

LOW-MASS STAR FORMATION AND THE INITIAL MASS FUNCTION IN
YOUNG CLUSTERS

by

Kevin Lee Luhman

A Dissertation Submitted to the Faculty of the
DEPARTMENT OF ASTRONOMY
In Partial Fulfillment of the Requirements
For the Degree of
DOCTOR OF PHILOSOPHY
In the Graduate College
THE UNIVERSITY OF ARIZONA

1 9 9 8

INFORMATION TO USERS

This manuscript has been reproduced from the microfilm master. UMI films the text directly from the original or copy submitted. Thus, some thesis and dissertation copies are in typewriter face, while others may be from any type of computer printer.

The quality of this reproduction is dependent upon the quality of the copy submitted. Broken or indistinct print, colored or poor quality illustrations and photographs, print bleedthrough, substandard margins, and improper alignment can adversely affect reproduction.

In the unlikely event that the author did not send UMI a complete manuscript and there are missing pages, these will be noted. Also, if unauthorized copyright material had to be removed, a note will indicate the deletion.

Oversize materials (e.g., maps, drawings, charts) are reproduced by sectioning the original, beginning at the upper left-hand corner and continuing from left to right in equal sections with small overlaps. Each original is also photographed in one exposure and is included in reduced form at the back of the book.

Photographs included in the original manuscript have been reproduced xerographically in this copy. Higher quality 6" x 9" black and white photographic prints are available for any photographs or illustrations appearing in this copy for an additional charge. Contact UMI directly to order.

UMI

A Bell & Howell Information Company
300 North Zeeb Road, Ann Arbor MI 48106-1346 USA
313/761-4700 800/521-0600

LOW-MASS STAR FORMATION AND THE INITIAL MASS FUNCTION IN
YOUNG CLUSTERS

by

Kevin Lee Luhman

A Dissertation Submitted to the Faculty of the
DEPARTMENT OF ASTRONOMY
In Partial Fulfillment of the Requirements
For the Degree of
DOCTOR OF PHILOSOPHY
In the Graduate College
THE UNIVERSITY OF ARIZONA

1 9 9 8

UMI Number: 9901759

UMI Microform 9901759
Copyright 1998, by UMI Company. All rights reserved.

**This microform edition is protected against unauthorized
copying under Title 17, United States Code.**

UMI
300 North Zeeb Road
Ann Arbor, MI 48103

THE UNIVERSITY OF ARIZONA ©
GRADUATE COLLEGE

As members of the Final Examination Committee, we certify that we have
read the dissertation prepared by Kevin Lee Luhman
entitled Low-Mass Star Formation and the Initial Mass Function
in Young Clusters

and recommend that it be accepted as fulfilling the dissertation
requirement for the Degree of Doctor of Philosophy

George Rieke
George Rieke

7/29/98
Date

James W. Liebert
James Liebert

7/29/98
Date

Erick T. Young
Erick Young

7/29/98
Date

Jonathan Lunine
Jonathan Lunine

7/29/98
Date

Date

Final approval and acceptance of this dissertation is contingent upon
the candidate's submission of the final copy of the dissertation to the
Graduate College.

I hereby certify that I have read this dissertation prepared under my
direction and recommend that it be accepted as fulfilling the dissertation
requirement.

George Rieke
Dissertation Director George Rieke

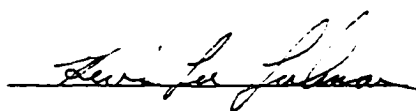
7/29/98
Date

STATEMENT BY AUTHOR

This dissertation has been submitted in partial fulfillment of requirements for an advanced degree at The University of Arizona and is deposited in the University Library to be made available to borrowers under rules of the Library.

Brief quotations from this dissertation are allowable without special permission, provided that accurate acknowledgment of source is made. Requests for permission for extended quotation from or reproduction of this manuscript in whole or in part may be granted by the head of the major department or the Dean of the Graduate College when in his or her judgment the proposed use of the material is in the interests of scholarship. In all other instances, however, permission must be obtained from the author.

SIGNED: _____



ACKNOWLEDGMENTS

An important factor in a successful thesis is a good advisor, and I couldn't have asked for a better one than George Rieke. The tireless efforts of George and Marcia in supporting countless observing runs are greatly appreciated. They've shown incredible patience and understanding while training myself and other young scientists. In addition, I thank George and Marcia for obtaining the grant which has supported me during much of my tenure at Steward (NASA grant NAGW-4083 under the Origins of Solar Systems program). Jim Liebert has played an important role as an educator, colleague, and fellow Kansas Jayhawks fan. I'm very grateful to Chad Engelbracht for writing the scripts used in reducing FSpec data and for putting up with my persistent questions concerning latex, perl, fortran, IRAF, etc. I thank Tim Pickering and Craig Kulesa for the computer expertise they've made available to myself and the rest of Steward. Chad, Tim, and Craig also acted as plump and readily explodable targets for my quad rockets in Quake, although not by their own volition. Margaret Hanson and Chad have provided a great deal of assistance and stimulating conversations regarding general observing and science in the infrared.

The large amount of observing time which produced the data presented in this thesis was made possible by the generosity of the Steward telescope allocation committee. I thank several scientists for providing helpful comments and access to their data and theoretical calculations: F. Allard, I. Baraffe, A. Burrows, F. D'Antona, L. Hartmann, G. Herbig, J. D. Kirkpatrick, M. Meyer, J. Stauffer, and F. Swenson.

DEDICATION

For Michael and Laurie.

TABLE OF CONTENTS

| | |
|--|----|
| LIST OF FIGURES | 10 |
| LIST OF TABLES | 13 |
| ABSTRACT | 14 |
| 1 Introduction | 15 |
| 2 Testing Theoretical Evolutionary Tracks | 18 |
| 2.1 Introduction | 18 |
| 2.2 CM Dra and YY Gem | 19 |
| 2.3 Pleiades and Globular Clusters | 19 |
| 2.4 Which Tracks Are Appropriate for Young, Embedded Clusters? | 20 |
| 3 A Young Object Near the Hydrogen Burning Limit: V410 X-ray 3 | 24 |
| 3.1 Introduction | 24 |
| 3.2 Observations | 26 |
| 3.3 Discussion | 27 |
| 3.3.1 Spectroscopic Results: Li Detection and Spectral Type | 27 |
| 3.3.2 Colors, Extinction, and Bolometric Luminosity | 28 |
| 3.3.3 H-R Diagram | 29 |
| 3.4 Conclusions | 31 |
| 4 A Young Object Below the Hydrogen Burning Limit: ρ Oph 162349.8 – 242601 | 37 |
| 4.1 Introduction | 37 |
| 4.2 Observations | 39 |
| 4.3 Discussion | 40 |
| 4.3.1 Cluster Membership | 40 |
| 4.3.2 Spectral Type and Effective Temperature | 41 |
| 4.3.3 Extinction and Bolometric Luminosity | 43 |

TABLE OF CONTENTS — *Continued*

| | | |
|-------|---|-----|
| 4.3.4 | Age and Mass | 44 |
| 4.4 | Conclusion | 45 |
| 5 | L1495E | 49 |
| 5.1 | Introduction | 49 |
| 5.2 | Observations | 51 |
| 5.3 | Discussion | 53 |
| 5.3.1 | IR Spectral Classification of Young Stars | 53 |
| 5.3.2 | Derivation of T_{eff} | 55 |
| 5.3.3 | Derivation of L_{bol} | 58 |
| 5.3.4 | H-R Diagram | 60 |
| 5.3.5 | The Initial Mass Function | 63 |
| 5.4 | Conclusions | 71 |
| 5.5 | Notes on IR Spectral Classification | 73 |
| 5.6 | Comments on Individual Source Classifications | 79 |
| 6 | IC 348 | 107 |
| 6.1 | Introduction | 107 |
| 6.2 | Observations | 108 |
| 6.3 | Individual Source Characteristics | 112 |
| 6.3.1 | Spectral Types | 112 |
| 6.3.2 | Substellar Members of IC 348 | 115 |
| 6.3.3 | Extinction | 117 |
| 6.3.4 | Derivation of T_{eff} and L_{bol} | 120 |
| 6.3.5 | X-ray Properties | 121 |
| 6.4 | Circumstellar Disks | 122 |
| 6.4.1 | Signatures of Disks | 122 |
| 6.4.2 | Disk Frequency and Lifetimes | 124 |

TABLE OF CONTENTS — *Continued*

| | | |
|-------|---|-----|
| 6.5 | The IC 348 Stellar Population | 125 |
| 6.5.1 | Cluster Membership | 125 |
| 6.5.2 | H-R Diagram | 126 |
| 6.5.3 | Dynamics | 127 |
| 6.5.4 | Star Formation History | 129 |
| 6.5.5 | The Initial Mass Function | 131 |
| 6.6 | Conclusions | 139 |
| 6.7 | Notes on IR Spectral Classification | 141 |
| 6.7.1 | G0 and Earlier | 142 |
| 6.7.2 | G0 to Early K | 143 |
| 6.7.3 | Late K | 143 |
| 6.7.4 | Early M | 144 |
| 6.7.5 | Mid M | 145 |
| 6.7.6 | Late M and Other Types | 146 |
| 6.8 | Notes on Optical Classification | 148 |
| 7 | ρ Ophiuchi | 171 |
| 7.1 | Observations | 174 |
| 7.2 | Individual Source Characteristics | 175 |
| 7.2.1 | IR Spectral Classification | 175 |
| 7.2.2 | Derivation of A_J , T_{eff} , and L_{bol} | 179 |
| 7.3 | The ρ Oph Stellar Population | 181 |
| 7.3.1 | Cluster Membership | 181 |
| 7.3.2 | Global Properties of the IR Spectra and Colors | 182 |
| 7.3.3 | The H-R Diagram and Star Formation History | 184 |
| 7.3.4 | The Initial Mass Function | 186 |
| 7.4 | Conclusions | 193 |
| 7.5 | Notes on Individual Sources | 195 |

TABLE OF CONTENTS — *Continued*

| | |
|-------------------------|-----|
| 8 Future Work | 213 |
| References | 216 |

LIST OF FIGURES

| | | |
|------|---|-----|
| 2.1 | Theoretical tracks tested against CM Dra and YY Gem | 22 |
| 2.2 | Theoretical tracks tested against the Pleiades | 23 |
| 3.1 | High-resolution Li I spectrum of V410 X-ray 3 | 33 |
| 3.2 | Low-resolution optical spectrum of V410 X-ray 3 | 34 |
| 3.3 | K -band spectrum of V410 X-ray 3 | 35 |
| 3.4 | H-R diagram for V410 X-ray 3 | 36 |
| 4.1 | Low-resolution optical spectrum of ρ Oph 162349.8 – 242601 | 47 |
| 4.2 | H-R diagram for ρ Oph 162349.8 – 242601 | 48 |
| 5.1 | K -band spectra of sources in L1495E | 91 |
| 5.2 | Finding chart for the K -band image of L1495E | 92 |
| 5.3 | Recent temperature scales for cool stars | 93 |
| 5.4 | $H - K$ vs. $J - H$ for L1495E | 94 |
| 5.5 | H-R diagram for L1495E | 95 |
| 5.6 | IMF for L1495E | 96 |
| 5.7 | K -band luminosity function for L1495E | 97 |
| 5.8 | Equivalent widths of K -band lines | 98 |
| 5.9 | K -band spectra of K0V stars | 99 |
| 5.10 | K -band spectra of K1V stars | 100 |
| 5.11 | K -band spectra of K7V stars | 101 |
| 5.12 | K -band spectra of M1V stars | 102 |
| 5.13 | K -band spectra of M2V stars | 103 |
| 5.14 | K -band spectra of M3V stars | 104 |
| 5.15 | Composite standard spectra for K -band classification | 105 |

LIST OF FIGURES — *Continued*

| | | |
|------|--|-----|
| 5.16 | Composite standard spectra for K -band classification | 106 |
| 6.1 | K -band spectra of sources in IC 348 | 154 |
| 6.2 | K -band spectra of sources in IC 348 | 155 |
| 6.3 | K -band spectra of sources in IC 348 | 156 |
| 6.4 | K -band spectra of sources in IC 348 | 157 |
| 6.5 | Low-resolution optical spectra of M6 sources in IC 348 | 158 |
| 6.6 | Low-resolution optical spectra of M7-M8 sources in IC 348 | 159 |
| 6.7 | H-R diagram for IC 348 with DM94 | 160 |
| 6.8 | H-R diagram for IC 348 with DM97 | 161 |
| 6.9 | $H - K$ vs. $J - H$ for disk sources in IC 348 | 162 |
| 6.10 | H-R diagram for late-type sources in IC 348 with DM94, DM97 | 163 |
| 6.11 | H-R diagram for late-type sources in IC 348 with Burrows, BCAH97 . | 164 |
| 6.12 | $H - K$ vs. $J - H$ for IC 348 | 165 |
| 6.13 | $F(\text{H}\alpha)$ versus $F(\text{Br}\gamma)/F(\text{H}\alpha)$ | 166 |
| 6.14 | Distribution of ages for core stars in IC 348 | 167 |
| 6.15 | K -band luminosity function for IC 348 | 168 |
| 6.16 | IMF for IC 348 | 169 |
| 6.17 | Simulated effect of binarity on the IMF | 170 |
| 7.1 | Finding chart for the spectroscopic sample in ρ Oph | 200 |
| 7.2 | K -band spectra of sources in ρ Oph ($< \text{F8}$ or $r_K < 0.25$) | 201 |
| 7.3 | K -band spectra of sources in ρ Oph ($r_K < 0.25$) | 202 |
| 7.4 | K -band spectra of sources in ρ Oph ($0.25 \leq r_K \leq 1$) | 203 |
| 7.5 | K -band spectra of sources in ρ Oph ($r_K \geq 1$) | 204 |
| 7.6 | K -band spectra of sources in ρ Oph ($r_K \geq 1$, III, K-M) | 205 |
| 7.7 | K -band spectra of IRAS64A and FU Ori objects | 206 |
| 7.8 | $H - K$ vs. $J - H$ for ρ Oph as a function of r_K | 207 |

LIST OF FIGURES — *Continued*

| | | |
|------|--|-----|
| 7.9 | $H - K$ vs. $J - H$ for ρ Oph as a function of position | 208 |
| 7.10 | H-R diagram for ρ Oph | 209 |
| 7.11 | K -band luminosity function for ρ Oph | 210 |
| 7.12 | $H - K$ vs. K for ρ Oph | 211 |
| 7.13 | IMF for ρ Oph | 212 |

LIST OF TABLES

| | | |
|-----|--|-----|
| 3.1 | Photometry of V410 X-ray 3 | 32 |
| 5.1 | Data for Spectroscopic Sample in L1495E | 84 |
| 5.1 | Data for Spectroscopic Sample in L1495E | 85 |
| 5.2 | Candidate Low-Mass Members of L1495E | 86 |
| 5.3 | Spectral Standards | 87 |
| 5.3 | Spectral Standards | 88 |
| 5.3 | Spectral Standards | 89 |
| 5.4 | Components of Composite Spectra | 90 |
| 6.1 | Data for Spectroscopic Sample in IC 348 | 151 |
| 6.1 | Data for Spectroscopic Sample in IC 348 | 152 |
| 6.1 | Data for Spectroscopic Sample in IC 348 | 153 |
| 7.1 | Data for Spectroscopic Sample in ρ Ophiuchi | 197 |
| 7.1 | Data for Spectroscopic Sample in ρ Ophiuchi | 198 |
| 7.1 | Data for Spectroscopic Sample in ρ Ophiuchi | 199 |

ABSTRACT

I have used optical and near-infrared spectroscopy and imaging to measure spectral types and luminosities for young ($\tau < 10$ Myr), embedded ($A_V = 0-50$), low-mass ($0.1-1 M_\odot$) stars in three nearby ($d < 300$ pc) clusters: L1495E, IC 348, and ρ Ophiuchi. In conjunction with theoretical evolutionary tracks, I have derived the star formation history and initial mass function for each stellar population. A large number of brown dwarf candidates have been identified in the photometry, several of which are confirmed through spectroscopy. Finally, I have measured the frequency and survival times of circumstellar disks and investigated the photometric and spectroscopic properties of protostars.

In § 2, I apply observational tests to the available sets of evolutionary models for low-mass stars, concluding that the calculations of D’Antona & Mazzitelli are preferred for the range of masses and ages considered here. In § 3 and § 4, I examine in detail the spectroscopic characteristics and substellar nature of two brown dwarf candidates. The study then expands to include the populations within the clusters L1495E (§ 5), IC 348 (§ 6), and ρ Ophiuchi (§ 7). In § 8, I briefly discuss the past, present, and future of scientific research related to this thesis.

CHAPTER 1

INTRODUCTION

The process by which interstellar gas clouds contract, fragment, and form stars is central to our picture of stellar evolution but is not well understood. One of the most fundamental constraints on this process is its final product, the initial mass function (IMF). Some theoretical models, such as those that invoke fragmentation into fractal structure (e.g., Larson 1985, 1992) predict that the low-mass cutoff of the IMF will depend on the gas kinetic temperature in the region of formation. Other models predict a low-mass turnover as a result of strong suppression of the formation of extremely low-mass stars and substellar objects by winds (Adams & Fatuzzo 1996). The IMF may be a function of the cluster density because of the influence of star-star interactions on the process of accretion (e.g., Price & Podsiadlowski 1995; Bonnell et al. 1997). Still other models (e.g., Silk 1995) are relatively insensitive to such environmental conditions.

The IMF can be determined in the solar neighborhood; however, as with most regions of space, the local stellar population represents a mixture of stars formed at different times and in differing environments. Consequently, any signature of the

dependence on conditions at the time of formation has been lost. Alternately, the IMF can be measured in evolved stellar clusters. However, low-mass star forming associations are quickly dissipated due to their internal velocity dispersions. In a Galactic lifetime, significant numbers of low-mass stars can escape even a massive cluster, due to a combination of internal cluster dynamics and Galactic tides (see, e.g., Vesperini & Heggie 1997). Thus, evolved clusters can be used only with caution to probe the IMF, and then only in a narrowly constrained set of conditions, namely formation in a very dense environment.

Consequently, only very young star forming regions are suitable to probe variations in the low-mass IMF. Typical star forming lifetimes in such regions appear to be ~ 10 Myr. Therefore, if I observe a system within this time interval, I have a chance of glimpsing a representative range of stellar masses independently of whether the system is destined to become a bound cluster. In addition, for their first ~ 10 Myr, the properties of substellar objects - brown dwarfs - are continuous with those of low-mass stars, largely as a result of the deuterium burning phase. After 5 to 10 Myr, the stars evolve toward a stable luminosity on the main sequence, whereas brown dwarfs continue to fade indefinitely and observational selection effects can produce a false indication of a low-mass cutoff in the IMF near the bottom of the main sequence.

Because very young clusters can be heavily embedded, near-IR observations have played an important role in determining their mass functions. Modeling of KLFs (e.g., McCaughrean & Stauffer 1994; Lada & Lada 1995; Lada, Alves, & Lada 1996) can constrain the IMF but may be subject to systematic uncertainties such as those arising from extinction and IR excesses. Models using multi-band IR photometry (e.g., Comerón et al. 1993; Strom, Kepner, & Strom 1995; Comerón,

Rieke, & Rieke 1996) can reduce these uncertainties. However, both techniques are sensitive to assumptions about the star formation rate as a function of time. A more definitive understanding of these young stellar populations requires spectroscopic surveys so mass functions can be derived from H-R diagrams which yield the star formation history directly, as illustrated by a number of optical spectroscopic surveys (e.g., Hartigan 1993; Hughes et al. 1994; SS94; Hillenbrand 1997). Although a number of these studies suggest a low mass turnover in the IMF, because they probe only the less-embedded members of the region, they also are potentially subject to biases. With the addition of IR spectral classification, these biases could be avoided. Meyer (1995) and Green & Meyer (1995) began such work by measuring spectral types through H and K -band spectra of embedded sources in NGC 2024 and ρ Oph. Because of technical limitations, these studies reach only a fraction of the cluster members, and they generally do not include the faintest and potentially least-luminous ones. In the following work, I have expanded on these previous studies by using deep IR and optical imaging and spectroscopy to obtain magnitude-limited samples of hundreds of young stars in several nearby clusters. From this data, I derive spectral types, luminosities, and reddenings for individual sources. Combining the resulting H-R diagrams with IR luminosity function modeling, I examine the star formation histories, mass functions, constraints on circumstellar disk lifetimes, and presence of brown dwarfs in young clusters.

CHAPTER 2

TESTING THEORETICAL EVOLUTIONARY TRACKS

2.1. Introduction

The initial mass functions (IMFs) derived in embedded clusters are strongly dependent on the adopted temperature scale and set of evolutionary tracks. In § 5 I justify the adoption of the temperature scale of Leggett et al. (1996). Over the last several years, evolutionary tracks by D'Antona & Mazzitelli (1994) (hereafter DM94), Burrows et al. (1993) (hereafter BHSL93), and Swenson (hereafter FJS) have been used widely in the analysis of embedded clusters. Only very recently have model interiors been coupled with sophisticated model atmospheres. New evolutionary tracks using Allard's latest NextGen atmospheres have been produced by both Burrows (private communication) and Baraffe et al. (1997) (hereafter BCAF97). I test these various tracks against the two low-mass eclipsing binaries (YY Gem, CM Dra), the Pleiades, and globular clusters.

2.2. CM Dra and YY Gem

In Figure 2.1 I present the observed properties of YY Gem and CM Dra with the theoretical predictions. For YY Gem, the stellar radii and ratio of component luminosities are from Budding et al. (1996) and the system L_{bol} is from Leung & Schneider (1978). For CM Dra, I repeated the calculation by Lacy (1976) of the component luminosities using new parallax data; the radii were taken from Metcalf et al. (1996). I then used the radii and luminosities for each system to calculate T_{eff} .

Chabrier & Baraffe (1995) found good agreement between the data on CM Dra and YY Gem and their evolutionary tracks using Allard's Base atmospheres. These tracks are not shown, but are similar to the Base tracks of Burrows. However, more recent interiors combined with Allard's latest NextGen atmospheres do not fit the binary data as well as the Base models and are only marginally better than the older tracks of DM94 and FJS. The fit actually worsens for CM Dra if its low metallicity (implied by kinematics) is included. The possible youth of YY Gem does not change the fits substantially. It is interesting to note that all three generations of models by Burrows (Model X, Base, NextGen) produce identical mass-radius relationships which fit perfectly with the data for CM Dra.

2.3. Pleiades and Globular Clusters

I have transformed the Pleiades $(V - I)_C$ colors of Stauffer (private communication) to spectral type using Bessell (1979) for $< M0V$ and Bessell (1990a) for $\geq M0V$. I converted from spectral type to T_{eff} using both Kirkpatrick et al. (1993) and Leggett et al. (1996). Visual magnitudes were converted to L_{bol} using the bolometric

corrections compiled by Kenyon & Hartmann (1995). In Figure 2.2, I have plotted the Pleiades with tracks of DM94, FJS, and BCAH97. Both DM94 and BCAH97 imply a mass-dependent age for the empirical Pleiades isochrone (~ 100 Myr), where lower mass sources appear progressively younger. If I use the synthetic colors produced by BCAH97 to transform between the theoretical and observation planes, I find that this trend is enhanced (i.e, the synthetic temperature scale is cooler). The FJS isochrones, on the other hand, are parallel to the Pleiades locus, but these stars then fall below the FJS main sequence.

Baraffe et al. (1997) find excellent agreement between their latest tracks and the main sequence down to $0.1 M_{\odot}$ in the globular cluster NGC 6397. The higher temperatures and reduced metallicities ($[\text{Fe}/\text{H}] = -1.9$) of such stars make them easier to model, whereas the solar abundance calculations do not match well with observations. For instance, the predicted solar metallicity main sequence falls equidistant between the NGC 6397 sequence and the Leggett et al. (1996) young disk sequence.

2.4. Which Tracks Are Appropriate for Young, Embedded Clusters?

Since the BCAH97 tracks only extend up to $0.7 M_{\odot}$, it is not possible to derive an IMF for the entire population. However, I can make the simple calculation of $N(> 0.7 M_{\odot})/N(< 0.7 M_{\odot})$ using each set of tracks. This ratio is 0.18, 0.18, and 1 using the DM94, FJS, and BCAH97 tracks, respectively, whereas Scalo (1986) predicts a value of 0.22. The strange IMF produced by BCAH97 may be due to the limitations of the NextGen atmospheres. The lowest gravity available in the atmospheric models ($\log g = 3.5$) is near that expected for low-mass stars at 1 Myr.

New model interiors by D'Antona & Mazzitelli (DM97) which treat convection in a more sophisticated manner produce a cooler main sequence than found in DM94, bringing it into better agreement with observations. Since model atmospheres are not used in DM97, the surface gravity constraints of the NextGen models are avoided and DM97 may be useful for studying young stars. The DM97 tracks must be tested with the binary and Pleiades data as well, but they may prove to be the most promising set of tracks for deriving IMFs in very young clusters.

New instrumental capabilities, particularly near-infrared (IR) spectroscopy, now permit placement of hundreds of embedded cluster members on the Hertzsprung-Russell (H-R) diagram. The uncertainties in evolutionary tracks, especially at young ages, loom as perhaps the largest obstacle in interpreting these new data to derive fundamental cluster properties such as the IMF. Further progress on interior models is essential in addition to more observational tests of the tracks at young ages.

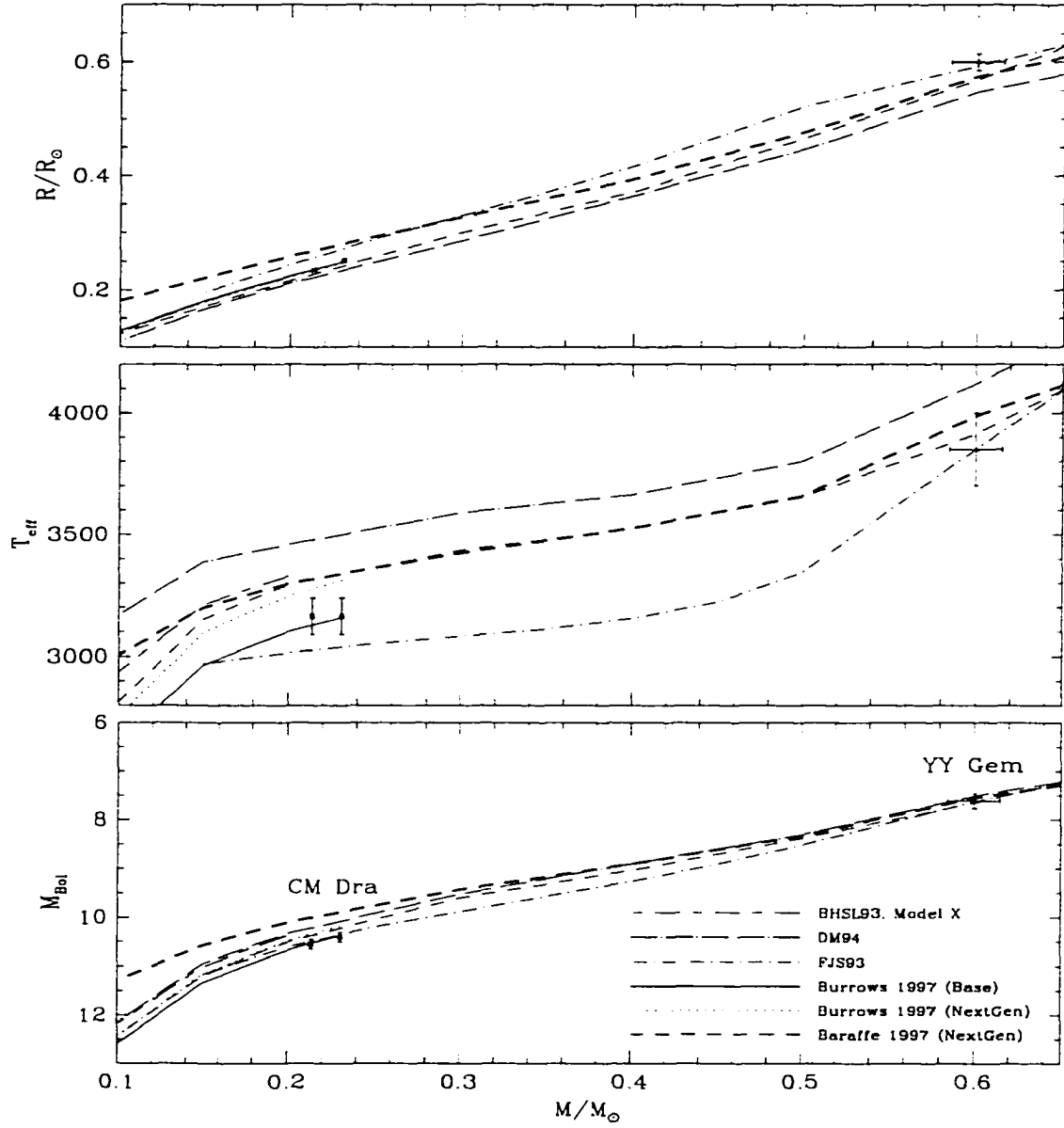


Figure 2.1 Comparison of stellar properties derived for YY Gem and CM Dra to the predictions of model interiors (solar metallicities). The bold dashed line represents 100 Myr as given by BCAH97.

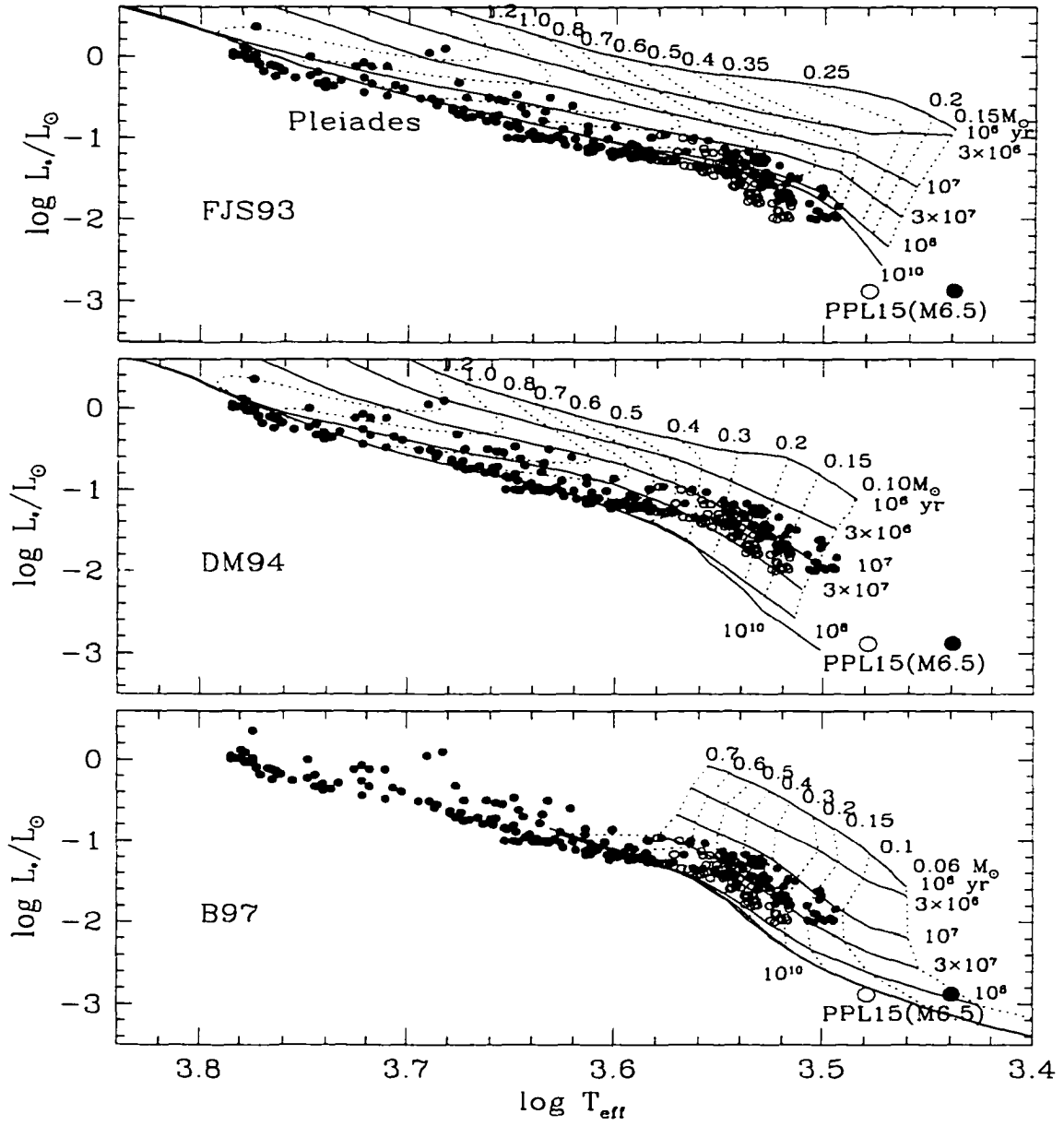


Figure 2.2 The Pleiades with evolutionary tracks of FJS, DM94, and B97. Solid and open circles were transformed with the Leggett et. al. (1996) and Kirkpatrick et al. (1993) temperature scales, respectively.

CHAPTER 3

A YOUNG OBJECT NEAR THE HYDROGEN BURNING LIMIT: V410 X-RAY 3

3.1. Introduction

A broad variety of astrophysical issues have motivated searches for brown dwarfs (Burrows & Liebert 1993). However, for many years, no definitive detections were made (Stevenson 1991). This situation has changed dramatically with the discovery of the stellar companion GL 229B (Nakajima et al. 1995; Oppenheimer et al. 1995) and of PPL 15 (M6.5), Teide 1 (M8), and Calar 3 (M8) in the Pleiades (Stauffer, Hamilton, & Probst 1994; Basri, Marcy, & Graham 1996; Rebolo, Zapatero Osorio, & Martín 1995; Zapatero Osorio, Rebolo, & Martín 1997). With a suite of prototype objects, the properties of relatively old brown dwarfs are becoming well-defined to guide future search programs.

To establish the properties of brown dwarfs for comparison with theoretical predictions, I require objects over a large range of ages and masses. Newly formed brown dwarfs should be luminous and relatively easy to detect, but they are difficult to distinguish from low-mass stars. Unlike evolved brown dwarfs such as GL 229B, young substellar objects are not drastically cooler than low-mass stars. Li depletion is useful in identifying brown dwarfs in the Pleiades since it marks the hydrogen burning limit for stars at ~ 100 Myr (Basri, Marcy, & Graham 1996), but a similar test is not available for very young sources.

Since I must rely on evolutionary tracks to identify young brown dwarfs, I have carefully examined the translation of the theoretical hydrogen burning limit into the observed spectral types. The Rosetta Stone for such a study is the young (~ 1 Myr), late-type (M6) source V410 X-ray 3 in L1495E within the star forming Taurus-Auriga complex. This source was first identified in ROSAT observations by Strom & Strom (1994) (SS94), making it one of the latest objects observed in Taurus at that time. Other young (≤ 10 Myr old) M6 sources observed to date include UX Tauri C and Ap J0323+4853 in α Persei (Magazzù et al. 1991; Zapatero Osorio et al. 1996). Since V410 X-ray 3 is nearby (~ 140 pc) and has no significant extinction or IR excess emission, I can accurately measure its bolometric luminosity and study it in both the optical and IR. I have obtained low-resolution optical and IR spectra of V410 X-ray 3 to establish the spectral type and examine the behavior of gravity-sensitive features. I have placed the source on the H-R diagram and used the latest evolutionary tracks to discuss the spectral type of the substellar boundary for very young sources. The following work has been in collaboration with L. Hartmann and C. Briceño.

3.2. Observations

C. Briceño obtained *VRI* photometry for V410 X-ray 3 using the 2048×2048 thinned CCD mounted on the 1.2 m telescope of the Smithsonian Astrophysical Observatory at Mt. Hopkins. The data were reduced using the standard IRAF routines for fixing bad pixels, bias-subtracting, and flat-fielding. Aperture photometry was performed using the APPHOT package. Instrumental magnitudes were transformed to the Cousins system using Landolt (1992) standard stars spanning a wide range of colors. The internal dispersion and systematic errors due to the transformation are at the ± 0.02 magnitude level. The new photometry is presented in Table 3.1 along with measurements of SS94 and from § 5.

K-band spectroscopy was performed on V410 X-ray 3 on 1994 December 9 using the near-IR long-slit spectrometer FSpec (Williams et al. 1993) at the Steward 2.3 m Bok Reflector on Kitt Peak. The observing and data reduction procedures are discussed in detail § 5. I obtained an optical spectrum of V410 X-ray 3 with the Boller and Chivens Spectrometer at the Bok Reflector on 1996 November 7. I used the 400 g mm^{-1} grating ($\lambda_{\text{blaze}} = 7506 \text{ \AA}$) to obtain a spectrum from 5600 to 9000 \AA with $\Delta\lambda = 6 \text{ \AA}$ and an integration time of 1200 s. To derive the sensitivity function of the array, I also observed Hiltner 102, a star whose intrinsic spectral distribution is known. The spectrum of V410 X-ray 3 was extracted from a bias-subtracted frame, corrected for the sensitivity function, and wavelength calibrated using He-Ar and Fe-Ne lamp spectra.

An intermediate-resolution optical spectrum of V410 X-ray 3 was obtained by L. Hartmann and C. Briceño on 1996 December 3 using the Blue Channel Spectrograph at the MMT equipped with the Loral 3072×1024 ($15 \text{ }\mu\text{m}$ square pixels) CCD binned by a factor 2:1 in the spatial direction. The spectrograph was

configured with a 1200 g mm^{-1} grating and a $1''.5 \times 180''$ slit. This combination yielded a spectral resolution of 1.8 \AA ($0.50 \text{ \AA pixel}^{-1}$) over the range $\sim 6000\text{--}7300 \text{ \AA}$. Two 1800 s exposures were obtained of the source, each one followed immediately by an exposure of the He-Ne-Ar comparison lamp. High signal-to-noise exposures were also taken of standard stars with spectral types in the range M0-M6 (Allen & Strom 1995; Gliese 1969). All sources were observed at an airmass ~ 1.5 . The data were reduced using the standard IRAF procedures.

3.3. Discussion

3.3.1. Spectroscopic Results: Li Detection and Spectral Type

Before discussing the other properties of V410 X-ray 3, I must first establish its membership to the L1495E star forming region. The X-ray ($\log L_X/L_{\text{bol}} = -2.8$) and $\text{H}\alpha$ ($W_\lambda = 16 \text{ \AA}$) emission of this source are indicative of a young star, but since the photometry and spectra imply little or no extinction, V410 X-ray 3 could also be a particularly active older foreground star. In the spectrum presented in Figure 3.1 I detect Li at $\lambda = 6707 \text{ \AA}$ ($W_\lambda = 0.45 \text{ \AA}$). This result confirms the pre-main-sequence nature of this object and its membership to the L1495E region, against which it is projected on the sky.

In Figure 3.2, the optical spectrum of V410 X-ray 3 is compared with the spectra of GL 406 (M6V), SAO 141344 (M5III), and VY Peg (M7III) (provided by J. D. Kirkpatrick.) Unfortunately, no M6III spectrum was available. Only the strongest features appearing in M stars are labeled. The M6V and an average of M5III and M7III spectra (referred to as M6III in the following discussion) provide the closest matches to the spectrum of V410 X-ray 3. I estimate the spectral type to be $\text{M}6 \pm 0.5$, which is consistent with the M6 type reported by SS94.

The remarkable aspect of the V410 X-ray 3 spectrum is the almost perfect match with M6III. As seen in Figure 3.2, CaH at 7000 Å is intermediate between M6V and M6III while the other gravity-dependent features (K I, Na I, and TiO/VO beyond 8200 Å) are all reproduced well by the giant. The Na I line appears to be particularly sensitive to gravity. Martín, Rebolo, & Zapatero Osorio (1996) also observed weak Na I in late-type Pleiades sources (M6-M8), which they attributed to non-dwarf surface gravities even though these sources are much less luminous than V410 X-ray 3 and have surface gravities within a factor of ~ 2 of those of dwarfs.

In Figure 3.3, the IR spectrum of V410 X-ray 3 is presented along with those of GL 406 (M6V), GL 644C (M7V), and R Lyr (M5III). The strengths of Ca, CO, and the feature near $2.28 \mu\text{m}$ match those of M6V or M7V but the Na is much weaker than in either standard. Na decreases in strength from dwarfs to giants, as seen in the M5III spectrum, so the weak Na in V410 X-ray 3 is probably due to a low surface gravity, which is consistent with the non-dwarf gravity implied by the optical spectrum. Greene & Meyer (1995) find similar behavior in *K*-band spectra of very young embedded stars in ρ Ophiuchi. I also find this effect in an M5 star in L1495E, which has detectable Sc ($2.195 \mu\text{m}$) and weak Na, which are giant-like, while other features remain dwarf-like, such as CO. In § 5 I show that most of the stars in L1495E have IR spectra similar to dwarf comparison stars, whereas the spectrum of V410 X-ray 3 appears intermediate between a dwarf and a giant, consistent with the very young age implied by its position on the H-R diagram.

3.3.2. Colors, Extinction, and Bolometric Luminosity

In Table 3.1 I present all available photometry of V410 X-ray 3. It appears to be moderately variable, possibly due to star spots. To compute photometric colors

for comparison with those of standard dwarf and giant colors, I have combined the data into colors labeled as “adopted” in Table 3.1 as follows: I take 1) $(V - I)_C$ from my measurement and $(R - I)_C$ as the average of my measurement and that of SS94; 2) $I_C - K$ from the data of SS94 for 1993 January 12, when simultaneous optical and IR data were obtained; and 3) the average of this SS94 JHK data and my measurements of 1994 December 19 to compute JHK colors (within the errors, the star was at the same brightness level for these two data sets). Standard M6V (young disk) and M6III colors are shown in Table 3.1, where I find that the colors of V410 X-ray 3 are matched closely by those of a normal M6V dwarf reddened by $A_V = 0.6$ with the extinction law of Rieke & Lebofsky (1985). Alternate choices of standard colors (e.g., Bessell 1991) imply lower extinctions. I also find that the colors of M6III do not match for any value of extinction. It is curious that the optical spectrum looks giant-like while the optical colors remain dwarf-like.

In the same manner as Leggett et al. (1996), I have calculated $\log L_{\text{bol}}/L_{\odot} = -1.23 \pm 0.1$ ($d = 140$ pc) by integrating the “adopted” broad-band photometry in Table 3.1. If I apply the bolometric correction of a standard M6V to I or J (Kenyon & Hartmann 1995) I arrive at nearly the same luminosity. The lack of excess emission at V and L' rules out significant contamination in the measured luminosity by a circumstellar disk.

3.3.3. H-R Diagram

To estimate the mass and age of V410 X-ray 3 I must use the H-R diagram in conjunction with theoretical evolutionary tracks. There are several sets of model interiors available. The tracks of DM94 BHSL93 are shown in the upper panel of Figure 3.4 and newer calculations of Burrows (1997) and BCAH97 using Allard’s latest NextGen atmospheres are given in the lower panel. In § 2 and § 5, I discuss

the comparison of the various models to the observations of YY Gem and CM Dra, globular clusters, embedded clusters, the Pleiades (particularly PPL 15), and the main sequence. The newer tracks appear to be well-suited for studying sources near the hydrogen burning limit, but I also show the tracks of DM94 and BHSL93 for reference since these calculations have been widely used.

The placement of V410 X-ray 3 on the H-R diagram now relies on the crucial step of converting the M6 spectral type to an effective temperature. In § 5 I find that the Leggett et al. (1996) M dwarf temperature scale is consistent with the empirical T_{eff} measurement of CM Dra and also gives a reasonable age and mass for PPL 15 when coupled with the latest evolutionary tracks. Synthetic colors are produced by the latest tracks of BCAH97 and the resulting $(I_C - K) - T_{\text{eff}}$ scale is quite similar to that of Leggett et al. When estimating T_{eff} for pre-main-sequence stars it is customary to use a dwarf scale, so in Figure 3.4 I first plot the position of V410 X-ray 3 with $T_{\text{eff}}(\text{M6V}) = 2840 \text{ K}$, as given by a fit to the Leggett et al. scale. The corresponding mass is $\sim 0.07 M_{\odot}$. However, since the optical spectrum matches well with M6III and the IR spectrum appears intermediate between a dwarf and giant, the temperature of V410 X-ray 3 may fall between that of M6V ($T_{\text{eff}} = 2840 \text{ K}$) and M6III ($T_{\text{eff}} = 3250 \text{ K}$) (Ridgway et al. 1980; Perrin et al. 1997). If the intrinsic $I_C - K$ of a young (1-3 Myr old) M6 star is similar to that of M6V, which is the case for V410 X-ray 3, then BCAH97 predict that such a source will have a temperature at $\sim 200 \text{ K}$ greater than that of M6V. Figure 3.4 shows the position of V410 X-ray 3 with this temperature, where the mass implied by the latest tracks ($\sim 0.08\text{-}0.15 M_{\odot}$) is now just above the hydrogen burning limit. I therefore estimate that the hydrogen burning limit occurs near M6 – M7 for young, embedded stars.

3.4. Conclusions

I have presented observations of the late-type source V410 X-ray 3 in Taurus, which exhibits X-ray and $H\alpha$ emission and Li absorption, clear signatures of youth. Because of its proximity, luminosity, and lack of heavy extinction, this source is a unique opportunity to study a low-mass young star from the optical into the IR. I show that:

1. The colors are consistent with those of a slightly reddened dwarf ($A_V = 0.6$).
2. The optical spectrum matches well with M6III and the IR spectrum shows both dwarf (weak CO) and giant (weak Na) characteristics.
3. Using recent model interiors and atmospheres of BCAH97, I estimate a temperature of ~ 200 K hotter than that of M6V, thus implying a mass of $\sim 0.08\text{--}0.15 M_\odot$. However, the mass of this source could be as low $0.07 M_\odot$ if the Leggett et al. dwarf temperature scale is used.
4. Consequently, with the latest evolutionary tracks the hydrogen burning limit for young stars (~ 1 Myr old) occurs at $\sim M6 - M7$. However, the theoretical models are uncertain at very young ages and low masses and require observational tests.

Table 3.1. Photometry of V410 X-ray 3

| I_C | $(V - I)_C$ | $(R - I)_C$ | $I_C - K$ | $J - H$ | $H - K$ | $K - L'$ | K | Comments |
|-------|-------------|-------------|-----------|---------|---------|----------|-------|--------------------------|
| 13.53 | ... | 2.27 | 3.04 | 0.57 | 0.44 | ... | 10.49 | 1993 Jan 12 ^a |
| ... | ... | ... | ... | 0.94 | 0.37 | ... | 10.77 | 1993 Mar 11 ^a |
| ... | ... | ... | ... | 0.69 | 0.40 | 0.05 | 10.54 | 1994 Dec 19 ^b |
| 14.07 | 4.18 | 2.25 | ... | ... | ... | ... | ... | 1995 Dec 11 |
| 13.80 | 4.18 | 2.26 | 3.04 | 0.63 | 0.42 | ... | ... | adopted |
| ... | 3.75 | 2.10 | 2.90 | 0.56 | 0.33 | ... | ... | M6V ^c |
| ... | 3.30 | 1.85 | 3.75 | 0.89 | 0.30 | ... | ... | M6III ^d |
| ... | 3.98 | 2.23 | 3.20 | 0.62 | 0.37 | ... | ... | M6V, $A_V = 0.6$ |
| ... | 3.53 | 1.98 | 4.05 | 0.95 | 0.34 | ... | ... | M6III, $A_V = 0.6$ |

^aSS94. JHK in CIT system.

^bMMT $JHKL'$. L' is centered at $3.4 \mu\text{m}$ with a FWHM of $0.2 \mu\text{m}$.

^cM6V colors from Leggett (1992).

^dM6III colors from Thé et al. (1990) and Frogel et al. (1978).

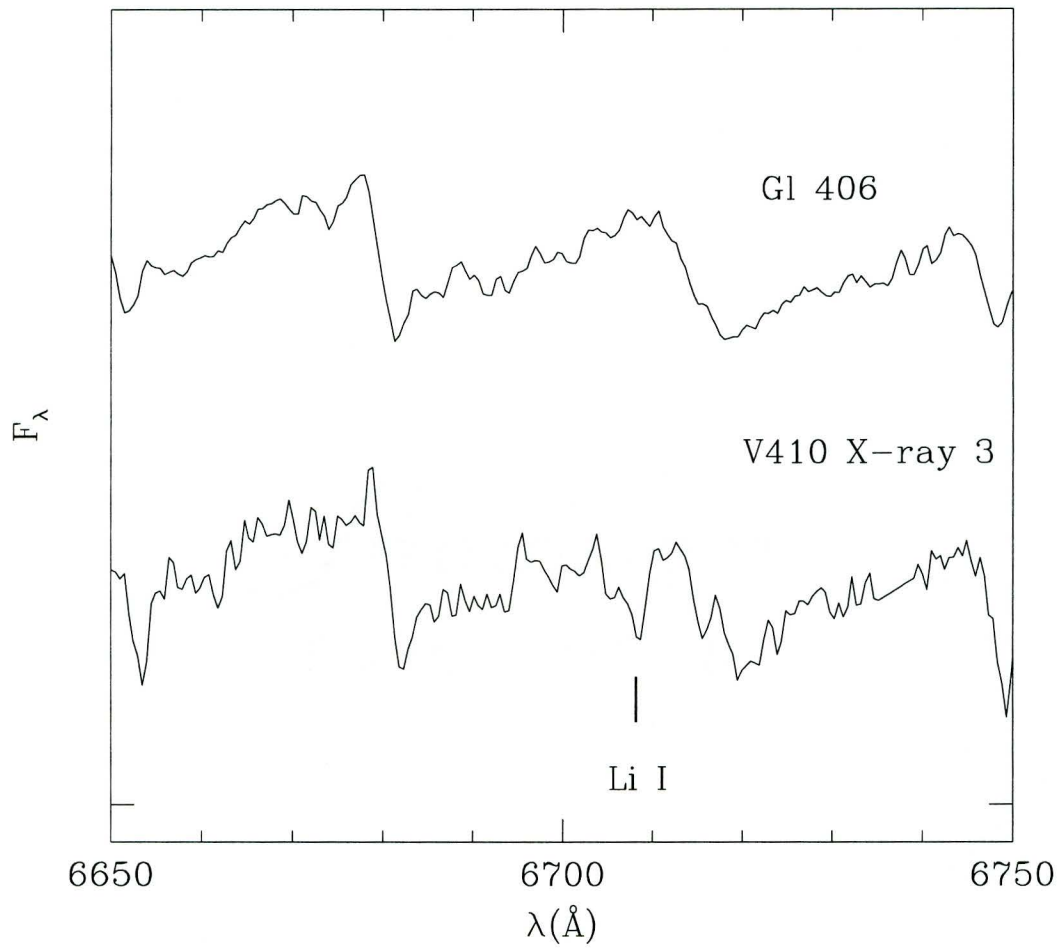


Figure 3.1 The Li I region for V410 X-ray 3 in my MMT spectra. For comparison purposes I show the same spectral region for the standard star GL 406 (M6V).

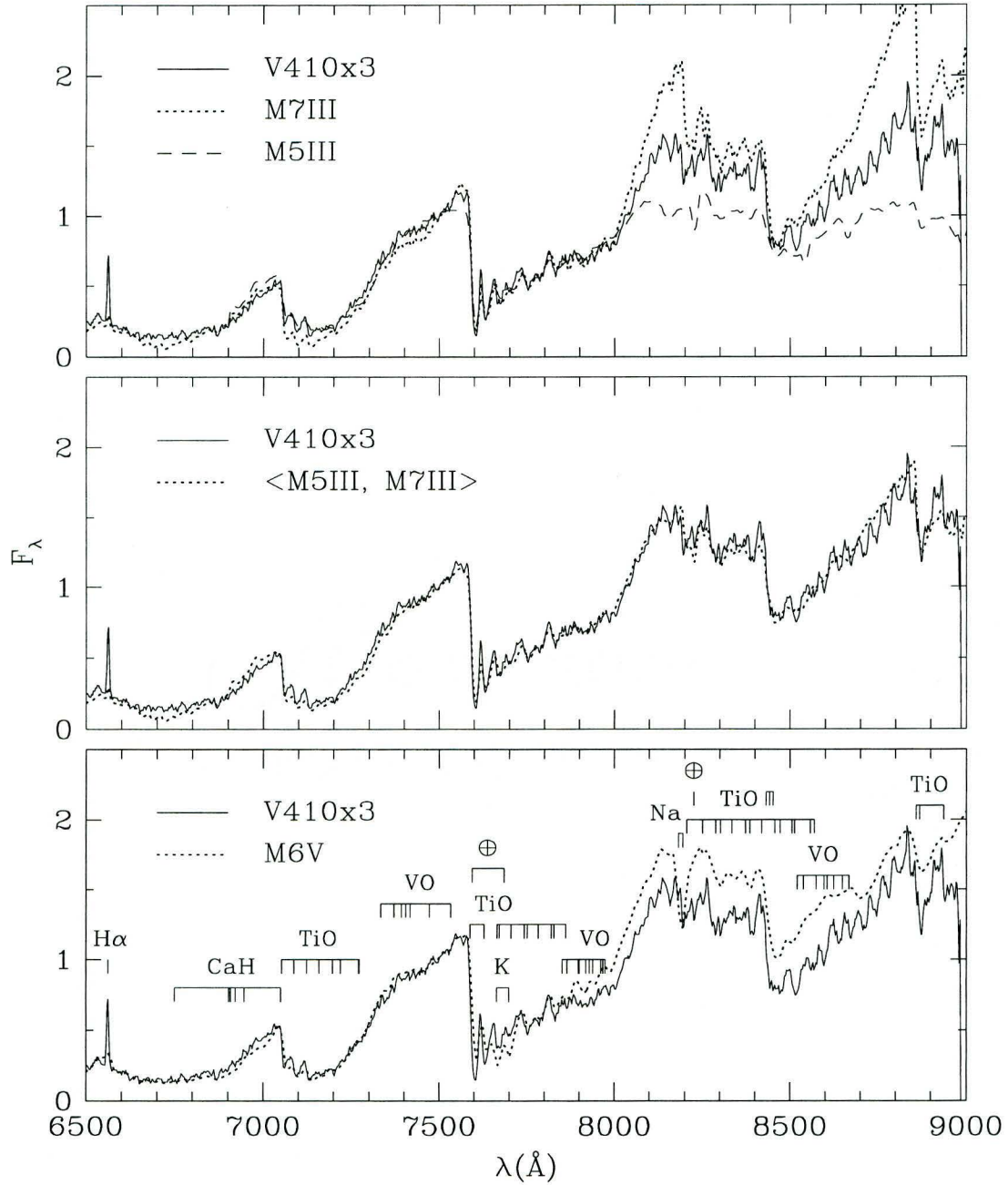


Figure 3.2 Optical spectrum of V410 X-ray 3 plotted with late-M spectral standards. All spectra are normalized at 7500 \AA .

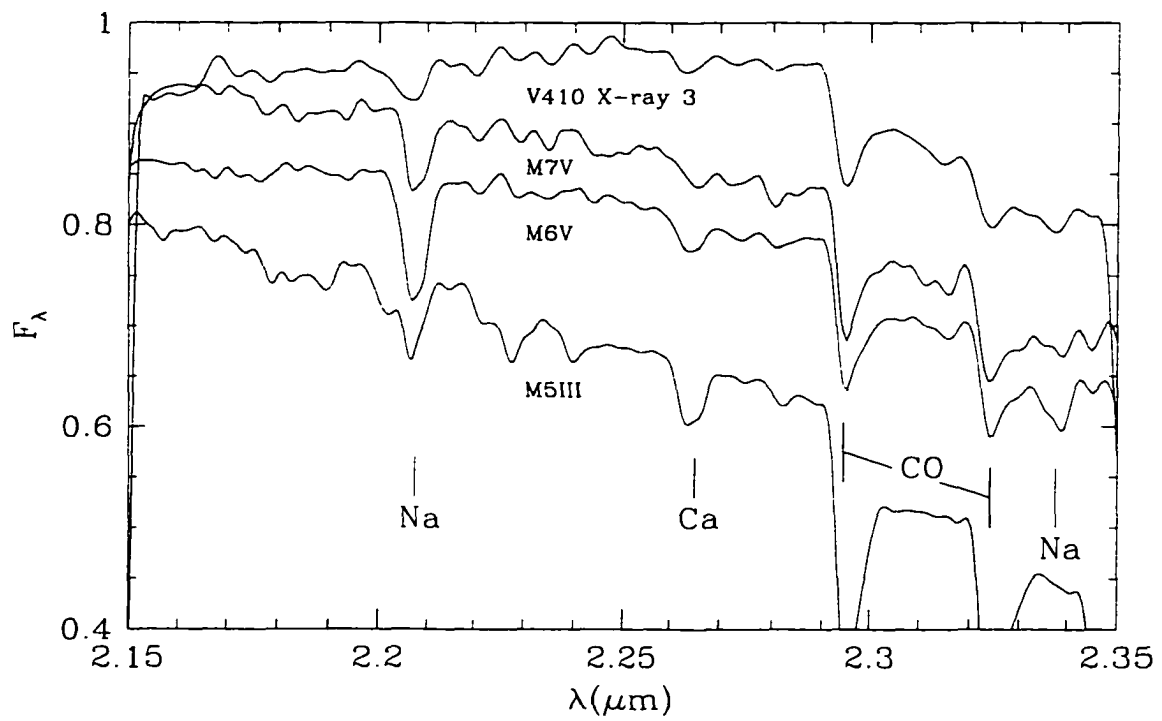


Figure 3.3 *K*-band spectrum ($R = 800$) of V410 X-ray 3 plotted with late-M dwarf and giant spectral standards, normalized at 2.2 μm with constant offsets.

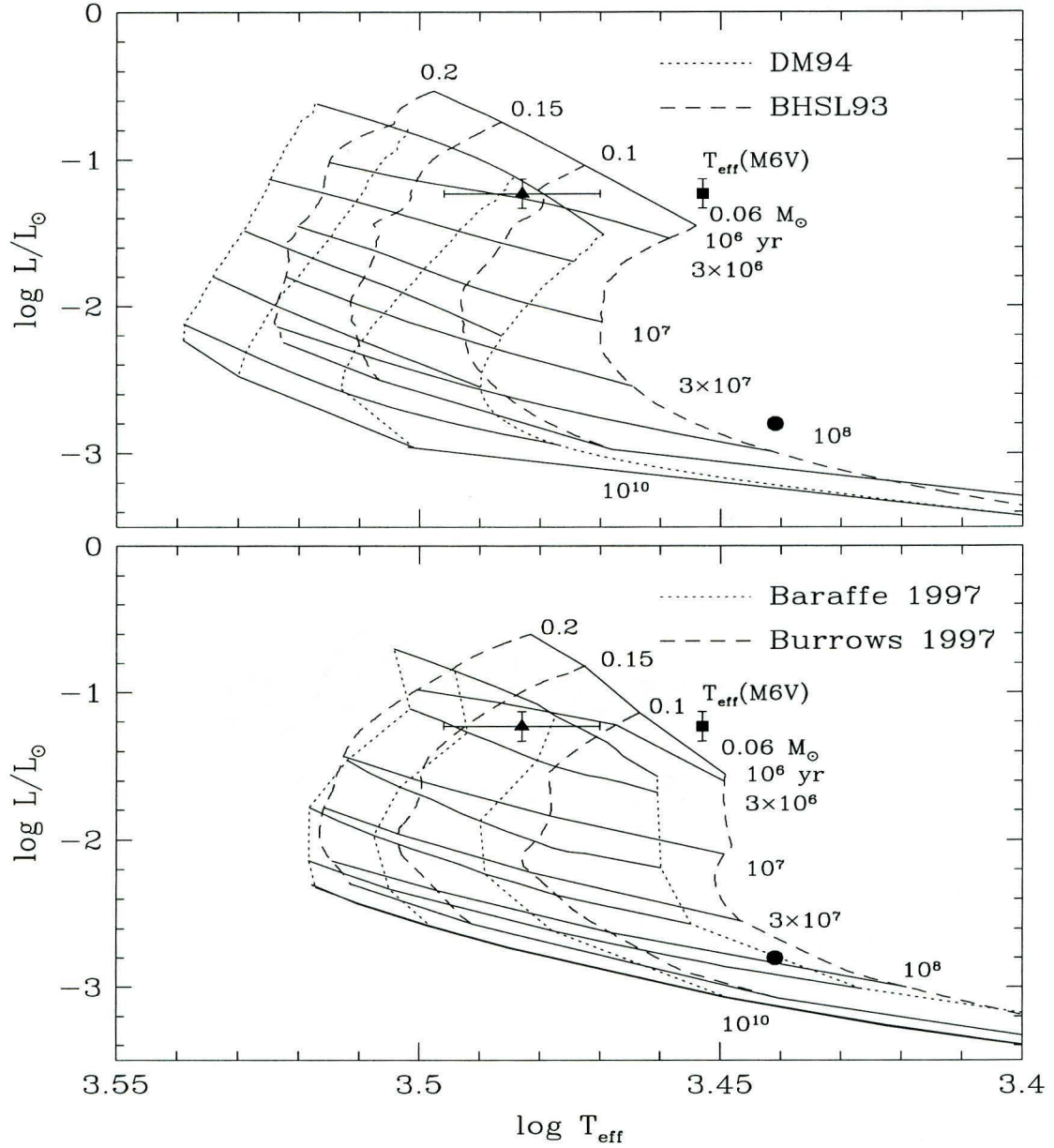


Figure 3.4 The H-R diagram near the hydrogen burning limit. V410 X-ray 3 is plotted with the Leggett et al. (1996) M6V temperature (square) and the theoretical temperature of a young M6 star (triangle). The error bar in effective temperature represents ± 0.5 subclass. For reference, PPL 15 (M6.5) is also shown (circle).

CHAPTER 4

A YOUNG OBJECT BELOW THE HYDROGEN BURNING LIMIT: ρ OPH 162349.8 – 242601

4.1. Introduction

Brown dwarfs are an elusive class of object which can offer insight into several fundamental questions. Do substellar objects contribute significantly to dark matter? If extreme brown dwarfs (e.g., Jupiter) form only in circumstellar disks and low-mass stars form in both single and multiple systems, at what mass does the transition in formation mechanism occur? Do other physical properties of the protostellar system affect this transition? The issues which motivate research in brown dwarfs are reviewed in detail by Burrows & Liebert (1993).

Many searches for brown dwarfs have concentrated on open clusters. If cluster membership can be established for a brown dwarf candidate then the cluster

age and distance can be assigned to the object. The mass is then derived from evolutionary tracks. For example, three promising candidates in the Pleiades are PPL 15 (M6.5), Teide 1 (M8), and Calar 3 (M8). A detection of weak Li in the former implies that it is a transitional object near the hydrogen-burning limit (Basri, Marcy, & Graham 1996). All of the available evolutionary tracks also imply substellar masses of 0.02-0.07 M_{\odot} for Teide 1 and Calar 3 (Rebolo, Zapatero Osorio, & Martín 1995). Zapatero Osorio (1997) has recently discovered several additional candidates in deep CCD imaging of the Pleiades.

Young, embedded clusters offer unique advantages and disadvantages in the study of brown dwarfs. Very young brown dwarfs (~ 1 Myr) should be quite luminous ($\log L_{\text{bol}}/L_{\odot} \sim -2$ to -1) and have properties similar to those of low-mass stars (e.g., T_{eff} , L , $[Li/H]$). Consequently, one could potentially detect brown dwarfs down to very low masses ($\sim 0.01 M_{\odot}$) and examine their mass function and binarity in the context of a fairly compact, well-defined region of star formation. Contamination by background stars is also minimized by extinction within the cluster. X-ray emission, $H\alpha$ emission, and Li absorption are likely to be strong in young brown dwarfs and should help in determining cluster membership. However, distinguishing young substellar objects from low-mass stars can be difficult and I must rely on evolutionary tracks for deriving masses of free-floating objects. Finally, emission from circumstellar material can hamper the measurement of effective temperatures and bolometric luminosities.

As one of the nearest (~ 160 pc) young, embedded clusters, the ρ Oph star forming region is a prime hunting ground for newly-formed brown dwarfs. Comerón et al. (1998) (CRCTL) have recently obtained 3-8 μm ISOCAM photometry of several low-mass candidates identified in ground-based near-IR imaging. After

modeling the spectral energy distributions, they have used the derived luminosities in conjunction with theoretical evolutionary tracks to estimate masses for individual sources. Four brown dwarf candidates are identified, three of which are heavily embedded and impossible to observe in the optical. One source which exhibits little reddening ($A_V < 2$) had been identified previously as either a foreground star or, if a ρ Oph member, a brown dwarf candidate (Rieke & Rieke 1990). I have obtained a low-resolution optical spectrum to determine its spectral type and optical photometry to test whether it is reddened. These data, along with the mid-IR excess reported by CRCTL, establish the cluster membership of this object. I place it on the H-R diagram and use the latest evolutionary tracks to discuss the question of its substellar nature. The following work has been in collaboration with J. Liebert.

4.2. Observations

I obtained an optical spectrum of ρ Oph 162349.8 – 242601 with the Red Channel Spectrograph at the Multiple Mirror Telescope on Mt. Hopkins, on 1997 April 14 and 15. I used the 270 g mm^{-1} grating ($\lambda_{\text{blaze}} = 7300 \text{ \AA}$) to obtain a spectrum from 5000 to 9000 \AA . A $2'' \times 180''$ aperture was used, providing a spectral resolution of $\Delta\lambda = 18\text{\AA}$. Since this source is invisible on the optical television guider ($m_V \sim 22.5$), I positioned an SAO star on the slit and offset to the coordinates of the ρ Oph source, $\alpha = 16^{\text{h}}23^{\text{m}}49^{\text{s}}.8$ and $\delta = -24^{\circ}26'01''$ (1950), as measured by Rieke & Rieke (1990). Three exposures of 1800 s were obtained during the two nights. To derive the sensitivity function of the array, I also observed the flux standards Feige 34, Ross 640, and BD+8 2015. The spectra were extracted from bias-subtracted frames, corrected for the sensitivity function, and wavelength

calibrated using He-Ar-Ne lamp spectra. The three exposures were finally combined and smoothed to a resolution of $\Delta\lambda \sim 25 \text{ \AA}$ (see Figure 4.1).

On 1997 June 8, I observed ρ Oph 162349.8 – 242601 with the Steward 1200×800 CCD at the 2.3 m Bok Reflector on Kitt Peak. I obtained six exposures of this source with a nearly-Mould *I*-band filter, each with an integration time of 480 s. I periodically observed the photometric standard Wolf 629 (Landolt 1992). After reducing the images and extracting photometry with standard procedures within IRAF, I applied an airmass correction (~ 0.03 mag) and transformed the photometry to the Cousins system (~ 0.04 mag). The latter was performed by convolving the transmission functions of the nearly-Mould and Cousins *I*-band filters with the spectra of 162349.8 – 242601 and a standard dwarf of a similar spectral type as Wolf 629 (M4). On 1997 June 17, I used the Steward Observatory 256×256 near-IR camera at the 1.6 m Bigelow Reflector to obtain *K*-band photometry. Using standard observing and reduction techniques, I measure $K = 14.25 \pm 0.1$ for 162349.8 – 242601.

4.3. Discussion

4.3.1. Cluster Membership

In a discussion of embedded brown dwarf candidates in ρ Oph, Rieke & Rieke (1990) suggested that 162349.8 – 242601 may be a foreground dwarf since its IR colors imply little reddening. However, the membership of this object to the ρ Oph star forming region is strongly supported by several new observations, the first of which is my measurement of H α emission ($W_\lambda \sim 60 \text{ \AA}$) (see Figure 4.1). Chromospheric emission in active late-M field dwarfs appears at a much lower intensity ($W_\lambda \leq 15 \text{ \AA}$) (Liebert et al. 1992; Hawley, Gizis, & Reid 1996), whereas

the circumstellar accretion disks of T Tauri stars often produce $H\alpha$ emission of $\sim 100 \text{ \AA}$. The three-sigma detection of mid-IR excess emission towards this source by CRCTL is also indicative of a young system with a circumstellar disk or envelope. Finally, I demonstrate in § 4.3.2 that the spectrum of 162349.8 – 242601 is intermediate between that of a dwarf and giant, consistent with its pre-main-sequence nature. I conclude that this object is almost certainly young and associated with ρ Oph. I note that Casanova et al. (1995) do not detect this source in ROSAT observations of ρ Oph. With their upper limit of $\log L_X/L_\odot \leq -6.1$, I calculate $\log L_X/L_{\text{bol}} \leq -3.6$ for this object, which is consistent with the typical ratio of -4 measured for low-mass T Tauri stars.

4.3.2. Spectral Type and Effective Temperature

Only the strongest features appearing in M stars are labeled in the spectrum of ρ Oph 162349.8 – 242601 in Figure 4.1. A more extensive line list (including telluric features) is found in Kirkpatrick, Henry, & McCarthy (1991). To classify the ρ Oph spectrum, I used the spectra of late M standard stars provided by J. D. Kirkpatrick, where each spectral type is represented by the following stars: M7V=vB 8, M7III=VY Peg, M8V=<LHS 2243, LHS 2397a, LP 412-31, vB 10>, M8III=IRAS 09540-0946, M9V=<BRI 1222-1222, LHS 2065, LHS 2924, TVLM 868-110639>, and M9III=<BR 1219-1336, IRAS 15060+0947>. I find features characteristic of both dwarfs and giants in the ρ Oph spectrum, which is not surprising given the surface gravity of a pre-main-sequence source. The same behavior is seen in late-type objects in Taurus and the Pleiades. In the optical spectrum of an M6 object in Taurus in § 3, I find that K I, Na I, and TiO/VO beyond 8200 \AA are reproduced well by a M6III spectrum while CaH is intermediate between that of a dwarf and giant. They also present an IR spectrum which shows

both dwarf (weak CO) and giant (weak Na) characteristics. In optical spectra of late-type Pleiades sources (M6-M8), Martín, Rebolo, & Zapatero Osorio (1996) observed weak Na I, which they attributed to non-dwarf surface gravities. In 162349.8 – 242601 I also see weak, giant-like Na while CaH, K I, and the continuum near Na I are intermediate between that of M8V and M8III. In future studies, these features should prove useful in distinguishing late field dwarfs from young, pre-main-sequence brown dwarfs.

For a given M subclass, I find that the closest match to the ρ Oph spectrum is achieved with an average of standard dwarf and giant spectra. These spectra for M7, M8, and M9 are shown in Figure 4.1 and clearly indicate a spectral type of $M8.5 \pm 0.5$ for ρ Oph 162349.8 – 242601. The strength of VO near 7450, 7900, and 8600 Å is particularly indicative of very late types. I arrived at the same spectral type by using the spectral indices discussed by Martín et al. (1996) and references therein.

To place ρ Oph 162349.8 – 242601 on the H-R diagram, I must convert the M8.5 spectral type to an effective temperature. However, the temperature scale for late M dwarfs is highly uncertain. Techniques in the derivation of temperature scales include fitting K -band photometry and bolometric fluxes to blackbodies (Berriman, Reid, & Leggett 1992), matching observed colors with those of synthetic spectra (Brett 1995), and fitting selected wavelengths of observed spectra to blackbodies (Jones et al. 1994). All of these studies imply relatively cool temperature scales where $T_{\text{eff}}(M8V) \leq 2500$ K. On the other hand, Kirkpatrick et al. (1993) performed spectral synthesis of individual stars with the model atmospheres of Allard (1990) and estimated $T_{\text{eff}}(M8V, M9V) = 2875, 2625$ K. Using Allard’s latest NextGen synthetic spectra, Leggett et al. (1996) have repeated this experiment for stars as

late as M6.5V and arrive at a scale cooler by ~ 200 -300 K. In § 5 the Leggett et al. temperature scale is consistent with the empirical T_{eff} measurement of CM Dra and gives a reasonable age and mass for PPL 15 when coupled with the latest evolutionary tracks. If I extrapolate the Leggett et al. scale to later types I arrive at $T_{\text{eff}}(M8.5V) \sim 2500$ K. This extrapolation is also consistent with the temperature of 2600 K adopted by Rebolo et al. (1996) for the M8 Pleiades brown dwarfs Teide 1 and Calar 3. Since the giant temperature scale, derived through angular diameter measurements, is warmer than the dwarf scale ($T_{\text{eff}}(M8III) \sim 2800$ K, Perrin et al. 1997), the temperature of a pre-main-sequence M8.5 object may be higher than that of a dwarf. If I assume that the intrinsic colors of a young M8.5 source fall between those of a dwarf and giant, then the evolutionary models of BCAH97 predict that such a source will have a temperature ~ 100 K greater than that of M8.5V. If I combine this offset with $T_{\text{eff}}(M8.5V) \sim 2500$ K, I arrive at a temperature of ~ 2600 K for 162349.8 – 242601, with an uncertainty of ± 200 K due to the spectral type (± 0.5 subclass = ± 100 K) and temperature scale (± 100 K).

4.3.3. Extinction and Bolometric Luminosity

Photometry of ρ Oph 162349.8 – 242601 was first obtained by Rieke & Rieke (1990) where they measured $J = 15.4$, $H = 14.7$, and $K = 14.2$ with uncertainties of ± 0.2 . In more recent observations, Barsony et al. (1997) have measured 10% CIT photometry of $J = 15.13$, $H = 14.37$, and $K = 13.87$. If I assume an intrinsic color of $J - K = 1.14$ -1.21, as reported by Leggett (1992) for typical M8V and M9V stars, then the $J - K$ measured for the ρ Oph source (1.2 ± 0.3 , 1.26 ± 0.14) implies an extinction of $A_V \sim 0.5 \pm 0.5$ when combined with the extinction law of Rieke & Lebofsky (1985). With my new optical and IR photometry ($I_C = 18.49 \pm 0.05$, $K = 14.25 \pm 0.1$), I can make a more accurate estimate of the extinction. The

intrinsic colors of an M6 pre-main-sequence object in L1495E are similar to those of a typical M6 dwarf, as shown in § 3. Assuming the intrinsic color of the ρ Oph source is similar to that of M8 and M9 dwarfs, ($I_C - K = 4.0-4.5$, Leggett 1992), my measurement of $I_C - K = 4.24 \pm 0.11$ implies $A_V = 0$ with an upper limit of 0.7, which is consistent with the values produced by $E(J - K)$. The presence of K -band excess emission can lead to an overestimate of extinction towards young stars, but this is not an issue here since I measure no extinction. To calculate the luminosity, I have used $BC_J = 2.05$ as measured for M8 and M9 dwarfs (Kirkpatrick et al. 1993; Tinney, Mould, & Reid 1993). Since the optical spectrum of the ρ Oph source does not match perfectly with standard dwarf spectra, I adopt an uncertainty of ~ 0.15 magnitudes in this bolometric correction. With $A_V = 0$ and an upper limit of 0.7, $J = 15.25 \pm 0.25$, and a distance modulus of 6.1 ± 0.1 (Bertiau 1958; Whittet 1974), I arrive at $\log L_{\text{bol}}/L_{\odot} = -2.58 \pm 0.18$. The diameter of the cluster is less than 1 pc, so the position of the source along the line of sight within the cloud is not important in the derivation of the luminosity.

4.3.4. Age and Mass

To examine the age and mass of ρ Oph 162349.8 – 242601, I have placed it on the H-R diagram in Figure 4.2 with the latest evolutionary tracks. In § 2 and § 5 I discuss the comparison of available model interiors to the observations of YY Gem and CM Dra, globular clusters, embedded clusters, the Pleiades (particularly PPL 15), and the lower main sequence. On both observational and theoretical bases, the tracks of Burrows (1997) and BCAH97 appear most appropriate for studying sources in the substellar regime. The age implied for 162349.8 – 242601 by BCAH97 is $\sim 3-10$ Myr, whereas a slightly older age is produced by Burrows, both of which are older than the canonical cluster age of 1 Myr. However, it is unclear

how seriously to take these age estimates given the uncertainties in the tracks at very young ages and cool temperatures. On the other hand, an H-R diagram for ρ Oph by Bouvier & Appenzeller (1992) shows sources as old as 10 Myr, so the age of 162349.8 – 242601 implied by the tracks is not unreasonable and may explain its low reddening.

From the models of BCAH97 and Burrows I derive a mass of $\sim 0.035 M_{\odot}$ for ρ Oph 162349.8 – 242601, with lower and upper limits of 0.01 and 0.06 M_{\odot} given the uncertainties in the temperature of this object. A more accurate mass estimate will require observational tests of the low-mass tracks and late-type temperature scale, particularly at young ages. To place this ρ Oph source in the context of other recently discovered brown dwarfs, I have plotted PPL 15, Teide 1, and Calar 3 in Figure 4.2. Regardless of uncertainties in the temperature scale and tracks, 162349.8 – 242601 appears to be less massive than the three Pleiades sources and could be a very young precursor to GL 229B (0.035-0.05 M_{\odot}) (Nakajima et al. 1995; Oppenheimer et al. 1995; Allard et al. 1996; Marley et al. 1996). This conclusion is in agreement with that of CRCTL, derived independently by isochrone fitting of multi-band photometry.

4.4. Conclusion

I have presented compelling evidence of a young brown dwarf in the ρ Oph star forming region. The youth and cluster membership of this source are strongly supported by its intense H α emission ($W_{\lambda} \sim 60 \text{ \AA}$), weak mid-IR excess emission (CRCTL), and simultaneous dwarf and giant optical spectral features. After measuring a spectral type of M8.5 and placing the source on the H-R diagram, I used state-of-the-art evolutionary tracks to derive a mass of $\sim 0.035 \pm 0.025 M_{\odot}$,

making it one of the youngest and least-massive brown dwarfs observed to date. These results add credence to the remaining ρ Oph brown dwarf candidates reported by CRCTL, which will require IR spectroscopic confirmation due to their embedded nature.

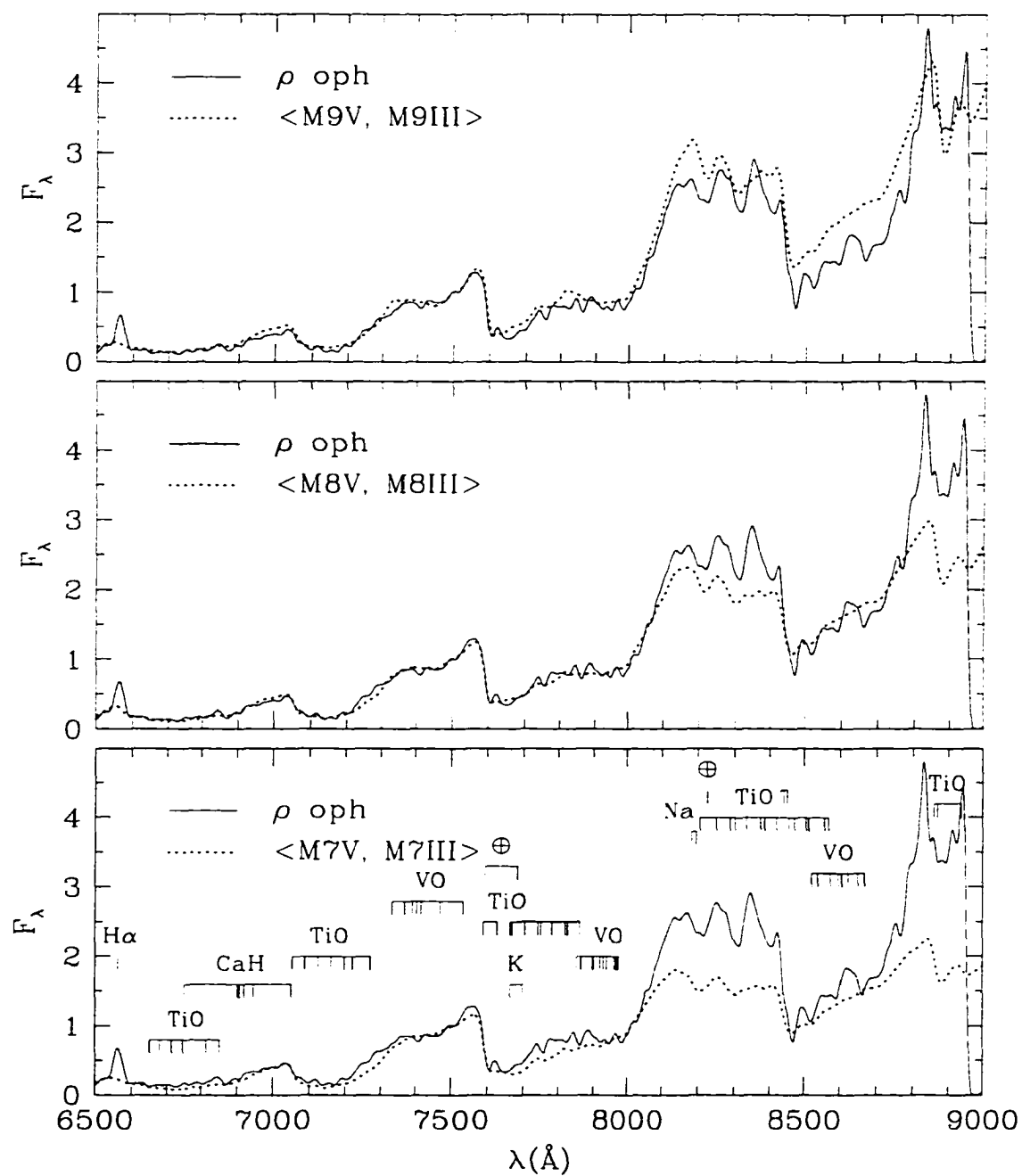


Figure 4.1 Optical spectrum of 162349.8 – 242601 plotted with averages of standard late M dwarfs and giants. All spectra are normalized at 7500 Å.

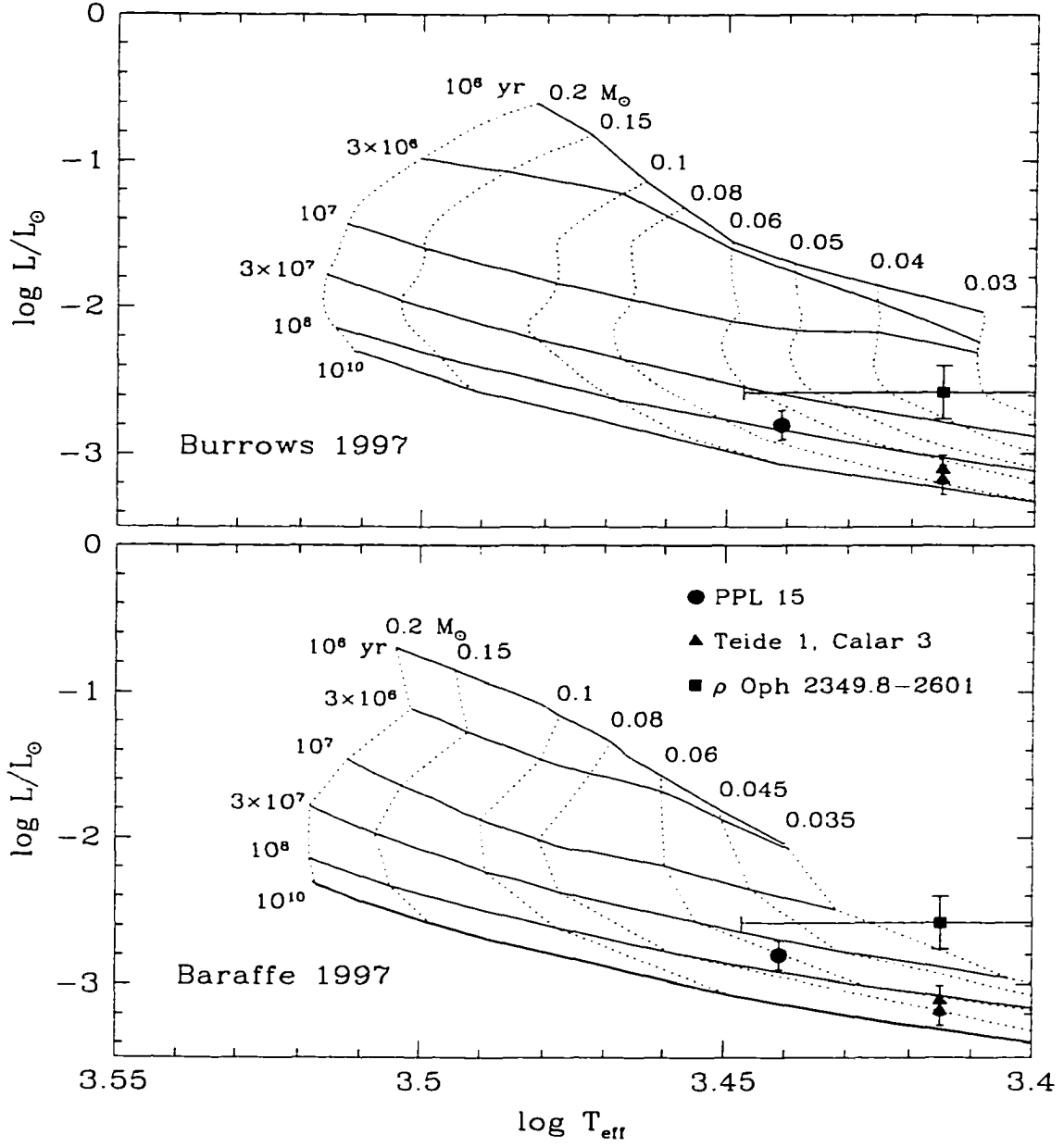


Figure 4.2 The H-R diagram near the hydrogen burning limit. 162349.8 – 242601 is plotted with the temperature I estimate for a young M8.5 object on the evolutionary tracks of Burrows (1997) and BCAH97. The Pleiades brown dwarfs PPL 15 (M6.5), Teide 1 (M8), and Calar 3 (M8) are shown for reference, using a dwarf temperature scale (without T_{eff} error bars).

CHAPTER 5

L1495E

5.1. Introduction

Near-IR surveys of molecular clouds (e.g., L1630) imply that the dominant mode of star formation occurs in clusters (Lada et al. 1991). However, the fundamental physical properties of the stars in these clusters are not well-established since they are deeply embedded and difficult to study with conventional techniques in the optical. By the time these clusters are exposed enough for optical observations, the stars have dispersed over a large area and nearly completed their pre-main-sequence (PMS) evolution. To probe the physical properties such as the IMF of young, embedded clusters, I must utilize IR tools both to measure luminosity functions and to place cluster members on H-R diagrams.

Deep $J(1.25\ \mu\text{m})$ $H(1.64\ \mu\text{m})$ $K(2.2\ \mu\text{m})$ imaging of nearby clusters (≤ 500 pc) such as ρ Oph, IC 348, NGC 1333, Taurus-Auriga, NGC 2024, the Trapezium, and NGC 2264 has been used to construct IR luminosity functions which constrain the star formation history and the IMF down to the hydrogen burning limit (Comerón

et al. 1993; Lada, Young, & Greene 1993; Greene et al. 1994; McCaughrean & Stauffer 1994; Lada & Lada 1995; Strom, Kepner, & Strom 1995; Comerón, Rieke, & Rieke 1996; Lada, Alves, & Lada 1996). H-R diagrams are more difficult to construct since spectral types must be measured along with luminosities, but in conjunction with PMS tracks, they also give the mass and age for individual sources. Until recently, H-R diagrams were restricted to exposed, optically visible young stellar objects (YSOs) in Orion, Taurus, Lupus, and Chameleon (Gauvin & Strom 1992; Hartigan 1993; Hughes et al. 1994; Kenyon & Hartmann 1995; Lawson, Feigelson, & Huenemoerder 1996; Hillenbrand 1997). Newly available IR spectrometers have allowed spectral classification of a number of more deeply embedded stars in L1641N, ρ Oph, and NGC 2024 (Hodapp & Deane 1993; Greene & Meyer 1995; Meyer 1995; Ali et al. 1997).

In deep X-ray observations of the young cluster L1495E, Strom & Strom (1994) (SS94) identified eight new PMS ($\sim 10^6$ yr old) sources and noted an additional five candidate members in IR imaging, increasing the known population to 35. They then used optical photometry and spectroscopy to place 25 of these objects on the H-R diagram from which they derived an IMF consistent with Scalo (1986).

To probe the most obscured candidate members of L1495E, I performed IR spectroscopy on the remaining objects in the X-ray and IR imaging samples. I also observed several of the optically visible stars, allowing a comparison between types derived from optical and IR spectra that shows my analysis of the IR spectra to provide accurate spectral types. To quantify IR excesses, I extended the photometry of the X-ray selected sources to L' ($3.4 \mu\text{m}$). In conjunction with theoretical evolutionary tracks, I use these new data to derive the star formation history and low-mass IMF complete to 0.15 and $0.35 M_{\odot}$ for tracks by D'Antona

& Mazzitelli (1994) and Swenson (1996), respectively. I imaged the cluster to $J \sim 18.5$ and $K \sim 17.5$ to determine the completeness of the identified sample of cluster members. After making the necessary completeness corrections, I find that the IMF of L1495E is probably similar to those of other much denser clusters of forming stars.

5.2. Observations

On 1994 December 8, 9, and 13, I performed K -band spectroscopy on 15 sources in L1495E using the near-IR long-slit spectrometer FSpec (Williams et al. 1993) at the Steward 2.3 m Bok Reflector on Kitt Peak. I used an IR camera to guide off the slit, providing positive identification of each object observed. The source and a telluric standard (HR 1406) were stepped through six positions along the $2''.4 \times 90''$ slit ($= 2 \times 75$ pixels). At one grating setting, I obtained a spectrum extending from 2.0 to 2.4 μm with a two-pixel resolution of $\lambda/\Delta\lambda = 800$. I also obtained follow-up spectra at $R = 1200$ for V410x6 and P04154+2823 at the Bok Reflector on 1996 October 30 and V410x8b and 8d at the Multiple Mirror Telescope on 1996 December 23.

IRAF routines and customized scripts within this environment were used to reduce the data. After dark subtraction and flat-fielding, adjacent images along the slit were subtracted from each other to remove sky emission. The six sky-subtracted images were aligned and combined, during which most transient bad pixels (e.g., cosmic rays) were rejected. A spectrum was extracted from this final image, divided by the extracted telluric standard spectrum, and wavelength calibrated using OH airglow lines. The intrinsic spectral slope and absorption features in the telluric standard (F7V) were removed by applying the solar spectrum, as discussed

by Maiolino, Rieke, & Rieke (1996). The spectra are shown in Figure 5.1.

Imaging was performed at the Bok Reflector on the nights of 1994 November 9 and 10 using the Steward Observatory NICMOS3 256×256 near-IR camera at a plate scale of $0''.64 \text{ pixel}^{-1}$ and a total field of $2'.7$ square. Six frames were taken at each position with offsets of $6''$ to allow for efficient flat-fielding and removal of bad pixels. A flat field was constructed by median combining the six exposures at a given position. A 4×4 grid of positions in the background field was imaged at K where neighboring cells were separated by $140''$. The southeast cell of this grid was centered at $\alpha = 4^{\text{h}}18^{\text{m}}24^{\text{s}}.1$, $\delta = 29^{\circ}32'21''$ (1950) (roughly 1° north of L1495E). Poor weather reduced my available observing time so only one cell in the grid was imaged at J . The total integration time (six frames combined) was 180 seconds on each background image. A similar 4×4 grid of images was obtained on the L1495E cloud at J and K , with integration times of 360 and 180 seconds, respectively. The grid of images was positioned so that Hubble 4 was centered in the southeast cell of the grid. For calibration, I observed a photometric standard star, HD 44612, periodically during the night.

The images were reduced with tasks available in the IRAF image analysis software. After dark-subtracting and flat-fielding the images, the six frames at a given position were shifted and combined into one image. The tasks DAOFIND and PHOT under the package APPHOT were used in measuring the stellar coordinates and performing photometry. The regions of overlap between neighboring cells were $20''$ wide and typically contained several stars, facilitating alignment of the cells into one image and producing an uncertainty of less than $2''$ in relative stellar coordinates across the grid. A map of the on-cloud image is shown in Figure 5.2.

On 1994 December 19 and 20 $JHKL'$ aperture photometry was obtained for

my spectroscopic sample at the Multiple Mirror Telescope on Mount Hopkins, Arizona. The facility near-IR photometer was used with an aperture of $5''.6$ and a chopper throw of $10''$ in elevation. The spectral bands were standard Arizona/Johnson J , H , K , and a filter centered at $3.4 \mu\text{m}$ with a bandwidth of $0.2 \mu\text{m}$. The data were calibrated using standard stars from the list of Elias et al. (1982). This aperture photometry is presented in Table 5.1 with previous photometry from SS94. Photometric errors should be < 0.05 magnitudes, unless noted otherwise.

5.3. Discussion

5.3.1. IR Spectral Classification of Young Stars

I selected for IR spectroscopy all sources from the list of SS94 which lacked measured spectral types, displayed evidence of cloud membership (X-ray or $\text{H}\alpha$ emission), and were bright enough ($K \leq 12.5$). In addition, I obtained spectra of anonymous sources for which SS94 only had IR photometry. Finally, to compare the optical and IR spectral types, I added several stars to the sample which were classified in the optical by SS94. Most of the spectra were observed at $R = 800$, but the grating providing this resolution was replaced permanently part way through my program with one giving $R = 1200$. After the installation of the new grating, I observed two of the faintest X-ray sources (V410x8b and 8d) and two stars previously observed. The latter two were observed again to compare the spectral types and r_K (a measure of veiling at K) derived at the two resolutions for a heavily veiled source (PSC04154+2823) and a star with strong CO and possibly giant-like features (V410x6). The spectra are organized in Figure 5.1 roughly in order of spectral type. Table 5.1 lists spectral types, r_K , and photometry of all of

the sources in L1495E with spectroscopy.

Low-resolution ($R = 800$) K -band spectroscopy was selected for this project for several reasons. The K -band suffers little extinction while also falling near the peak of the spectral energy distribution of YSOs. Beyond $2\ \mu\text{m}$ there are several temperature-sensitive metallic absorption features (Na, Ca, Mg) in cool stars ($>G0$) whose equivalent widths can be measured adequately at low resolution. However, the only strong K -band feature exhibited by stars between B0 and G0 is $\text{Br}\gamma$ (which can be filled in by emission in young stars); H -band spectroscopy is required for classification in this domain. In the H -band, on the other hand, extinction is larger and higher resolution is required to determine spectral types. A disadvantage of observations at K is possible contamination of the stellar spectrum by continuum emission, also referred to as continuum veiling, from a circumstellar envelope or disk. I developed techniques that allow derivation of spectral types for class II and III sources without serious interference by veiling. Class I sources typically are featureless in the near-IR (Greene & Lada 1996). A detailed description of the spectral classification, along with discussion of individual sources, is provided in § 5.5.

An important aspect of this work is the comparison of classifications of young, embedded objects in the IR with those in the optical from SS94. Of seven objects in common between the two studies, five agree in type to within one subclass. However, two sources, V410x8e and Anon 13, disagree by more than one letter class. In both of these discordant cases, the IR spectrum indicates a hotter object than the optical one does, so binarity is not a plausible explanation for the different classifications. IR continuum veiling also cannot be the source of the discrepant types (see § 5.5). It appears that these cases arise either from extreme variability

(no large scale variations are apparent in my photometry, but it is not coincident in time with the spectroscopy) or to mis-identifications. Because I used an IR guider and took a spectrum of the nearest bright IR object (within $5''$ of the expected position), and the optical spectra used an optical guider, the latter possibility seems most likely. In general, though, I conclude that the IR classification agrees well with that from the optical, and that objects classified by either method can be discussed together with no systematic errors.

5.3.2. Derivation of T_{eff}

To construct an H-R diagram for comparison with evolutionary tracks, I must derive T_{eff} and L_{bol} from observable quantities. I have adopted the conversion of spectral type to T_{eff} given in Schmidt-Kaler (1982) for early dwarfs ($\leq M0V$). Most temperature scales agree fairly well for dwarfs between A and K types. For instance, when the Schmidt-Kaler temperature scale is combined with the Johnson (1966) colors, the resulting $T_{\text{eff}} - (V - I)_C$ relationship is consistent with that of Alonso, Arribas, & Martinez-Roger (1996).

For M dwarfs, on the other hand, published temperature scales differ significantly (Allard et al. 1997). For many years, blackbody techniques were used to derive temperature scales (Veeder 1974; Reid & Gilmore 1984; Berriman & Reid 1987; Berriman, Reid, & Leggett 1992). More recently, Kirkpatrick et al. (1993) and Leggett et al. (1996) have fit Allard's original synthetic spectra (Allard 1990) and latest NextGen spectra to observed M dwarf spectra. These two temperature scales are shown in Figure 5.3, where the Leggett et al. scale is divided into kinematically young and old stars. The temperature scale for cool giants does not rely on such modeling of photometry or spectra since angular diameter measurements allow the direct calculation of T_{eff} (Dyck et al. 1996). This T_{eff} -spectral type conversion for

giants is plotted in Figure 5.3 using the giant colors of Bessell & Brett (1988). The dwarf scales should be more applicable to cool PMS stars than this giant scale, but the latter is shown to illustrate the magnitude of change in temperature scales as we go to lower surface gravities. Recent stellar interior models using Allard's NextGen atmospheres provide not only T_{eff} but synthetic colors and magnitudes as well (BCAH97), which is equivalent to a built-in synthetic temperature scale in the evolutionary tracks. The resulting theoretical $T_{\text{eff}} - (V - I)_C$ and $T_{\text{eff}} - (I_C - K)$ at the main sequence and 1 Myr are shown with the observed scales in Figure 5.3.

Rather than arbitrarily adopting a temperature scale for cool dwarfs, I have tested the scales in Figure 5.3 with the independent T_{eff} measurements for the two known low-mass double-lined eclipsing spectroscopic binaries, YY Gem and CM Dra. To plot YY Gem, T_{eff} was derived from the stellar radii and ratio of component luminosities of Budding et al. (1996) and the system L_{bol} of Leung & Schneider (1978). The $(V - I)_J$ and K_{CTIO} measured by Leung & Schneider and Leggett (1989) were then transformed to $(V - I)_C$ and $I_C - K$. For CM Dra, I repeated the calculation of the component luminosities of Lacy (1976) using new parallax data (van Altena, Lee, & Hoffleit 1991). The inclusion of the radii measurements of Metcalf et al. (1996) then produced T_{eff} . $(V - I)_C$ and $I_C - K$ were taken from Leggett (1992) and were nearly the same as the values found by transforming Lacy's $(V - I)_J$ to Cousins. Note that these colors are consistent with those expected given the published spectral types of YY Gem (M0-1V) and CM Dra (M3-5V).

In Figure 5.3 I find that the temperature scales of both Kirkpatrick et al. and BCAH97 agree with the measurements of YY Gem. The young disk locus of Leggett et al. also reproduces the data for YY Gem, which is consistent with the

youth (~ 100 Myr old) suggested by Chabrier & Baraffe (1995) for this system. Since the photometry and kinematics of CM Dra are indicative of a halo star, I expect that this source will have colors affected by low metallicity. The locus of old stars in the Leggett et al. scale matches well with the observations of CM Dra in both colors, whereas the scale of Kirkpatrick et al. is too hot. If the BCAH97 scale were plotted for low metallicity, it would move to cooler temperatures and agree with CM Dra in $I_C - K$. On the other hand, the synthetic $(V - I)_C$ scale, which is already too cool for solar metallicity, would deviate further from CM Dra at lower abundances. The synthetic $I_C - K$ scale of BCAH97 is similar to the Leggett et al. scale and should be applicable to the color-magnitude diagrams of older, exposed clusters (e.g., Pleiades). Along with CM Dra, these two scales also produce the expected age and mass for PPL 15 when combined with the latest tracks. For young, embedded clusters, however, the stellar colors are contaminated by effects of extinction and circumstellar emission so I must use the Leggett et al. scale to convert spectral types to T_{eff} . After taking $M0V = 3850$ K (typical value for most scales), I find $T_{\text{eff}} = 3850 - 168.1 \times (\text{M subclass})$ as the best fit to the Leggett et al. (1996) data. As a final caveat, although I adopt this dwarf scale for all sources discussed here, a somewhat hotter (~ 100 -200 K) scale which is intermediate between the dwarf and giant scales may be more appropriate for very young, late M stars (§ 3 and § 4).

In § 5.3.4, I use the Pleiades to test evolutionary tracks. The Pleiades is attractive for such tests because the small extinction allows colors to be converted directly to effective temperatures. I have transformed the $(V - I)_C$ colors of Stauffer (private communication) to spectral type using Bessell (1979) for $<M0V$ and Bessell (1990a) for $\geq M0V$. The spectral types were translated to T_{eff} with the same scale used for the young stars in L1495E. Note that available spectral

type-color scales can differ substantially, even for early-type stars. For instance, for G0V Bessell (1979) and Bessell (1990b) give $(V - I)_C = 0.625$ and 0.715 , respectively. The first conversion produces good agreement between the theoretical main sequence and G-type Pleiades members while the latter does not.

5.3.3. Derivation of L_{bol}

Since young stars (≤ 10 Myr) are embedded and often have excess UV (disk boundary layer) and IR (circumstellar disk or envelope) emission, I cannot derive their luminosities by simply integrating the broad-band photometry. Kenyon & Hartmann (1990) found that the I and J bands suffer the least contamination from either source of excess emission. Since the extinction correction is smaller at J and I have J photometry for my entire spectroscopic sample, I use this band in the derivation of stellar luminosities. For sources with multiple photometric measurements, I used my MMT J photometry in the calculation of the luminosity. In general, I find that the photometry from different epochs agrees well and the variability is restricted to changes of ≤ 0.3 mag. The exceptions are V410x8b and 8e, which have discrepant spectral types and are possible mis-identifications, and PSC04154+2823, which exhibits the largest IR excess and is probably the most active source in the sample.

The $R - I$ color should be mostly free of both UV and IR excess, so to determine the extinction I assume the intrinsic $R - I$ of the young star is that of a dwarf of my measured spectral type. Using the interstellar reddening law of Rieke & Lebofsky (1985), I find that $A_J = 1.34((R - I)_C - (R - I)_C(\text{dwarf}))$, where A_J is in the Johnson-Glass photometric system. The intrinsic colors and bolometric corrections of standard dwarfs are taken from Kenyon & Hartmann (1995). When both optical and IR spectral types were available for a source, I used

the optical type to estimate its intrinsic colors and T_{eff} . I combined the extinction, BC_J , and a distance modulus of 5.88 for Taurus to derive the luminosities. Seven stars in my sample are known binaries and their luminosities were corrected for the contribution of the secondary in the same manner as SS94. In two of these systems (V892 Tau and LkCa7) the secondaries are faint enough that no corrections are necessary. The final extinctions, effective temperatures, and luminosities are given in Table 5.1.

For the six reddest sources and one optically visible star, optical photometry is not available so I must use $J - H$ to derive the extinction. These stars are circled in Figure 5.4 where I plot $J - H$ versus $H - K$ of the spectroscopic sample. The main sequence and classical T Tauri star (CTTS) locus are shown along with the reddening bands of each. The CTTS locus shown here was derived by using $E(R - I)$ to deredden 30 optically visible CTTS in Taurus (Meyer 1995). Here I repeat this process and use $E(R - I)$ to create a dereddened color-color diagram for my sample, which is shown in the lower panel of Figure 5.4. Assuming that I have now corrected for all extinction towards each star, these positions on the diagram should reflect only the contribution of photospheric and circumstellar emission. The sources appear roughly consistent with the CTTS locus found by Meyer, which has been successfully modeled as colors arising from star-disk systems (Lada & Adams 1992; Meyer, Calvet, & Hillenbrand 1997). The large scatter around the locus is not surprising and can be explained by differences in the disk inclination, spectral type, and the size of an inner hole in the disk. I assume that the sources without optical photometry are also CTTS and derive their extinctions by dereddening the stars to the CTTS locus: $A_J = 2.63((J - H) - (J - H)_{\text{CTTS}})$. For late-type stars falling in the reddening band of the main sequence, dereddening to the main sequence or CTTS locus produces similar extinctions. The absence of a color

correction for these embedded sources results in steadily increasing uncertainties in colors as we go to very red sources. This fact coupled with the intrinsic scatter in the CTTS locus produces the largest extinction and luminosity uncertainties in the sources dereddened with $J - H$.

5.3.4. H-R Diagram

I use T_{eff} and L_{bol} to place sources measured spectroscopically on an H-R diagram as shown in Figure 5.5. I have omitted V410x8d from Figure 5.5 since it falls well below the main sequence and is probably a background dwarf. The spectral types of V410x8b and 8e are too uncertain to place them on the H-R diagram or assess their cluster membership.

To derive the star formation history and IMF implied by the H-R diagram of L1495E, several sets of low-mass evolutionary tracks are available. These include calculations for $\leq 0.2 M_{\odot}$ (BHSL93; Nelson, Rappaport, & Joss 1993), $0.25\text{--}5 M_{\odot}$ (FJS), $\leq 2.5 M_{\odot}$ (DM94), $\leq 0.2 M_{\odot}$ (Burrows 1997) and $\leq 0.7 M_{\odot}$ (Baraffe et al. 1995; BCAH97) with Allard's Base and NextGen atmospheres. D'Antona & Mazzitelli are also currently completing a suite of model interiors with a sophisticated treatment of convection. In § 2 I briefly discusses the comparison of these various tracks to stellar populations ≥ 100 Myr old, using the data on YY Gem and CM Dra, Pleiades, main sequence, and globular clusters. I conclude that the interior models with NextGen atmospheres provide only marginally improved fits to the observations over previous generations of tracks. I also find that neither DM94 or FJS is clearly better than the other when these tests are performed.

For use with the young cluster L1495E (~ 1 Myr old), it is therefore not

clear which set of tracks is preferred. Consequently, rather than using only one set of tracks, in Figure 5.5 I have plotted the H-R diagram of L1495E with the calculations of FJS, DM94 (Alexander Opacities, CM Convection), and BCAH97.

In previous studies of young, embedded clusters, temperature scales and evolutionary tracks have been adopted without justification or consistency checks against main sequence data. As pointed out by Stauffer, Hartmann, & Barrado (1995), if an observed H-R diagram is used to derive ages for PMS sources, then the adopted temperature scale and evolutionary tracks should be consistent with the observed main sequence, otherwise the age estimate may not be meaningful. For instance, the empirical Pleiades isochrone can be matched by several combinations of scales and tracks, where DM94 requires a scale hotter than Kirkpatrick et al. (1993) and FJS requires a much cooler scale, similar to blackbody ones. However, since the Leggett et al. scale makes use of the latest synthetic spectra and agrees with measurements of CM Dra, I do not believe it is valid to adopt alternative scales for each set of tracks simply to make them consistent with observations. I note that, as demonstrated § 2, none of the three sets of tracks I show in Figure 5.5 match the main sequence or Pleiades data when combined with the Leggett et al. scale.

To provide a useful reference point for the stars in L1495E and an additional check of the tracks, I have also plotted the M6.5 Pleiades member PPL 15 in Figure 5.5. The depleted Li abundance in this object implies it falls near the hydrogen burning limit. The position of PPL 15 on the BCAH97 tracks is consistent with that of a transition object at an age of 100 Myr. However, Basri & Martín (1997) have recently proposed that PPL 15 is a system of binary brown dwarfs where the Li may not be depleted as previously believed. Future observations of

PPL 15 should provide the component luminosities and dynamical mass constraints which could alter the present agreement with the tracks of BCAH97 and Burrows.

I now examine the star formation history of L1495E implied by the H-R diagram in Figure 5.5. The tracks of DM94 indicate a coeval population where most of the stars have an age of ≤ 1 Myr with a few as old as 10 Myr. The calculations of BCAH97 only reach up to $0.7 M_{\odot}$, making it difficult to estimate the coevality. The ages are slightly older than those produced by DM94, with the oldest stars appearing at 30 Myr. FJS, on the other hand, implies a distinct trend where the less massive stars are much older. Several sources also fall near the FJS 100 Myr isochrone, which is the age of the Pleiades. Of the five oldest sources less than $1 M_{\odot}$, SS94 suggested that three (Anon 3, 12, 17) may be foreground main sequence stars since they have very little extinction or $H\alpha$ emission. They also lack an IR excess in my $JHKL'$ photometry. SS94 estimated that ~ 10 foreground M stars should fall within a circle of $r < 25'$ towards Taurus, so it is certainly plausible that these three stars are foreground objects. These stars are indicated as open circles in Figure 5.5. On the other hand, CK Tau 1 exhibits significant extinction and $H\alpha$ emission and appears to be a cluster member despite its implied age of $\sim 10, 30$, and 100 million years respectively for the tracks of DM94, BCAH97, and FJS. PSC04158+2805 is also a likely member, since it is embedded and has an IR excess. Uncertainties in its spectral type could make it as young as 10 Myr with the BCAH97 tracks, or even somewhat younger with those of DM94. However, with any reasonable spectral type for either of these sources, the ages implied by the FJS tracks (30-100 Myr) are difficult to understand.

SS94 point out that the velocity dispersion ($\sim 1 \text{ km s}^{-1}$) of sources in L1495E can be used to limit the expected ages. A star with this velocity on the plane of

the sky at the distance of L1495E will travel nearly 4° in 10 Myr. Since the stellar density in L1495E is too low for a bound cluster, sources which have not escaped should in general have ages ≤ 1 Myr. Only the DM94 tracks satisfy this constraint.

5.3.5. The Initial Mass Function

Comparison with SS94

In conjunction with the evolutionary tracks of DM94 and FJS, SS94 used the observed T_{eff} and L_{bol} to derive masses for individual sources in L1495E and hence a cluster IMF. Since the sensitivity of their ROSAT observations fell sharply beyond a radius of $25'$ centered on V410 Tau, SS94 only included stars within this area in the calculation of the IMF.

I perform a parallel derivation to allow comparison with the results of SS94. I restrict my study to the same area as SS94 and reject the seven PMS sources with $r > 25'$ indicated in Table 5.1. Within the inner region, the IMF of SS94 included 12 previously known PMS stars, eight new X-ray sources, Anon 9, Anon 13, and five secondaries. For the updated IMF calculation, I supply spectral types for four of these sources which were not observed spectroscopically but were assumed to be M2 by SS94 (PSC04154+2823, PSC04158+2805, V410x2, V410x4). I also add three heavily embedded sources (Anon 20, 24, 25) to the IMF determination. Since the spectral type for V410x8e is uncertain I have omitted it from the sample, but I have included all of the other sources used by SS94 to derive an IMF. The three probable foreground sources discussed earlier (Anon 3, 12, 17) are excluded from the sample. To estimate masses for the secondaries, I assume that the extinction is the same towards both the primary and secondary and that the ratio of bolometric luminosities is equal to the ratio of K -band fluxes. If I also assume that the

components are coeval I can derive secondary masses from the evolutionary tracks. Of course, these masses are highly uncertain since the age spread observed on my H-R diagram can translate to masses between $0.1\text{--}0.5 M_{\odot}$ for $\log L_{\text{bol}} = -0.5$. Also, if a companion has an IR excess I will overestimate its mass. The IMFs I derive from FJS and DM94 are given in Figure 5.6, which are similar to those found by SS94. However, there is an unexplained discrepancy between the forms of the Scalo (1986) IMF plotted in Figure 5.6 and the corresponding figure in SS94.

Completeness Correction

However, the IMFs derived by SS94 and by us from the spectroscopically observed samples will not represent the true IMF of the cluster unless the sample is representative of the full cluster membership. The most likely source of bias is incompleteness for faint sources, which is likely to translate into an under-representation of low-mass members. Because X-ray luminosity scales roughly with IR (or bolometric) luminosity (e.g., Feigelson et al. 1993; Casanova et al. 1995), the search for cluster members in the X-ray by SS94 does not assure that the faint cluster members have been completely identified.

To estimate the completeness of the spectroscopic sample, I have imaged a relatively uniform and opaque $10' \times 10'$ region of L1495E at J and K (see Figure 5.2). The large extinction within this field provides an excellent screen against background stars, in contrast to other parts of L1495E where extinction is low and it is difficult to distinguish low-mass sources from field stars. The identically-sized off-cluster field I imaged provides an excellent model of the distribution of field stars behind L1495E. For the bright sources which were saturated in my on-cloud image ($K \leq 10$), I used the K magnitudes of SS94.

The resulting K -band luminosity functions (KLFs) for the on and off fields are shown in the top panel of Figure 5.7. I obtained the best fit to the reddened background population behind L1495E by applying an extinction of $A_K = 2.25$ ($E(J - K) = 3.4$) to the off-field KLF. This value is a reasonable estimate of the typical extinction through the cloud since it is similar to the largest extinction I derive toward stars in the spectroscopic sample. The average $J - K$ observed for sources between $K = 14$ -15 (presumably background stars) is also consistent with my model of the reddening. Instead of a single value of $A_K = 2.25$, if I apply an extended distribution of extinctions (e.g., Gaussian) to the off-field KLF, there is little change in the fit unless large extinction variations are assumed, in which case the fit worsens.

In the second panel of Figure 5.7 I examine the sources which fall above the reddened background distribution. Nine of the sources in this histogram (shown as shaded boxes) have spectroscopy and are included in the IMF in § 5.3.5. Eight of these sources are at $K < 11$. Any low-luminosity objects fainter than $K = 14$ would be lost in the background. There is an excess of ~ 9 sources above the background model between $K = 11$ and 14 which lack spectroscopy and may be cluster members. These candidate cluster members are either too faint or too red to be foreground stars. By their dereddened luminosities, the two least reddened stars ($J - K = 1.0, 2.1$) are probably background stars shining through less opaque regions of the cloud. I would also expect a few of the stars with $J - K = 4$ -5 to be the brightest background stars. Therefore, I can estimate the completeness of the sample by taking the sources at $J - K = 1.0, 2.1, > 4, > 4$ (8-11 in Table 5.2) as background stars. The remaining eight sources (1-7, 12) cannot be explained with my model of the background population and are possible cluster members.

After dereddening the candidate members, I obtain the histogram of $K_{\text{dereddend}}$ in the lower panel of Figure 5.7. For stars with spectroscopy, I simply used the extinctions given in Table 5.1. To deredden the other eight sources, I used $E(J - K)$ and assumed an intrinsic color of 0.9. Since $J - K$ varies only between 0.8 and 1.0 for M stars and my bins are 0.5 magnitudes wide, errors in the assumed intrinsic colors will have little effect on the histogram of $K_{\text{dereddend}}$. If any of these sources have excess emission at K , I will overestimate the luminosity and mass. If I examine the histogram of $K_{\text{dereddend}}$ in Figure 5.7 I see that the completeness limit for the spectroscopic sample is (at best) $K_{\text{dereddend}} = 10$. On the H-R diagram in Figure 5.5, this completeness limit intersects the locus of stars near 0.15 and 0.35 M_{\odot} for DM94 and FJS, respectively. These mass completeness limits are shown with the IMFs in Figure 5.6. The first conclusion I can draw is that despite the extensive spectroscopy available for L1495E, completeness corrections are significant near 0.1 M_{\odot} .

I can now estimate a completeness correction for the IMF. In the region of L1495E I imaged, there are 10 and 8 stars brighter and fainter than $K_{\text{dereddend}} = 10$, respectively. Of these, there is one bright source lacking spectroscopy and one faint source with spectroscopy. Consequently, the completeness of the spectroscopic sample is approximately 90% and 10% on either side of $K_{\text{dereddend}} = 10$. The secondary of V410 Tau is not shown in Figure 5.7 but has $K_{\text{dereddend}} = 9.5$ and is included in this discussion. In the IMF calculated in § 5.3.5, there are 29 sources (5 secondaries) where 10 sources (9 at $K < 10$, 1 at $K > 10$) fall within the area I imaged. Out of the other 19 stars, 11 (2 secondaries) have $K < 10$ and 8 (2 secondaries) have $K > 10$. Thus, $N(K < 10)/N(K > 10) = 11/8$ in the region not imaged, which is very similar to the ratio of 10/8 predicted by my completeness correction. Apparently only the most opaque region of L1495E, which I imaged, is

seriously incomplete. To apply a completeness correction to the IMF, I only need to add the 8 sources which were dereddened in Figure 5.7 and lack spectroscopy (1-7, 12 in Table 5.2). By combining the extinction derived from $E(J - K)$ and an assumed $BC_J = 1.75$ (which varies between 1.5 and 2.0 for M stars) I can estimate L_{bol} for these sources. In Table 5.2 I present the photometry and luminosities of the low-mass candidates with $K < 14$ which appear in the lower panel of Figure 5.7. I also provide these properties for five additional sources identified by SS94 in images of other regions of L1495E.

If I assume an age for these low-mass candidates, I can use a given set of evolutionary tracks to derive their masses. The low-luminosity sources I add to the IMF (1-7, 12) would fall in the lowest mass bins and significantly affect the FJS IMF. However, I do not attempt to estimate masses with the FJS tracks since they imply much older ages for low-mass stars and the models are truncated at $0.15 M_{\odot}$. On the other hand, the tracks of DM94 imply a coeval population of ≤ 1 Myr, so I assume this age range applies to the low-mass candidates and derive their masses. This completeness correction to the DM94 IMF is indicated by the shaded regions in Figure 5.6. At the lowest masses, the new DM94 IMF deviates dramatically from the uncorrected version and that of Scalo (1986). The corrected IMF shows no evidence for a peak near $\log M = -0.5$ ($M \sim 0.3 M_{\odot}$). Instead, it becomes nearly flat in logarithmic units, assuming the DM94 tracks. If I relax my age assumption for the low-mass candidates and allow some to be as old as 3 Myr, a few sources will move from the lowest mass bin into the next higher one, but I still find that the mass function fails to peak at $\log M = -0.5$ as found by Scalo (1986).

The sources in Table 5.2 are excellent candidates for very low-mass stars and

brown dwarfs. Because of the uncertainties in the models and the assumed physical properties, I refrain from listing masses for individual sources. However, Anon 14 is a particularly good brown dwarf candidate because of its low luminosity combined with a large L' -band excess that indicates it is almost certainly a cluster member.

Comparison with Previous IMF Studies

A number of previous works have used photometry to derive IMFs in the ρ Oph and NGC 2024 young, embedded clusters (e.g., Comerón et al. 1993, updated in Comerón, Rieke, & Rieke 1996; Strom, Kepner, & Strom 1995; Comerón et al. 1996). These works have all been based on evolutionary tracks of DM94, or a combination of these models and the compatible calculations of BHSL93. The results of these studies are nearly identical (see Williams et al. 1995), finding a nearly flat or slowly rising trend toward lower masses, if the IMF is expressed in logarithmic mass units. Hillenbrand (1997) reports a possible low-mass turnover at $\log M = -0.7$ in the young Orion population, but this feature occurs near the completeness limit of the survey and requires confirmation.

As Figure 5.6 shows, the IMF derived for L1495E is very similar to those found in ρ Oph and NGC 2024. The similarity of the IMFs is of substantial interest, since the density of forming stars varies by two orders of magnitude among the three regions, from ~ 10 -100 pc^{-3} in L1495E (this work) to ~ 4000 pc^{-3} in the core of NGC 2024 (Lada et al. 1991). The form of the IMFs may change with improvements in the evolutionary tracks (see below). However, I expect that changes would affect all three derived IMFs in a similar manner, particularly because the three regions have similar ages. Thus, it appears that the IMF may be approximately invariant over a large range of star forming environments.

If the low-mass IMF is roughly independent of cluster density, then I might expect the IMFs found in older, exposed clusters to match those of embedded clusters. Most studies of older clusters indicate an IMF that is roughly flat in logarithmic mass units down to the bottom of the main sequence, in agreement with the completeness-corrected IMF in Figure 5.6 based on the DM94 tracks and those derived from photometric studies of ρ Oph and NGC 2024. Examples include: 1.) globular clusters studied by De Marchi & Paresce (1995); 2.) the Hyades (Bryja 1994); 3.) Praesepe (Williams, Rieke, & Stauffer 1995); and 4.) the Pleiades (Williams et al. 1996).

Implications of Recent Evolutionary Tracks

Because the BCAH97 tracks only extend up to $0.7 M_{\odot}$, it is not possible to use these models to derive an IMF for the entire population. However, I can make the simple calculation of $N(> 0.7 M_{\odot})/N(< 0.7 M_{\odot})$ using each set of tracks. This ratio is 0.16, 0.16, and 1 using the DM94, FJS, and BCAH97 tracks, respectively, whereas Scalo (1986) predicts a value of 0.22 and other proposed forms for the field IMF (e.g., Basu & Rana 1992) would be still lower. My completeness correction in § 5.3.5 reduced these observed values, but the incompleteness would have to be much larger than I estimate to bring the BCAH97 IMF to a plausible form.

The anomalous IMF produced by the BCAH97 tracks may be due to the limitations of the NextGen atmospheres for very young stars. The lowest surface gravity ($\log g = 3.5$) available in the atmospheric models is near and possibly larger than that expected for low-mass stars at 1 Myr. Another issue which is relevant for low-mass PMS stars is the treatment of convection. DM94 examined the sensitivity of T_{eff} to the free parameters $\alpha = l/H_p$ and a in the mixing-length

theory (MLT) and Canuto & Mazzitelli (CM) models of convection, respectively. While there was little variation of T_{eff} with α in CM convection, T_{eff} increased by ~ 600 K from $l/H_p = 1$ to 2 in the solar model. DM94 found that below $\sim 0.2 M_\odot$ the PMS tracks no longer depended substantially on l/H_p , which agrees with the results of Burrows et al. (1989). Consequently, the use of MLT with $l/H_p = 1$ by BCAH97 and Burrows (1997) should be acceptable below $\sim 0.2 M_\odot$, but at higher masses this choice of l/H_p could be responsible for the cool PMS tracks produced by BCAH97 (relative to FJS and DM94) and the strange form of the resulting IMF for L1495E.

At masses below $0.2 M_\odot$, the tracks of BCAH97 and Burrows (1997), which both use NextGen atmospheres, agree fairly well, while they are both 100-200 K cooler than the gray atmosphere calculations of DM94. However, Model X of BHSL93 also uses a gray atmosphere but is closer to the newer NextGen calculations than DM94. The difference between DM94 and the other tracks may be largely due to the treatment of the surface boundary condition. DM94 compute gray atmospheres with the Eddington approximation ($T(\tau)$) whereas the models of BHSL93, BCAH97, and Burrows (1997) solve the radiative transfer explicitly, as recommended by BHSL93 and Baraffe et al. (1995) for $2500 \text{ K} < T_{\text{eff}} < 4000 \text{ K}$.

The strange BCAH97 IMF and reasonable DM94 IMF for L1495E above $0.2 M_\odot$ stress the need for sophisticated convection models for young, intermediate-mass stars. On the other hand, the agreement of the BCAH97 and Burrows (1997) tracks with the observations of PPL 15 (assuming my temperature scale is valid) demonstrate the importance of synthetic, non-gray atmospheres and non-Eddington boundary conditions below $0.2 M_\odot$.

5.4. Conclusions

I have used IR spectroscopy to derive spectral types for young, embedded stars in L1495E and complement those obtained in the optical. IR spectral classification is nontrivial and must be performed with care, but I find that I can account for the effects of non-dwarf surface gravities and continuum veiling on the observed spectra. I find that:

1. The optical and IR spectral types agree to within one subclass for five of seven sources. The remaining two objects differ so dramatically that there is probably a mis-identification in one band or the other.
2. Non-solar abundances have a significant effect on the K -band spectra of stars, so solar-metallicity spectral standards must be selected for classifying young stars.
3. $R \geq 1000$ is a suitable spectral resolution for classifying late-type ($>G0$) young stars in the K -band.
4. The ~ 3 very young (< 1 Myr), luminous M stars in my sample exhibit weak Na (presumably due to low surface gravity) while the strength of CO remains dwarf-like.
5. The one star showing a large veiling in the K -band spectrum ($r_K \sim 2$) also had the largest IR excess in the $JHKL'$ photometry.

After carefully arriving at a T_{eff} scale for cool stars and constructing an H-R diagram for L1495E, I can compare the placement of the cluster population with the predictions of various evolutionary tracks for young, low-mass stars. The Swenson

(1996) models imply that the stars are progressively older with lower masses, with many members being unrealistically old compared with the escape time from the cluster. Even though they include modern atmospheric models, the tracks of BCAH97 also tend to make the cluster members uncomfortably old and indicate an implausible form for the IMF. Although these tracks reproduce observations of globular clusters and of CM Dra and YY Gem (two pairs of eclipsing binaries with well-determined luminosities and temperatures) and may be useful at the main sequence, they still appear to have significant shortcomings for very young stars, possibly due to the inadequacies of MLT convection above $0.2 M_{\odot}$. The tracks of DM94 provide the more satisfactory result that the star formation is roughly coeval at ~ 0.5 Myr, and also they lead to a an IMF that is approximately in agreement with those derived for older clusters that are not dust embedded and where the stellar parameters can be related to masses more reliably. These tracks and those of Swenson (1996) do not match the data for CM Dra and YY Gem as well as those in BCAH97, but they do produce reasonable IMFs at young ages.

Nonetheless, since the DM94 tracks have been used in previous studies, they can be used in a comparative sense. I find that the IMF derived with these tracks and optical spectroscopy by Strom & Strom (1994) agrees well with that derived with the addition of IR spectroscopy; the more heavily obscured sources reached by the latter technique do not differ in intrinsic properties significantly from the other members of the cluster. However, from IR imaging of the cluster core and of a control field, I conclude that both spectroscopic samples may be incomplete for faint, low-luminosity objects with masses near $0.1 M_{\odot}$. If the candidate low-mass sources identified in the imaging are added to the IMF, I find that the IMF does not turn over near $0.3 M_{\odot}$ (and does not agree with the Scalo (1986) field star IMF). Instead, the mass function of L1495E is roughly flat in logarithmic mass

units below $\sim 0.4 M_{\odot}$. This behavior agrees well with that deduced for a number of other nearby very young star formation regions interpreted with DM94 tracks and indicates that the IMF may be roughly invariant over two orders of magnitude of density in a forming cluster, from $\sim 10\text{-}100 \text{ pc}^{-3}$ in L1495E (this work) to $\sim 4000 \text{ pc}^{-3}$ in NGC 2024 (Lada et al. 1991). To test these conclusions, the sources in the photometric completeness correction must be spectroscopically confirmed as low-mass cluster members rather than background stars. Further improvements and observational testing of theoretical models for very young stars are also required for a definitive determination of the low-mass IMF in these clusters.

5.5. Notes on IR Spectral Classification

To classify YSOs through their IR spectra, I have observed a large number (~ 50) of cool dwarfs which have standard spectral types and supplemented these spectra with those of giants from Kleinmann & Hall (1986). In Table 5.3 all available metallicity estimates are listed for this sample. The majority of the early K dwarfs have relatively well-known metallicities from spectral analyses (Cayrel de Strobel et al. 1992), whereas the cooler dwarfs only have very uncertain metallicity estimates derived through their displacements from the main sequence (Eggen 1996). The kinematic and photometric populations of Leggett (1992) are also presented, providing an additional hint to the metallicities of late-type dwarfs. In Figs. 5.9-5.14, I compare the spectra within each well-populated spectral subclass of our sample. The spectra are ordered from weakest to strongest features from top to bottom in each figure. Although a few of the stars do not have metallicity estimates, this comparison clearly illustrates that the photospheric absorption features change noticeably with metallicity, where a change of ~ 0.1 in $\log(\text{Fe}/\text{H})$

appears detectable. In lower resolution spectra ($R=500$), Leggett et al. (1996) also find that Na, Ca, and CO differ significantly in strength between metal-poor and metal-rich stars. There is one exception in our sample to this trend. Hearnshaw (1974) derived an iron abundance of 0.36 for HR 511, whereas our spectrum does not have particularly strong features and implies a roughly solar metallicity. Hearnshaw noted that the star is subluminescent on the color magnitude diagram, which is the behavior expected of a metal-poor rather than metal-rich star. More recently, metallicity measurements by Gorgas et al. (1993) imply that HR 511 is overabundant in iron while close to solar in other species, possibly explaining the appearance of its infrared spectrum.

Since the strengths of K -band features in stars outside an abundance range of $-0.2 \lesssim [Fe/H] \lesssim 0.2$ depart noticeably from those of solar-metallicity stars, I have rejected the spectra which indicate low or high metallicities and combined the rest into one composite spectrum representing that subclass. For subclasses containing only one or two stars, I used the neighboring subclasses and any metallicity information to check for extreme metallicity. I used the data for the stars in Table 5.4 to create a network of composite standard spectra ($>G0$) shown in Figs. 5.15-5.16 at the original resolution ($R = 1200$) and smoothed to the resolution of the spectra in L1495E ($R = 800$).

The IR classification of young stars is challenging. Circumstellar dust emission and surface gravities intermediate between those of dwarfs and giants can produce spectra which depart from those of spectral standards. To derive spectral types of young stars, I have developed a classification procedure which accounts for the effects of continuum veiling and gravity. Na and Ca are strong features and have weak dependences on gravity (with exceptions which will be pointed out later), so

they are used in the first step of the classification. For each spectral type in the network, I determine the continuum veiling that must be applied to the standard to match the Na and Ca strengths in the YSO spectrum. I quantify veiling through the parameter r_K , where $r_K = I_{2.2 \mu\text{m}}(\text{IR excess})/I_{2.2 \mu\text{m}}(\text{star})$. The equivalent width of a feature in a stellar spectrum contaminated by continuum veiling is $W_\lambda(\text{veiled}) = W_\lambda(\text{intrinsic})/(1 + r_K)$. For a particular spectral type in the standard network, the best fit r_K minimizes the least squares residual:

$$[W_\lambda(\text{Na, standard})/(1 + r_K) - W_\lambda(\text{Na, YSO})]^2 + [W_\lambda(\text{Ca, standard})/(1 + r_K) - W_\lambda(\text{Ca, YSO})]^2.$$

For instance, if I have a young star with $W_\lambda(\text{Na}) = 4 \text{ \AA}$ and $W_\lambda(\text{Ca}) = 4 \text{ \AA}$ and the M0V standard has $W_\lambda(\text{Na}) = 6 \text{ \AA}$ and $W_\lambda(\text{Ca}) = 6 \text{ \AA}$, then the best match for M0V is with a veiling of $r_K = 0.5$ and a least squares residual of zero. The r_K and residual of the fit is determined for each dwarf subclass later than G0. Note that since my network of standards is not perfectly sampled across each subclass, I interpolated equivalent widths across empty subclass bins. This should be a reasonable approach since the variation of feature strengths with spectral type is smooth.

Each standard dwarf is artificially veiled to match Na and Ca in a given YSO, with the least squares residual as an indication of how good the fit was for a particular spectral type. I then over-plot the YSO spectrum with each of these veiled standards to compare the weaker features and derive the final spectral type interactively. At $R = 800$, the only features other than $\text{Br}\gamma$, Na, Ca, and CO which are detectable are Mg ($2.28 \mu\text{m}$) and a blend of Mg and Al ($2.11 \mu\text{m}$). The typical uncertainties in spectral type and r_K are $\pm 1\text{-}2$ subclasses and 0.25, respectively. Since $\text{Br}\gamma$ absorption changes in an opposite manner relative to the other strong

features, stars earlier than K4 are readily typed. However, since $\text{Br}\gamma$ can be filled in by emission in YSOs, I take the measured equivalent width as only a lower limit to the intrinsic absorption. Dwarfs later than M2 are also easily classified since $W_\lambda(\text{Ca})$ steadily declines with cooler temperatures while $W_\lambda(\text{Na})$ peaks at M6. Stars between K4 and M2 are the most difficult to classify since the relative strengths of Na and Ca are fairly constant in this range. A veiled M2 star can look very similar to an unveiled K5. The strength of Mg relative to Na and Ca is a crucial temperature constraint in this range.

Since the strengths of the CO band heads are sensitive to gravity, and the embedded objects might be expected to have feature strengths between those for dwarfs and giants, I do not use them to estimate the spectral type in the above process. Initially, CO is only used to identify background giants which are behind the molecular cloud. Giant-like CO absorption can occur in FU Ori objects (due to circumstellar disk) or extremely young stars (due to extended, low-gravity photosphere). These sources should be distinguishable from giants through the presence of an IR excess or line emission, for instance. After deriving the best estimate of the spectral type, I measure the ratio of the equivalent widths of the first two CO band heads in the YSO to those of the best fit veiled standard (usually a dwarf).

I now address an important question: Is it valid to use spectra of standard dwarfs to classify YSOs which presumably have gravities intermediate between those of giants and dwarfs? For instance, I expect that T Tauri stars with ages ≤ 1 Myr could have $\log g \sim 2-3$, halfway between that of dwarfs and giants. To examine the sensitivity to surface gravity of the K -band absorption features, I can compare the standard dwarfs and giants. As shown in Figure 5.8, Na, Ca, and

Mg have similar strengths for a given dwarf and giant spectral type earlier than K7. Br γ is slightly weaker in dwarfs, but the difference is small considering the surface gravities of dwarfs and giants differ by ~ 5 -6 dex. Therefore, for stars earlier than K7, I feel that I can use Br γ , Na, Ca, and Mg to derive spectral types independent of the surface gravity. However, the behavior of these features changes later than K7. Na and Ca continue to increase slowly in strength toward late giant types. In dwarfs, the equivalent widths of Na and Ca increase more rapidly after K7V before falling off after M2V and M6V, respectively. The relative strengths of Ca, Na, and Mg are relatively constant from dwarfs to giants for K7 to M2, so using a dwarf to type a low-gravity star in this range will only introduce error in r_K and not the spectral type. For M3 and later, the relative strengths of Na and Ca differ significantly from dwarfs to giants. In M3 and M4, the strength of Ca is unchanged from dwarfs to giants, whereas Na is twice as strong in dwarfs as in giants. As Ca weakens in dwarfs later than M4, the ratio of $W_\lambda(\text{Na})/W_\lambda(\text{Ca})$ increases dramatically in dwarfs while remaining fairly constant in giants.

It is among mid-to-late M types where I must be especially careful in the classification of young stars. Since Na is much stronger in late dwarfs than in late giants, the spectrum of a low-gravity late M YSO may exhibit a weakened Na line which would not be reproduced by the standards M dwarfs. In § 3 a discussion is given on the effects of low gravity on the optical and IR spectra of the M6 star V410x3, which include weak, giant-like Na in both bands. Using these dwarfs I would mistakenly derive a spectral type of \sim M0V for such a star, which is the latest M dwarf with Na and Ca in comparable strengths. Fortunately, there are other features which can indicate when such a misclassification is present. The CO band heads may appear stronger in the low-gravity young star than in dwarfs. Giants also exhibit many small absorption features not detectable in dwarfs, some

of which might appear in the YSO. For example, Sc absorption at the blue edge of Na is very strong in giants and barely detectable (at $R \leq 1200$) in M2V and M3V.

Mg ($2.28 \mu\text{m}$) provides another important constraint on the spectral type. The strength of Mg is virtually constant across all K and M giants. For dwarfs, Mg is visible earlier than M2V. As Mg disappears at M2V and later, two other features happen to appear $\sim 10 \text{ \AA}$ to the blue and red of Mg and are prominent for later dwarf types. On the other hand, these lines are weak and the single Mg line dominates in all giants. After examining the ultra-high resolution spectra of Wallace & Hinkle (1996), I identify the red line as Ca but it is unclear what species produces the other feature. These two lines are resolved in my $R = 1200$ standard spectra, while at $R \leq 1000$ they are blended together and can be easily mistaken for Mg. As discussed earlier, the strength of Mg relative to Na and Ca is very helpful in deriving spectral types, but the two features which replace Mg at late types are also critical since their presence places an upper limit to the temperature. Consequently, a low-gravity M5 star may have weakened Na relative to M5V and thus $W_\lambda(\text{Na})/W_\lambda(\text{Ca})$ which matches that of M0V, but the detection of two lines instead of a single Mg line at $2.28 \mu\text{m}$ would clearly indicate that a late M type should be assigned.

The uncertainties in spectral type and τ_K can be reduced by observing at $R = 1200$, which is the resolution of my standard star observations. In these spectra several additional features are detected which help constrain the spectral type more tightly. As I discussed, the two lines which replace Mg in M dwarfs are very useful and require $R \geq 1000$ to be resolved. The Al and Mg lines near $2.11 \mu\text{m}$ are also resolved at such resolution and are excellent indicators of spectral type independent of continuum veiling since their relative strengths change noticeably

from K to M stars. The spectra of K and M giants are riddled with moderately strong features across the entire K -band, producing a particularly distinctive continuum structure at such resolution and making it relatively easy to differentiate between background giants and cluster members. In both dwarfs and giants there are also several Si, Ti, and Fe lines apparent at this resolution. The amount of veiling present in a YSO is much easier to estimate if these weaker features can be detected. When deriving the spectral types of cool ($>G0$), embedded YSOs in the K -band, I find that spectra at $R = 1000$ -1200 produce the best compromise between sensitivity and accurate spectral types.

5.6. Comments on Individual Source Classifications

Anonymous 24: It has strong $\text{Br}\gamma$ absorption and weak Mg/Al ($2.11\ \mu\text{m}$), Na, Ca, Mg, and CO. G1V with $r_K = 0$ fits well.

V410x8e: Although the signal-to-noise is fairly low, $\text{Br}\gamma$ absorption is still clearly detected with no other features obvious. By this spectrum alone, after accounting for the possibility of continuum veiling I derive a spectral type of G2 or earlier. However, SS94 observed a heavily veiled optical spectrum of M4 or later type. They go on to propose this star as the most likely source of the V410x8 X-ray emission. I was confident that I observed the correct star, but I obtained a follow-up spectrum to be sure. Again I detected only $\text{Br}\gamma$ absorption in a spectrum (not shown in Figure 5.1) very similar to the original. If there was a misidentification of sources on the part of SS94 and V410x8e is earlier than G2, then it falls below the main sequence at the distance of L1495E and is probably a background star. Otherwise, if we have both observed the same star, then the difference in the IR and optical spectral types is very puzzling. I also note that

although my MMT aperture photometry agrees well with that of SS94 for most sources, there is significant disagreement for this source (and also V410x8d and 8e).

V410x8d: I observed this source since it was low luminosity and is a good low-mass candidate. I plot in Figure 5.1 both the original spectrum ($R = 1200$) and a version smoothed to the resolution of the other data ($R = 800$). I detect $\text{Br}\gamma$ and CO absorption with no other features appearing above the considerable noise. The $\text{Br}\gamma$ strength constrains the type to G3-K3 independent of luminosity class. The CO strength is indicative of stars between late-G giants and mid-K dwarfs. These two constraints together produce a type of approximately K0. There should not be any significant veiling since $\text{Br}\gamma$ and CO cannot simultaneously be stronger than I observe.

Anonymous 20: The spectrum shows strong absorption in Mg/Al, $\text{Br}\gamma$, Na, Ca, Mg, and CO. The $2.28\ \mu\text{m}$ Mg line is particularly deep with $W_\lambda = 3\ \text{\AA}$, which is 1.5 times stronger than measured in any of my standard dwarfs or giants. The relative strengths of all the K -band features match well with a K3V, but the absolute strengths of the lines are significantly stronger than those of a K3V (equivalent to $r_K = -0.3$). In my analysis of metal-poor and metal-rich standard stars, I have found that all of these K -band metal features scale to together with metallicity to first order. If the anomalously strong K -band features in Anon 20 are a metallicity effect, then I estimate $[Fe/H] \sim 0.25$ by comparing to the metal-rich dwarfs I have observed. Such an abundance would not be expected from a young star in Taurus, but I have no other explanation for the line strengths observed.

V410x2: I detect absorption in Mg/Al, Na, Ca, Mg, and CO. This spectrum fits well with M0V and $r_K = -0.1$, indicating that the lines were slightly stronger than my standard.

Anonymous 25: This spectrum is very similar to that of V410x2 but with weaker Mg, no Mg/Al, and slightly stronger Na, Ca, and CO. All of these features are consistent with M1 and $r_K = 0$.

PSC04158+2805: 1-0 S(1) ($2.12 \mu\text{m}$) and 1-0 S(0) ($2.22 \mu\text{m}$) H_2 emission is detected along with absorption in Na, Ca, Mg, and CO. If I add a small amount of continuum veiling to Anon 25 ($r_K = 0.1$), the resulting spectrum is almost identical to PSC04158+2805 so I adopt M1 and $r_K = 0.1$ for this source.

CY Tau: This spectrum shows $\text{Br}\gamma$ emission and has similar line ratios as Anon 25 and PSC04158+2805. The absolute strengths of the features imply $r_K = 0.15$ for M1. The spectral slope indicates less reddening than in the previous stars two stars.

PSC04154+2823: I obtained spectra at both $R = 800$ and $R = 1200$ for this object where the observations were separated by two years. They both show similar $\text{Br}\gamma$ emission strengths and highly reddened spectral slopes. In the original $R = 800$ spectrum, the profile of Na appears quite broad while I discover in the $R = 1200$ data that this is due to absorption by Sc in the blue edge of Na. I detect Sc in all of my cool giants and also in dwarfs between M2V and M3V (though very weak). The strength of CO relative to Na and Ca is dwarf-like, so the presence of Sc implies a spectral type between M2 and M3. It is in this range of types that the transition occurs from a single Mg line to two other features at nearly the same wavelength. In the higher resolution spectrum I can see that the Mg line is indeed replaced by two other lines. The relative strengths of these two features, Na and Ca, also imply spectral type of M2 or M3, so I estimate M2.5 and $r_K = 2$ for this source.

Anonymous 12, V410x4, V410x5a: V410x4 and x5a have virtually identical

spectra. Anon 12 is also very similar to these sources but with slightly weaker CO. I find that the Na, Ca, and CO strengths of these stars match well with those of an M4V with $r_K = 0$. Even at $R = 800$, the feature at $2.285 \mu\text{m}$ appears slightly broader than the Mg lines in earlier type stars, implying that it is probably not Mg but actually the two lines which replace it in mid-to-late M dwarfs.

V410x6: The ambiguity that I discussed earlier in classifying a low-gravity late M star is present for this source. The relative strengths of Na and Ca are consistent with either a late K/early M dwarf or any M star of lower gravity. To distinguish between the two possibilities, I can use the Mg line since it should be obvious in a late K/early M dwarf but replaced by two features for M3 and later. In the original $R = 800$ spectrum, the feature at $2.285 \mu\text{m}$ appears broad and may be two lines rather than one Mg line. The blue edge of Na also seems depressed, possibly by Sc absorption. To check these two important features I obtained another spectrum of this source at $R = 1200$ where I do indeed resolve two features at $2.285 \mu\text{m}$ and Sc absorption near Na. The double feature at $2.285 \mu\text{m}$ and the CO strength constrain the type to $\geq \text{M3}$ and $\leq \text{M6}$, respectively. The strength of the Ca line is the maximum I see in any standard giant or dwarf, so the veiling is probably close to zero. I derive M4.5 and $r_K = 0$ for this source. I also note that although the gravity departs enough from that of a dwarf to weaken Na and enhance Sc, the CO is not appreciably stronger than that of an M4.5 dwarf. Once placed on the H-R diagram, this source does indeed appear very luminous for its temperature, well above the 1 Myr isochrone.

V410x3: The large ratio of Na to Ca in this spectrum is only found in dwarfs later than M4. The relative and absolute strengths of Ca and the feature at $2.285 \mu\text{m}$ imply M6V or M7V. But the Na line is weaker than in these dwarfs,

which may result from a low surface gravity. However, the CO in this source still matches that of an M6 or M7 dwarf and does not appear enhanced by low gravity. This behavior of Na and CO is the same as observed in V410x6, hence V410x3 may simply be a cooler version of V410x6.

Anonymous 13: The relative strengths of Na, Ca, and Mg match well with those of a K4 star with no veiling, while the CO is 25% stronger than that of a dwarf of this type. However, SS94 derived an optical spectral type of M5 for this source. Even after accounting for effects of veiling and gravity (as for V410x3 and x6), I cannot find an M star which matches my spectrum. The Mg line is simply too strong to match any late M giant or dwarf, hence continuum veiling cannot be the problem. A follow-up spectrum at $R = 1200$ could constrain the IR spectral type further. If this star is actually an M star, at this higher resolution the feature at $2.285 \mu\text{m}$ should appear as two features rather than one Mg line.

V410x8b: As with V410x8d, this is a very faint source that I observed in follow-up work in L1495E. I clearly detect absorption in Na and CO, but since the signal-to-noise is fairly low I do not have tight constraints on the Ca and Mg strengths. A giant which matches the CO strength in this source (G8III) should also have detectable $\text{Br}\gamma$ absorption, so this is probably not a background giant. If the CO strength is not affected significantly by a non-dwarf surface gravity (as implied by the rest of my sources), then the CO strength implies a type of K5 to M3 (or later if veiled). The ratio of Na to CO, which should be independent of veiling, implies either a heavily veiled late M star or mid K star with no veiling. This source is not very embedded and should be observed in the optical to derive a more accurate spectral type.

TABLE 5.1
DATA FOR SPECTROSCOPIC SAMPLE IN L1495E

| # | star | opt ^a | IR | T_{eff} | A_J | L_{bol} | R_C^a | I_C^a | J | H | K | L' | comments ^b |
|-----------------|-------------------|------------------|---------|------------------|-------|------------------|---------|---------|-------|-------|-------|--------------------|-----------------------|
| 1 | Anon 3 | M4.5 | ... | 3095 | 0.13 | 0.006 | 17.31 | 15.45 | 14.43 | 13.84 | 13.49 | 13.2 ^c | MMT, foreground? |
| 2 | Anon 9 | A2 | ... | 8970 | 2.79 | 14.9 | 15.49 | 13.38 | 10.45 | 8.77 | 7.89 | 7.47 | MMT |
| | | | | | | | | | 10.15 | 8.84 | 7.96 | ... | SS94 |
| 3 | Anon 12 | M4+ | M4(1) | 3180 | 0.03 | 0.039 | 14.94 | 13.29 | 12.25 | 11.64 | 11.38 | 11.32 ^c | MMT, foreground? |
| | | | | | | | | | 12.18 | 11.63 | 11.36 | ... | SS94 |
| 4 | Anon 13 | M5 | K4(2) | 3010 | 0.95 | 0.044 | 18.58 | 15.97 | 12.97 | 11.71 | 10.93 | 10.29 | MMT |
| | | | | | | | | | 12.82 | 11.64 | 10.90 | ... | SS94 |
| 5 | Anon 17 | M1.5 | ... | 3595 | 0.00 | 0.063 | 13.81 | 12.76 | 11.92 | 11.27 | 11.27 | ... | MMT, foreground? |
| 6 | Anon 20 | ... | K3(2) | 4730 | 6.87 | 0.56 | ... | ... | 16.72 | 13.54 | 11.93 | 11.18 ^c | MMT, $r_K = -0.3$ |
| | | | | | | | | | ... | 13.58 | 11.92 | ... | SS94 |
| 7 | Anon 24 | ... | G1(2) | 5945 | 6.97 | 2.61 | ... | ... | 15.55 | 12.31 | 10.64 | 9.89 | MMT |
| | | | | | | | | | 14.84 | 12.27 | 10.65 | ... | SS94 |
| 8 | Anon 25 | ... | M1(2) | 3680 | 7.43 | 3.31 | ... | ... | 15.07 | 11.68 | 9.95 | 9.39 | MMT |
| | | | | | | | | | 14.75 | 11.73 | 9.88 | ... | SS94 |
| 9 ^d | BP Tau | K7 | ... | 4060 | 0.11 | 0.89 | 11.23 | 10.39 | 9.30 | 8.42 | 8.05 | ... | SS94 |
| 10 | CK Tau 1 | M2:e | ... | 3510 | 0.55 | 0.061 | 16.40 | 14.83 | 12.49 | 11.35 | 10.83 | ... | SS94 |
| | | | | | | | | | 12.53 | 11.36 | 10.80 | ... | SS94 |
| | | | | | | | | | 12.69 | 11.26 | 10.83 | ... | SS94 |
| 11 | CY Tau | M2 | M1(2) | 3510 | 0.03 | 0.47 | 12.38 | 11.20 | 9.76 | 9.05 | 8.83 | ... | SS94, $r_K = 0.15$ |
| 12 | CZ Tau | M3 | ... | 3350 | 0.48 | 0.38 | 13.53 | 11.80 | 9.90 | 9.24 | 8.77 | ... | SS94, $b = 0.69$ |
| 13 | DD Tau | M4 | ... | 3180 | 0.00 | 0.29 | 12.63 | 11.19 | 9.56 | 8.8 | 8.37 | ... | SS94, $b = 0.65$ |
| 14 ^d | DE Tau | M1 | ... | 3680 | 0.26 | 1.04 | 11.87 | 10.66 | 9.15 | 8.26 | 7.71 | ... | SS94 |
| 15 ^d | FO Tau | M2 | ... | 3510 | 0.27 | 0.37 | ... | ... | 9.70 | 8.77 | 8.19 | ... | SS94, $b = 0.6$ |
| 16 | FQ Tau | M4 | ... | 3180 | 0.12 | 0.071 | 13.49 | 11.77 | 10.98 | 10.31 | 9.83 | ... | SS94, $b = 0.52$ |
| 17 ^d | HDE 283592 | G5 | ... | 5770 | 0.19 | 8.23 | 8.34 | 7.83 | 7.46 | 7.04 | 6.93 | ... | SS94 |
| 18 | Hubble 4 | K7 | ... | 4060 | 0.68 | 2.98 | 11.92 | 10.65 | 8.56 | 7.68 | 7.29 | ... | SS94 |
| 19 ^d | LkCa 4 | K7 | ... | 4060 | 0.30 | 1.07 | 11.54 | 10.56 | 9.28 | 8.57 | 8.35 | ... | SS94 |
| 20 | LkCa 5 | M2: | ... | 3510 | 0.03 | 0.36 | 12.51 | 11.33 | 10.05 | 9.34 | 9.12 | ... | SS94 |
| 21 ^d | LkCa 7 | K7 | ... | 4060 | 0.39 | 1.19 | 11.63 | 10.58 | 9.26 | 8.56 | 8.33 | ... | SS94 |
| 22 | PSC04154 +2823 | ... | M2.5(2) | 3430 | 5.20 | 0.64 | ... | 19.60 | 14.52 | 11.56 | 9.61 | 7.86 | MMT, $r_K = 2$ |
| | | | | | | | | | 15.00 | 11.80 | 10.13 | ... | SS94 |
| 23 | PSC04158 +2805 | ... | M1(2) | 3680 | 1.50 | 0.077 | 17.11 | 14.97 | 13.23 | 11.89 | 10.86 | 10.70 | MMT, $r_K = 0.1$ |
| | | | | | | | | | 13.15 | 11.92 | 10.80 | ... | SS94 |

TABLE 5.1—Continued

| # | star | opt ^a | IR | T_{eff} | A_J | L_{bol} | R_C^a | I_C^a | J | H | K | L' | comments ^b |
|-----------------|----------|------------------|---------|------------------|-------|------------------|---------|---------|--------------------|--------------------|--------------------|--------------------|-----------------------|
| 24 ^d | RY Tau | K1 | ... | 5080 | 0.30 | 4.55 | 10.28 | 9.63 | 8.00 | 6.78 | 5.74 | ... | SS94 |
| 25 | V410 Tau | K7 | ... | 4060 | 0.00 | 1.69 | 10.18 | 9.48 | 8.33 | 7.73 | 7.54 | ... | SS94, $b = 0.86$ |
| 26 | V410x1 | M3.5-4 | ... | 3180 | 0.21 | 0.12 | 14.15 | 12.36 | 11.25 | 10.01 | 9.25 | ... | SS94 |
| 27 | V410x2 | ... | M0(2) | 3850 | 4.42 | 0.62 | ... | 20.00 | 13.91 | 11.14 | 9.18 | ... | MMT, $r_K = -0.1$ |
| | | | | | | | | | 13.86 | 10.94 | 9.43 | ... | SS94 |
| 28 | V410x3 | M6 | M6.5(2) | 2840 | 0.00 | 0.061 | 15.80 | 13.53 | 11.63 | 10.94 | 10.54 | 10.49 | MMT |
| | | | | | | | | | 11.50 | 10.93 | 10.49 | ... | SS94 |
| | | | | | | | | | 12.08 ^c | 11.14 | 10.77 | ... | SS94 |
| 29 | V410x4 | ... | M4(1) | 3180 | 5.32 | 1.26 | ... | 19.30 | 13.76 | 11.10 | 9.72 | 9.18 | MMT |
| | | | | | | | | | 13.46 ^c | 11.07 | 9.69 | ... | SS94 |
| 30 | V410x5a | M5 | M4(1) | 3010 | 0.79 | 0.084 | 17.14 | 14.65 | 12.10 | 10.81 | 10.19 | 9.74 | MMT |
| | | | | | | | | | 11.88 | 10.80 | 10.12 | ... | SS94 |
| 31 | V410x6 | M5 | M4.5(2) | 3010 | 0.24 | 0.21 | 15.08 | 13.00 | 10.54 | 9.67 | 9.05 | ... | SS94 |
| 32 | V410x7 | M1 | ... | 3680 | 2.15 | 0.48 | 17.79 | 15.17 | 11.88 | 10.05 | 9.16 | ... | SS94 |
| 33 | V410x8d | ... | K0(3) | 5250 | 1.79 | 0.039 | 18.51 | 16.79 | 14.70 | 13.39 | 12.45 | 11.92 ^c | MMT, background? |
| | | | | | | | | | 14.31 ^c | 13.03 ^c | 12.47 ^c | ... | SS94 |
| 34 | V892 Tau | B9 | ... | 5250 | 1.77 | 11.09 | 13.14 | 11.43 | 8.55 | 6.91 | 5.64 | ... | SS94 |
| 35 | V819 Tau | K7 | ... | 4060 | 0.48 | 0.96 | 11.57 | 10.45 | 9.59 | 8.65 | 8.00 | ... | SS94 |
| 36 | V410x8b | ... | K-M | ... | ... | ... | 18.14 | 16.22 | 14.52 | 13.19 | 12.67 | 12.34 ^c | MMT |
| | | | | | | | | | 13.82 | 12.74 | 11.96 | ... | SS94 |
| 37 | V410x8e | M4: | <G2 | ... | ... | ... | 19.24 | 17.30 | 15.12 | 13.73 | 13.04 | 13.10 ^c | MMT, background? |
| | | | | | | | | | 14.63 ^c | 13.76 ^c | 12.88 | ... | SS94 |

^aSS94.^b r_K was derived from the IR spectra and was approximately zero if not given. "b" is the factor by which the luminosity was multiplied to correct for a binary companion. SS94=CIT JHK photometry from SS94 and references therein. MMT= $JHKL'$ photometry obtained at MMT for this program.^cPhotometric uncertainty larger than 0.05 mag.^dAt $r > 25'$ from cluster center and not included in IMF.

TABLE 5.2
CANDIDATE LOW-MASS MEMBERS OF L1495E

| # | $\alpha(1950)$ | $\delta(1950)$ | Imaging | | MMT Photometry | | | | | SS94 ID | $\log(L_{\text{bol}})$ |
|----|----------------|----------------|---------|-------|----------------|-------|-------|-------------|-----|---------|------------------------|
| | | | J | K | J | H | K | L' | | | |
| 1 | 4 15 35.23 | 28 20 12 | 16.55 | 11.20 | ... | ... | ... | ... | ... | ... | -0.1 |
| 2 | 4 15 22.13 | 28 20 59 | 16.77 | 12.38 | ... | ... | ... | ... | ... | ... | -0.9 |
| 3 | 4 15 06.53 | 28 12 22 | 16.09 | 12.51 | ... | ... | ... | ... | ... | Anon19 | -1.1 |
| 4 | 4 15 40.64 | 28 13 30 | 17.18 | 12.57 | 16.97 | 14.04 | 12.53 | 11.88(0.1) | ... | Anon21 | -0.9 |
| 5 | 4 15 35.97 | 28 21 08 | 17.23 | 13.25 | ... | ... | ... | ... | ... | ... | -1.3 |
| 6 | 4 15 15.55 | 28 13 03 | 17.36 | 13.25 | ... | ... | ... | ... | ... | ... | -1.3 |
| 7 | 4 15 39.91 | 28 19 19 | 16.49 | 13.39 | ... | ... | ... | ... | ... | ... | -1.6 |
| 8 | 4 15 43.84 | 28 20 35 | 15.54 | 13.45 | ... | ... | ... | ... | ... | ... | -1.9 |
| 9 | 4 15 29.90 | 28 19 03 | >18 | 13.53 | >18 | 16.03 | 13.23 | 12.12 | ... | Anon26 | -1.3 |
| 10 | 4 15 20.96 | 28 12 56 | 14.66 | 13.68 | ... | ... | ... | ... | ... | ... | -2.3 |
| 11 | 4 15 31.66 | 28 17 59 | >18 | 13.71 | ... | ... | ... | ... | ... | ... | -1.4 |
| 12 | 4 15 17.18 | 28 14 09 | 18.73 | 13.73 | ... | ... | ... | ... | ... | ... | -1.3 |
| 13 | 4 15 24.49 | 28 10 15 | ... | ... | 15.00 | 13.90 | 13.45 | 13.3(0.4) | ... | Anon1 | -2.1 |
| 14 | 4 15 24.95 | 28 11 12 | ... | ... | 14.73 | 13.50 | 12.79 | 12.45(0.15) | ... | Anon2 | -1.8 |
| 15 | 4 14 59.26 | 28 20 45 | ... | ... | 15.42 | 13.61 | 12.84 | 9.97(0.06) | ... | Anon14 | -1.5 |
| 16 | 4 15 01.31 | 28 16 18 | ... | ... | 18.00 | 15.58 | 14.20 | >13.3 | ... | Anon23 | -1.9 |
| 17 | 4 15 31.66 | 28 17 59 | ... | ... | >19.6 | 15.92 | 13.64 | >13.1 | ... | Anon27 | -2.2 |

NOTE.—Stars 1-12 fall within the region imaged in Figure 5.2 and appear as unshaded boxes labeled with $J - K$ in Figure 5.7.

TABLE 5.3
SPECTRAL STANDARDS

| star | type | ref | [Fe/H] | ref | comments ^a |
|----------|----------|---------|--|-----|-----------------------|
| HR7162 | F9V | KMb | ... | ... | ... |
| HR7503 | G1.5Vb | KMb | (0.22, 0.2, 0.0), 0.11 | C,G | KH,16 Cyg A |
| HR7504 | G3V | KMb | (0.11, 0.08, 0.07, 0.0), 0.06 | C,G | KH,16 Cyg B |
| HR5072 | G4V | KMb | -0.11, -0.21 | C,L | ... |
| HR8631 | G4V | KMb | ... | ... | ... |
| HR7260 | G4.5V | KMb | ... | ... | ... |
| HR7462 | K0V | KMb | -0.23, -0.25 | C | σ Dra |
| HR511 | K0V | C | 0.36 | C | ... |
| HR7368 | K0V | KMb | 0.08 | WG | ... |
| HD145675 | K0V | KMb | 0.22, 0.18, 0.35, 0.31 | C | ... |
| HD25329 | K1Vsb | C | -2.3, -1.32, -1.34, -1.6 -1.56, -1.56, -1.8 | C | ... |
| HD190404 | K1V | C | -0.2, -0.1, -0.15, -0.3, -0.14 | C | ... |
| HR493 | K1V | KMb | -0.2 | C | ... |
| HD109011 | K2V | KMb | ... | ... | ... |
| HD184467 | K2V | KMb | ... | ... | ... |
| HD160346 | K3-V | KMb | ... | ... | ... |
| HR8832 | K3V | KMb | 0.0, 0.1, 0.0, -0.21, 0.0, -0.01, 0.2 | C | ... |
| HR8085 | K5V | KMb | 0.0, -0.05, -0.1, -0.06 | C | 61 Cyg A |
| HD196795 | K5V | KMb | ... | ... | ... |
| HR8086 | K7V | KMb | -0.65, -0.15, -0.05, -0.1, 0.0 | C | OD,Y/O,61 Cyg B |
| GL338B | K7V | HKS | 0.06 | E | ... |
| GL673 | K7V | HKS | 0.4 | C | OD,O/H |
| GL380 | K7V,K6eV | HKS,KMb | 0.28, 0.1 | C,E | Y/O,O/H |

TABLE 5.3---*Continued*

| star | type | ref | [Fe/H] | ref | comments ^a |
|---------|----------|---------|--------------------------|------|-----------------------|
| GL338A | M0V | HKS | 0.08 | E | ... |
| GL328 | M0V | KHM | ... | ... | O/H,Y/O |
| GL846 | M0.5V | KMb | ... | ... | OD,YD |
| GL908 | M1V | KMb,HKS | -1 | KMb | OD,O/H |
| GL412A | M1V | HKS | -0.19 | E | OD,OD |
| GL411 | M2V,M2+V | HKS,KMb | -0.2, -0.07 ^b | C,E | KH,OD,O/H |
| GL625 | M1.5V | HKS | ... | ... | YD,OD |
| GL104 | M2 | RHG | ... | ... | ... |
| GL382 | M2V | KHM | 0.46 | E | YD,YD |
| GL352AB | M3V | KHM | ... | ... | Y/O,OD |
| GL436 | M3V | KHM | 0.18 | E | OD,Y/O |
| GL752A | M3V | KHM | 0.41 | E | OD,Y/O |
| GL725A | M3V | KHM | -0.08 | E | Y/O,O/H |
| GL725B | M3.5V | KHM | -0.15 | E | Y/O,O/H |
| GL896A | M3.5V | HKS | ... | ... | YD,YD |
| GL402 | M4V | HKS | ... | ... | Y/O,YD |
| GL406 | M6V | HKS | ... | ... | Wolf 359,OD,NA |
| GL644C | M7V | KHM | ... | ... | OD,NA |
| GL752B | M8V | KHM | -0.8 | E | OD,NA |
| HR6014 | K1.5IV | KMb | ... | ... | ... |
| HR8905 | F8III | MAT | ... | ... | KH, ν Peg |
| HR4883 | G0IIIp | KMb | ... | ... | KH,31 Com |
| HR6608 | G2IIIb | KMb | ... | ... | KH,84 Her |
| HR3323 | G5IIIa | KMa | -0.02, 0.03 | C,BG | KH,o U Ma |

TABLE 5.3—*Continued*

| star | type | ref | [Fe/H] | ref | comments ^a |
|----------|----------|-----|--|-------------|-----------------------|
| HR4932 | G8IIIab | KMb | −0.15, 0.04, −0.03, −0.15, 0.02 0.04, −0.1, −0.06, 0.0, −0.02 0.17, −0.05, 0.21, −0.08 | C C C | KH,ε Vir |
| HR8694 | K0III− | KMb | 0.09, 0.14 | C | KH,ι Cep |
| HR6299 | K2III | KMb | 0.07, −0.06 | C | KH,κ Oph |
| HR7806 | K2.5III | KMb | −0.5 | KMa | KH,39 Cyg |
| HR6705 | K5III | KMb | 0.33 | C | KH,γ Dra |
| HR7635 | M0III− | KMb | ... | ... | KH,γ Sge |
| HR8284 | M1IIIab | KMb | ... | ... | KH,75 Cyg |
| HR45 | M2III+ | KMb | ... | ... | KH,ξ Peg |
| HR7157 | M5IIIvar | KMa | ... | ... | KH,R Lyr |
| HD108849 | M7III− | KMb | ... | ... | KH,BK Vir |
| HD114961 | M7III | KMb | ... | ... | KH,SW Vir |

^aNames used in Kleinmann & Hall (1986) are given. KH indicates spectra taken from Kleinmann & Hall. Kinematic and photometric populations from Legget (1992): YD=young disk, OD=old disk, Y/O=young-old disk, O/H=old-disk/halo.

^bInfrared spectra of Jones et al. (1996) and Wallace & Hinkle (1996) indicate a much lower metallicity.

NOTE.—KMa=Keenan & McNeil (1976); MAT=Morgan, Abt, & Tapscott (1978); L=Laird (1985); Bell & Gustafsson (1989); KMb=Keenan & McNeil (1989); KHM=Kirkpatrick, Henry, & McCarthy (1991); C=Cayrel de Strobel et al. (1992); HKS=Henry, Kirkpatrick, & Simons (1994); WG=Wyse & Gilmore (1995); E=Eggen (1996); RHG=Ried, Hawley, & Gizis (1996); G=Gonzalez et al. (1997).

Table 5.4. Components of Composite Spectra

| type | component stars |
|--------|----------------------|
| F9V | HR7162 |
| G1.5V | HR7503 |
| G3V | HR7504 |
| G4V | HR5072+HR8631+HR7260 |
| K0V | HR511+HR7368 |
| K1V | HR493 |
| K2V | HD109011+HD184467 |
| K3V | HD160346+HR8832 |
| K5V | HR8085+HD196795 |
| K7V | HR8086+GL338B+GL673 |
| M0.5V | GL846 |
| M2V | GL104 |
| M3V | GL352AB+GL436+GL896A |
| M4V | GL402 |
| M6V | GL406 |
| M7V | GL644C |
| M8V | GL752B |
| K1.5IV | HR6014 |
| F8III | HR8905 |
| G0III | HR4883 |
| G2III | HR6608 |
| G5III | HR3323 |
| G8III | HR4932 |
| K0III | HR8694 |
| K2III | HR6299 |
| K5III | HR6705 |
| M0III | HR7635 |
| M1III | HR8284 |
| M2III | HR45 |
| M5III | HR7157 |
| M7III | HD108849+HD114961 |

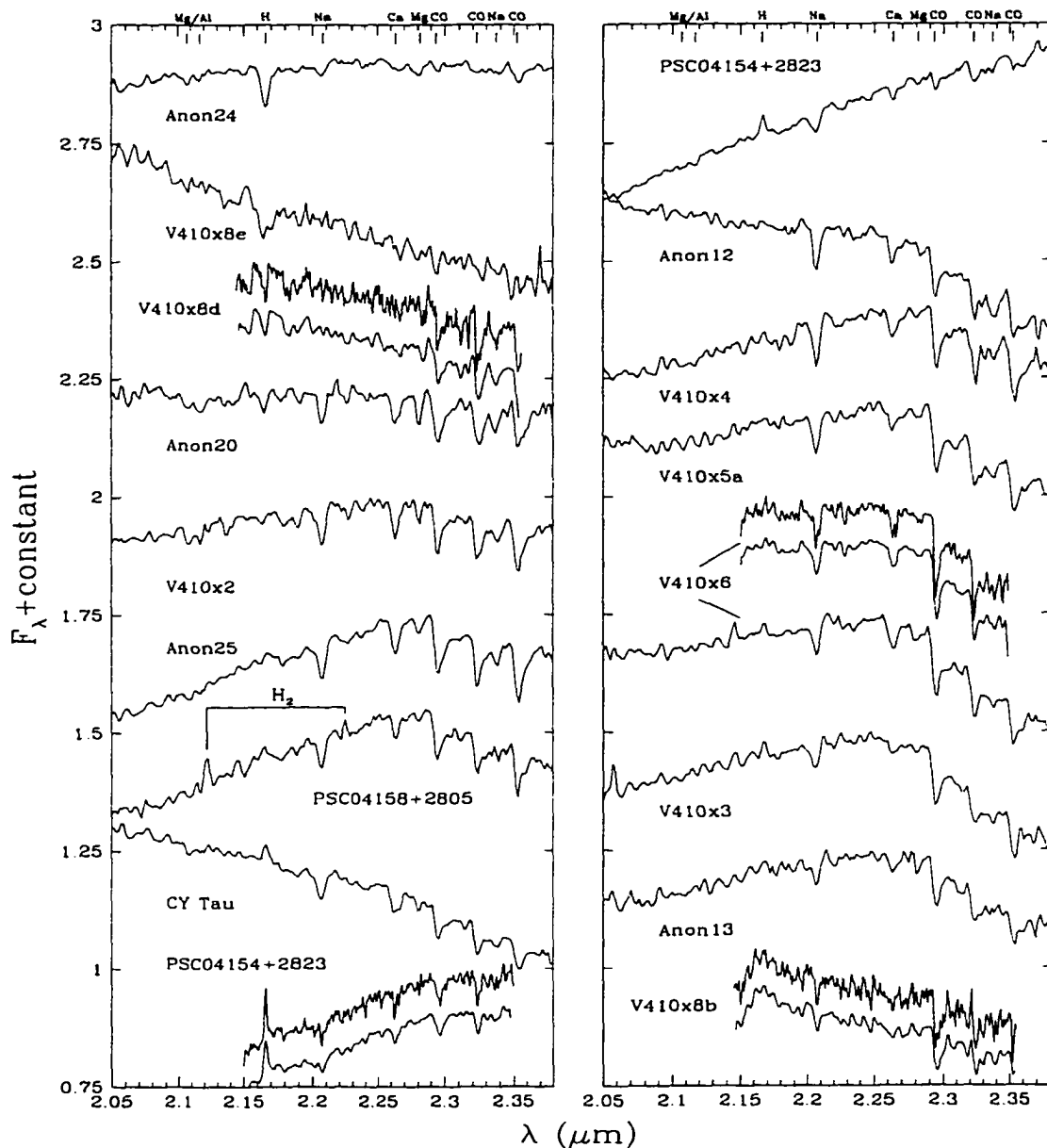


Figure 5.1 K -band spectra of sources in L1495E from earlier (upper right) to later (lower right) IR spectral types. The spectra are normalized at $2.2 \mu\text{m}$ and offset by additive amounts. For V410x8d, PSC04154+2823, V410x5a, and V410x8b, the original spectrum at $R = 1200$ (upper) and a version smoothed to $R = 800$ (lower) are shown. All other spectra were observed at $R = 800$.

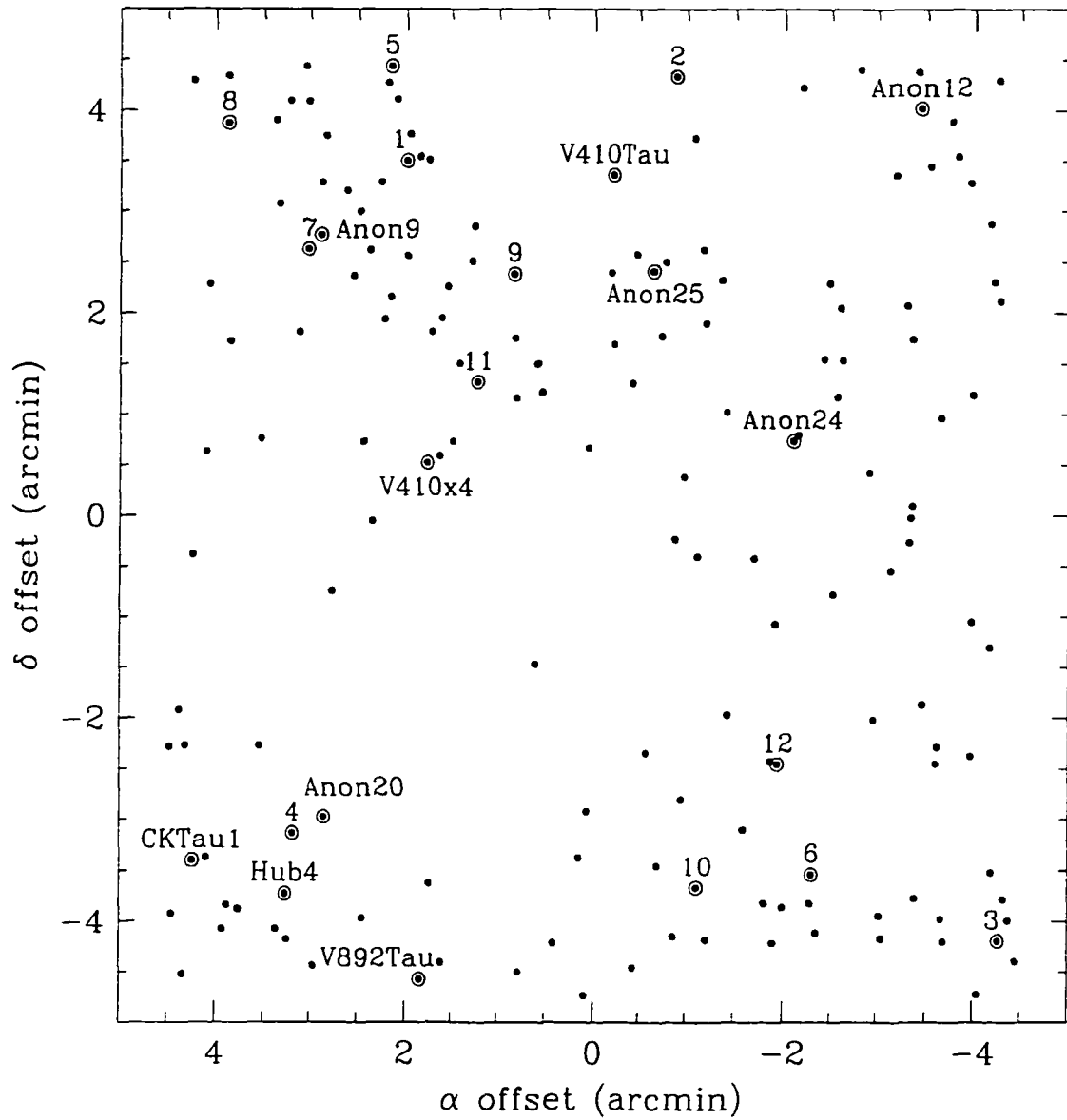


Figure 5.2 The finding chart for the *K*-band image of L1495E. The origin corresponds to $\alpha = 4^{\text{h}}15^{\text{m}}26^{\text{s}}.1$, $\delta = 28^{\circ}16'38''$ (1950). Number identifications refer to sources in Table 5.2 which appear as labeled, unshaded boxes in Figure 5.7.

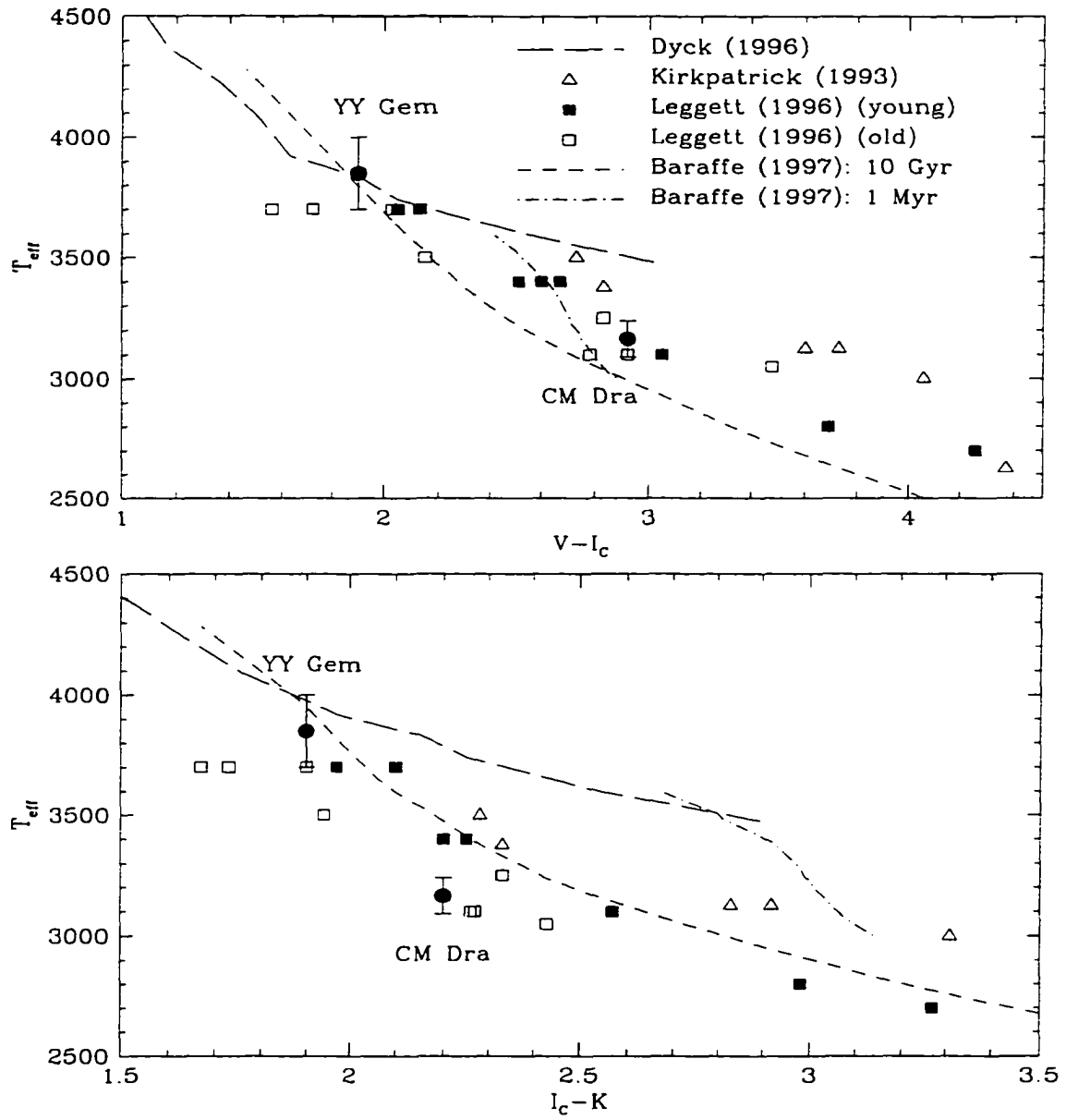


Figure 5.3 Recent temperature scales for cool stars. T_{eff} measurements for YY Gem and CM Dra are indicated by the error bars.

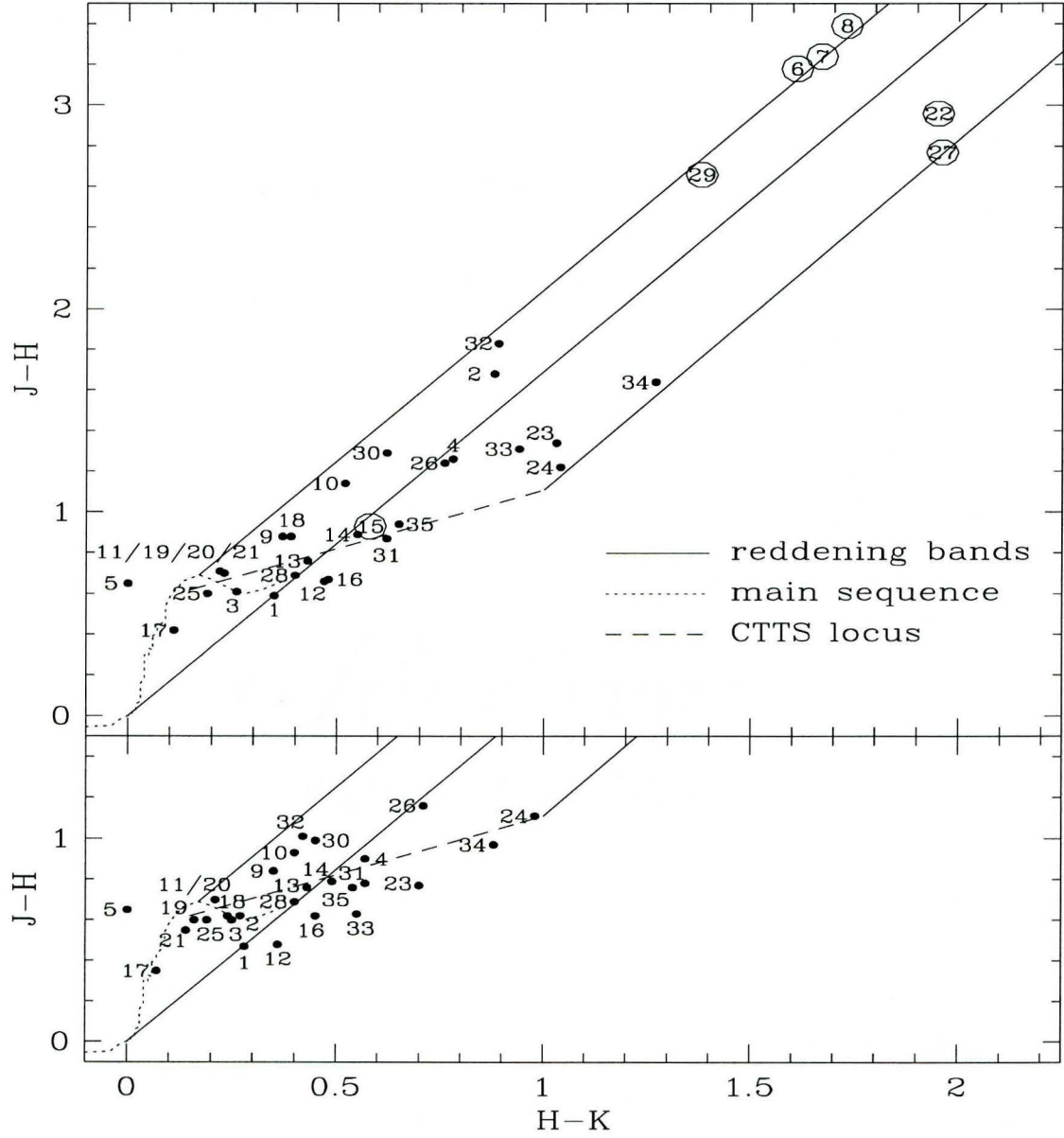


Figure 5.4 $H - K$ vs. $J - H$ of the entire spectroscopic population of L1495E (upper panel). Number designations are from Table 5.1. The circles indicate sources without optical photometry. After correcting the IR colors for the extinction derived from $E(R - I)$, the sources scatter around the classical T Tauri locus (CTTS) (lower panel).

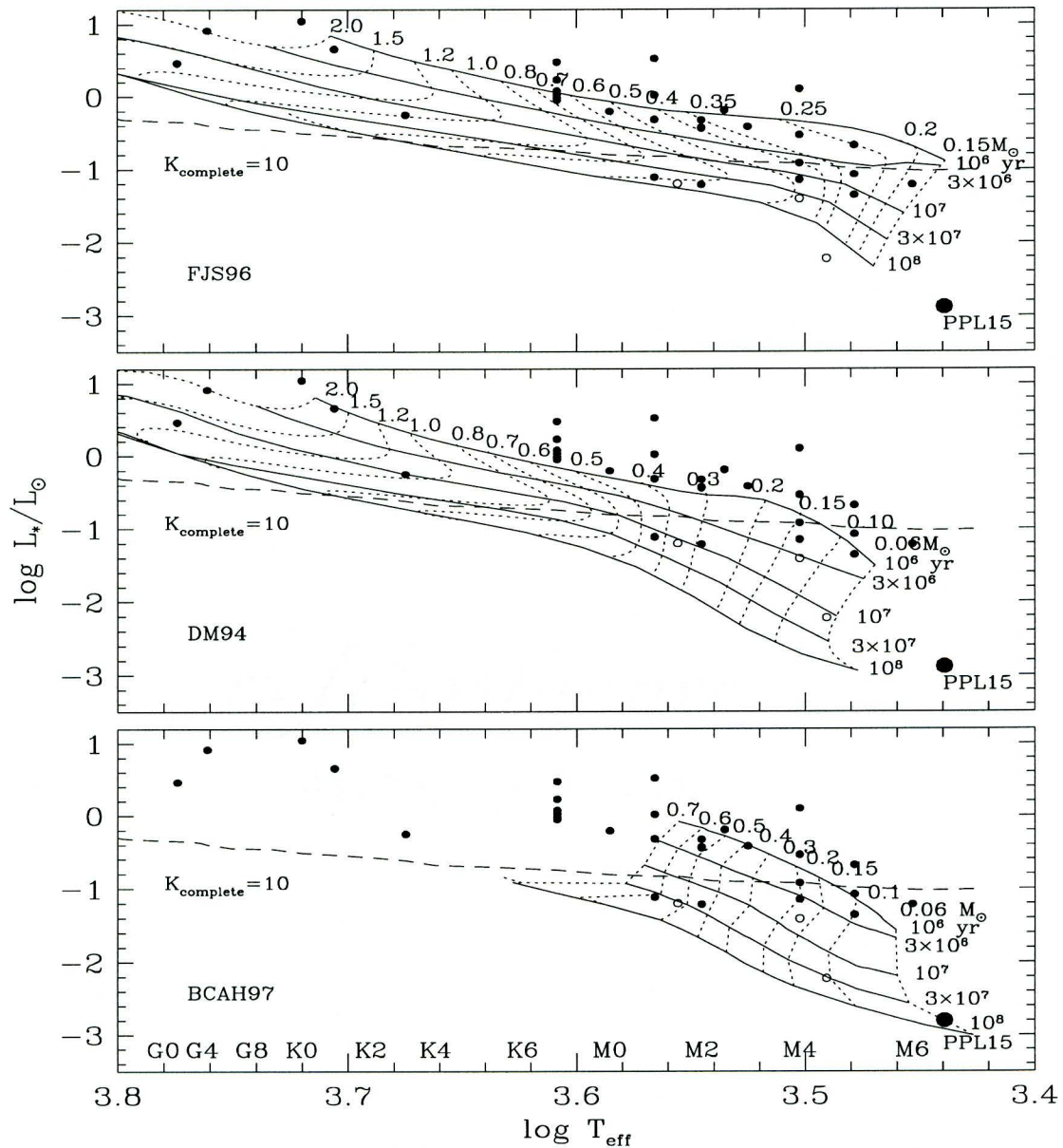


Figure 5.5 The H-R diagram of L1495E with tracks of FJS, DM94, and BCAH97. The Pleiades source PPL 15 (M6.5) is shown for reference. The Leggett et al. (1996) spectral type- T_{eff} scale for dwarfs is given on the bottom of the plot. The dashed line represents the completeness limit at dereddened $K = 10$. Open circles are probable foreground stars (Anon3, 12, 17).

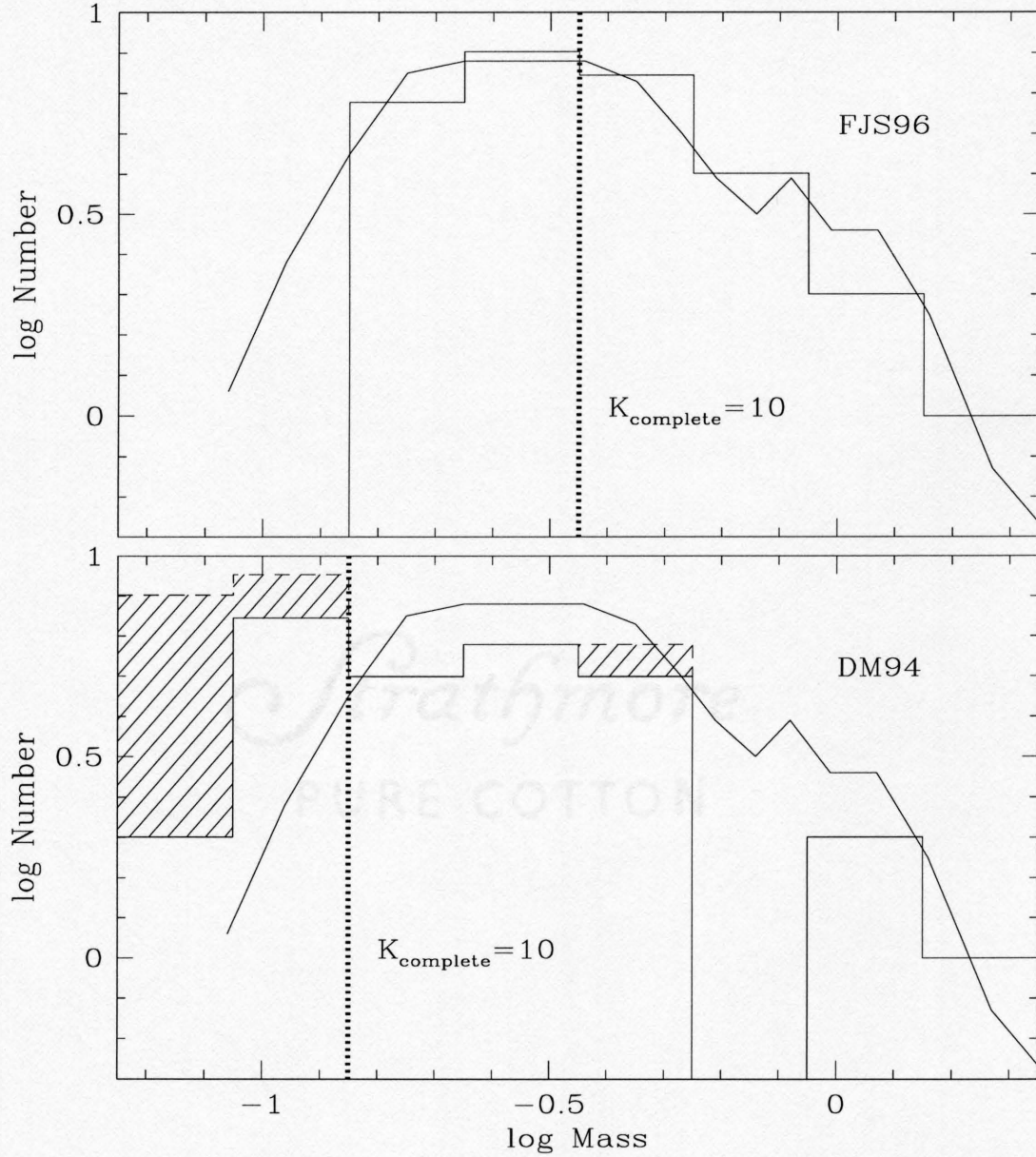


Figure 5.6 The solid histograms are the IMFs derived from the spectroscopic sample with the tracks of FJS and DM94. The mass completeness limit corresponding to a completeness of $K_{\text{dereddened}} = 10$ is given for each set of tracks. We have estimated a completeness correction for the IMF derived from DM94, shown as the shaded areas. No completeness correction was attempted for the FJS IMF. For reference, the field IMF of Scalo (1986) is also given as the solid curve.

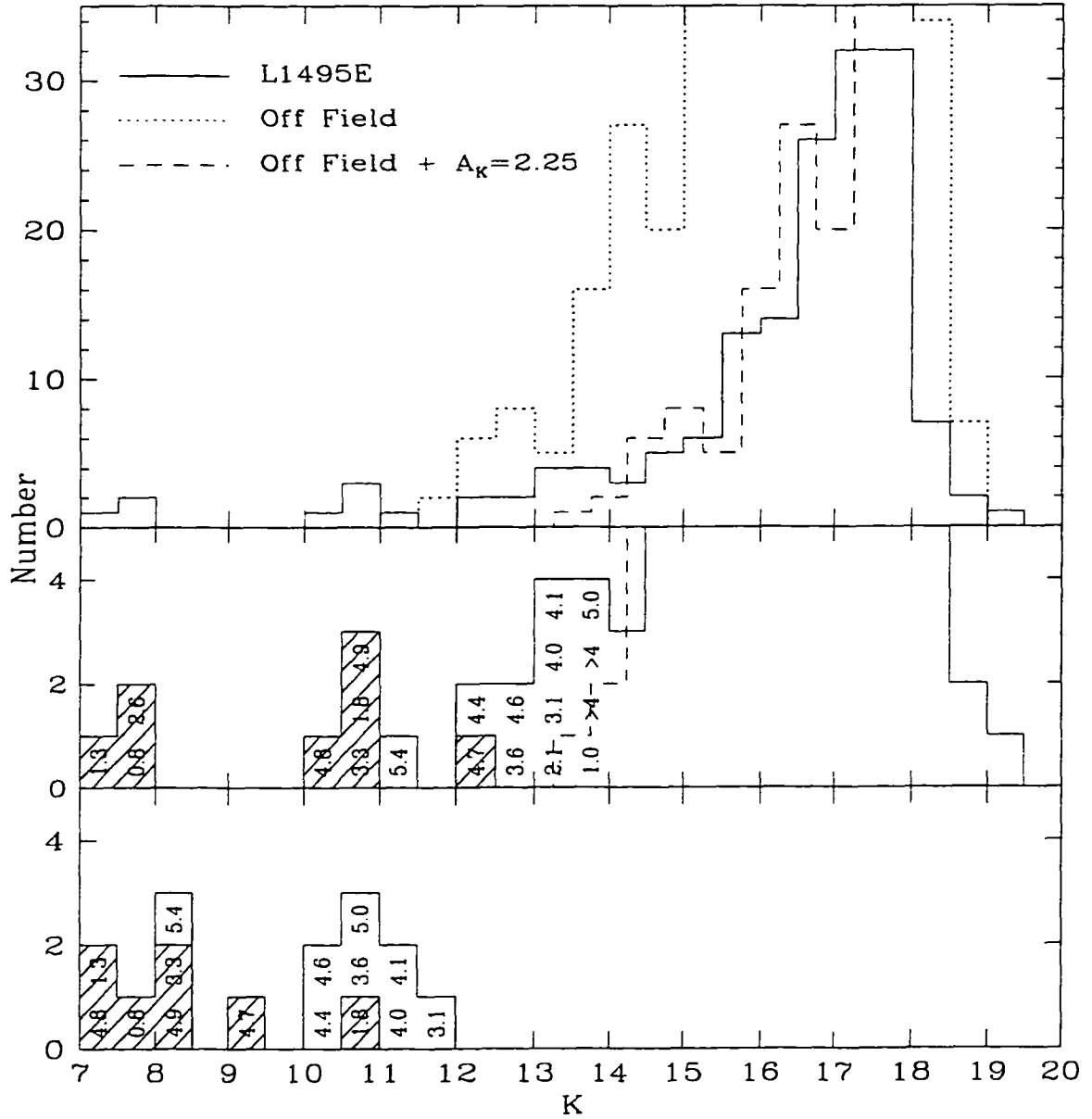


Figure 5.7 K -band luminosity function toward the region of L1495E presented in Figure 5.2 and a nearby off-field location of the same size. Note that V892 Tau ($K = 5.64$) does not fall within the boundaries of this plot. Sources falling above the reddened background are labeled with $J - K$. Shaded boxes indicate stars with spectroscopy. Anon 12 is not shown since it is probably a foreground star. The histogram after dereddening of the sources is given in the lower panel.

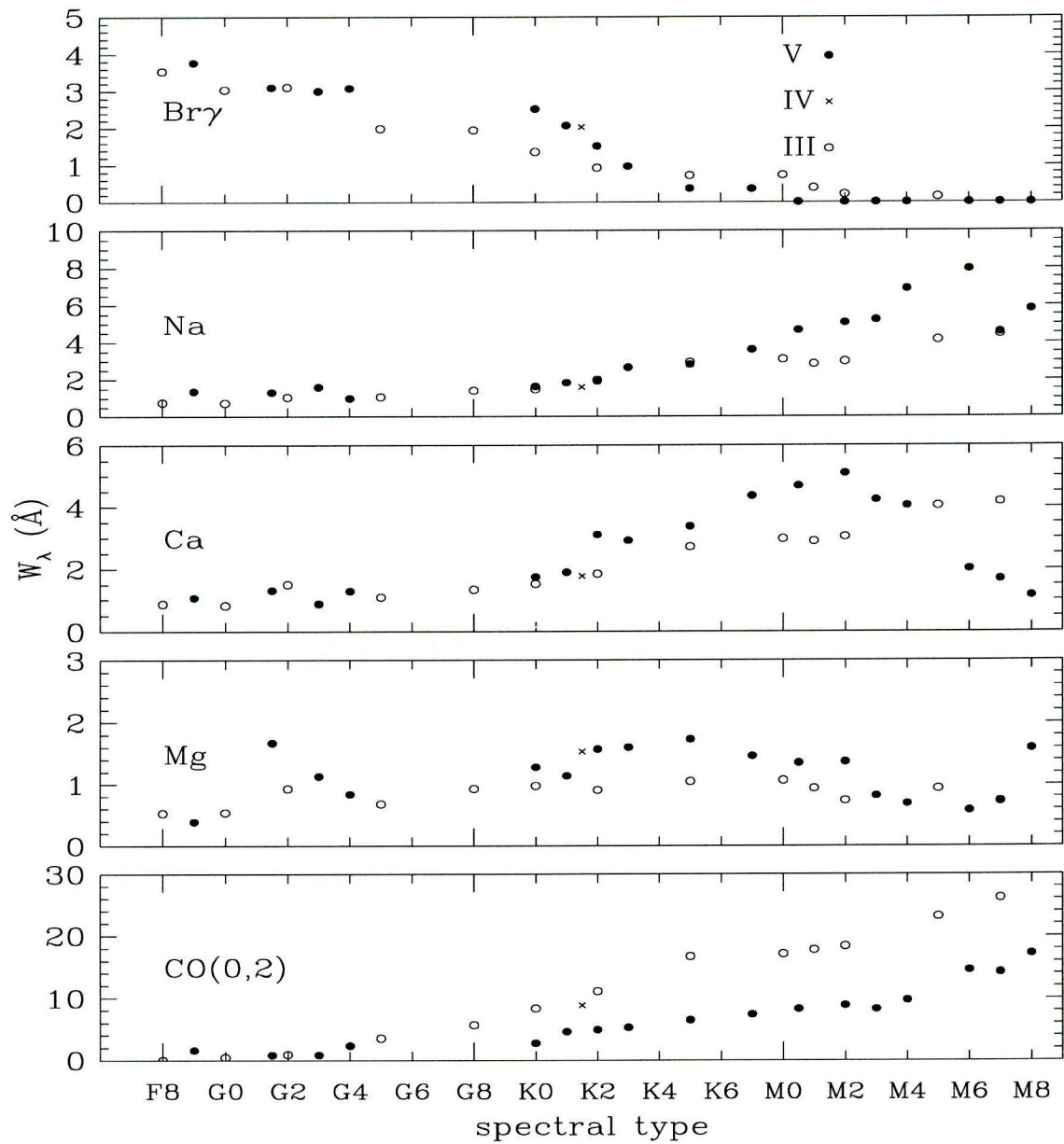


Figure 5.8 Equivalent widths of the prominent K -band absorption features measured from $R = 1200$ spectra of (approximately) solar-metallicity composite dwarfs and giants.

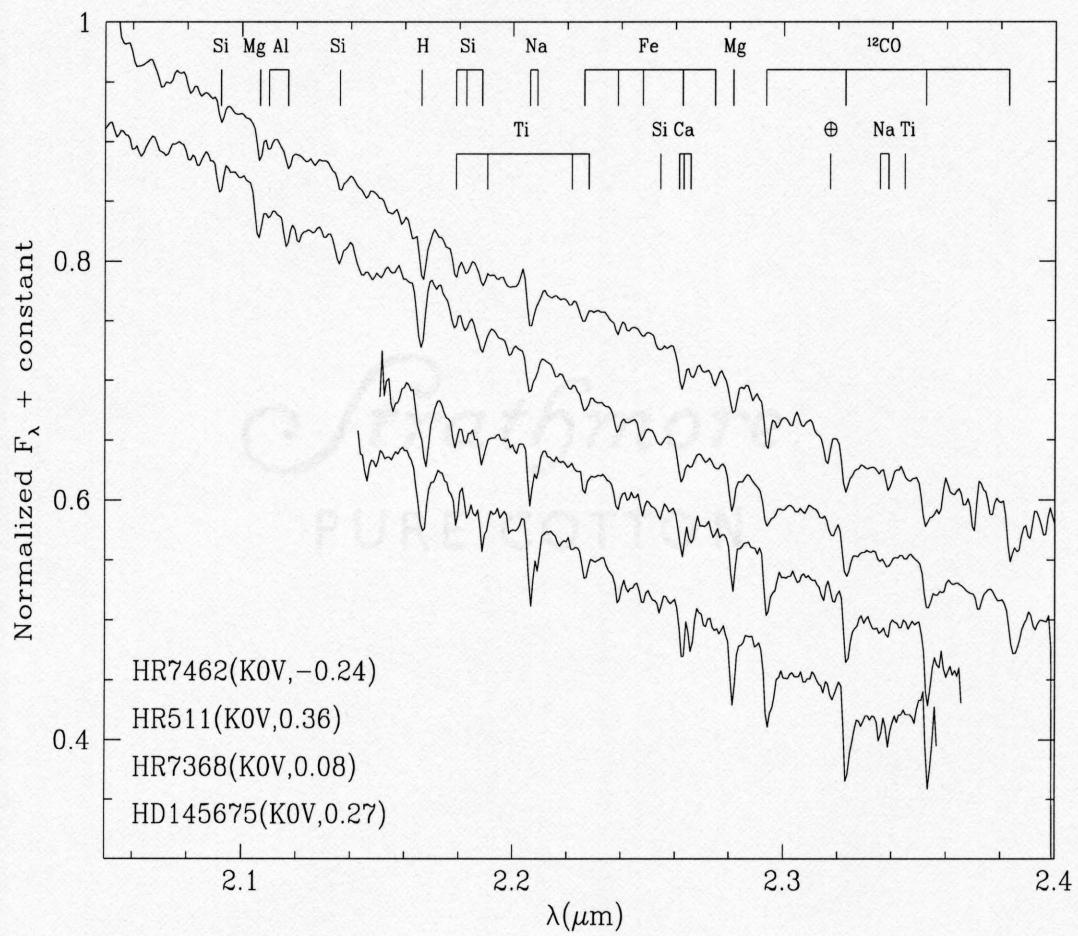


Figure 5.9 *K*-band spectra of K0V stars.

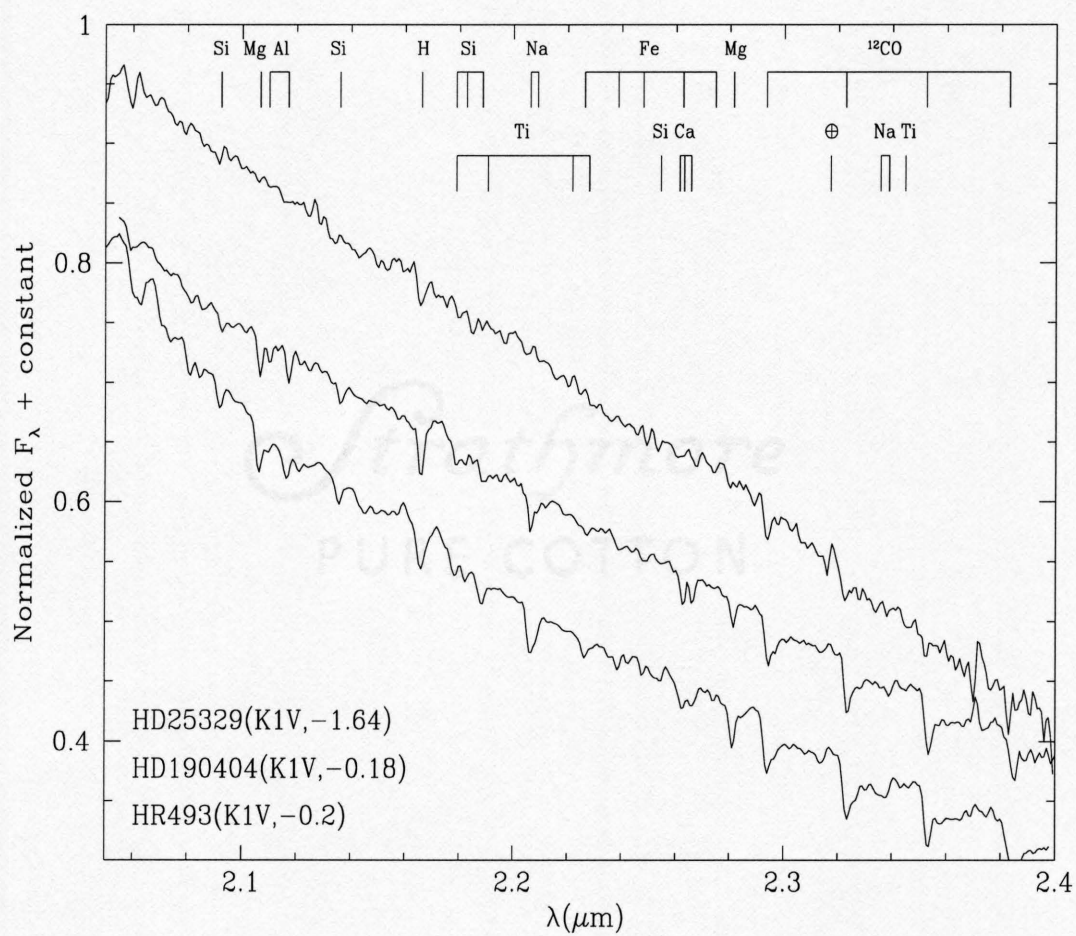


Figure 5.10 *K*-band spectra of K1V stars.

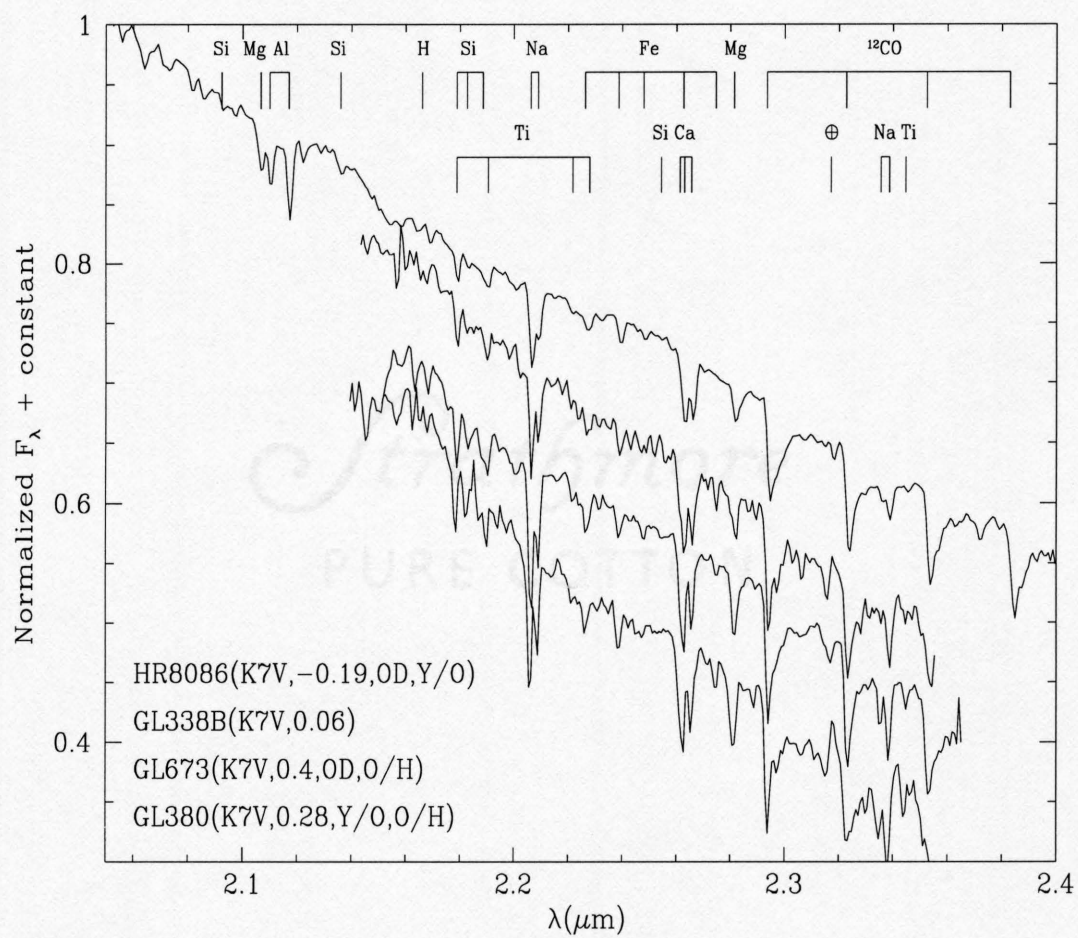


Figure 5.11 *K*-band spectra of K7V stars.

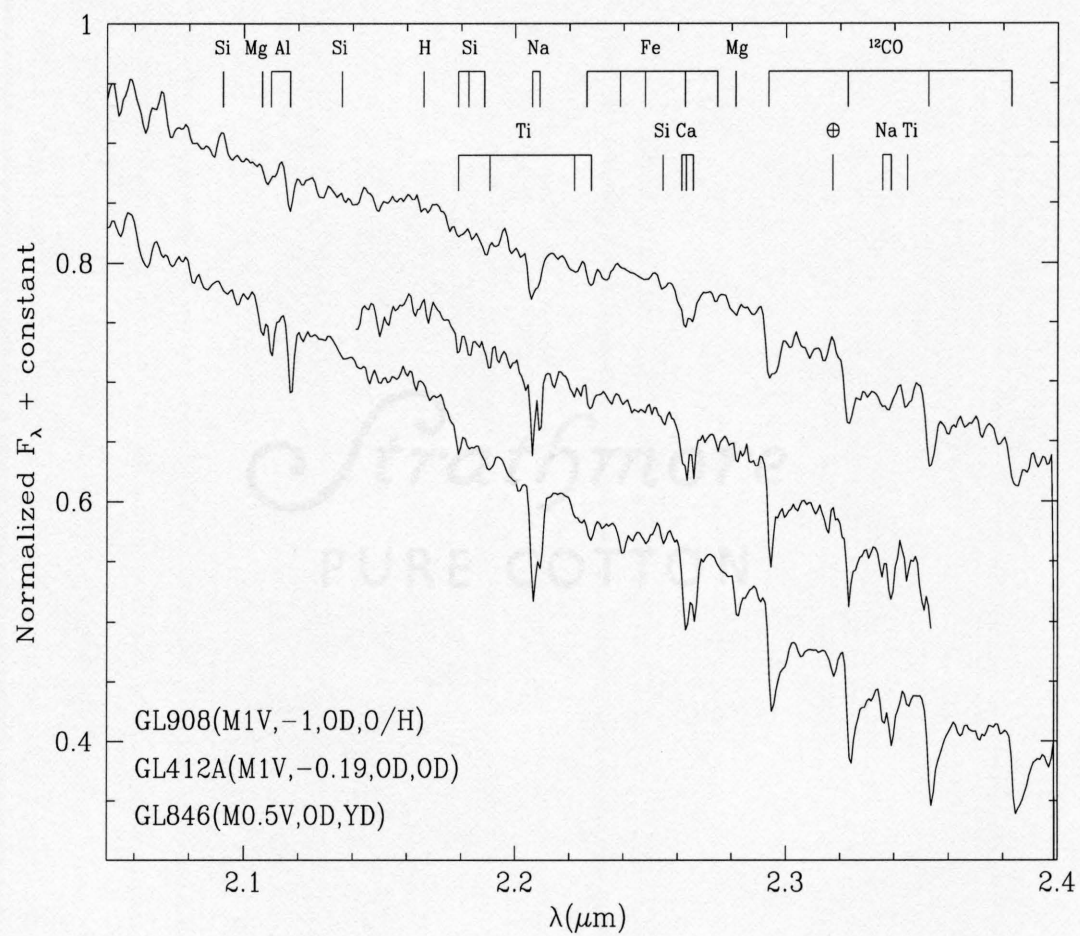


Figure 5.12 *K*-band spectra of M1V stars.

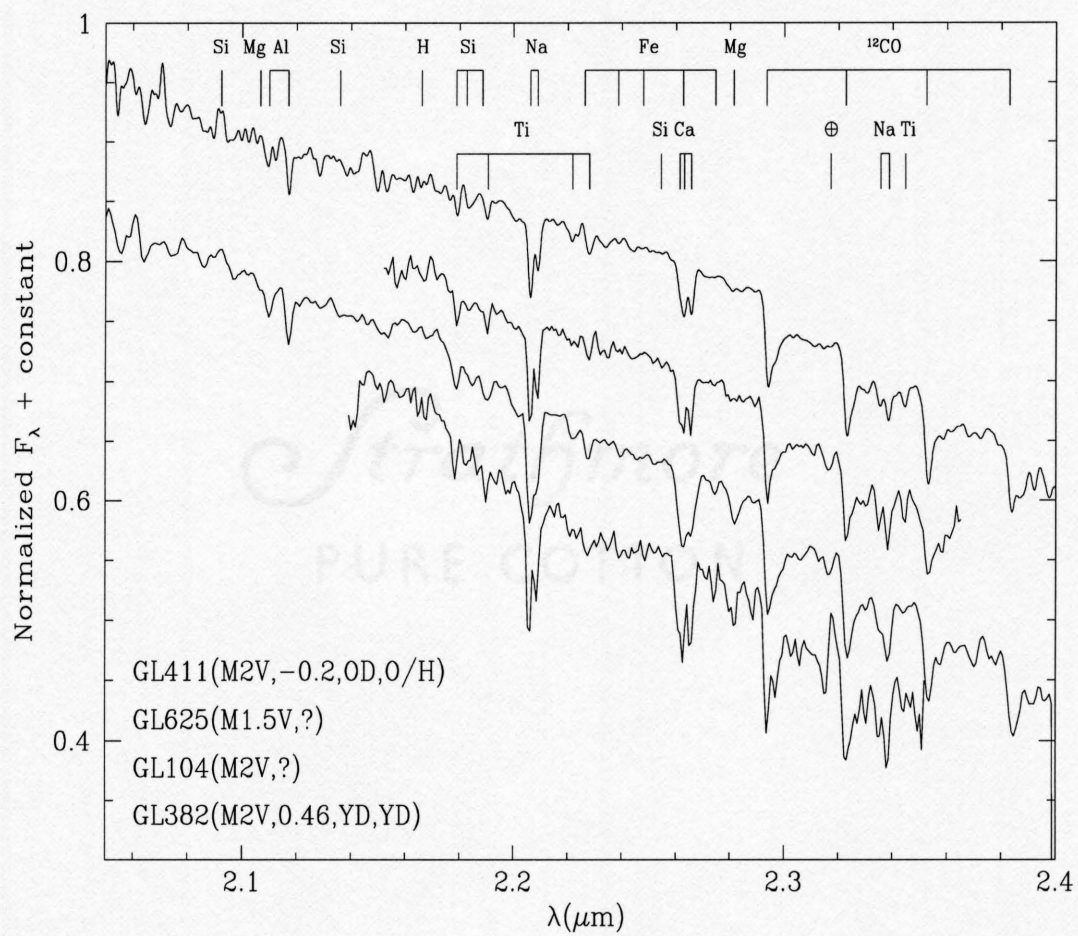


Figure 5.13 *K*-band spectra of M2V stars.

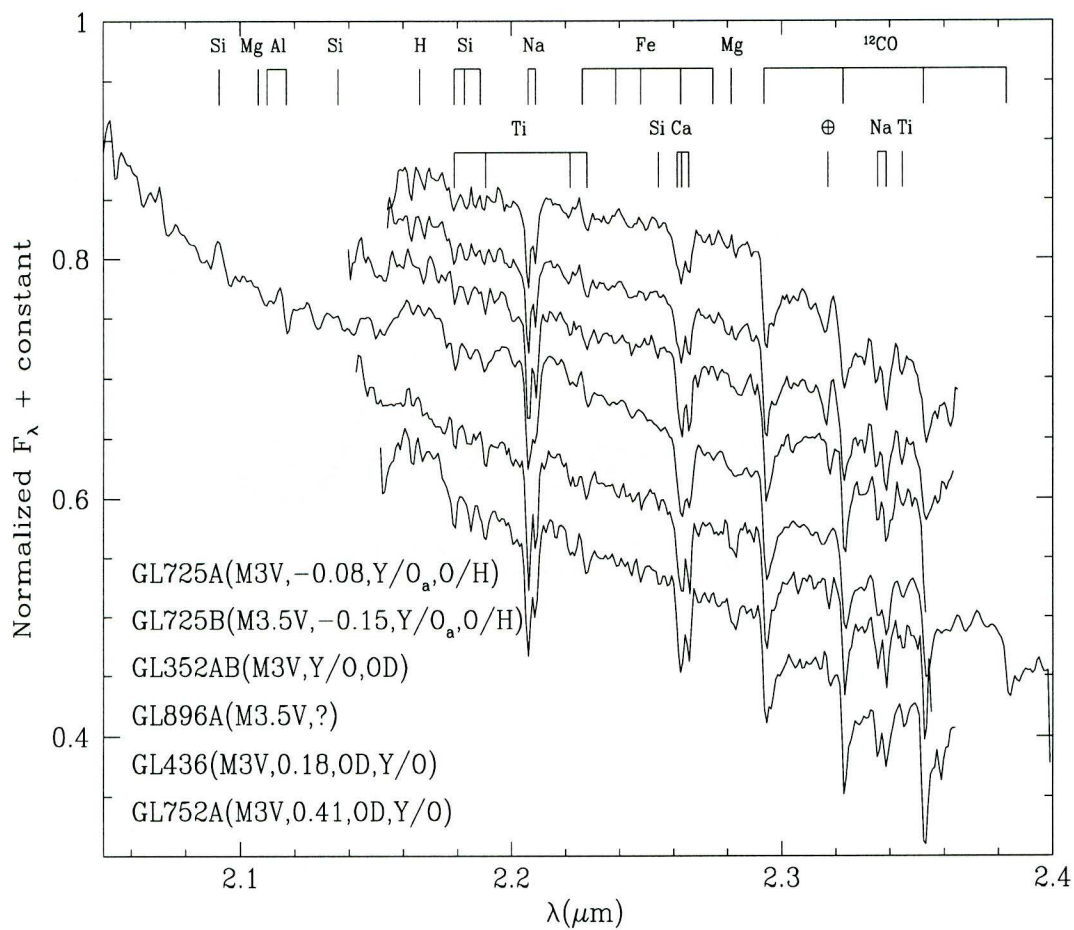


Figure 5.14 *K*-band spectra of M3V stars.

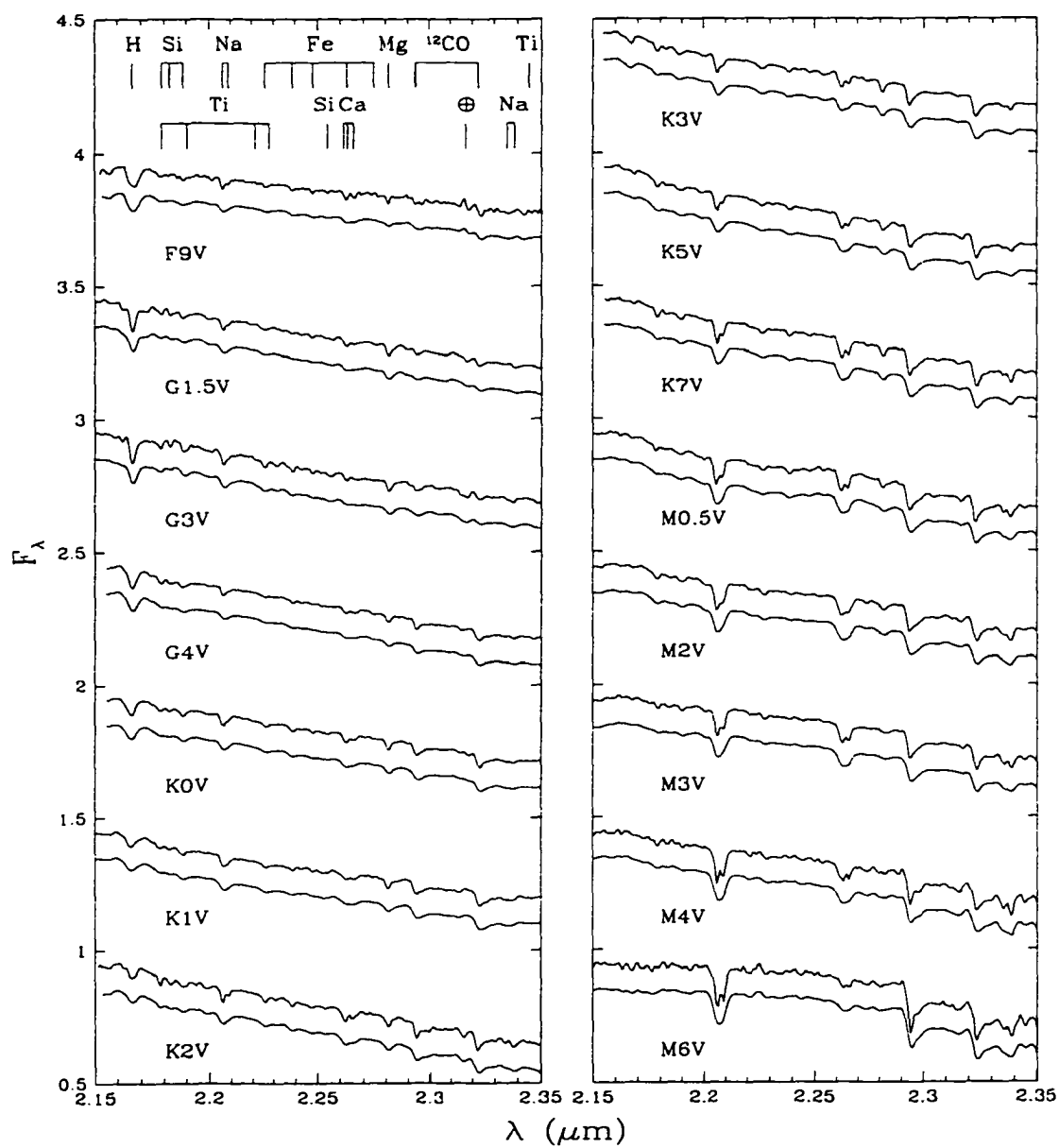


Figure 5.15 Composite standard spectra for K -band classification at $R = 800$ (lower) and $R = 1200$ (upper).

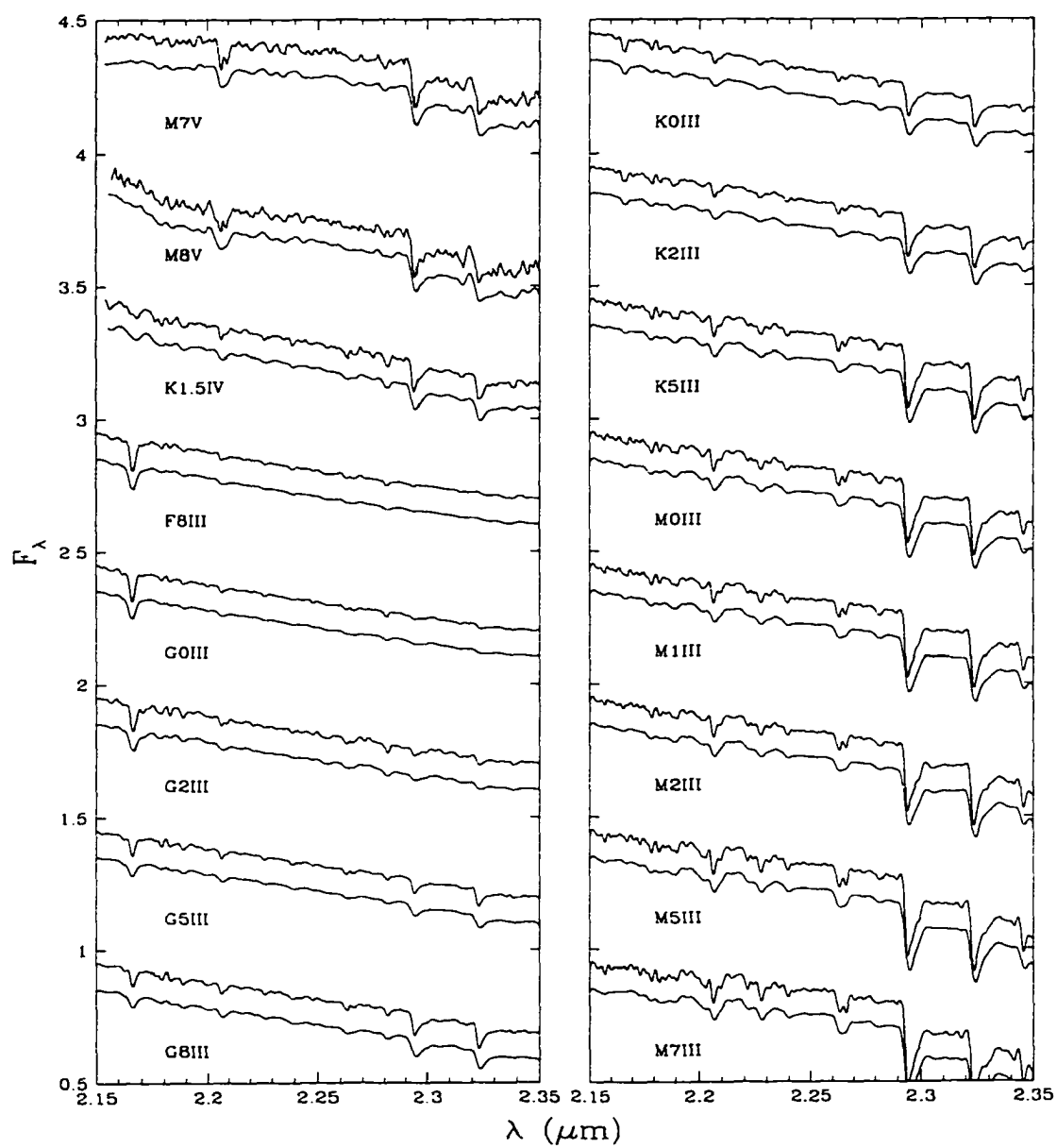


Figure 5.16 Composite standard spectra for K -band classification at $R = 800$ (lower) and $R = 1200$ (upper).

CHAPTER 6

IC 348

6.1. Introduction

A combination of optical and near-IR observations is required to obtain a deep and unbiased stellar census of young clusters. In § 5 I obtained IR spectra and photometry towards L1495E, which I used to complement the optical and X-ray observations of SS94. This study demonstrated techniques for combining spectroscopy and imaging in both the optical and IR to obtain a thorough understanding of the stellar population. The young (≤ 10 Myr), nearby ($d = 300$ pc) cluster IC 348, within the Perseus complex, is an ideal target in which to extend these techniques. It has been observed through proper motion measurements (Fredrick 1956), spectroscopy and photometry (Gingrich 1922; Harris, Morgan, & Roman 1954; Strom, Strom, & Carrasco 1974), IR imaging (Lada & Lada 1995), and deep ROSAT pointings (Preibisch, Zinnecker, & Herbig 1996).

Therefore, I have obtained optical and K -band spectra of more than 100 stars

in IC 348, with emphasis on the $5' \times 5'$ core where my spectroscopic sample is complete to $K = 12.5$ and $\sim 50\%$ complete to $K = 14.5$. I have also imaged the cluster and a nearby off field to a limit of $K \sim 16.5$. An independent and comparably extensive optical study of this cluster has recently become available (Herbig 1998; hereafter H98), along with improved theoretical models of young, low-mass stars and brown dwarfs (D'Antona & Mazzitelli 1997; hereafter DM97). I use this extensive database to achieve a broad overview of the star formation occurring in this cluster, including the star formation history, circumstellar disk lifetimes, the shape of the low-mass IMF, and the spectroscopic identification of young brown dwarfs. Finally, I discuss the IMF in IC 348 in the context of recent results in the field and in other young clusters. The following work has been in collaboration with C. Lada and E. Lada.

6.2. Observations

I performed K -band spectroscopy on sources in IC 348 using the near-IR long-slit spectrometer FSpec (Williams et al. 1993) at the Steward 2.3 m Bok Reflector on Kitt Peak on 1995 December 2-4 and at the Multiple Mirror Telescope (MMT) on Mount Hopkins on 1995 November 3-9 and 1996 October 24 and 29. I used an IR camera to guide off the slit, providing positive identification of each object observed. Sources were stepped through six positions along a $2''.4 \times 90''$ slit at the Bok Reflector and four positions along a $1''.2 \times 30''$ slit at the MMT. These apertures correspond to 2×75 and 2.5×75 pixels, respectively, on the detector array. At each position along the slit, the integration times ranged between 5 and 120 s. At one grating setting, I obtained a spectrum extending from 2.0 to $2.4 \mu\text{m}$ with a two-pixel resolution of $R = \lambda/\Delta\lambda = 800$. During the observations in 1996, I

obtained a few follow-up spectra with a new grating which provided $R = 1200$.

In addition to the sources in IC 348, I observed an A0 V star (HR 1019) every ~ 20 minutes during the night. At $R \sim 1000$, A stars are featureless across the entire K band except for absorption in $\text{Br}\gamma$ ($2.166 \mu\text{m}$), thus making excellent standards to correct telluric absorptions. Following a few of the A0 V star observations each night, I also obtained a spectrum of a G0 V star (HR 1489). The solar spectrum was used to remove the $\text{Br}\gamma$ absorption in the G0 V star and with the resulting spectrum I corrected the atmospheric absorption near $\text{Br}\gamma$ in the A0 V spectrum. I then derived the intrinsic profile of $\text{Br}\gamma$ absorption in the A0 V and used it to remove $\text{Br}\gamma$ from all of the standard spectra. These modified A0 V star spectra served as telluric-correction standards across the entire K band. If a G star alone is used to correct telluric absorptions (Maiolino, Rieke, & Rieke 1996), it needs to have nearly solar metallicity for accurate correction of the photospheric features with the solar spectrum.

IRAF routines and customized scripts within this environment were used to reduce the data. After dark subtraction and flat-fielding, adjacent images along the slit were subtracted from each other to remove sky emission. The sky-subtracted images were aligned and combined, during which most transient bad pixels (e.g., cosmic rays) were rejected. A spectrum was extracted from this final image, divided by the extracted A0 V standard spectrum, and wavelength calibrated using OH airglow lines. The intrinsic spectral slope of the standard was removed with an artificial blackbody spectrum of $T_{\text{eff}} = 10000 \text{ K}$.

I selected for IR spectroscopy the 75 sources from the IR imaging of Lada & Lada (1995) with $K \leq 12.5$ and falling within a $5' \times 5'$ region centered on the cluster as defined by the boundaries of $\alpha = 3^{\text{h}}41^{\text{m}}13^{\text{s}}.2, 36^{\text{s}}.8$ and $\delta = 31^{\circ}58'0''$,

32°3'0" (1950). In addition, as time permitted, I observed the 29 brightest sources ($K \lesssim 10$) in the remaining outer regions of IC 348. These spectra are presented in Figs. 6.1-6.4, in order of IR spectral type. Since I cannot classify the early-type stars ($< G0$) in the K -band, the spectra for these sources are ordered by optical types. Spectra from my network of standard stars (see § 5) and data for V410 X-ray 3 in L1495E are also given. The latter star was useful in classifying stars in IC 348 since it is one of a few young (~ 1 Myr old), late-type sources discovered to date (M6; SS94; § 3).

I obtained optical spectra of sources in IC 348 with the Boller and Chivens Spectrometer at the Bok Reflector on 1995 January 11-12 and 1996 November 6-7. I used the 400 g mm⁻¹ grating ($\lambda_{\text{blaze}} = 7506 \text{ \AA}$) to obtain spectra from 5600 to 9000 Å with $\Delta\lambda = 6 \text{ \AA}$ and integration times between 5 and 1800 s. To derive the sensitivity function of the array, I observed Hiltner 102, a star whose intrinsic spectral distribution is known. The spectra were extracted from bias-subtracted frames, corrected for the sensitivity function, and wavelength calibrated with He-Ar and Fe-Ne lamp spectra. Fringing beyond 8000 Å could not be removed completely by flat-fielding the optical spectra and is apparent to varying degrees in the data. I obtained spectra of the optically brightest 70 sources in the IR imaging survey of Lada & Lada (1995), 53 of which have IR spectroscopy.

Additional optical spectroscopy was performed towards 18 of the faintest sources ($I = 16\text{-}18.5$) in the core of IC 348 using the Red Channel Spectrograph at the Multiple Mirror Telescope on Mt. Hopkins, on 1997 November 27-29. I used the 270 g mm⁻¹ grating ($\lambda_{\text{blaze}} = 7300 \text{ \AA}$) to obtain a spectrum from 5500 to 9500 Å. A 2" × 180" aperture was used, providing a spectral resolution of $\Delta\lambda = 18 \text{ \AA}$. One to four exposures of 1800 s were obtained for each source, which were combined

and smoothed to a resolution of $\Delta\lambda \sim 25 \text{ \AA}$. The spectra of the sources M6 and later are shown in Figs. 6.5 and 6.6.

Imaging was performed at the Bok Reflector on the nights of 1995 December 8 and 10 using the Steward Observatory NICMOS3 256×256 near-IR camera at a plate scale of $0''.64 \text{ pixel}^{-1}$, corresponding to a total field of $2'.7$ square. I observed a 2×2 grid of positions centered on the core of IC 348 at $\alpha = 3^{\text{h}}41^{\text{m}}25^{\text{s}}.0$, $\delta = 32^{\circ}0'30''$ (1950), where the positions were separated by $140''$. At each position, I obtained images with dithers of $8''$ in a 4×4 grid, facilitating efficient flat-fielding and removal of bad pixels. A flat field was constructed by median combining the 16 exposures at a given position. The integration times were 90, 30, and 30 s at J , H , and K , respectively. With the same dithering technique, I observed a background field of equal area at $\sim 1^{\circ}$ north of the cluster at J and K with integration times of 45 and 30 s. For calibration, I observed a photometric standard star, GL 105.5, periodically during the night. After dark-subtracting and flat-fielding the images, the 16 frames at a given position were shifted and combined into one image. The tasks DAOFIND and PHOT under the package APPHOT were used in measuring the stellar coordinates and extracting photometry. The density of stars was low enough that I could measure the background emission in an annulus around each star and subtract it from the photometry. The data were calibrated with the CIT photometry of GL 105.5 from Elias et al. (1982). Typical photometric errors are 0.05-0.1 mag at $K < 14$, which is the region of interest in the KLF. The regions of overlap between neighboring cells were $20''$ wide and typically contained several stars, facilitating alignment of the cells into one image. The on and off-cloud images are saturated at $K < 11$ -12 and the latter are complete to $K \sim 17.5$. Determining the completeness of the images towards IC 348 is problematic due to crowding and nebulosity, but incompleteness probably begins near $K \sim 16.5$.

Due to saturation of the brighter sources, this photometry was used only in the completeness correction in § 6.5.5. Colors, extinctions, and luminosities for the spectroscopic sample were calculated from the photometry of Lada & Lada (1995), which is given in Table 6.1.

6.3. Individual Source Characteristics

6.3.1. Spectral Types

IR Spectral Classification

A technique was developed in § 5 to use K -band spectra ($R \sim 1000$) to derive the spectral types and continuum veilings of young, late-type stars (~ 1 Myr, $>G0$). I have used the same method for the sources in IC 348, types for which are listed in Table 6.1 along with other spectroscopic properties ($W_\lambda(\text{Br}\gamma)$, r_K , CO enhancement). In § 6.7 I present a detailed description of the IR spectral classification of the sources in my sample.

For a given spectral type earlier than M4, the strength of Na absorption at $2.2 \mu\text{m}$ is roughly the same in dwarfs and giants (Green & Lada 1997). However, at later spectral types, Na is much stronger in dwarfs than in giants (§ 5) and therefore I might expect Na to deviate from dwarf strengths in pre-main-sequence stars, as observed for the M6 star V410 X-ray 3 in L1495E (§ 3). Indeed, I do find that Na is consistently weaker in the young stars later than M3 in IC 348 than observed in dwarfs of similar types. The source of this trend is not continuum veiling since the other absorption features (Ca, Mg, CO) match those of unveiled dwarfs. Greene & Meyer (1995) and Greene & Lada (1997) have found that the ratio of $[W_\lambda(\text{Na}) + W_\lambda(\text{Ca})]/W_\lambda(\text{CO})$ for young stars in ρ Oph and Taurus appears

intermediate between that of dwarfs and giants, which was attributed to enhanced CO absorption in the pre-main-sequence stars. In late-M stars, I suggest that much of this behavior is instead due to the weakening of Na with lower surface gravities. I also find that only five sources (49, 71, 74, 128, 252) in IC 348 clearly exhibit CO absorption more than 1.25 times that of a dwarf. In the H-R diagram in Figs. 6.7 and 6.8, these stars appear luminous and young but not systematically the most luminous of the sample. Interestingly, the sources with CO enhancement fall within the reddening band of the main sequence in Figure 6.9 and do not show signatures of disk activity.

Optical Spectral Classification

For the optical spectra, I used the spectral standards of Torres-Dodgen & Weaver (1993), Allen & Strom (1995), and J. D. Kirkpatrick (private communication) to classify the stars in a similar manner as Hillenbrand (1997). Details are provided in § 6.8. Since my constraints on the early types are generally consistent with those derived previously in the literature, I adopt the latter, more accurate types. While star 12 appeared as a single object in the IR data of Lada & Lada (1995), it is resolved into two stars (H139, H140) in the optical images of H98. I was not aware of the binarity at the time of the spectroscopic observations, therefore it is not clear whether I obtained spectra of one component or the composite system. Since H98 reports a spectral type of G0 for H139, for the analysis here I assume that the A type I measure applies to H140. In Table 6.1 I list the optical spectral types and measurements of $H\alpha$ emission. The uncertainties in $W_\lambda(H\alpha)$ are $\sigma \sim 0.3\text{-}0.5 \text{ \AA}$ for most stars, but are 10 \AA or more for the coolest objects where the measurement is highly sensitive to the placement of

the continuum.

Comparison of IR and Optical Classifications

The optical and IR spectral types derived in L1495E (§ 5) agreed to within one subclass for five of seven sources. For IC 348, I have the opportunity to perform a similar test in a much larger sample of young stars. Of 53 sources falling in both my optical and IR spectroscopic samples, 34 stars have both IR and optical types which are well-defined (not <F8 or >K5). For 28 of these stars, the two spectral types agree within the uncertainties while 6 do not. No systematic difference in types is apparent for these latter stars, which are as follows (optical, IR type): 32 (K8, K4-K7), 33 (M2, M4-M5), 65 (K7+, M2-M4), 100 (M1, M2-M4), 141 (M1, K5-M0), and 145 (M5, M2-M4).

When the optical classifications of H98 and the IR types are compared, I find a larger difference in spectral types. Of 45 stars which fall in both samples, 31 have precise spectral types where 17 of these agree within the uncertainties. The 14 stars with discordant types are as follows (H98, IR type): 35 (G8, K3-K6), 42 (H203) (M3, M4-M6), 52 (K6, M2-M4), 59 (G7, K2-K4), 75 (K8, M2-M4), 77 (M1, K5-M0), 83 (K8, M2-M4), 88 (M2, K6-M1), 91 (M1, M2-M4), 103 (K8, M1-M3), 151 (M3, K6-M1), 171 (M2, M3-M5), 217 (M3, M4-M6), and 252 (M4, M0-M3). For 10 of these 14 stars, I derive IR classifications which are later than the optical types of H98.

The final comparison is between the my optical classifications and those of H98. Excluding the binary systems (12, 24) and stars with uncertain spectral types (16, 38), the two optical classifications agree for 5 stars. For the remaining

discordant classifications, 2 stars have earlier spectral types in my data, 5 (K0, F8-G8) and 86 (M3, M2), while I derive later spectral types than those of H98 for 11 (H98, this work): 32 (K7, K8), 40 (K6, K8-M0), 59 (G7, G8-K2), 71 (M2, M3) 74 (M1, M2), 103 (K8, M2), 145 (M3, M5), 165 (M4, M5), 237 (M3, M5), 360 (M4, M5), and 413 (M4, M5). This systematic difference in optical spectral types may be due the reliance of H98 on a much smaller wavelength coverage (5800-7100 Å) in the spectral classification. A systematic error to earlier types on the part of H98 is suggested by my analysis of optical and IR colors in the derivation of extinctions in § 6.3.3.

In summary, my optical and IR spectral classifications agree for $\sim 80\%$ of the sample and differ by a few subclasses for the remaining sources. Both my IR and optical spectral types appear systematically later than the optical classifications of H98. Although optical classifications with the broad wavelength coverage used here are probably more accurate than IR types, I conclude both that my IR classifications are reliable and that the IR and optical classifications can be combined consistently in my study.

6.3.2. Substellar Members of IC 348

Objects at the age of IC 348 with spectral types later than M6 are likely to be substellar (§ 3). Previous studies of young clusters have frequently failed to locate any objects with spectral types later than M5 to M6 (e.g., SS94; Hartigan 1993). However, photometric studies have inferred the existence of numerous brown dwarfs (e.g., Comerón et al. 1993, 1996; § 5) Either young brown dwarfs are uncommon and some other phenomenon is appearing in the photometry, or the spectroscopic studies have been biased against these low-luminosity, cool objects.

I can distinguish these possibilities, since my IR selected sample in IC 348 is sensitive to objects with masses well below the stellar cutoff. Although the faintest sources I can distinguish from the background are beyond the reach of my IR spectral classification technique even on a 4 meter telescope, many of them are sufficiently lightly obscured that I have been able to obtain spectra in the far red (see Figs. 6.5 and 6.6). Virtually all the faint objects with spectroscopy that would be assigned brown dwarf candidacy from my photometry are indeed very cool and appear as substellar when placed on the H-R diagrams in Figs. 6.10 and 6.11. Previous spectroscopy of faint objects in ρ Oph has supported (Williams et al. 1995) or established (§ 4) the substellar nature of a number of faint sources. However, IC 348 is the first young cluster where a substantial portion of the apparent brown dwarf population has been confirmed unambiguously.

Accurate masses for young, late-M objects await observational tests, preferably in the form of spectroscopic binaries, of both the tracks and temperature scales at very young ages and cool temperatures. Without such data, the masses derived for these objects depend on the adopted set of evolutionary tracks and the choice of temperature scale. In the H-R diagrams shown here, I use the dwarf conversion of spectral types to effective temperatures described in § 4, which is an extrapolation of the Leggett et al. (1996) scale. The adoption of a temperature scale for giants, which is warmer by 100-200 K and may be partially applicable to pre-main-sequence stars, moves the late-M stars to higher masses on the evolutionary tracks. Although in § 4 used a temperature scale adjusted to higher temperatures to interpret the data for ρ Oph 2349.8 – 2601, here I instead apply the dwarf scale for late-type sources so that the same scale is used for all sources in IC 348. However, regardless of the choice of temperature scale or evolutionary tracks, at least 3 sources appear substellar.

6.3.3. Extinction

In the top panel of Figure 6.12 I show the $H - K$ versus $J - H$ diagram for all sources in my spectroscopic sample. The main sequence and CTTS locus are shown along with the reddening bands of each. The CTTS locus was derived using $E(R - I)$ to deredden 30 optically visible CTTS in Taurus (Meyer 1995) and has been successfully modeled as arising from star-disk systems (Lada & Adams 1992; Meyer, Calvet, & Hillenbrand 1997). With the exception of four sources with anomalously red $H - K$, the distribution of colors in IC 348 is indicative of a mixture of normal stars and CTTSs subject to extinction up to $A_V \sim 10$.

Using the reddenings measured from $E(R - I)$ for the CTTS ($W_\lambda(H\alpha) > 10 \text{ \AA}$) in my sample, I have calculated the intrinsic JHK colors of these sources, as illustrated in the color-color diagram in Figure 6.12. I also show the dereddened JHK colors of early-type stars with extinctions derived from optical photometry. Assuming that I have now corrected for all extinction towards each star, the positions on the diagram should reflect only the contribution of photospheric and circumstellar emission. We see that the dereddened positions of the CTTS in IC 348 are consistent with the CTTS locus. Most of the early-type stars appear to have roughly dwarflike JHK colors while a few show significant K -band excess emission, resembling Herbig Ae/Be stars. Star 5 falls intermediate between the CTTS locus and the region populated by Ae/Be stars, which is consistent with its G spectral type. In an optical study of WTTS in Taurus, Gullbring et al. (1998) found anomalous colors which were progressively redder from B to J with respect to colors of main sequence stars. However, I fail to find this trend or any other systematic color anomaly in the data for IC 348. Consequently, in this analysis I have assumed that the intrinsic colors, particularly $R - I$ and $J - H$, of young

stars are similar to those of main sequence stars.

It is often customary to use $E(R - I)$ in deriving extinctions for young stars (e.g., Meyer 1995; § 5). Trullols & Jordi (1997) reported deep $UBVRI$ photometry over much of the cluster, but their data produces anomalous extinction measurements. If I use my spectral classifications and calculate reddenings separately from $E(V - R)$ and $E(R - I)$, the values of A_J derived from the first color are systematically larger (0.2-1.3 mag) than those measured from the second color. The source of this trend is apparent when I compare the colors of Trullols & Jordi (1997) to those recently reported by H98. The $(R - I)_{\text{TJ}}$ color is systematically lower than $(R - I)_{\text{H98}}$, while the opposite behavior is seen to a lesser extent with $V - I$. Since the colors of Trullols & Jordi (1997) deviate most dramatically at large $R - I$ (by up to 2 magnitudes), it would appear that they used an inadequate color transformation to the Cousins photometric system for reddened, late-type stars.

Since the photometric sample of Trullols & Jordi (1997) is more complete than that of H98 for sources earlier than K0 and the anomalous extinction estimates do not appear in the former data set for these types, I have computed extinctions for them by dereddening $(V - I)_{\text{TJ}}$ to the standard dwarf colors corresponding to the adopted spectral types in Table 6.1. Extinctions for early-type stars without optical photometry are derived in the same manner but with $E(J - H)$ and the IR photometry of Lada & Lada (1995). For spectral types of K0 and later where the photometry at V is more uncertain, I have dereddened $(R - I)_{\text{H98}}$ to the main sequence colors to arrive at extinction estimates. When optical photometry was not available, I used $J - H$ and dereddened to the main sequence or to the CTTS locus ($A_J = 2.63[(J - H) - (J - H)_{\text{CTTS}}]$) when the stars fell within or to the

right of the reddening band of the main sequence. Since the three objects later than M6 are quite faint ($I > 18$), I have used the most accurate color, $I - K$, to calculate the extinctions. The presence of K -band excess emission could lead to an overestimate of extinctions, but no such emission is obvious for these three objects in the IR color-color diagram and the reddenings I calculate are small.

For ~ 20 stars, the reddenings from $R - I$ imply intrinsic colors of $J - H$ which are bluer than the main sequence values by more than 0.2 mag. This discrepancy indicates that either the intrinsic IR colors are bluer than those of main sequence stars, or the optical colors are redder. Whereas no mechanism is obvious for the source of the first proposition, red optical colors could be due to cool companions. The source of this anomaly may also be the adopted spectral types. There were eight stars for which I had no optical spectra and uncertain IR classifications. I therefore adopted the optical spectral types of H98 and found that all of these stars exhibit optical colors which are too red relative to the spectral type and IR colors. In light of the results in § 6.3.1 where I found my optical types to be later than those of H98 by 1-2 subclasses, this color anomaly could be largely explained by a systematic error in the classification of H98 in the direction of early types. For most of the remaining stars which show this discrepancy and are not classified by H98, no optical spectra were available and the IR types were used. In these cases, an adjustment to a later subclass within the uncertainties of the classification would eliminate the color anomaly (e.g., adopt M3 instead of M2 for the classification of M1-M3). To address this issue in the calculation of extinctions, whether the discrepancy is due to a cool companion or spectral classification error, I do not deredden $R - I$ beyond the point where the dereddened $J - H$ color becomes 0.1 mag bluer than the main sequence color, where 0.1 mag represents the largest typical uncertainties in $J - H$.

The source extinctions at J are listed in Table 6.1, where the interstellar reddening law of Rieke & Lebofsky (1985) is used with A_J in the Johnson-Glass photometric system. The typical uncertainties in A_J are 0.1-0.2 for B through G stars, 0.2-0.3 for K and early-M stars, and 0.3-0.5 for mid and late-M stars. The average extinction corresponds to $A_V = 3.2$, somewhat larger than the value of $A_V = 2.8$ derived for the optically selected sources in H98. This result is not surprising since the IR selected sample includes a number of objects with $A_J \geq 2$, which will not be found in equivalent numbers by optical selection. In addition, the strong central concentration of the cluster in the near-IR compared with the optical (see H98 Figure 15) can most readily be explained by high extinction in the core region that causes sources to drop below the detection limit in the optical.

6.3.4. Derivation of T_{eff} and L_{bol}

To transform from observable (spectral type, photometry) to theoretical (T_{eff} , L_{bol}) parameters, I follow the strategies utilized in § 5. I adopt the conversion between spectral types and T_{eff} given in Schmidt-Kaler (1982) for early dwarfs ($\leq M0$ V). Since published temperature scales differ significantly for M dwarfs. I tested the available conversions with the independent T_{eff} measurements for the two known low-mass double-lined eclipsing spectroscopic binaries, YY Gem and CM Dra (§ 5). The scale of Leggett et al. (1996), which we express as $T_{\text{eff}} = 3850 - 168.1 \times (\text{M subclass})$, currently provides the most satisfactory match to the binary data. After combining this conversion with that of Schmidt-Kaler (1982), I transformed the adopted spectral types to effective temperatures (see Table 6.1).

Since young stars (≤ 10 Myr) are embedded in molecular clouds and often have excess UV (accretion onto stellar surface) and IR (circumstellar disk or envelope)

emission, I cannot derive their luminosities by simply integrating the broad-band photometry. To avoid contamination by these types of non-stellar emission, I must derive luminosities using colors where veiling is expected to be relatively small. Therefore, I have estimated the extinction from $E(R - I)$ or $E(J - H)$, and used J (extinction corrected) to estimate the bolometric luminosity, except in the case of the three sources later than M6 for which I use K . These calculations were carried out by transforming the CIT $J - H$ colors of Lada & Lada (1995) to the Johnson-Glass photometric system, taking the intrinsic colors and bolometric corrections of standard dwarfs from Kenyon & Hartmann (1995), and assuming a distance modulus of 7.5 (H98). To estimate the luminosities of the sources with uncertain but clearly late spectral types ($>K5$), I deredden the JHK photometry to the CTTS locus and adopt $BC_J = 1.75$, which is the average value for dwarfs between M0 ($BC_J \sim 1.5$) and M6 ($BC_J \sim 2$). The bolometric luminosities and JHK photometry of Lada & Lada (1995) are given in Table 6.1.

6.3.5. X-ray Properties

The comparison of X-ray and IR properties of the sources in IC 348 by Preibisch et al. (1996) can be improved in a number of ways. Within the $5' \times 5'$ core of the cluster, my study and that of H98 provide complete and accurate spectral types and identify the cluster membership, and my work gives a complete sample in bolometric luminosity to a range well below the corresponding X-ray detection limit. Taking all stars of type G, K, and M within the core, we find that the ratio L_X/L_{bol} scatters between $10^{-2.5}$ and 10^{-4} , consistent with the results of Preibisch et al. (1996). I also find a slight tendency for L_X/L_{bol} to decrease with increasing L_{bol} , with a formal slope of -0.27 ± 0.19 in $\log L_X/L_{\text{bol}}$ versus $\log L_{\text{bol}}$.

6.4. Circumstellar Disks

6.4.1. Signatures of Disks

Theoretical modeling of hydrogen emission lines in T Tauri stars has recently focused on magnetospheric accretion as the emission mechanism, (Muzerolle, Calvet, & Hartmann 1998, references therein). With the inner circumstellar disk truncated by a stellar magnetosphere, these models suggest that matter accretes from the inner regions of the disk along magnetic field lines. As material collides with the stellar surface, energy from the accretion shock eventually leaves the system as UV and optical emission. The observed hydrogen line profiles of several T Tauri stars are fit well by the predictions of magnetospheric accretion. Another test of such models can be made through measurements of the relative strengths of $H\alpha$ and $Br\gamma$ for CTTS in IC 348. Since the emitting regions are quite dense and optically thick, the predicted line ratios depart substantially from case B recombination and depend on several properties of the accretion process, such as the inner and outer radius of the accreting disk region (r_{mi} , r_{mo}) and maximum of the temperature distribution (T_{max}). The relative IR and optical line fluxes, particularly from optically thin high- n transitions, may be useful diagnostics in measuring accretion rates if the models are found to agree with observations.

The $Br\gamma$ line fluxes were calculated by using the K -band photometry of Lada & Lada (1995) to calibrate the IR spectra. By deducing the photospheric K magnitude from the veiling (r_K) measured in these spectra and adopting the color $R - K$ corresponding to the spectral type of a given star, I converted $W_\lambda(H\alpha)$ to a line flux at a surface of $R_* = 2 R_\odot$. Alternatively, if I convert the equivalent widths and dereddened R photometry to line fluxes, I arrive at the same values to within 0.2 dex in most cases. The line fluxes for both $Br\gamma$ and $H\alpha$ were corrected

for extinction with the values given in Table 6.1. My $H\alpha$ measurements were used in preference to those of H98, when possible, since the former were taken closer in time to the $Br\gamma$ observations. The results for all CTTS in my IR sample are shown in Figure 6.13. I find that the model predictions of Muzerolle, Calvet, & Hartmann (1998) can reproduce the measurements when the input model parameters are varied from $r_{mi} = 2.2-4 R_*$, $r_{mo} = 3-6 R_*$, and $T_{max} = 8000-10000$ K for a star of $M_* = 0.5 M_\odot$ and $R_* = 2 R_\odot$. The models also imply plausible accretion rates between 10^{-9} and $10^{-8} M_\odot \text{ yr}^{-1}$ for all the sources in question. On the other hand, if stellar winds are invoked as the source of the hydrogen emission, then the models of Natta, Giovanardi, & Palla (1988) can reproduce the relative strengths of $H\alpha$ and $Br\gamma$ observed in IC 348, but the luminosities of these lines would imply anomalously high mass loss rates exceeding $10^{-6} M_\odot \text{ yr}^{-1}$. However, high-resolution spectra are needed to resolve the profiles of $H\alpha$ and $Br\gamma$ and conclusively determine whether the emission is due to infall or outflow (e.g., Najita, Carr, & Tokunaga 1996). An independent measurement of accretion rates for these stars would also be valuable, as performed for T Tauri stars through a detailed analysis of their blue spectra by Valenti, Basri, & Johns (1993).

K -band excess emission in T Tauri stars is probably due to accreting circumstellar disks (Lada & Adams 1992; Meyer et al. 1997). As I might expect, all nine stars exhibiting significant continuum veiling in their K -band spectra ($r_K \geq 0.5$) have strong hydrogen emission. Three of these sources (15, 26, 40) also show emission in Ca III near 8500 Å. The one other star in my optical sample with such emission, star 37, was not observed spectroscopically in the IR. In the following discussion, I designate sources with evidence for circumstellar disks as those exhibiting $W_\lambda(H\alpha) > 10 \text{ Å}$, $W_\lambda(Br\gamma) > 1 \text{ Å}$, or $r_K \geq 0.5$.

6.4.2. Disk Frequency and Lifetimes

In a study of the frequency and survival time scales of circumstellar disks, Strom et al. (1989) and Strom, Edwards, & Skrutskie (1993) derived the magnitude of K -band excess emission towards 83 young stars in the Taurus-Auriga star-forming complex. Strom et al. (1993) calculated that reprocessing disks are optically thick at $2.2\ \mu\text{m}$ (at $r < 1\ \text{AU}$) when $\Delta K \geq 0.2$, where $\Delta K = \log [F_{2.2}(\text{PMS star})/F_{2.2}(\text{standard})]$. In the Taurus sample, they found that $\sim 50\%$ of sources younger than 3 Myr (22/48) and between 3 and 10 Myr (10/23) exhibited K -band excess emission indicative of an optically thick disk, whereas only one star older than 10 Myr met the criterion. These results implied survival times for massive circumstellar disks ranging between $\tau \ll 3\ \text{Myr}$ and $\tau \sim 10\ \text{Myr}$.

In the extensive $\text{H}\alpha$ survey across most of IC 348 ($15' \times 25'$), H98 identified 58 WTTS ($2\ \text{\AA} < W_\lambda \leq 10\ \text{\AA}$) and 51 CTTS ($W_\lambda > 10\ \text{\AA}$). This fraction of WTTS is larger than found in Taurus or Chamaeleon, which H98 attributes to either incompleteness or the differing environments, where the higher stellar densities in the IC 348 could truncate disks more rapidly and convert CTTS to WTTS. Such a process would also account for the concentration of WTTS (H98) and IR excess sources (Lada & Lada 1995) in the core of IC 348 relative to the outer regions of the cluster. While the $\text{H}\alpha$ study of H98 covered a very large area, I provide a much deeper spectroscopic sample limited to the $5' \times 5'$ cluster core. Combining the $\text{H}\alpha$ data of H98 with the my measurements of $\text{H}\alpha$, $\text{Br}\gamma$, and r_K . I find that $\sim 24\%$ (16/67) of core stars with spectral types of F and later and younger than 3 Myr (using DM94) have disks, where the disk signature is defined in the previous section. These sources are indicated in the distribution of ages shown in Figure 6.14, where I see that no sources with evidence of disks appear

older than 3 Myr in the core. These results imply a somewhat lower disk frequency and shorter disk lifetimes in the core of IC 348 as compared to the remainder of the cluster and Taurus, consistent with the possibility that disks are destroyed more rapidly in dense star forming environments.

6.5. The IC 348 Stellar Population

6.5.1. Cluster Membership

While measurements of Li at $\lambda = 6707 \text{ \AA}$ from low-resolution spectra are not reliable for stars earlier than $\sim M0$, the detection of Li (0.3-0.4 \AA) in most of the early and mid-M stars in my optical sample provides a good indication of their youth and cluster membership (Favata, Micela, & Sciortino 1997). Most of the warmer stars and ones which were too faint for a Li detection, particularly the late-M stars, are almost certainly cluster members as well. They fall above the main sequence (i.e., not background stars) and show reddened spectra and colors (i.e., not foreground stars). In addition, several stars have very strong H α emission and the late-M stars exhibit spectral features indicative of both giants and dwarfs, implying their pre-main-sequence nature. A particularly good diagnostic for distinguishing pre-main-sequence M stars from dwarfs is the weak, giantlike nature of Na absorption near 8200 \AA in the former (Martín, Rebolo, & Zapatero Osorio 1996; § 3), as illustrated in Figure 6.5.

Since I am studying such a small area of the sky, there should be negligible contamination from foreground and background stars. I do not find any foreground stars towards the $5' \times 5'$ core, which is consistent with the calculations of H98 for the expected density of foreground objects. I identify five likely foreground stars outside of the $5' \times 5'$ core. Stars 54, 57, 107, 134, and 189 fail to exhibit Li

absorption or extinction in either the JHK colors or the optical spectra. Stars 18 and 28 are omitted from further analysis since they were identified as probable foreground objects in the proper motion study of Blaauw (1952). The optical spectra of stars 14, 127, 131, 152, 352, and 442 are indicative of background giants and background early-type stars. I reach the same conclusion with the IR spectra of stars 14, 127, and 131. The expected contamination by background stars at very faint magnitudes is discussed in more detail in § 6.5.5 and Figure 6.15.

6.5.2. H-R Diagram

I use T_{eff} and L_{bol} to place the spectroscopic sample on H-R diagrams in Figs. 6.7 and 6.8. I have omitted the foreground and background stars and sources with uncertain IR spectral types ($>K5$). The incomplete sample of sources observed outside of the core of IC 348 is presented in the top panel of Figs. 6.7 and 6.8. The core stars are shown in the second panel, with the completeness limit of $K_{\text{dereddened}} = 12$ indicated by the dashed line. While the completeness limit of the IR spectroscopic sample is $K = 12.5$ in the cluster core, the combined IR and optical spectroscopic study is complete to $K_{\text{dereddened}} = 12$ and 50% complete to $K_{\text{dereddened}} = 14.5$, as shown in Figure 6.15.

To interpret the H-R diagram of IC 348, several sets of low-mass evolutionary tracks are available (DM94; BCAH97 DM97; FJS; Burrows, private communication). In § 2 and § 5 discussed the differences between the recent model interiors at low masses and young ages and compared the model predictions with observations of YY Gem and CM Dra, Pleiades, the main sequence, and globular clusters. DM97 also discuss in more detail the current state of models of convection and deuterium and lithium burning in low-mass stars. D'Antona & Mazzitelli (private communication) have recently found that a more precise

treatment of deuterium burning produces little change with respect to the DM97 isochrones, differences which are marginal considering the intrinsic uncertainties in the treatment of convection and the atmospheric opacities. Although no set of calculations was clearly preferred, I found in § 5 that the tracks of DM94 (Alexander opacities, CM convection) provide the satisfactory result that star formation in L1495E is roughly coeval at ~ 0.5 Myr, with the locus of stars having the same age as a function of mass. More recently, the DM97 set of tracks has been made available, which match the data for CM Dra and YY Gem much better than DM94 and produce a comparable match to those of BCAH97 and A. Burrows (see § 2). When used with the Leggett et al. (1996) temperature scale, I also find that the DM97 tracks imply a nearly coeval Pleiades population as a function of mass, which was not the case for DM94 (§ 2). The DM94 and DM97 calculations are quite similar except at masses below $0.2 M_{\odot}$, as seen in Figs. 6.10 and 6.11. Like DM94, the tracks of DM97 have the advantage that they extend over a wide range of masses (0.02 - $3 M_{\odot}$) and can be used to interpret observations for all stars in IC 348, unlike those of BCAH97 and Burrows. In addition to DM97, I will use the DM94 tracks in the discussion below to maintain continuity with previous studies, particularly H98.

6.5.3. Dynamics

Lada & Lada (1995) used measurements of the total cluster membership and of the velocity dispersion to conclude that IC 348 is on the border between becoming a bound cluster and eventually dissipating. This calculation suggests that dynamical evolution may have an influence on the cluster mass function. To consider this issue I follow the discussion in Williams, Rieke, & Stauffer (1995), who give references to previous work. Encounters between cluster members will tend to establish a

Maxwellian velocity distribution, and the stars in the high velocity tail of this distribution will escape the cluster. Because of equipartition, this process favors loss of the low-mass stars. Hence, it causes the cluster mass function to flatten and favor higher masses.

Taking a half-mass radius for IC 348 of 0.47 pc and a total ~ 230 members (Lada & Lada 1995), I find that the half-mass relaxation time that characterizes the evaporation process is about 2 Myr. Fortunately, detailed calculations show that the relaxation effects on the IMF enter relatively slowly (Terlevich 1987; Vesperini & Heggie 1997 and references therein), leading to a gradual flattening of the IMF over 3 - 10 relaxation times. Given the time dependence of star formation in IC 348, evaporation of low-mass members has probably not strongly affected the observed mass function, but it may have modestly decreased the numbers of the lowest mass members. Thus, the mass function I derive below should be considered to give a lower limit to the rise of the IMF toward low masses.

Although IC 348 may evolve into a bound cluster, the structure of the cluster can change substantially on the time scales over which star formation has occurred. For example, at a typical relative velocity of 2 km s^{-1} , a star with an age of 10 Myr will have traveled 20 pc, more than 3° on the sky if in a straight line and perpendicular to the line of sight. Thus, in a bound cluster a star will have traversed many orbits in 10 Myr, and will not necessarily be close to its initial formation site. For example, a simple potential energy estimate suggests that a star with a random velocity of 2 km s^{-1} could be found $5'$ from its formation site.

6.5.4. Star Formation History

As shown in the H-R diagrams of the cluster core in Figs. 6.7 and 6.8, the tracks of DM94 imply a population of stars spread between 0.5 and 10 Myr of age, with most members < 3 Myr old and a few sources older than 10 Myr. The distributions of ages derived from DM94 and DM97 are shown in Figure 6.14, which both appear fairly similar to that derived from the color-magnitude diagram of H98. The H-R diagrams imply a slightly younger population than that found by Lada & Lada (1995), where the KLF suggested star formation had occurred at a roughly constant rate for 5-7 Myr.

Has star formation ceased in IC 348 or is it ongoing? If the typical lifetimes of the youngest protostars, Class 0 and Class I sources, are ~ 0.1 Myr and star formation has continued at a constant rate for 10 Myr, then I expect $\sim 1\%$ of the few hundred stars in IC 348 to be currently in these protostellar phases. Indeed, I find that one source, star 51, exhibits a featureless K -band spectrum and a very large IR excess in the JHK colors, indicating strong continuum veiling ($r_K > 5$), possibly due to emission from a circumstellar envelope in a Class I source (Greene & Lada 1996). In near-IR observations of an H_2 jet in IC 348, McCaughrean, Rayner, & Zinnecker (1994) suggested that the exciting source may be a star deeply embedded within a NH_3 core and detected only at $\lambda \geq 350 \mu m$, possibly indicative of a Class 0 source. Near these Class 0 and Class I candidates, I also find two very luminous sources, stars 13 and 49, appearing well above the 1 Myr isochrone and near the birthline. Strom et al. (1974) discovered source 13, also known as IC 348 IR and the Flying Ghost Nebula (Boulard et al. 1995), and proposed that it was an embedded B star due to its high luminosity. Boulard et al. (1995) have recently modeled the broad-band photometry and derived a spectral

type of B7.5. However, as shown in my IR spectra, stars 13 and 49 are both late K or early M and appear very young on the upper H-R diagram of Figs. 6.7 and 6.8, making them very young Class II sources. In conclusion, the likely presence of Class 0, Class I, and early Class II sources implies that star formation is currently underway in IC 348.

H98 shows that a population of emission-line stars is centered on the cluster core, with a mean $\log \tau$ of 1.3 Myr representing a star formation duration of about 3 Myr. He suggests that this very young cluster is superimposed on a more broadly distributed non-emission-line population that permeates the region, with a mean $\log \tau$ of about 3 Myr and representing star formation from about 1 Myr to 10 Myr ago.

I can use the IR selected sample to probe the origin of this older population component. Figure 15 of H98 shows that the IR selected sample is more centrally concentrated than the optical one, presumably because it is less affected by extinction in the cluster core. Calculating the areal density of the older population from counts between 6 and 10' in radius and the core density within a radius of 2.8' (and thus coincident with and equal in area to my 5' box), I find that 33% of the 83 core sources should be from the older population. This portion is significantly smaller than the 54% found by H98 for the optical sample. On the other hand, from the IR-selected H-R diagram for the DM97 tracks, about 25% of the stars in the core have ages >3 Myr. Thus, as suggested by H98, the IR data imply that the older population component is not peaked on the cluster core, although this result is not definitive because of the small number statistics. However, the core star formation must have a duration of at least 3 Myr, given the observed age distribution and the degree of peaking of counts on the core. Some of the older

and more widely distributed stars may originate at the same sites as the younger emission-line stars, given that a star on a plunging orbit could escape to a distance $\sim 5'$ from a formation site at the cluster center. However, since the older stars are not centrally concentrated, they are likely to have formed at other sites.

In summary, a vigorous episode of star formation has occurred in the core of IC 348 from at least 3 Myr ago to the present time. Star formation may have begun near this site much earlier, as long ago as 10 Myr; however, the entire cluster appears to be permeated by a 1 to 10 Myr-old population, so that the older core stars may have been generated by formation at positions outside of the core which are no longer apparent. On the other hand, the fewer K -band excess sources observed by Lada & Lada (1995) towards the core could imply a more evolved population, but also could indicate lower disk lifetimes in the core, consistent with the conclusions of § 6.4.2. Any difference in star formation history from the core to the outer cluster remains subtle at this point. A spectroscopic study of the outer cluster to the same completeness as presented here for the core is necessary to address this issue properly.

6.5.5. The Initial Mass Function

The Spectroscopic Sample

In conjunction with the evolutionary tracks of DM94 and DM97, I can use T_{eff} and L_{bol} to derive masses for individual sources in IC 348 and hence a cluster IMF. Since my spectroscopy and imaging were concentrated on the $5' \times 5'$ core of IC 348, I restrict the analysis of the mass function to sources within this region. After omitting background and foreground stars and sources with uncertain spectral types ($>K5$), I derive the DM94 and DM97 IMFs for the core spectroscopic sample,

as shown by the solid histograms in Figure 6.16. However, these IMFs may not be representative of the full cluster membership. The most likely source of bias is incompleteness in faint sources, which will translate into an under-representation of older and less massive members. Fortunately, since extinction is relatively small at $2\ \mu\text{m}$, the K -band completeness limit and range of extinctions present in IC 348 correspond to a well-defined completeness in terms of bolometric luminosity, as represented by the dashed line in Figs. 6.7 and 6.8. It is apparent from the H-R diagram that my spectroscopically determined mass function is complete to $\sim 0.3\ M_{\odot}$ for stars at ages of 10 Myr.

A Completeness Correction with the KLF

To estimate a completeness correction to the spectroscopically derived IMF, I have obtained JHK images of the cluster core and an off-field region of equal size, similar to the procedure applied to L1495E (§ 5). For the bright sources which were saturated in my images of IC 348 ($K \leq 11-12$), I have used the photometry of Lada & Lada (1995). The resulting KLFs for the on and off fields are shown in the top panel of Figure 6.15. In the second panel of Figure 6.15, stars with spectral types are represented by solid stripes while sources with classifications of $>K5$ are indicated by dotted stripes. Spectroscopically identified background stars are shown as “B”. The sources with $K < 16$ in the on-cloud KLF were dereddened to the distribution given in the bottom panel. Sources with $K > 16$ only had accurate K photometry, so no attempt was made to deredden them. For stars with spectroscopy, I used the extinctions given in Table 6.1. For sources which lacked spectroscopy or had types of $>K5$, I estimated extinctions by dereddening $J - H$ to the CTTS locus and I derived bolometric luminosities by assuming $BC_J = 1.75$,

which is a typical value for late-type sources. In the case of stars with inaccurate J magnitudes, I arrived at reddenings and luminosities with $E(H - K)$, an intrinsic color of $H - K = 0.25$, and $BC_H = 2.4$. Since my bins are 0.5 mag wide, errors in the assumed intrinsic colors will have little effect on the histogram of $K_{\text{dereddened}}$ in the lower panel of Figure 6.15.

Given the dereddened cluster KLF in Figure 6.15, I now have a well-defined completeness limit at $K_{\text{dereddened}} = 12$. The three arrows in Figure 6.15 indicate the hydrogen burning limit at 1, 3, and 10 Myr, demonstrating that the spectroscopic sample is nearly complete to $0.08 M_{\odot}$ for stars younger than 1 Myr. The K magnitude corresponding to this mass is virtually the same with any set of tracks discussed in § 6.5.2. There are several sources in the dereddened cluster KLF which fall above the background distribution and lack spectroscopy. In the optical, the reddening vectors are roughly parallel to the theoretical isochrones (see, e.g., H98 Figure 12), making mass and reddening partially degenerate variables. However, the reduced extinction in the IR makes it feasible to derive approximate masses from the photometry. If I subtract the background KLF from that of the cluster and assume ages for the remaining sources, I can use the evolutionary tracks to convert the bolometric luminosities to masses. Since 1 and 3 Myr represent the approximate average ages for low-mass stars in IC 348 with DM94 and DM97, respectively, these ages were assumed for the sources lacking spectroscopy. The derived masses do not change substantially if I instead adopted other ages between 1 and 10 Myr. After adding these photometrically derived masses to the IMF for the spectroscopic sample, I arrive at the distribution indicated by dashed lines in Figure 6.16. As shown in Figure 6.15, the completeness correction for $K < 14.5$ pushes the mass completeness limit of the IMF to $0.08 M_{\odot}$ for ages less than 10 Myr, which is an upper limit for the bulk of the population (see Figure 6.14).

Given the rapid increase of the background distribution and the completeness limit of my on-field KLF, no completeness correction is possible at $K_{\text{dereddened}} > 14.5$. Consequently, below the hydrogen burning limit I can only provide a lower limit to the mass function.

Effects of Binarity

In the above derivations, I have ignored the existence of binary systems. This assumption is commonly made in studies of young stellar clusters because the distances of even the nearest examples are too great to allow direct detection of most binaries.

To assess the effects of binaries, I modeled the influence of unresolved binaries on the derived mass functions. In the spectroscopic sample, unresolved binaries should have spectra and thus spectral types dominated by the primary star. The luminosities measured will have contributions from both sources, but this does not introduce a significant error to the measurement of the primary mass since stars of a given mass evolve vertically on the H-R diagram at young ages and low masses. To estimate the effect of binarity on the photometric completeness correction to the IMF (see § 6.5.5), I used the theoretical M_K -mass relationship of DM94 for 3 Myr. With the Monte Carlo program described later in this section, a large set of binary and single systems were created, converted from individual component masses to K -band magnitudes, and the total system luminosity translated back to an observed mass. For virtually any input mass function or binarity fraction, the shapes of the observed and primary star mass functions were identical. After performing a similar experiment with the M_V -mass luminosity relationship used by Kroupa, Tout, & Gilmore (1991), I found that the visual luminosity functions

produce the primary star mass functions as well.

The lack of significant influence by the secondary stars on the IMF I deduce for the primaries has an important corollary: it is not possible to correct the IMF directly from my observations for the numbers of stars in binary systems. Thus, a single-star mass function (SSMF) that includes all the stars that have formed must be constrained by modeling, using what is known about binary systems as a boundary condition. Duquennoy & Mayor (1991) describe the characteristics of binaries in the general field, finding that these systems “can be formed by random association of stars from the same IMF”. And that “each primary star has actually 0.5 companion, on the average”. They estimate a completeness correction of a factor of 1.33 in this count, but also some small portion of their systems may be brown dwarfs and stars rather than two stars. I therefore conclude that the systems in the field exhibit between 0.5 and 0.67 stellar companions on the average, drawn randomly from the same IMF as the primaries. Simon et al. (1995) observed binary systems in the young star forming regions in Taurus and ρ Ophiuchi and found, within the errors, that the incidence of companions is similar to that found for field stars by Duquennoy & Mayor (1991).

I have estimated the difference between the SSMF and observed IMFs using a Monte Carlo technique. The simulation assumes that the SSMF is a power law of index α_1 for $0.05 M_\odot \leq M \leq 0.6 M_\odot$ and index α_2 for $0.6 M_\odot < M \leq 2.5 M_\odot$. The slope α is defined in logarithmic mass units, where a Salpeter value is 1.35. The results of the simulations were independent of the low-mass cutoff of the mass function as long as it fell below $0.1 M_\odot$. The program selected a large number of stars ($\sim 10^7$) from the assumed IMF and added companions drawn from the same mass function. To meet the constraint set by the observed stellar binary

rate, the fraction of stellar primaries with stellar companions was restricted to be either 0.5 and 0.67 in two separate simulations. In Figure 6.17, I show the SSMFs for $\alpha_1 = 0$ and 0.5 and $\alpha_2 = 1.5$ along with the subsequent primary star mass functions. The shapes of the primary IMFs, which should match those of the observed functions, flatten by $\Delta\alpha_1 = 0.4-0.7$ over the range of α_1 and binary rate discussed here. In addition, I investigated the effect of correlations between the primary and secondary masses. In a second simulation, I assumed that the secondary stars were drawn from the same IMF so long as they lay within a factor of ten of the primary mass, but that no secondaries fell outside this range. This simulation showed only a minor difference between the IMF for the primary stars and the SSMF, with $\Delta\alpha_1 \sim 0.2$. Over the wide range of assumptions made in these simulations (e.g., reducing the low-mass cutoff) I find that the slope of the SSMF can differ by $\Delta\alpha_1 = 0.2-0.7$ from that of the primary star mass function.

General Behavior of the IMF

Most studies of young (1-10 Myr old) clusters utilize the tracks of DM94 and do not include corrections for binarity. If I make the same assumptions, I can compare the results from cluster to cluster to search for changes in the primary stellar mass function. In ρ Oph (Comerón et al. 1993, updated in Comerón, Rieke, & Rieke 1996; Strom et al. 1995) and in NGC 2024 (Comerón et al. 1996) IMFs were derived using the DM94 tracks and IR luminosity function modeling. Because of the significant statistical errors and the limited accuracy of the methods, the IMF was fitted with a single power law from the lowest masses to $\sim 1 M_\odot$. In § 5 I determined the IMF of L1495E, using the DM94 tracks and a combination of spectroscopic measurements and luminosity function modeling. Both studies found

mass functions which were approximately flat in logarithmic units from ~ 0.05 to $\sim 1 M_{\odot}$.

If the range of stellar ages in a cluster is included correctly, the luminosity function modeling has no biases in estimated masses (Comerón et al. 1996). However, since it cannot place young stars on the H-R diagram, unique ages cannot be assigned. As a result, this technique will tend to spread objects at a given true mass over a range of possible masses and the derived IMF will be less sensitive to detailed structures. Keeping this tendency in mind as well as the broad range of masses fitted by a single power law in the references listed above, inspection of the upper panel of Figure 6.16 demonstrates that the IMF of IC 348 would also appear roughly flat over the ~ 0.05 to $\sim 1 M_{\odot}$ mass range, if it had been determined with the same luminosity function modeling.

The shape of the IMF can also be measured in older clusters where the uncertainties in the isochrones should be reduced. A flat substellar mass function has recently been derived through brown dwarf searches in the Pleiades open cluster (~ 100 Myr) (Zapatero Osorio et al. 1997; Martín, Rebolo, & Zapatero Osorio 1997). Similarly, Leggett, Harris, & Dahn (1994) find a flat IMF for the low-mass stars in the Hyades (~ 800 Myr). Although IMF studies of globular clusters cannot reach the highly evolved and faint substellar population, recent HST observations of ω Centauri (Pulone et al. 1998) and NGC 6397 (King et al. 1998) reveal a flat IMF down to $0.1 M_{\odot}$.

Overall, as noted by Scalo (1998), no significant variation in the low-mass IMF is evident among these various clusters. On the other hand, in an extensive spectroscopic study of Orion, Hillenbrand (1997) found a steep turnover at $0.2 M_{\odot}$. However, this behavior appears not to be compatible with deep K -band luminosity

function modeling of Orion (Muench, Lada, & Lada 1998). Although the situation in Orion requires clarification, in general it appears that the IMF is not strongly affected by star forming environment, since the YSO density varies by a factor of ~ 30 from L1495E to NGC 2024.

Although the DM94 tracks are useful when comparing my results with earlier work, they probably underestimate masses below $0.2 M_{\odot}$ (§ 5) while DM97 agrees better with binary and Pleiades data (§ 6.5.2). Hence, the IMF derived from DM97 may be the most accurate that can be obtained currently. The extensive spectroscopy in IC 348 discussed in this paper gives the first opportunity to improve our understanding of the low-mass IMF as derived with the DM97 tracks. As shown in the bottom panel of Figure 6.16, at $\sim 3 M_{\odot}$ the DM97 IMF does not fall as steeply toward higher masses as the IMF derived by Scalo (1986) and is actually better matched by the IMF of Miller & Scalo (1979), which Scalo (1986) supplanted. The IMF in IC 348 peaks at $\sim 0.25 M_{\odot}$ and slowly rises to this value with a slope of ~ -0.4 (where Salpeter is 1.35) in logarithmic units from the hydrogen burning limit, falling between the IMFs of Miller & Scalo (1979) and Scalo (1986). However, since the DM97 models are new versions of DM94 and the adequacy of the new input physics remains in question, the variation between the DM94 and DM97 IMFs in Figure 6.16 roughly represents the uncertainty in the IMF that can be derived for a very young cluster.

Combining all the arguments in this paper, it appears that all, or nearly all, star forming regions have very similar IMFs for primary stars (i.e., ignoring binary companions). With the DM94 calculations, young clusters exhibit low-mass IMFs with slopes between -0.5 and 0.5 in logarithmic units. In IC 348 there is a slow rise from the substellar regime to a peak near 0.2 to $0.3 M_{\odot}$, above which the

results agree with the Scalo (1986) and (even better) Miller & Scalo (1979) IMFs. Corrected for binarity, the single star mass functions are probably approximately flat in logarithmic units at masses lower than $0.3 M_{\odot}$.

6.6. Conclusions

I have used deep IR and optical spectroscopy with IR imaging to study the star formation history, disk properties, and mass function of the stellar population within the $5' \times 5'$ core of IC 348. My conclusions are as follows:

1. I find that my IR spectral types are in good agreement with those determined optically. A minor unexplained discrepancy is present in which the optical classifications of Herbig (1998) are systematically earlier than my IR and optical measurements by ~ 1 subclass for K and M stars.
2. By combining optical measurements with moderate-resolution ($R = 800$ -1200) K -band spectroscopy of the embedded population in IC 348, I have obtained spectroscopy for the core cluster members complete to $K_{\text{dereddened}} = 12$ and 50% complete to $K_{\text{dereddened}} = 14.5$.
3. Contrary to previous suggestions that IC 348-IR is an embedded B star, IR spectroscopy indicates that this source is an embedded T Tauri star (K7-M2).
4. Spectroscopic measurements of K -band continuum veiling, presumably arising in circumstellar disks or envelopes, are correlated with emission in $H\alpha$ and $Br\gamma$. The relative and absolute strengths of the H emission features can be explained in terms of magnetospheric accretion models where the accretion rates are 10^{-9} - $10^{-8} M_{\odot} \text{ yr}^{-1}$.

5. Combining my data with H α measurements of Herbig (1998), I find that $\sim 25\%$ of stars within the core of IC 348 and younger than 3 Myr exhibit signatures of disks. Since no sources older than 3 Myr show evidence for massive disks, disk lifetimes in the core of IC 348 appear to be shorter than those observed in Taurus or in the outer regions of IC 348.
 6. Using the evolutionary tracks of DM94 and DM97 to interpret the H-R diagram for IC 348, I measure stellar ages ranging between 0.5 and 10 Myr with most of the star formation occurring in the last 3 Myr.
 7. The young stellar population includes several very low-mass ($< 0.1 M_{\odot}$), late-type ($\geq M6$) sources. Although accurate masses require observational tests of the evolutionary tracks and temperature scale, three sources are brown dwarfs regardless of these uncertainties, supporting the idea that some of the faintest sources in the K -band luminosity function are indeed substellar.
 8. Comparisons with other IMF studies must take care to account for differences in approach. It appears that the IMFs of the other young clusters L1495E, ρ Oph, and NGC 2024 (but possibly not Orion) and of the Pleiades and Hyades are very similar to each other and to the IMF of IC 348. The low-mass IMF does not appear to be strongly dependent on the star forming environment, since the stellar densities vary by a large factor among these clusters.
 9. After using a deep KLF of the cluster core to make a completeness correction to the spectroscopic sample, the IMF derived from the latest evolutionary tracks of D'Antona & Mazzitelli (private communication) slowly rises from the hydrogen burning limit to $\sim 0.25 M_{\odot}$. The slope (in logarithmic units) is
-

~ -0.4 , as compared to slopes of 1.35, 0, and -2.6 for Salpeter (1955), Miller & Scalo (1979), and Scalo (1986), respectively. However, the exact shape of the low-mass IMF (the peak at $0.25 M_{\odot}$ and slope to the hydrogen burning limit) remains a function of the theoretical evolutionary tracks, which require observational tests at low masses and very young ages.

10. The inclusion of binary companions in the IMF will produce a single star mass function with a low-mass slope of ~ 0.5 greater than the measured primary star mass function, i.e. a roughly flat IMF below $0.3 M_{\odot}$.

6.7. Notes on IR Spectral Classification

Due to the large number of sources in my sample (~ 100), I visually organized the data into groups of spectra appearing approximately identical. I then classified each group by line ratios and the same spectral type was assigned for each star in the group. As described in § 5, to determine spectral types I rely on line ratios, which are independent of continuum veiling. I quantify veiling through the ratio of the IR excess flux to the photospheric flux at $2.2 \mu\text{m}$, represented by $r_K = I_{2.2}(\text{IR excess})/I_{2.2}(\text{star})$. Since the change of $W_{\lambda}(\text{Na})/W_{\lambda}(\text{Ca})$ with spectral type is subtle in standard K stars, the relative strengths of Al, Mg ($2.11, 2.28 \mu\text{m}$), and $\text{Br}\gamma$ must also be used in the classification. As discussed in § 6.7.5 and § 6.7.6, the strength of Na is highly dependent on surface gravity in M stars and cannot be used to derive reliably spectral types or veilings. Instead, I estimated veilings in M stars with Ca, which is the strongest feature relatively unaffected by surface gravity. The typical uncertainty in the measured veilings is $r_K \sim 0.25$. I could not estimate veilings in the early-type stars since the only absorption feature in these spectra is $\text{Br}\gamma$, which can be filled in by line emission.

While I do not list values of r_K for sources with uncertain spectral types ($>K5$), the strong CO band heads in these spectra imply little veiling. After deriving a spectral type for a source, I calculated percentage increase in the strength of the CO absorption over that of the standard dwarf of that type, which is listed as a CO percentage in Table 6.1. If no value is given, then the CO enhancement was less than $\sim 25\%$. For comparison, the CO absorption of a giant is 2-2.5 times stronger than that of a dwarf.

The recent K -band spectra ($R = 3000$) of Wallace & Hinkle (1997) proved useful as supplements to the standard spectra I obtained for L1495E and those of Kleinmann & Hall (1986). The major features appearing in the low-resolution K -band spectra of cool dwarfs are indicated at the top of Figs. 6.1-6.4 and are as follows: Mg I (2.1065, 2.1067 μm), Al I (2.1099, 2.1170 μm), Br γ (2.1661 μm), Na I (2.2062, 2.2090 μm), Ca I (2.2614, 2.2631, 2.2657 μm), Mg I (2.2814 μm), $^{12}\text{CO}(2,0)$ (2.2936 μm), $^{12}\text{CO}(3,1)$ (2.3227 μm), Na I (2.3355, 2.3386 μm), and $^{12}\text{CO}(4,2)$ (2.3525 μm). Several other weaker atomic lines (Fe, Si, Ti, Sc) are marginally resolved at the low resolution of my spectra.

6.7.1. G0 and Earlier

Except for strong Br γ absorption, stars with spectral types earlier than G0 are featureless in the K -band at a resolution of $R = 800$. Since Br γ emission can cause line veiling of the photospheric feature, as in the spectrum of star 12, I made no attempt at deriving spectral types for the early-type sources. However, the presence of Br γ absorption in sources 127 and 131 does place a constraint on their spectral types such that they fall below the main sequence at the distance of IC 348 and therefore must be background stars. This conclusion is consistent with the lack of any signatures of youth (e.g., IR excess, X-ray emission) and the

position of the stars near the outskirts of the cloud.

6.7.2. G0 to Early K

For stars later than G0, several absorption features (Al, Na, Ca, Mg, CO) are detectable as they become stronger with later types. Since $\text{Br}\gamma$ absorption decreases in strength until it disappears at K3-K4, its equivalent width relative to those of the other features is an excellent indicator of spectral type. Line emission can contaminate photospheric $\text{Br}\gamma$ absorption, but this did not appear to be the case with any of the sources in this spectral type range since the relative strengths of all features, including $\text{Br}\gamma$, were consistent with one type. I cannot derive an IR spectral type for source 5 due to its featureless spectrum. Given the optical classification of this star, the continuum veiling must be $r_K \geq 1$, which is consistent with the large IR excess observed in the JHK colors. Star 5 also exhibits $\text{Br}\gamma$ emission (1.8 \AA) in a high-resolution spectrum ($R = 3200$). Since star 232 falls below the main sequence with the spectral type I derive, it is probably a background star shining through the cluster center, which is consistent with the measured extinction of $A_V \sim 7.5$.

6.7.3. Late K

In late-K stars, Al and Mg ($2.11, 2.28 \mu\text{m}$) peak in strength and can be used relative to Na and Ca to derive spectral types. However, the line ratios are not significantly different from those of late-G and early-K stars. If the features of a young star are intrinsically strong than only a late-K star would fit both the relative and absolute line strengths. However, either a veiled late-K star or an early-K star with no veiling could produce a match to a spectrum with weak features. For instance, the lack of $\text{Br}\gamma$ absorption in star 26 implies a late-K type, but this feature could be

veiled by line emission. Since the $J - H$ color implies an extinction of $A_V \sim 10$ while the slope of the spectrum indicates $A_V \sim 20$, a substantial IR excess is likely. This is consistent with the IR excess seen in the JHK colors and the presence of intense $H\alpha$ emission (44 \AA) in source 26. It therefore appears likely that significant veiling is present in the spectrum, so rather than a late-G or early-K type I arrive at an IR spectral type of K4-K7 with $r_K = 0.75\text{-}1.5$. This range of types agrees with the independent optical classification of K7-K8.

I have two separate observations of star 32, where the first spectrum is similar to that of star 26 and could arise from a veiled ($r_K = 0.5\text{-}1$) late-K star or an early-K star with line veiling in $\text{Br}\gamma$. The second spectrum exhibits stronger features (except for Na) and implies a late-K type with little veiling. From these two spectra, I conclude that the star is late K and shows variable continuum veiling, which is consistent with the optical type of K8, JHK IR excess, strong $H\alpha$ emission (57 \AA), and $U - B$ excess (Trullols & Jordi 1997).

6.7.4. Early M

Near M0 and later, Al and Mg ($2.11, 2.28 \mu\text{m}$) begin to weaken while Na, Ca, and CO continue to increase in strength. In the stars classified as K6-M1, the second Mg line is still detectable and its strength relative to Ca is important in classifying these types. Sources such as 169 and 218 appear to have Mg and Ca indicative of this range of types. However, since the spectra have substantial noise, the Mg detection is

uncertain and the types could be late M, similar to the sources classified as $>K5$. For source 40, I have two spectra ($R = 800, 1200$) which exhibit strong emission in both He $2.058 \mu\text{m}$ and $\text{Br}\gamma$. The photospheric absorption line ratios

imply a spectral type near M0 with a veiling of $\tau_K \sim 1$, both of which are consistent with the optical type and IR and $U - B$ excesses. Star 100 also shows similar excesses with $\text{Br}\gamma$ and weak He emission. Other examples of late-K/early-M stars which show significant veilings include stars 15 and 60. Some of these sources can be mistaken for early-K stars with no continuum veiling and $\text{Br}\gamma$ line emission filling the photospheric absorption expected for such types. For star 149, atomic line ratios imply late-K/early-M types while the CO absorption appears enhanced relative to a that of dwarf of this type.

6.7.5. Mid M

Al and Mg disappear at my resolution in dwarfs later than M2 while Na and Ca reach their maximum strengths in M2 and M6 dwarfs, respectively. Since some of the sources which are classified as M2-M4 have substantial noise near Mg ($2.28 \mu\text{m}$), this line could be present and a late-K type may apply (e.g., star 120). As discussed in § 5, at the same point that Mg disappears, two features appear in dwarfs later than M2 at $\sim 10 \text{ \AA}$ on either side of the wavelength of Mg ($2.28 \mu\text{m}$). I identify the red line as Ca but it is unclear what species produces the other feature. These two lines are resolved in my $R = 1200$ standard spectra, while at $R \leq 1000$ they are blended together and can be easily mistaken for Mg.

The atomic lines in stars 49 and 252 imply early to mid-M dwarf types while the strong CO and hint of Sc (in the blue shoulder of Na) are reminiscent of giant spectra. Star 128 shows similar effects of low gravity in its spectrum, but I arrive at a slightly later type due to the lack of Mg ($2.28 \mu\text{m}$). Sources 71 and 74 appear to have enhanced CO and no veiling. The weak atomic features and strong CO in 75, 95, and 100 require both enhanced CO and moderate continuum veiling ($\tau_K \sim 0.5$). These spectra could also arise from unresolved binaries where the components are

early and late-M stars (see § 6.3.1 and § 6.7.6). There are several other M2-M4 sources (52, 78, 85, 120, 167, 193) with weak atomic features which could be veiled slightly ($r_K \leq 0.5$).

In the spectra of several sources classified as M2-M4, the lack of Al and Mg implies mid-M types while the weakness of Na relative to Ca indicates a late-K type. The latter effect is probably due to low surface gravity since Na becomes much weaker from dwarfs to giants, which is observed in the M6 source V410 X-ray 3 in Taurus (see Figure 6.3 and § 6.7.6). In § 6.3.1 I compare the optical and IR spectral types and find that Na appears to be systematically weak in the young stars relative to that of dwarfs.

6.7.6. Late M and Other Types

In late-M stars, Ca is weak while CO continues to become stronger. Na peaks in strength at M6 and drops rapidly thereafter in dwarfs, but as discussed in the last section this feature appears to weaken at earlier types in young stars due to the low surface gravity. The two features which have replaced Mg ($2.28 \mu\text{m}$) are blended together at my resolution and are quite weak. As seen in the spectrum of the unreddened M6 star V410 X ray 3, the continuum slope between 2.0 and $2.2 \mu\text{m}$ is fairly red (due to H_2O absorption) and is useful in distinguishing late-type M stars from earlier M stars and background K giants, all of which have similar CO strengths. The presence of Al, Mg, and $\text{Br}\gamma$ absorption are also useful in identifying field K giants. In addition, the Na line at $2.337 \mu\text{m}$ is present in dwarfs but not in giants. In my sample, I find three sources (14, 34, 80) which exhibit spectra closely matching those of standard K giants. FU Ori stars can also show strong, giantlike CO absorption, but these three stars show no signs of such phenomena (IR excess, emission lines). In the low signal-to-noise spectra of several sources,

strong CO absorption constrains the types to K5 or later, as classified in Table 6.1. The weakness of atomic lines in these spectra and the continuum slopes between 2.0 and 2.2 μm imply late-M types for these sources, which is confirmed by the M5 optical spectral type for star 135.

In the first observation of binary source 42 at $R = 800$, the spectrum was of the composite system. But in follow-up observations with the new grating at $R = 1200$, the seeing was improved and I was able to obtain spectra of the individual stars, which I have classified as \sim M2 and M5. When I attempt to classify the original composite spectrum (which matches the sum of the new data) as one star, I find that the atomic lines are weak while the CO is strong, implying a veiled, CO enhanced star of mid-M type. This classification has been assigned to sources 75, 95, and 100, which have spectra almost identical to the composite of each component of 42. Consequently, these three stars may be unresolved binaries with early-M/late-M components. Star 95 has an optical type of M4, which is consistent with such a composite classification. Sources 13 and 41 exhibit unique spectra relative to other sources in my sample. They both show Br γ emission, very weak Na absorption, no Al or Mg features, and a dwarflike ratio of Ca to CO. Since these sources are very luminous and fall near the birthline (see Figs. 6.7 and 6.8), they should have low surface gravities. The Na appears weakened by low gravity but the CO remains dwarflike, which is the same pattern I have seen for the very young M6 star V410 X-ray 3 in L1495E (§ 3). With both dwarf and giant standard references, the lack of Al and Mg implies types of M2 or later. Meanwhile, the strength of Ca relative to CO indicates a type of M2 or earlier. Assuming these are early-M stars, I derive continuum veilings of $\tau_K \sim 1$ from the absolute strengths of Ca and CO. In addition, after calculating the extinctions towards 13 and 41 from $E(J - H)$, I find that the continuum slopes are significantly affected

by both reddening and IR excess emission. Both stars, particularly 13, exhibit strong IR excess emission in the JHK colors as well. The spectrum of the star PSC04154+2823 in L1495E (§ 5), which is classified in the K -band as M1-M4 with $r_K = 2$, appears almost identical to those of 13 and 41. All three stars appear to be heavily embedded, active CTTS. In addition, star 40 has many of these spectral characteristics, but with strong Na absorption. It exhibits an optical type of K8-M0, which is consistent with the range of IR types I derive for stars 13, 41, and PSC04154+2823.

6.8. Notes on Optical Classification

Although the broad spectral coverage and low resolution are optimum for measuring spectral types of faint, late-type sources, O I and the blend of Ba II, Fe I, and Ca I are useful in classifying A and F stars. While the relative strengths of He I and O I in the spectrum of BD + 31°643 imply a type of B3 to B4 when compared with the standards of Torres-Dodgen & Weaver (1993), I refrain from classifying the spectrum with these features alone and adopt the B5 designation of Harris et al. (1954). G and K stars were classified with absolute and relative strengths of Na (5893 Å), Ca I, and the metallic blend at 6497 Å. However, absorption in Na must be used with caution due to contamination by interstellar absorption and emission in He I in CTTS. Emission in H α prevents the use of this absorption feature in the classification. For mid-K types and later, various molecular features deepen rapidly, allowing accurate classification of these stars. Optical continuum veiling, defined as the ratio of excess flux divided by photospheric flux at 5800 Å (r_{5800}), may be significant in the most active CTTS, weakening the observed spectral features and producing inaccurate types which are too early. Since most CTTS have veilings

of $r_{5800} < 1$ (Hartigan et al. 1995), the errors in spectral types of K and M stars should be restricted to a few subclasses. The Ca II triplet (a luminosity indicator) proved useful in identifying star 14 as a background giant, which agrees with the classification of the IR spectrum (see § 6.7.6).

In the study of the young M6 object V410 X-ray 3 in § 3, I found that the optical and IR (see § 6.3.1) spectra exhibited both dwarf and giant characteristics. In Figure 6.5, we see that CaH at 7000 Å is intermediate between M6V and M6III while the other gravity-dependent features (K I, Na I, and TiO/VO beyond 8200 Å) are all reproduced well by the giant. The Na I line appears to be particularly sensitive to gravity, as noted by Martín, Rebolo, & Zapatero Osorio (1996) in observations of late-type Pleiades sources. When various reddenings are applied to the spectrum of V410 X-ray 3, which has negligible extinction ($A_V < 0.5$), I find excellent matches with the spectra of five sources in IC 348, as shown in Figure 6.5. In other words, the mixture of dwarf and giant features seen in V410 X-ray 3 appears consistently for other pre-main-sequence M6 sources.

For types later than M6, averages of dwarf and giant spectra provide the best matches to the young sources shown in Figure 6.6. The effects of reddening can make it difficult to use the spectral slope as a spectral type indicator. For instance, $M6+A_V = 0$, $M7+A_V = 2$, and $M8+A_V = 3$ all exhibit similar slopes. Instead, the features used in the classification were VO (7400-7500 Å), VO (7900-8000 Å) relative to the continuum from 8100-8400 Å, and TiO/VO (8500 Å) (particularly for $>M8$). For sources 415 and 478, VO (7400-7500 Å) implies types of $\geq M7$ while VO (7900-8000 Å) indicates a type of $< M8$, as shown in Figure 6.6. TiO at 7200 Å is deepest at M7 and is of comparable strength in M6 and M8. The shallow TiO features in objects 415 and 478 therefore imply types of $\leq M6$ or

\geq M8, but continuum veiling may affect the depth of the TiO. The classification of sources later than M8 can be quite precise, as demonstrated by the rapid change in TiO/VO (8500 Å) and VO (7900-8000 Å) relative to the continuum from 8100-8400 Å from source 355 (M8) to ρ Oph 2349.8 – 2601 (M8.5).

TABLE 6.1
DATA FOR SPECTROSCOPIC SAMPLE IN IC 348

| # | Other ID ^a | α (1950) | δ (1950) | $\Delta\alpha$ ($''$) | $\Delta\delta$ ($''$) | previous ^b | optical ^c | IR | adopt ^d | T_{eff} | A_J | L_{bol}^e | I | J-H | H-K | K | r_k^f | Br γ ,CO Σ | center? ^h |
|-----------------|-----------------------|-----------------|-----------------|-------------------------|-------------------------|-----------------------|----------------------|----------|--------------------|------------------|-------|--------------------|-------|------|-------|-------|---------|--------------------------|----------------------|
| 1 | G20,BD+31.643 | 3 41 25.8 | 32 00 20.5 | ... | ... | B5V | B3-B4 | <F8 | B5 | 15400 | 0.69 | 573 | ... | 0.11 | 0.66 | 6.97 | ? | 0 | yes |
| 2 | P65,G12 | 3 41 27.0 | 32 00 38.7 | ... | ... | A2 | ok | <F8 | A2 | 8970 | 0.89 | 84.9 | ... | 0.27 | 0.56 | 7.45 | ? | 0 | yes |
| 3 | P88,G16 | 3 41 42.4 | 32 09 41.0 | ... | ... | A0 | ok | <F8 | A0 | 9520 | 0.76 | 76.8 | ... | 0.29 | 0.48 | 7.71 | ? | 0 | no |
| 4 | G11,H254 | 3 41 22.8 | 31 56 56.0 | -1.7 | -1.4 | F0m | ok | <F8 | F0 | 7200 | 0.61 | 31.4 | ... | 0.27 | 0.35 | 7.93 | ? | 0 | no |
| 5 | P51,H114 | 3 41 17.7 | 31 55 05.4 | -1.3 | -0.2 | K0/23 | F8-G8/2.1 | ? | G8 | 5520 | 1.35 | 8.28 | 12.37 | 1.18 | 1.02 | 7.95 | >1 | 1.9 | no |
| 6 | P68,G13,H166 | 3 41 28.6 | 31 57 19.2 | -0.6 | -2.0 | F8 | F8-G8 | G3-G7 | G3 | 5830 | 0.97 | 15.4 | ... | 0.63 | 0.38 | 8.21 | 0 | 0 | no |
| 7 | G4 | 3 41 00.1 | 31 57 51.6 | ... | ... | A0V | ok | <F8 | A0 | 9520 | 0.46 | 39.1 | ... | 0.13 | 0.12 | 8.66 | ? | 0 | no |
| 8 | G5 | 3 41 00.8 | 31 57 44.4 | ... | ... | A2V | ok | <F8 | A2 | 8970 | 0.45 | 30.9 | ... | 0.16 | 0.09 | 8.68 | ? | 0 | no |
| 9 | P75,H184 | 3 41 30.8 | 31 59 52.2 | -0.3 | -1.9 | G5-K0 | G6-K1 | G8 | 5520 | 1.35 | 10.1 | 12.16 | 0.79 | 0.40 | 8.75 | 0 | 0 | yes | |
| 10 | G9,H261 | 3 41 16.3 | 32 00 49.4 | -0.1 | -0.5 | F2 | ok | <F8 | F2 | 6890 | 0.63 | 15.0 | ... | 0.33 | 0.15 | 8.82 | ? | 0 | yes |
| 11 | P104 | 3 41 59.5 | 31 54 36.2 | ... | ... | F7-G6 | G2-G7/1.5 | G4 | 5800 | 1.62 | 10.9 | ... | 0.91 | 0.49 | 8.82 | 0 | 0 | no | |
| 12 ⁱ | H139 | 3 41 23.7 | 32 02 18.7 | 1.7 | -0.5 | G0 | A0-A5? | <F8? | G0 | 6030 | 1.20 | 4.81 | 12.60 | 0.63 | 0.42 | 8.90 | ? | 0 | yes |
| 12 ⁱ | H140 | 3 41 23.7 | 32 02 18.7 | 0.4 | -0.7 | ... | A0-A5? | <F8? | A3 | 8720 | 2.11 | 42.5 | ... | 0.63 | 0.42 | 8.90 | ? | 0 | yes |
| 13 | IC348-IR | 3 40 51.3 | 31 52 28.5 | ... | ... | ... | K7-M2 | M0.5 | 3765 | 3.44 | 2.08 | ... | 2.45 | 1.84 | 8.93 | 1 | 1.2,1.9 | no | |
| 14 | ... | 3 41 46.6 | 32 02 45.7 | ... | ... | ... | K1-2III | b | ... | ... | ... | ... | 0.93 | 0.41 | 8.94 | ... | 0 | no | |
| 15 | P86 | 3 41 36.3 | 31 54 37.0 | ... | ... | ... | M0.5/36 | K7-M1 | M0.5 | 3765 | 0.57 | 1.20 | ... | 1.01 | 0.60 | 9.33 | 0.75 | 0 | no |
| 16 | P59,H144 | 3 41 24.3 | 31 59 12.5 | -1.5 | -0.4 | K | G5-K0 | G2-G7 | G6 | 5700 | 0.77 | 5.23 | 11.74 | 0.56 | 0.22 | 9.36 | 0 | 0 | yes |
| 17 | ... | 3 41 39.4 | 32 09 46.3 | ... | ... | ... | A0-A9 | ... | A4 | 8460 | 1.51 | 20.1 | ... | 0.60 | 0.31 | 9.38 | ... | ... | no |
| 18 | G3,H20 | 3 40 49.7 | 32 00 21.7 | -0.5 | 1.1 | F8 | ok | ... | f | ... | ... | ... | 0.30 | 0.07 | 9.39 | ... | ... | no | |
| 19 | G10,H252 | 3 41 22.5 | 32 00 30.2 | 0.5 | -0.9 | A2 | ok | <F8 | A2 | 8970 | 0.76 | 18.6 | ... | 0.24 | 0.15 | 9.41 | ? | 0 | yes |
| 20 | P102,G17 | 3 41 59.3 | 32 01 01.9 | ... | ... | G0-G2 | ok | ... | G1 | 5945 | 0.46 | 4.70 | ... | 0.46 | 0.14 | 9.42 | ... | ... | no |
| 21 | ... | 3 41 47.8 | 31 59 49.0 | ... | ... | ... | G8-K2/4.7 | ... | K0 | 5250 | 1.36 | 3.87 | ... | 0.93 | 0.49 | 9.48 | ... | ... | no |
| 22 | P14,G2 | 3 40 42.9 | 32 03 44.1 | ... | ... | ... | F8-G0 | ... | G5 | 5770 | 0.65 | 4.07 | ... | 0.58 | 0.25 | 9.48 | ... | ... | no |
| 23 | P73,H182 | 3 41 30.4 | 31 59 16.1 | 0.4 | -1.8 | ... | G8-K4 | K3-K6 | K3 | 4730 | 1.64 | 3.59 | 13.91 | 1.08 | 0.50 | 9.51 | 0 | 0 | yes |
| 24 ⁱ | H157 | 3 41 26.7 | 31 58 11.1 | -0.4 | -1.5 | K7 | K6 | K6-M1 | K6.5 | 4132 | 0.67 | 1.03 | 12.88 | 0.82 | 0.36 | 9.52 | 0 | 0 | yes |
| 24 ⁱ | H158 | 3 41 26.7 | 31 58 11.1 | -4.6 | -0.8 | K8/32 | M0.5 | K6-M1 | M0 | 3850 | 1.11 | 0.74 | 14.31 | 0.82 | 0.36 | 9.52 | 0 | 0 | yes |
| 25 | ... | 3 41 53.0 | 31 55 35.1 | ... | ... | ... | A0-A9 | ... | A4 | 8460 | 1.09 | 14.0 | ... | 0.44 | 0.24 | 9.58 | ... | ... | no |
| 26 | ... | 3 40 47.7 | 31 52 47.9 | ... | ... | ... | K7-K8/44 | K4-K7 | K7 | 4060 | 1.94 | 1.50 | ... | 1.58 | 0.99 | 9.61 | 1.5 | 0 | no |
| 27 | ... | 3 40 27.8 | 32 04 08.3 | ... | ... | ... | F7-G6 | ... | G2 | 5860 | 1.20 | 4.78 | ... | 0.75 | 0.34 | 9.65 | ... | ... | no |
| 28 | G7,H89 | 3 41 12.7 | 31 58 13.6 | -0.8 | 0.2 | F8 | ok | ... | f | ... | ... | ... | 0.27 | 0.07 | 9.67 | ... | ... | no | |
| 29 | P57,H137 | 3 41 23.2 | 31 59 19.8 | -0.1 | -0.5 | K2 | G8-K2 | K2-K3 | K2 | 4900 | 0.48 | 2.17 | 12.15 | 0.64 | 0.24 | 9.68 | ... | ... | no |
| 30 | G6,H83 | 3 41 10.8 | 32 00 05.6 | 0.1 | -0.3 | F0 | ok | ... | F0 | 7200 | 0.44 | 6.60 | ... | 0.24 | 0.10 | 9.73 | ... | ... | no |
| 32 | H173 | 3 41 29.5 | 31 58 38.7 | -0.8 | -1.3 | K7/68 | K8/57 | K4-K7 | K7 | 4060 | 1.18 | 1.25 | 14.08 | 1.11 | 0.76 | 9.75 | 0.3,0.8 | 0 | yes |
| 33 | H143 | 3 41 24.2 | 31 59 17.3 | -0.6 | -0.6 | .../3 | M2/5.9 | M4-M5 | M3 | 3350 | 0.34 | 0.93 | 13.25 | 0.70 | 0.27 | 9.82 | 0 | 0 | yes |
| 34 | ... | 3 41 07.1 | 31 53 09.6 | ... | ... | ... | G8III | b | b | ... | ... | ... | 1.78 | 1.03 | 9.89 | ... | ... | no | |
| 35 | H187 | 3 41 30.9 | 31 58 09.6 | -0.3 | -1.8 | G8 | G8-K4 | K3-K6 | K3 | 4730 | 1.21 | 2.07 | 13.03 | 0.96 | 0.40 | 9.90 | 0 | 0 | yes |
| 36 | P72,H178 | 3 41 30.1 | 31 58 09.8 | -0.6 | -1.7 | K6/2 | K5-K6/3.9 | K6-M1 | K6 | 4205 | 0.81 | 1.34 | 13.07 | 0.91 | 0.37 | 9.91 | 0 | 0 | yes |
| 37 | P71 | 3 41 29.6 | 31 54 04.0 | ... | ... | ... | K6/47 | ... | K6 | 4205 | 0.63 | 1.10 | ... | 0.82 | 0.36 | 10.05 | ... | ... | no |
| 38 | P46,G8,H103 | 3 41 15.6 | 32 01 34.6 | -0.1 | -0.3 | F8,G5 | ok | F6-G1 | G0 | 6030 | 0.63 | 3.21 | 11.79 | 0.45 | 0.11 | 10.06 | 0 | 0 | yes |
| 40 | H124 | 3 41 21.4 | 32 01 14.3 | 0.6 | -0.8 | K6/145 | K8-M0/104 | K6-M1 | K8 | 3955 | 0.83 | 0.70 | 14.26 | 1.03 | 0.66 | 10.16 | 0.75 | 9.4,9.6 | yes |
| 41 | P42,H94 | 3 41 13.3 | 32 01 12.1 | 0.6 | -0.4 | K7/48 | ... | K7-M2 | K7 | 4060 | 1.17 | 0.71 | 14.94 | 1.17 | 0.85 | 10.20 | 1 | 3.5,5.2 | yes |
| 42 ⁱ | H202 | 3 41 33.7 | 31 59 34.8 | 0.4 | -1.2 | M1/32 | ... | M1-M3 | M1.5 | 3595 | 1.19 | 0.55 | 14.85 | 1.07 | 0.72 | 10.20 | 0 | 0 | yes |
| 42 ⁱ | H203 | 3 41 33.7 | 31 59 34.8 | -1.1 | -3.3 | M3/74 | ... | M4-M6 | M4 | 3180 | 0.32 | 0.088 | 15.16 | 1.07 | 0.72 | 10.20 | 0 | 0 | yes |
| 44 | P28 | 3 41 00.5 | 32 06 45.6 | ... | ... | ... | G8-K2 | ... | K0 | 5250 | 0.88 | 1.78 | ... | 0.75 | 0.30 | 10.22 | ... | ... | no |
| 45 | P47,H104 | 3 41 15.9 | 32 00 53.9 | -0.4 | -0.6 | K5 | K5 | K4-K7 | K5 | 4350 | 0.60 | 1.24 | 13.12 | 1.06 | -0.26 | 10.29 | 0 | 0 | yes |
| 47 | P16,H14 | 3 40 47.1 | 32 00 06.8 | -1.8 | 1.3 | ... | G8-K2 | ... | K0 | 5250 | 0.85 | 1.86 | 12.71 | 0.64 | 0.23 | 10.32 | ... | ... | no |
| 49 | ... | 3 40 49.2 | 31 52 12.0 | ... | ... | ... | ... | K7-M2 | M0.5 | 3765 | 4.93 | 2.96 | ... | 2.50 | 1.47 | 10.36 | 0 | 125-50% | no |
| 51 | ... | 3 41 04.6 | 31 52 10.0 | ... | ... | ... | ... | class I? | ... | ... | 0.77 | 0.03 | ... | 2.08 | 2.35 | 10.41 | >2 | 0 | no |
| 52 | P82,H211 | 3 41 35.2 | 31 58 16.8 | 0.0 | -2.2 | K6 | ... | M2-M4 | M1 | 3680 | 1.11 | 0.71 | 14.86 | 1.18 | 0.44 | 10.43 | 0.25 | 0 | yes |
| 54 | ... | 3 41 41.3 | 32 07 20.2 | ... | ... | ... | K1-K2 | ... | f | ... | ... | ... | 0.44 | 0.11 | 10.47 | ... | ... | no | |

TABLE 6.1—Continued

| # | Other ID ^a | $\alpha(1950)$ | $\delta(1950)$ | $\Delta\alpha(^{\prime\prime})$ | $\Delta\delta(^{\prime\prime})$ | previous ^b | optical ^c | IR | adopt ^d | T_{eff} | A_J | L_{bol}^e | I | J-H | H-K | K | r_k^f | Br γ , CO g | center? ^h |
|-----------------|-----------------------|----------------|----------------|---------------------------------|---------------------------------|-----------------------|----------------------|--------|--------------------|------------------|-------|--------------------|-------|------|------|-------|------------|-----------------------|----------------------|
| 57 | ... | 3 41 40.2 | 32 08 02.7 | ... | ... | ... | K3-K4 | ... | f | ... | ... | ... | ... | 0.57 | 0.16 | 10.53 | ... | ... | no |
| 58 | P74,H179 | 3 41 30.2 | 31 58 35.3 | -0.3 | -1.2 | K7/9 | ... | K6-M1 | K7 | 4060 | 1.11 | 0.92 | 14.10 | 0.93 | 0.41 | 10.54 | 0-0.3 | 0 | yes |
| 59 | P77,H190 | 3 41 31.8 | 32 02 08.6 | 0.9 | -1.3 | G7 | G8-K2 | K2-K4 | K2 | 4900 | 1.06 | 1.38 | 13.53 | 0.78 | 0.29 | 10.56 | 0 | 0 | yes |
| 60 ⁱ | P50,H109+110 | 3 41 17.2 | 32 02 05.6 | 0.1 | 0.1 | ...-K8/51 | ... | K7-M1 | M0 | 3850 | 1.27 | 0.71 | 15.13 | 1.02 | 0.62 | 10.59 | 0.75-1 | 4.1 | yes |
| 65 | P61,H148 | 3 41 25.6 | 31 59 28.4 | -0.6 | -1.3 | .../2 | K7+/-0.9 | M2-M4 | M0 | 3850 | 0.42 | 0.52 | 13.45 | 0.77 | 0.26 | 10.68 | 0 | 0 | yes |
| 68 | ... | 3 41 20.2 | 31 50 29.1 | ... | ... | ... | M3/5.1 | ... | M4 | 3180 | 0.00 | 0.22 | ... | 0.78 | 0.47 | 10.69 | ... | ... | no |
| 71 | H142 | 3 41 24.2 | 31 59 30.6 | -0.4 | -0.7 | M2/5 | M3/5 | M1-M3 | M3 | 3350 | 0.72 | 0.44 | 14.32 | 0.90 | 0.38 | 10.71 | 0 | 25% | yes |
| 74 | P62,H150 | 3 41 25.9 | 32 01 24.0 | 0.3 | -1.2 | M1/3 | M2/5.4 | M1-M3 | M2 | 3510 | 0.90 | 0.59 | 14.36 | 0.86 | 0.35 | 10.80 | 0 | 25% | yes |
| 75 | H214 | 3 41 35.4 | 32 01 04.5 | 0.1 | -2.0 | K8 | ... | M2-M4 | M1 | 3680 | 0.77 | 0.47 | 14.31 | 0.96 | 0.38 | 10.81 | 0.5? | 25-50%? | yes |
| 77 | P84,H210 | 3 41 35.1 | 31 58 51.9 | 0.0 | -1.6 | M1 | ... | K5-M0 | M0 | 3850 | 0.09 | 0.43 | 12.81 | 0.59 | 0.19 | 10.82 | 0 | 0 | yes |
| 78 | H115 | 3 41 18.3 | 31 58 55.1 | -0.9 | -0.5 | .../42 | ... | M2-M4 | M3 | 3350 | 0.86 | 0.24 | 16.00 | 1.26 | 0.69 | 10.84 | 0.5 | 1.7 | yes |
| 80 | ... | 3 41 19.5 | 32 01 26.8 | ... | ... | ... | ... | K1111 | b | ... | ... | ... | ... | 1.92 | 0.99 | 10.86 | ... | ... | no |
| 83 | P69,H170 | 3 41 29.1 | 31 59 35.0 | 0.4 | -1.7 | K8/7 | ... | M2-M4 | M1 | 3680 | 0.83 | 0.46 | 14.64 | 0.92 | 0.43 | 10.89 | 0 | 0 | yes |
| 86 | H119 | 3 41 19.5 | 31 58 05.9 | -1.0 | -0.9 | M3/3 | M2/3.9 | M1-M3 | M2 | 3510 | 0.72 | 0.48 | 14.06 | 0.79 | 0.29 | 10.97 | 0 | 0 | yes |
| 88 | H145 | 3 41 24.4 | 31 59 50.4 | -0.3 | -0.9 | M2/4 | ... | K6-M1 | M1 | 3680 | 0.90 | 0.49 | 14.63 | 0.86 | 0.38 | 10.99 | 0 | 0 | yes |
| 90 | P60,H146 | 3 41 25.0 | 32 00 13.7 | 0.6 | -1.4 | ... | ... | M1-M3 | M2 | 3510 | 0.77 | 0.44 | 14.55 | 0.81 | 0.36 | 11.03 | 0.25 | 0 | yes |
| 91 | H185 | 3 41 30.9 | 32 00 18.8 | 0.9 | -2.0 | M1/8 | ... | M2-M4 | M2 | 3510 | 0.94 | 0.44 | 14.76 | 0.92 | 0.40 | 11.03 | 0 | 0 | yes |
| 95 | ... | 3 41 13.6 | 32 02 46.5 | ... | ... | ... | ... | M4/5.5 | M4 | 3180 | 0.52 | 0.30 | ... | 0.75 | 0.33 | 11.07 | 0.25? | 25%? | yes |
| 96 | H154 | 3 41 26.5 | 32 00 27.4 | 0.0 | -1.7 | ... | ... | >K5 | ... | ... | 0.00 | 0.22 | 14.97 | 0.62 | 0.31 | 11.08 | ? | 0 | yes |
| 100 | P44 | 3 41 14.0 | 32 02 35.6 | ... | ... | ... | M1/90 | M2-M4 | M2 | 3510 | 0.56 | 0.31 | ... | 0.83 | 0.45 | 11.10 | 0.5? | 4.1,125-50%? | yes |
| 103 | P85,H219 | 3 41 36.2 | 31 58 47.1 | -0.6 | -1.7 | K8/44 | M2/26 | M1-M3 | M1 | 3680 | 1.07 | 0.31 | 15.38 | 1.09 | 0.70 | 11.12 | 0 | 2.5 | yes |
| 107 | ... | 3 40 47.4 | 32 10 19.8 | ... | ... | ... | M1 | K6-M1 | f | ... | ... | ... | ... | 0.48 | 0.21 | 11.20 | ... | 0 | no |
| 108 | H181 | 3 41 30.3 | 31 59 30.8 | -0.6 | -1.7 | M2/3 | ... | M2-M4 | M2 | 3510 | 0.69 | 0.37 | 14.37 | 0.78 | 0.31 | 11.22 | 0 | 0 | yes |
| 110 | P70 | 3 41 29.1 | 32 02 58.7 | ... | ... | ... | ... | K6-M1 | K8 | 3955 | 1.18 | 0.37 | ... | 1.07 | 0.59 | 11.24 | 0 | 0 | yes |
| 113 | H168 | 3 41 28.8 | 31 59 50.1 | -0.6 | -1.7 | ... | ... | K4-K7 | K5.5 | 4278 | 0.74 | 0.43 | 14.23 | 0.83 | 0.27 | 11.26 | 0-0.3 | 0 | yes |
| 115 | H127 | 3 41 21.6 | 31 59 55.5 | -0.6 | -0.8 | M1 | ... | K6-M1 | M1 | 3680 | 2.26 | 0.58 | 17.14 | 1.45 | 0.68 | 11.27 | 0-0.3 | 0 | yes |
| 120 | H98 | 3 41 14.6 | 32 02 32.2 | 0.1 | 0.1 | ... | ... | M2-M4? | M3 | 3350 | 0.36 | 0.22 | 14.40 | 0.79 | 0.32 | 11.30 | 0 | 0 | yes |
| 121 | ... | 3 41 17.6 | 32 07 06.1 | ... | ... | ... | ... | K4-K7 | K5.5 | 4278 | 0.18 | 0.32 | ... | 0.64 | 0.17 | 11.31 | 0 | 0 | no |
| 122 | ... | 3 41 24.9 | 32 06 03.8 | ... | ... | ... | ... | K5-M0 | K6.5 | 4132 | 0.36 | 0.30 | ... | 0.73 | 0.31 | 11.31 | 0 | 0 | no |
| 125 | H95 | 3 41 13.3 | 31 56 59.4 | -1.0 | -0.3 | ... | ... | K4-K7 | K5.5 | 4278 | 0.92 | 0.48 | 14.59 | 0.82 | 0.28 | 11.33 | 0-0.3 | 0 | no |
| 127 | ... | 3 41 51.4 | 31 57 21.3 | ... | ... | ... | F2-F5 | <F8 | b | ... | ... | ... | ... | 0.49 | 0.18 | 11.34 | ... | 0 | no |
| 128 | H87 | 3 41 11.8 | 31 59 30.9 | -0.5 | -0.4 | M1/47 | ... | M1-M4 | M2 | 3510 | 0.72 | 0.30 | 14.77 | 0.79 | 0.39 | 11.36 | 0 | 25% | no |
| 130 | ... | 3 40 55.9 | 32 04 24.3 | ... | ... | ... | M5/5 | >K5 | M5 | 3010 | 0.50 | 0.20 | ... | 0.76 | 0.34 | 11.38 | ? | 0 | no |
| 131 | ... | 3 40 38.5 | 32 05 44.4 | ... | ... | ... | F0-F4 | <F8 | b | ... | ... | ... | ... | 0.46 | 0.23 | 11.39 | ... | 0 | no |
| 133 | ... | 3 41 33.4 | 32 02 37.0 | ... | ... | ... | M4-M5 | M5-M6 | M5 | 3010 | 1.31 | 0.26 | ... | 1.07 | 0.56 | 11.39 | 0 | 0 | yes |
| 134 | H26 | 3 40 51.5 | 32 01 51.7 | -1.0 | 1.7 | ... | M4 | M2-M4 | f | ... | ... | ... | 13.56 | 0.55 | 0.21 | 11.40 | ... | 0 | no |
| 135 | ... | 3 41 30.9 | 32 10 43.8 | ... | ... | ... | M5/20 | >K5 | M5 | 3010 | 0.00 | 0.12 | ... | 0.69 | 0.44 | 11.41 | ? | 0 | no |
| 137 | P31 | 3 41 03.1 | 32 10 15.4 | ... | ... | ... | M4/8 | M4-M6 | M4 | 3180 | 0.42 | 0.20 | ... | 0.71 | 0.32 | 11.45 | 0 | 0 | no |
| 139 | H107 | 3 41 17.0 | 32 00 47.2 | 0.8 | -0.6 | M3/51 | ... | >K5 | M3 | 3350 | 0.60 | 0.23 | 15.39 | 0.70 | 0.39 | 11.47 | ? | 0 | yes |
| 141 | H131 | 3 41 22.2 | 31 57 03.7 | -0.6 | -1.5 | ... | ... | K5-M0 | M0.5 | 3765 | 0.90 | 0.33 | 15.00 | 0.87 | 0.33 | 11.48 | ? | 0 | no |
| 142 | P17,H16 | 3 40 47.9 | 31 59 10.9 | -0.6 | 1.4 | ... | M0-M1/4 | K5-M0 | M0 | 3850 | 0.83 | 0.33 | 14.38 | 0.86 | 0.28 | 11.48 | 0 | 0 | no |
| 144 | ... | 3 41 30.1 | 32 03 34.0 | ... | ... | ... | M0/2 | K5-M0 | M0 | 3850 | 0.36 | 0.22 | ... | 0.77 | 0.32 | 11.50 | 0 | 0 | no |
| 145 | H198 | 3 41 33.0 | 32 00 59.3 | 1.0 | -1.8 | M3/3 | M5/4 | M2-M4 | M4.5 | 3095 | 0.61 | 0.23 | 14.68 | 0.70 | 0.27 | 11.51 | 0 | 0 | yes |
| 149 | H167 | 3 41 28.6 | 31 59 08.5 | -0.6 | -1.6 | M3/8 | ... | K6-M1? | M3 | 3350 | 1.18 | 0.26 | 15.61 | 0.92 | 0.54 | 11.56 | 0.25-0.75? | 25-75%? | yes |
| 151 | H153 | 3 41 26.5 | 32 01 52.4 | 0.8 | -1.1 | M3 | ... | K6-M1 | M2 | 3510 | 0.64 | 0.24 | 14.85 | 0.76 | 0.34 | 11.60 | 0-0.3 | 0 | yes |
| 152 | ... | 3 40 39.2 | 32 10 19.9 | ... | ... | ... | F0-F6 | b | ... | ... | ... | ... | ... | 0.42 | 0.18 | 11.60 | ... | ... | no |
| 153 | P83,H206 | 3 41 34.4 | 31 59 08.0 | -0.3 | -1.9 | M2/91 | ... | >K5 | M2 | 3510 | 0.87 | 0.24 | 15.78 | 0.85 | 0.50 | 11.60 | ? | 0 | yes |
| 154 | ... | 3 41 29.5 | 32 02 52.7 | ... | ... | ... | ... | K6-M1 | K8 | 3955 | 0.37 | 0.19 | ... | 0.76 | 0.41 | 11.61 | 0-0.3 | 0 | yes |
| 158 | H191 | 3 41 31.8 | 31 59 46.9 | -0.1 | -1.9 | ... | ... | >K5 | M5 | 3010 | 1.22 | 0.22 | 16.40 | 0.95 | 0.52 | 11.66 | ? | 0 | yes |
| 165 | H159 | 3 41 27.1 | 31 59 30.4 | -0.3 | -1.7 | M4/50 | M5/74 | >K5 | M5 | 3010 | 0.89 | 0.17 | 16.07 | 0.81 | 0.50 | 11.77 | ? | 0 | yes |
| 166 | H204 | 3 41 34.2 | 32 00 36.5 | 0.1 | -1.8 | ... | ... | K6-M1 | K8 | 3955 | 1.44 | 0.28 | 17.08 | 1.07 | 0.60 | 11.78 | 0-0.3 | 0 | yes |
| 167 | H195 | 3 41 32.8 | 32 00 44.1 | 0.1 | -1.9 | ... | M3 | M2-M4 | M3 | 3350 | 1.48 | 0.21 | 16.75 | 1.19 | 0.58 | 11.79 | 0 | 0 | yes |

TABLE 6.1—Continued

| # | Other ID ^a | α (1950) | δ (1950) | $\Delta\alpha$ (") | $\Delta\delta$ (") | previous ^b | optical ^c | IR | adopt ^d | T_{eff} | A_J | L_{bol}^e | I | J-H | H-K | K | r_k^f | Bry,CO ^g | center? ^h |
|-----|-----------------------|-----------------|-----------------|--------------------|--------------------|-----------------------|----------------------|--------|--------------------|------------------|-------|--------------------|-------|------|-------|-------|---------|---------------------|----------------------|
| 168 | H133 | 3 41 23.0 | 32 01 21.5 | 0.3 | -0.8 | M2/12 | ... | >K5 | M2 | 3510 | 1.16 | 0.23 | 15.91 | 0.96 | 0.54 | 11.81 | ? | 0 | yes |
| 169 | H74 | 3 41 09.4 | 31 55 22.2 | -1.5 | 0.0 | M3/5 | ... | K6-M1? | M3 | 3350 | 0.73 | 0.17 | 15.69 | 0.75 | 0.45 | 11.81 | 0-0.3 | 0 | no |
| 170 | ... | 3 41 20.1 | 32 01 57.2 | ... | ... | ... | ... | M2-M4 | M3 | 3350 | 3.08 | 0.42 | ... | 1.74 | 0.83 | 11.83 | 0 | 0 | yes |
| 171 | H221 | 3 41 36.5 | 32 01 39.8 | 0.8 | -1.9 | M2 | ... | M3-M5 | M3 | 3350 | 0.77 | 0.18 | 15.28 | 0.85 | 0.30 | 11.85 | 0 | 0 | yes |
| 189 | ... | 3 40 33.2 | 32 05 36.0 | ... | ... | ... | M0 | ... | f | ... | ... | ... | 0.53 | 0.35 | 12.01 | ... | ... | no | |
| 191 | H172 | 3 41 29.5 | 32 00 41.5 | 0.5 | -1.6 | ... | ... | M1-M3 | M2 | 3510 | 1.54 | 0.19 | 17.42 | 1.30 | 0.51 | 12.05 | 0 | 0 | yes |
| 193 | H174 | 3 41 29.7 | 32 02 11.5 | 1.1 | -1.2 | .../10 | ... | M2-M4 | M3 | 3350 | 0.84 | 0.16 | 15.57 | 0.79 | 0.37 | 12.08 | 0 | 0 | yes |
| 194 | H117 | 3 41 18.9 | 32 01 11.8 | 0.3 | -0.7 | M1/26 | ... | >K5 | M1 | 3680 | 0.87 | 0.16 | 16.23 | 0.84 | 0.49 | 12.09 | ? | 0 | yes |
| 197 | H122 | 3 41 20.7 | 31 58 26.3 | -1.2 | 0.0 | ... | ... | G6-K1 | G8 | 5520 | 2.30 | 0.60 | 17.33 | 1.25 | 0.60 | 12.10 | 0 | 0 | yes |
| 207 | H130 | 3 41 21.9 | 31 58 16.9 | -1.0 | -1.1 | ... | ... | K6-M1 | K8 | 3955 | 1.90 | 0.28 | 17.06 | 1.24 | 0.54 | 12.16 | 0 | 0 | yes |
| 217 | H207 | 3 41 34.7 | 32 00 49.3 | 0.4 | -1.8 | M3/4 | ... | M4-M6 | M4 | 3180 | 0.97 | 0.14 | 16.13 | 0.82 | 0.33 | 12.24 | 0 | 0 | yes |
| 218 | H220 | 3 41 36.3 | 31 58 04.2 | -0.4 | -2.1 | M4/8 | ... | K6-M1? | M4 | 3180 | 1.39 | 0.15 | 16.72 | 0.98 | 0.51 | 12.24 | 0-0.3 | 0 | yes |
| 221 | H192 | 3 41 31.9 | 32 00 07.1 | 0.3 | -1.9 | .../26 | ... | >K5 | ... | ... | 0.13 | 0.05 | 16.59 | 0.89 | 0.58 | 12.27 | ? | 0 | yes |
| 226 | H136 | 3 41 23.1 | 32 02 04.1 | 0.9 | -0.6 | ... | ... | M2-M4 | M3 | 3350 | 0.44 | 0.10 | 15.98 | 0.64 | 0.37 | 12.31 | 0 | 0 | yes |
| 230 | H160 | 3 41 27.2 | 31 58 39.2 | 0.1 | -1.1 | ... | ... | >K5 | b | ... | 0.20 | 0.06 | 16.17 | 0.82 | 0.43 | 12.32 | ? | 0 | yes |
| 232 | H165 | 3 41 28.1 | 31 59 53.7 | 0.4 | -1.7 | ... | ... | F7-G7 | b | ... | ... | ... | 17.63 | 1.08 | 0.67 | 12.34 | ... | 0 | yes |
| 237 | H99 | 3 41 15.2 | 32 00 08.1 | -0.3 | -0.8 | M3/5 | M5/7 | M4-M6? | M5 | 3010 | 0.50 | 0.089 | 15.66 | 0.65 | 0.34 | 12.37 | 0 | 0 | yes |
| 248 | H163 | 3 41 27.6 | 31 59 58.2 | 0.0 | -1.7 | ... | ... | >K5 | ... | ... | 0.00 | 0.05 | 16.54 | 0.62 | 0.46 | 12.48 | ? | 0 | yes |
| 252 | H123 | 3 41 20.7 | 31 58 32.6 | -1.3 | -0.1 | M4/4 | ... | M0-M3 | M3 | 3350 | 0.99 | 0.12 | 15.71 | 0.93 | 0.29 | 12.50 | 0 | 75% | yes |
| 287 | H196 | 3 41 32.7 | 31 58 42.0 | -1.3 | -1.3 | ... | M5.5 | ... | M5.5 | 2925 | 1.21 | 0.066 | 17.89 | 0.97 | 0.60 | 12.81 | ... | ... | yes |
| 294 | H106 | 3 41 16.2 | 32 00 37.4 | -0.3 | -0.7 | ... | M4.5 | ... | M4.5 | 3095 | 0.44 | 0.052 | 16.42 | 0.66 | 0.38 | 12.89 | ... | ... | yes |
| 309 | H134 | 3 41 23.0 | 32 00 03.7 | 0.1 | -0.8 | M3/10 | ... | ... | M3 | 3350 | 0.39 | 0.048 | 16.72 | 0.58 | 0.47 | 13.01 | ... | ... | yes |
| 324 | H223 | 3 41 36.9 | 32 01 29.8 | 0.9 | -1.9 | ... | M6 | ... | M6 | 2840 | 0.46 | 0.037 | 17.18 | 0.63 | 0.42 | 13.20 | ... | ... | no |
| 325 | H128 | 3 41 21.7 | 31 59 23.6 | -0.4 | -0.7 | ... | M6 | ... | M6 | 2840 | 0.67 | 0.035 | 17.47 | 0.83 | 0.49 | 13.20 | ... | ... | yes |
| 335 | H216 | 3 41 35.9 | 31 59 21.6 | 0.1 | -1.8 | ... | M6/6 | ... | M6 | 2840 | 0.68 | 0.031 | 17.23 | 0.95 | 0.43 | 13.27 | ... | ... | yes |
| 351 | H113 | 3 41 17.4 | 31 59 40.3 | -0.1 | -0.8 | ... | M5.5 | ... | M5.5 | 2925 | 0.87 | 0.042 | 17.61 | 0.79 | 0.39 | 13.36 | ... | ... | yes |
| 352 | H101 | 3 41 15.4 | 32 02 30.9 | 0.4 | -0.1 | ... | b | ... | b | ... | ... | ... | 17.40 | 1.09 | 0.37 | 13.36 | ... | ... | yes |
| 353 | H176 | 3 41 29.8 | 32 00 55.6 | 0.3 | -1.6 | ... | M6/12 | ... | M6 | 2840 | 0.19 | 0.027 | 16.96 | 0.58 | 0.35 | 13.38 | ... | ... | yes |
| 355 | H186 | 3 41 30.9 | 31 58 48.1 | 0.3 | -1.5 | ... | M8 | ... | M8 | 2600 | 0.40 | 0.019 | 18.12 | 0.65 | 0.61 | 13.42 | ... | ... | yes |
| 360 | H212 | 3 41 35.4 | 32 01 22.1 | 1.0 | -1.9 | M4/8 | M5/9 | ... | M5 | 3010 | 0.26 | 0.027 | 16.41 | 0.68 | 0.24 | 13.49 | ... | ... | yes |
| 366 | H156 | 3 41 26.7 | 31 59 31.3 | 0.4 | -1.7 | ... | M5/5 | ... | M5 | 3010 | 0.37 | 0.036 | 17.27 | 0.57 | 0.14 | 13.51 | ... | ... | yes |
| 404 | H218 | 3 41 36.1 | 32 00 39.3 | 0.5 | -2.6 | M3 | M3 | ... | M3 | 3350 | 0.29 | 0.024 | 16.64 | 0.58 | 0.18 | 13.96 | ... | ... | yes |
| 413 | H227 | 3 41 37.3 | 32 01 44.5 | 0.6 | -2.1 | M4/3 | M5 | ... | M5 | 3010 | 0.21 | 0.017 | 17.33 | 0.55 | 0.33 | 14.01 | ... | ... | no |
| 414 | H217 | 3 41 35.9 | 32 01 10.5 | 0.0 | -2.3 | ... | M5.5/7 | ... | M5.5 | 2925 | 0.13 | 0.012 | 17.73 | 0.50 | 0.61 | 14.03 | ... | ... | yes |
| 415 | H126 | 3 41 21.6 | 32 00 13.8 | -0.3 | -0.9 | .../50 | M7.5/250 | ... | M7.5 | 2660 | 0.28 | 0.011 | 18.23 | 0.67 | 0.12 | 14.03 | ... | ... | yes |
| 442 | H193 | 3 41 32.3 | 32 00 14.8 | -0.1 | -2.3 | ... | b | ... | b | ... | ... | ... | 17.27 | 0.84 | 0.01 | 14.18 | ... | ... | yes |
| 454 | H201 | 3 41 33.2 | 32 01 13.3 | 0.1 | -1.9 | .../65 | M6/140 | ... | M6 | 2840 | 0.01 | 0.0078 | 17.82 | 0.88 | 0.31 | 14.31 | ... | ... | yes |
| 478 | H162 | 3 41 27.6 | 32 01 51.3 | 0.6 | -1.6 | ... | M7.5/100 | ... | M7.5 | 2660 | 0.14 | 0.0059 | 18.58 | 1.13 | 0.40 | 14.64 | ... | ... | yes |

^aDesignations of Gingrich (1922), Preibisch, Zinnecker, & Herbig (1996), and Herbig (1998).^bOptical spectral types of Harris, Morgan, & Roman (1954), Fredrick (1956), Strom, Strom, & Carrasco (1974), and Herbig (1998) with Herbig's measurements of $W_\lambda(\text{H}\alpha)$.^cOptical spectral types and $W_\lambda(\text{H}\alpha)$ measured in this work. "ok" indicates an uncertain early type which is consistent with the previous spectral type from the literature.^dBackground and foreground stars are indicated by "b" and "f".^eFor sources with spectral types of >K5, L_{bol} was calculated by dereddening the JHK colors to the CTTS locus and assuming $\text{BC}_J = 1.75$.^fDerived from the IR spectra in this work.^gThe detection limit for Bry emission is typically $\sim 0.5\text{--}1.5$ Å. The strength of the CO bandhead is given as a percentage increase in CO absorption over that of a dwarf of the same spectral type.^hThe position of the source relative to the central $5' \times 5'$ of the cluster, as defined in the text.ⁱSources 12, 24, 42, and 60 appear as single stars in the JHK photometry of Lada & Lada (1995) while resolved into two stars in the optical images of Herbig (1998).NOTE.—Sources are designated by their rank in K magnitude in the imaging of Lada & Lada (1995), which provides the coordinates and CIT JHK photometry presented here. Cousins I photometry is from Herbig (1998). $\Delta\alpha$ and $\Delta\delta$ represent the coordinates of Herbig subtracted from those of Lada & Lada.

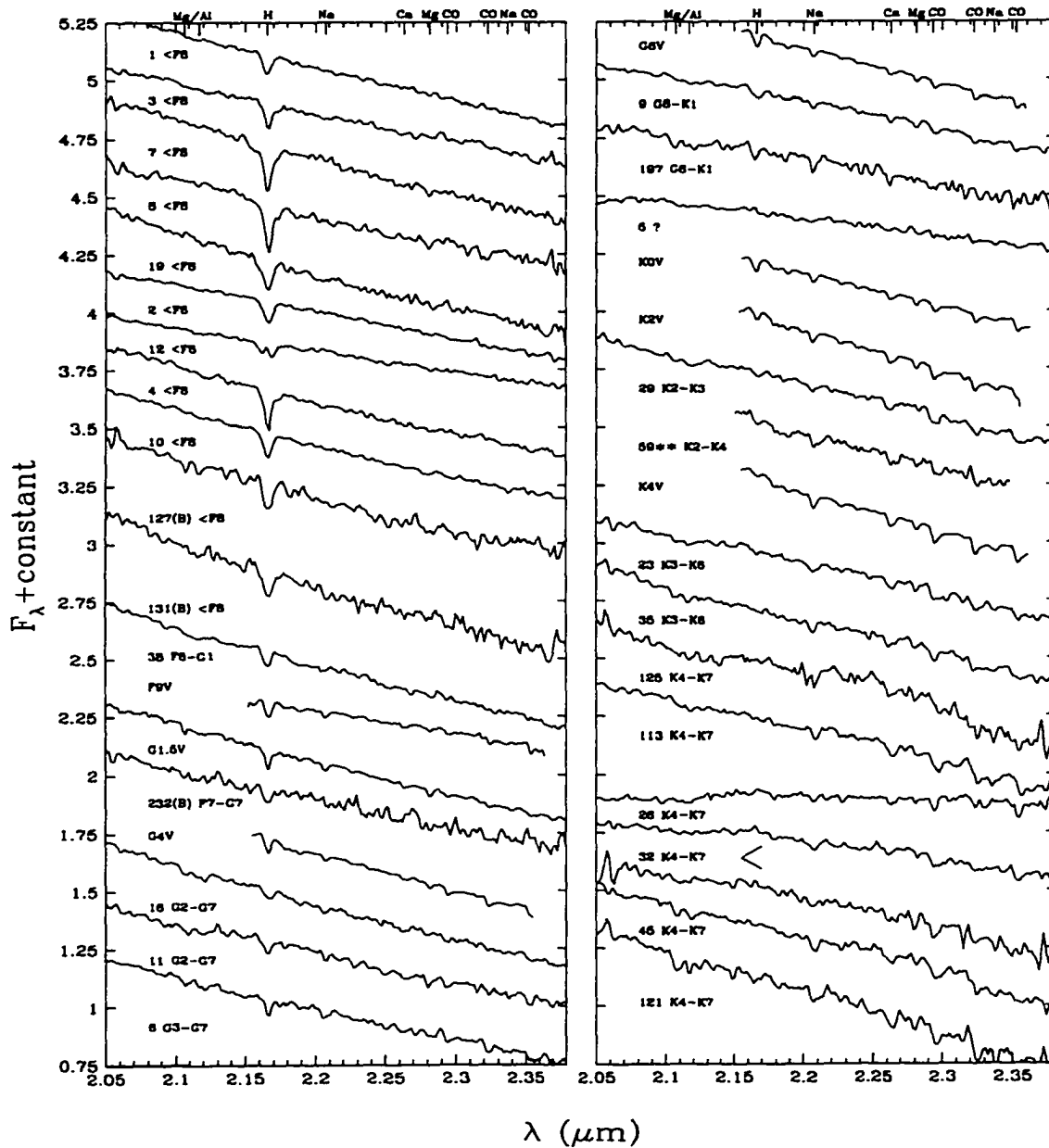


Figure 6.1 K -band ($R = 800$) spectra of sources in IC 348 in order of spectral type. Each spectrum is labeled with the number designation from Table 6.1 and IR spectral type. Background stars, foreground stars, previously published spectral types, and spectra observed at $R = 1200$ and smoothed to $R = 800$ are indicated with B, F, one star (*), and two stars (**). Spectra are normalized at $2.2 \mu\text{m}$ with constant offsets.

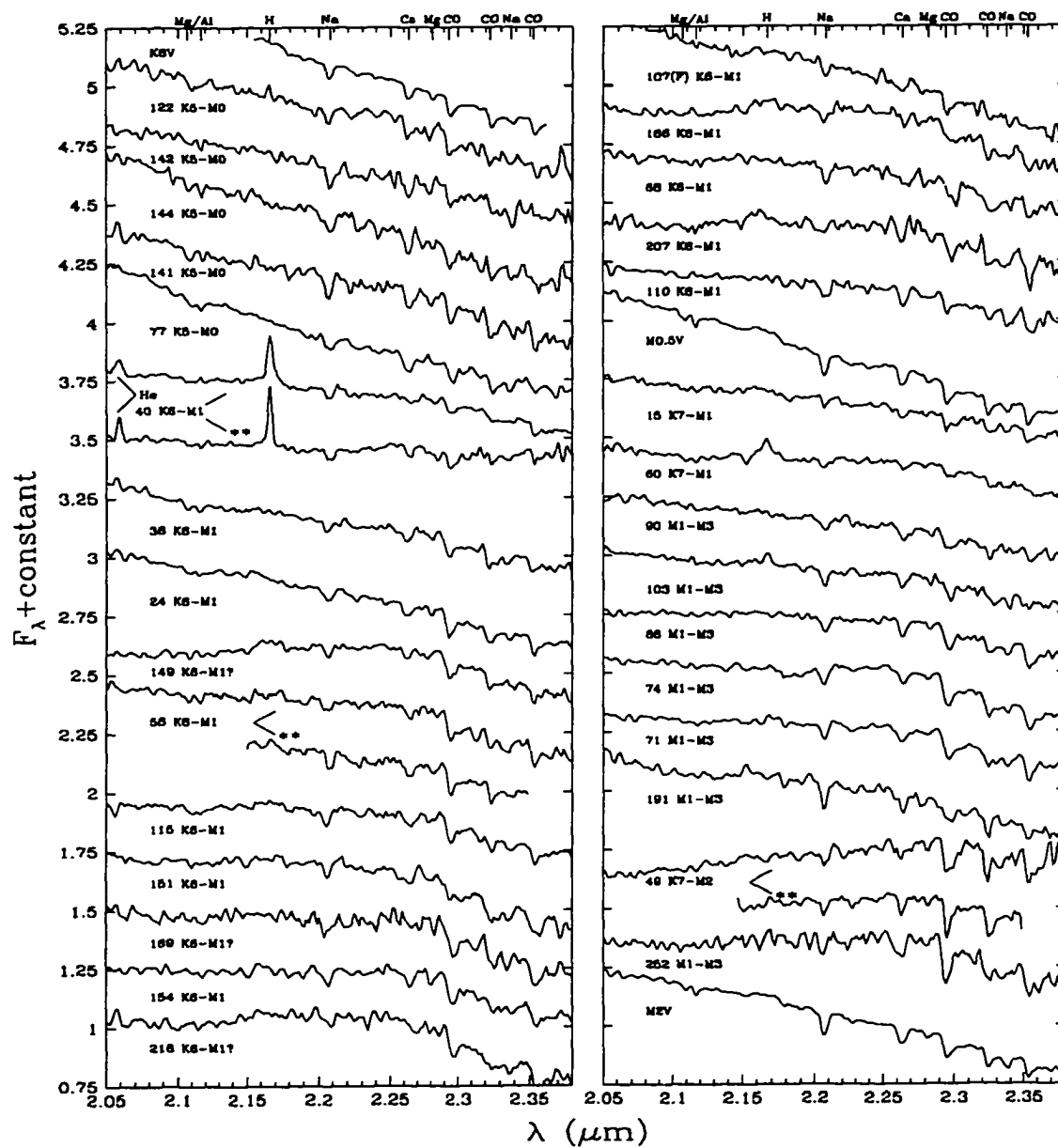


Figure 6.2 Same as Figure 6.1.

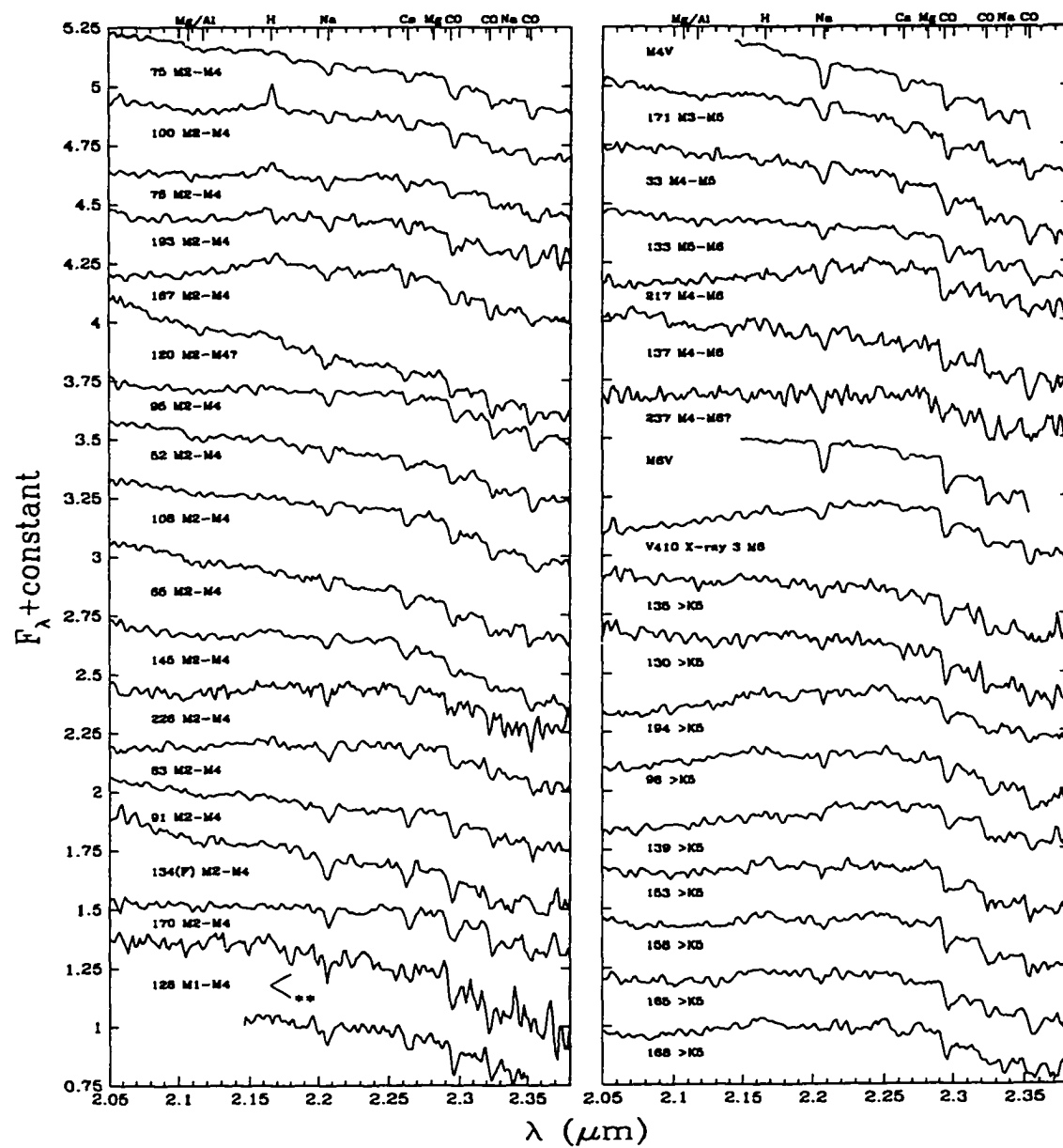


Figure 6.3 Same as Figure 6.1.

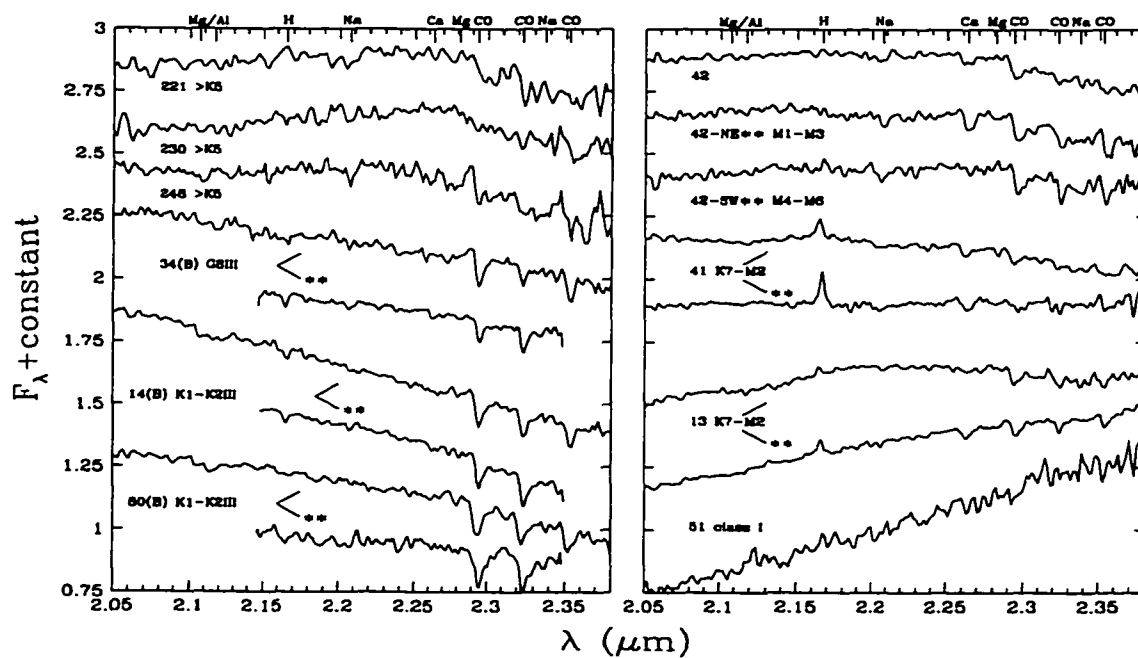


Figure 6.4 Same as Figure 6.1.

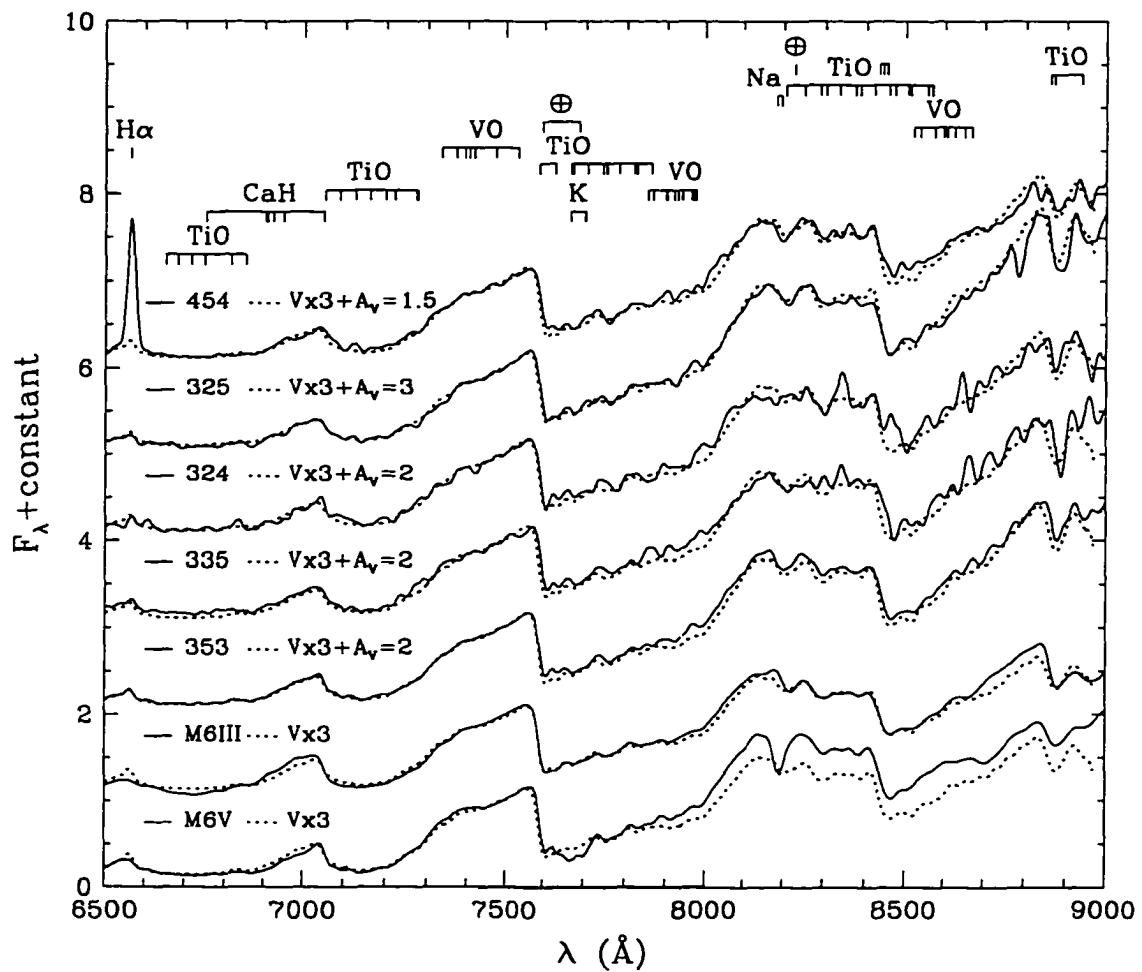


Figure 6.5 Optical spectra of M6 sources in IC 348 (solid lines). Extinction has been applied to the spectrum of the M6 object V410 X-ray 3 in L1495E to produce the best match with each source (dotted lines). Standard M6V and M6III spectra are also compared to the spectrum of V410 X-ray 3. All spectra are normalized at 7500 Å.

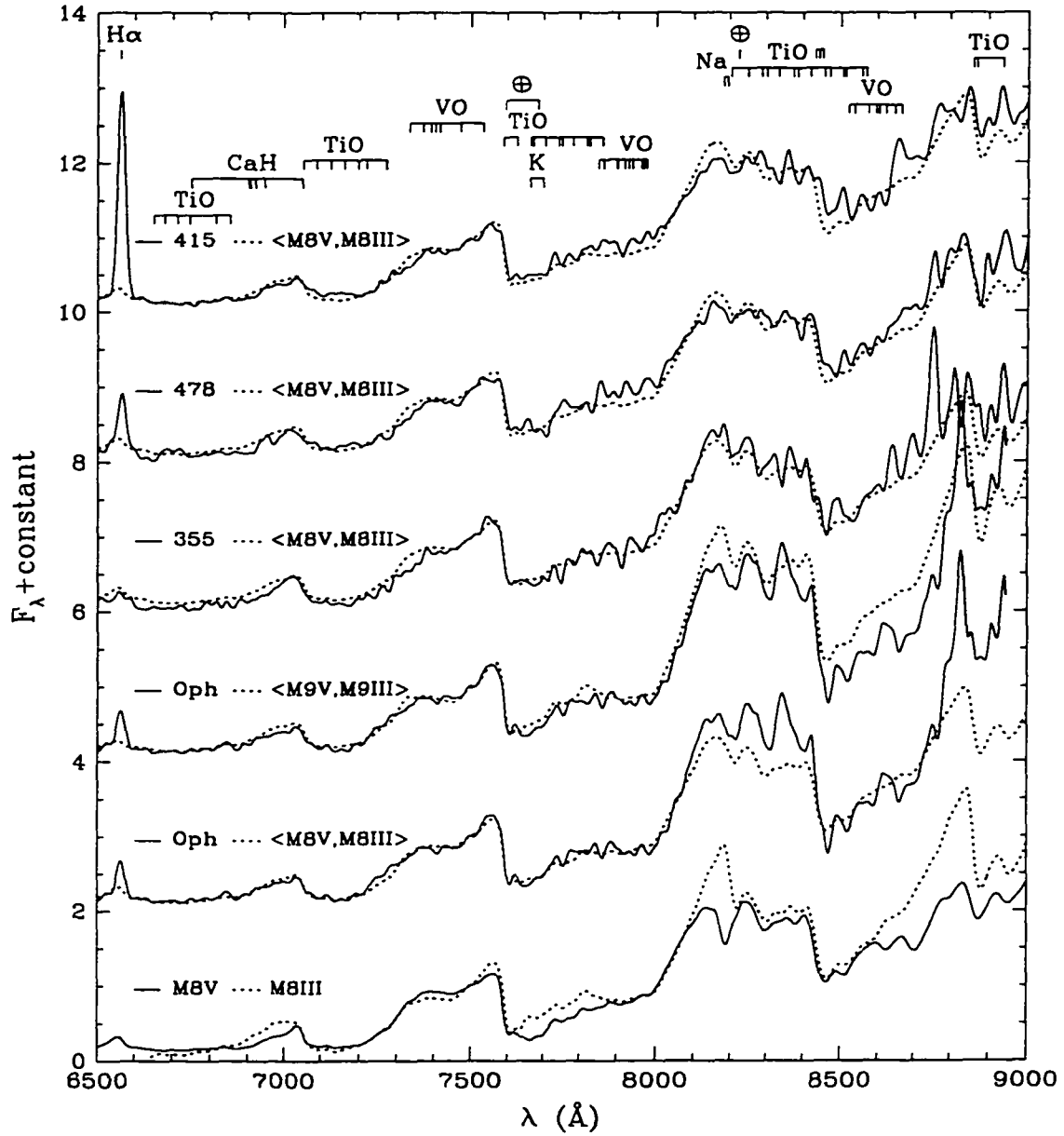


Figure 6.6 The three latest sources observed in IC 348 (415=M7.5, 478=M7.5, 355=M8) and ρ Oph 162349.8–242601 (M8.5) (solid lines) are plotted with averages of standard M8 and M9 dwarfs and giants (dotted lines). Features which are sensitive to surface gravity are apparent in the comparison of the M8 V and M8 III spectra. All spectra are normalized at 7500 Å.

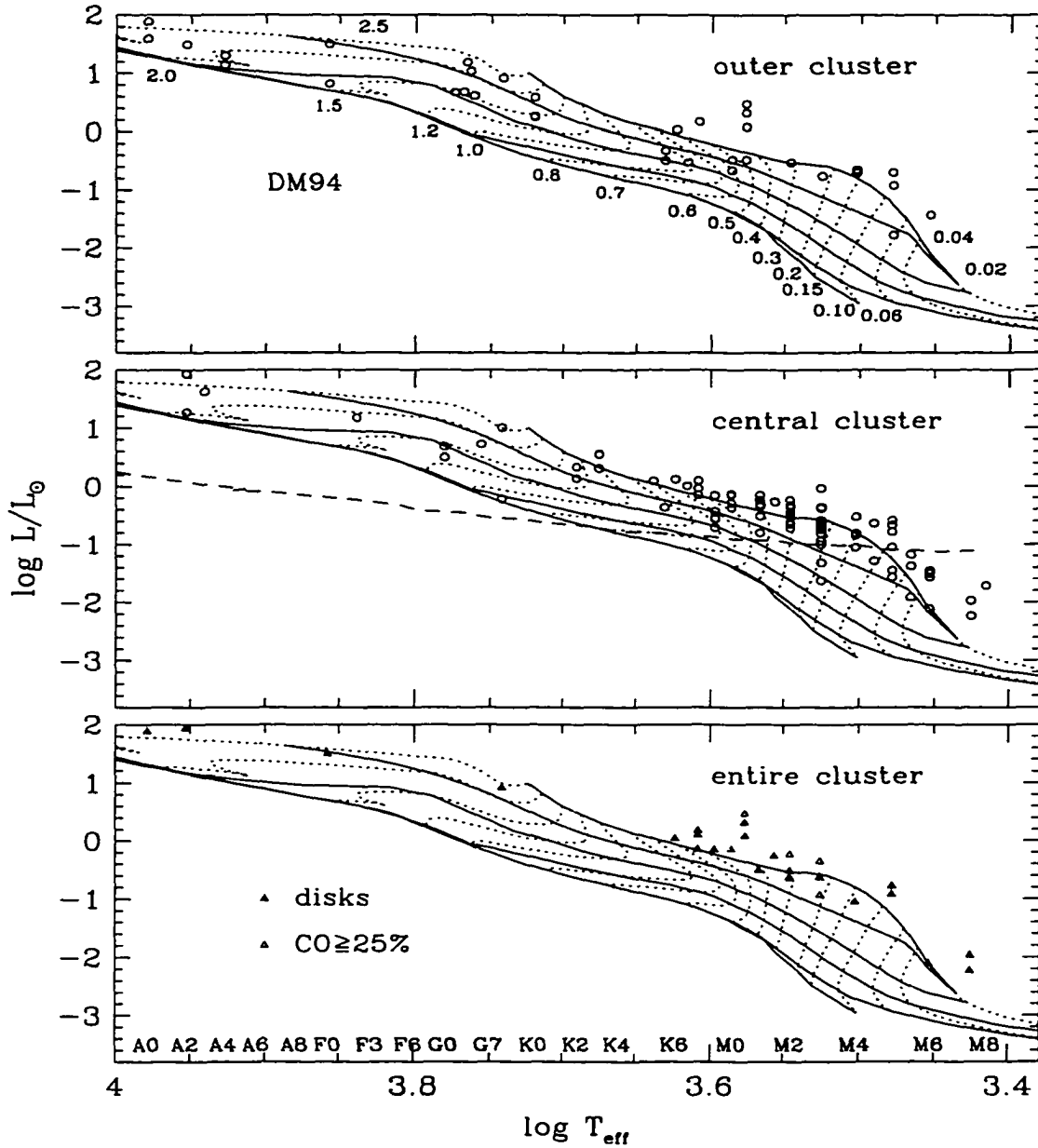


Figure 6.7 H-R diagram for IC 348 with the tracks of DM94 for the outer cluster (upper panel), the cluster core (middle panel), and all sources showing signs of disk activity ($W_{\lambda}(\text{H}\alpha) \geq 10 \text{ \AA}$, $W_{\lambda}(\text{Br}\gamma) > 0$, $r_K \geq 0.5$) and CO absorption ≥ 1.25 times that of a dwarf. Three early-type sources with significant K -band excess emission in Figure 6.12 are also indicated. The horizontal solid lines are isochrones representing ages of 1, 3, 10, 30, and 100 Myr, from top to bottom. The completeness limit of $K_{\text{dereddened}} = 12$ in the cluster core is represented by the dashed line.

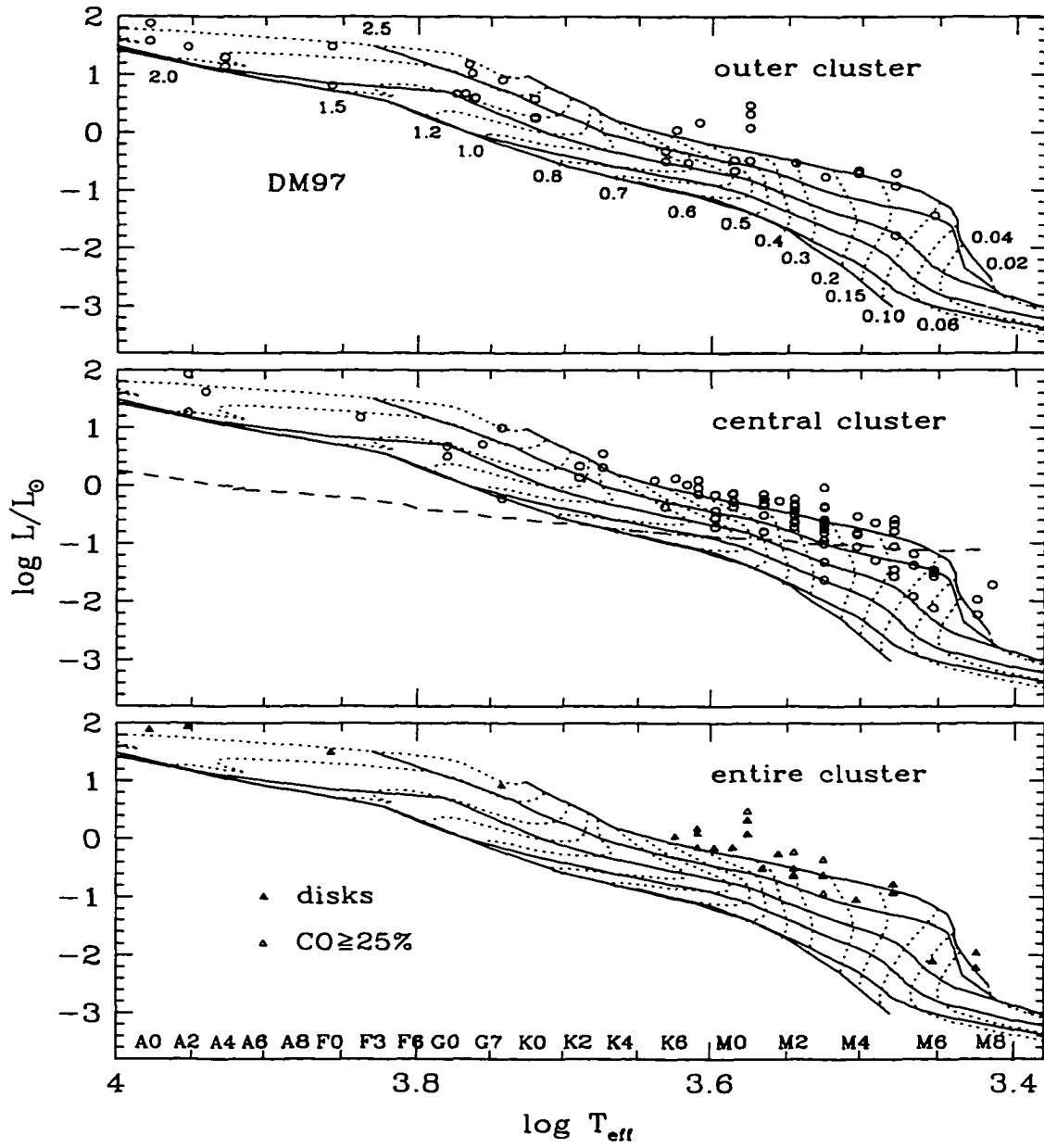


Figure 6.8 Same as Figure 6.7, but with the evolutionary tracks of DM97.

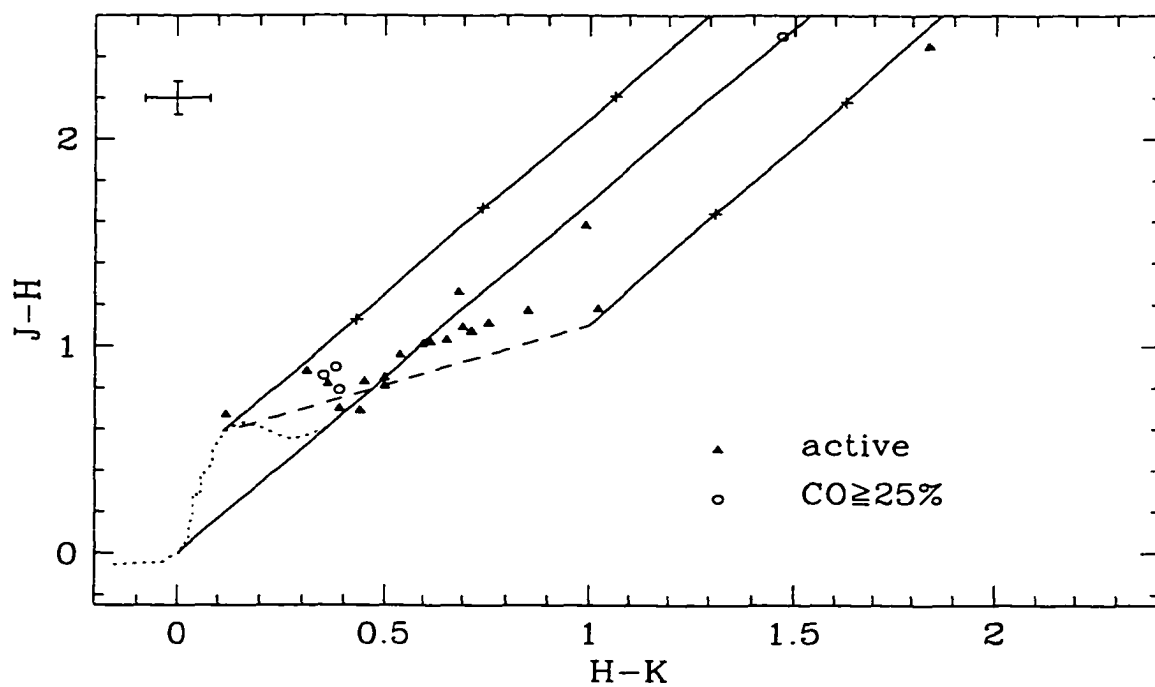


Figure 6.9 $H - K$ vs. $J - H$ for sources showing signs of disk activity ($W_{\lambda}(\text{H}\alpha) \geq 10 \text{ \AA}$, $W_{\lambda}(\text{Br}\gamma) > 0$, $r_K \geq 0.5$) and CO absorption ≥ 1.25 times that of a dwarf. Typical uncertainties of ± 0.08 in the colors are represented in the upper left corner. Pluses on the reddening lines appear at intervals of five magnitudes of visual extinction.

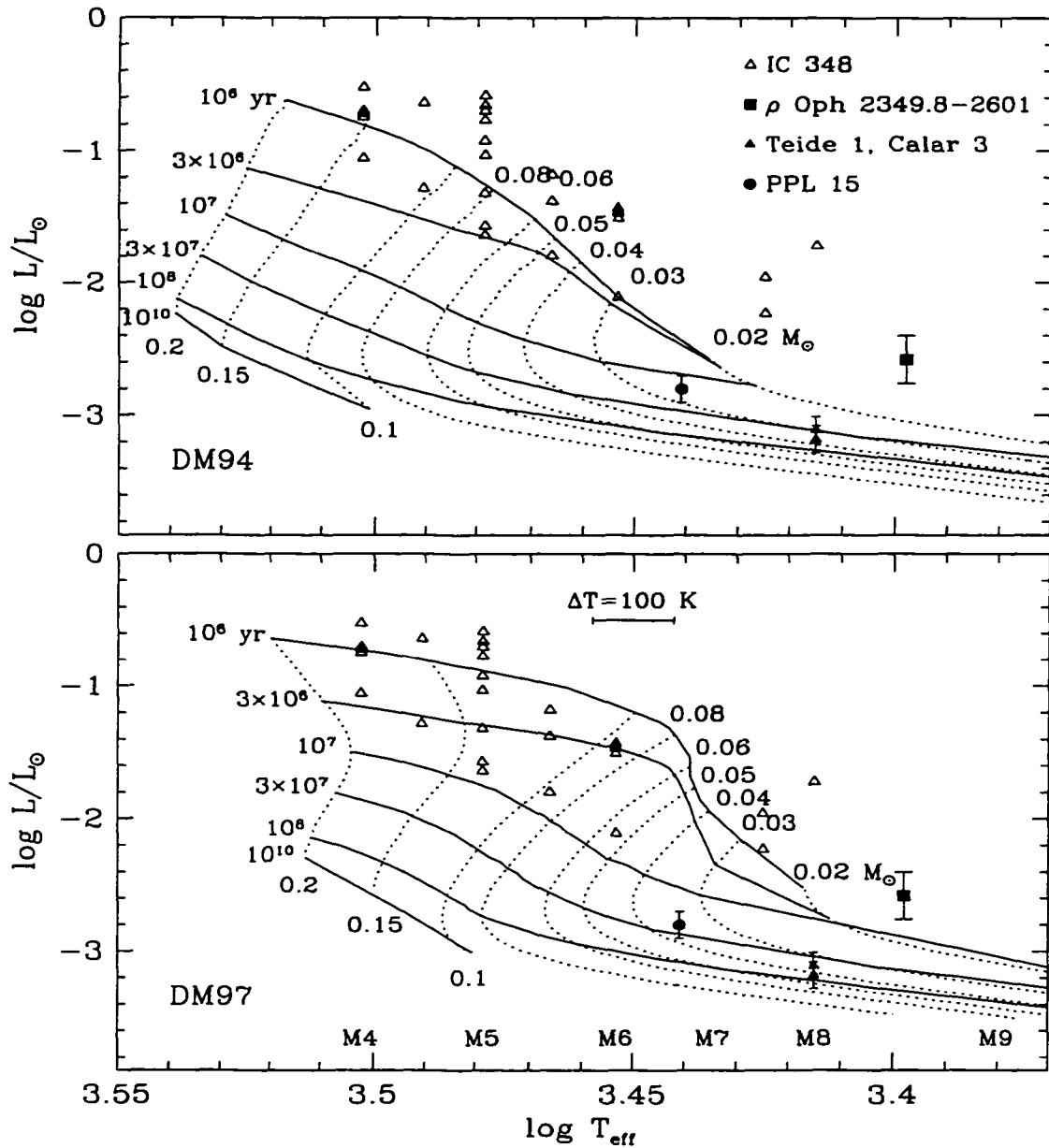


Figure 6.10 The H-R diagram for all late-type sources observed in IC 348 with evolutionary tracks of DM94 and DM97. The brown dwarf ρ Oph 162349.8–242601 and Pleiades brown dwarfs PPL 15, Teide 1, and Calar 3 are shown for reference. Uncertainties in spectral types and temperature scale are typically ± 0.5 subclass and ± 100 K, respectively.

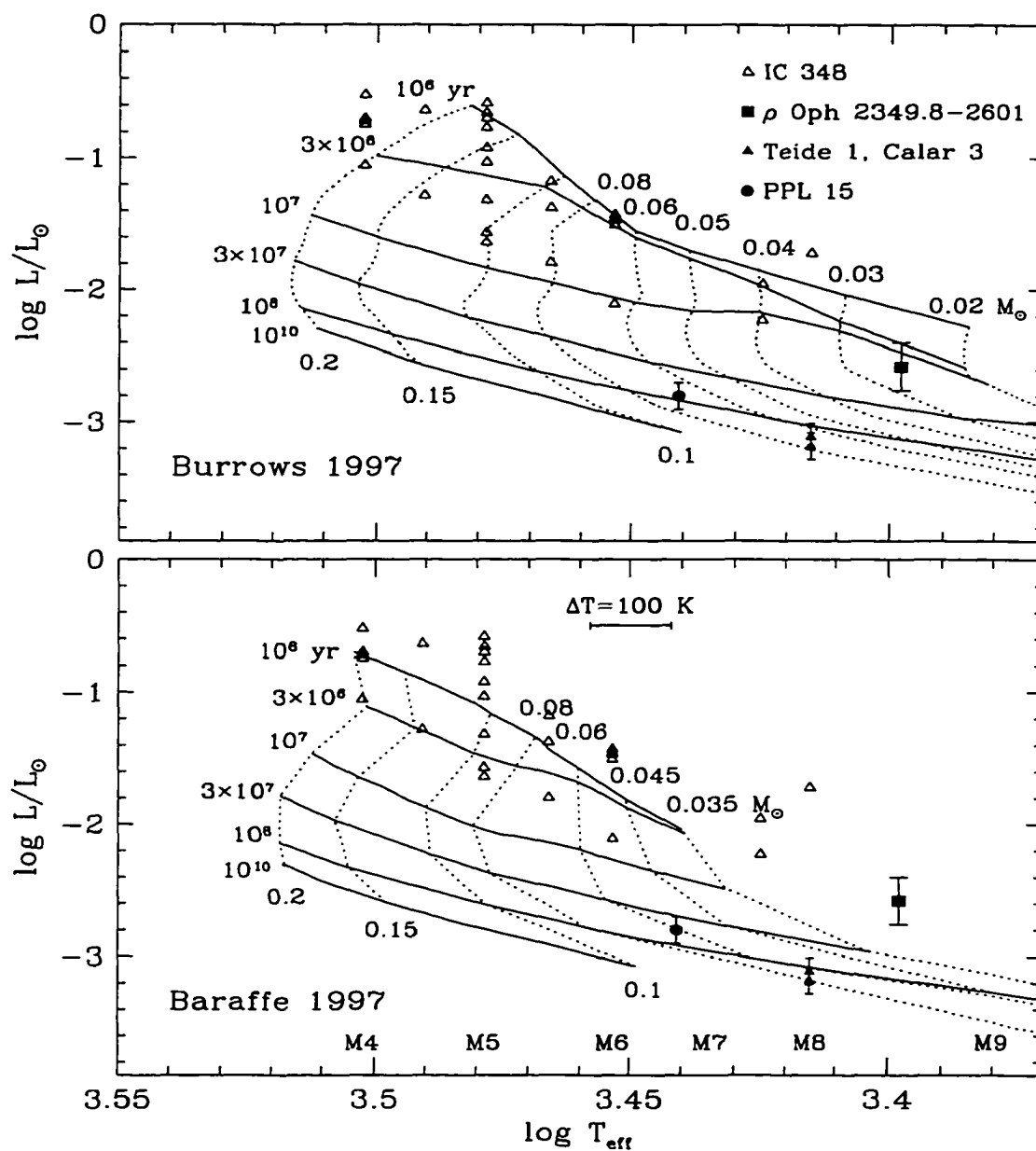


Figure 6.11 Same as Figure 6.10, but with the evolutionary tracks of Burrows (1997) and Baraffe 1997.

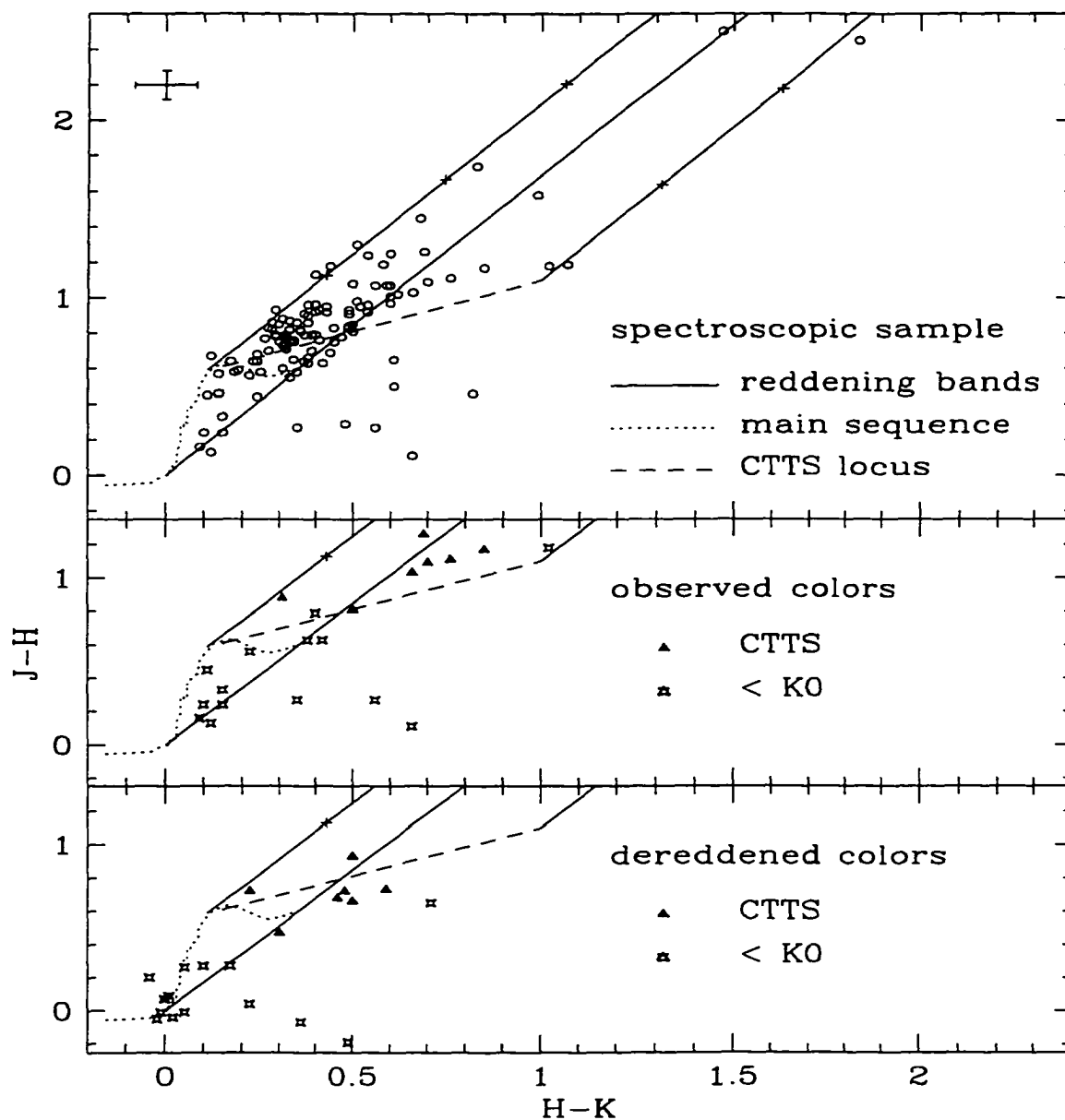


Figure 6.12 $H - K$ vs. $J - H$ for the spectroscopic sample in IC 348 in the upper panel, where the crosses indicate sources uncertain with spectral types. Typical uncertainties of ± 0.08 in the colors are represented in the upper left corner. For the T Tauri stars with optical spectra, we used extinctions derived from the spectra to deredden the sources from the observed colors (middle panel) to the intrinsic colors (lower panel). The stars represent early-type stars ($< K0$) which were dereddened with $E(V - I)$. Pluses on the reddening lines appear at intervals of $A_V = 5$.

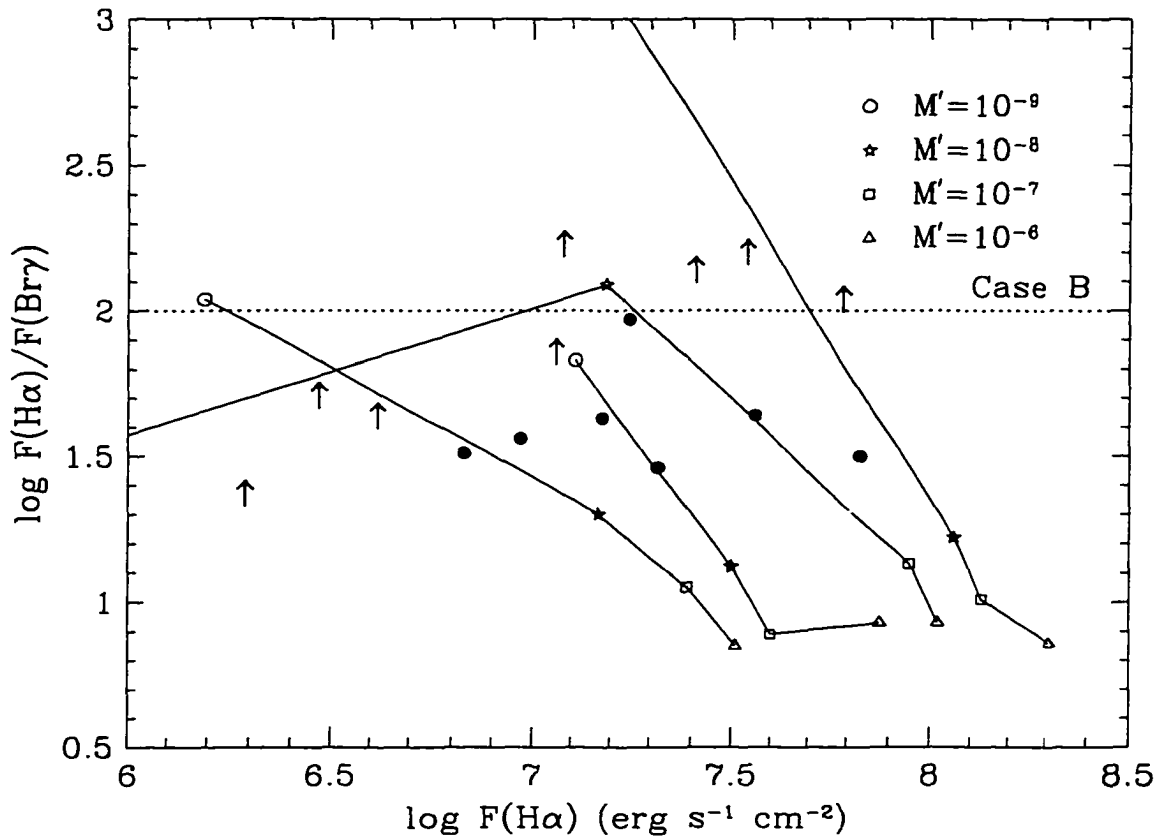


Figure 6.13 The $H\alpha$ line flux vs. the ratio of $Br\gamma$ to $H\alpha$. The solid points and arrows are observed values and lower limits for CTTS in IC 348 for which we have IR spectra. The uppermost solid point is CY Tau in L1495E. The magnetospheric accretion model predictions of Muzerolle, Calvet, & Hartmann (1998) are represented by solid lines from left to right for $r_{mi} = 2.2 R_*$, $r_{mo} = 3 R_*$, $T_{max} = 8000$ and 10000 K, $r_{mi} = 4 R_*$, $r_{mo} = 6 R_*$, $T_{max} = 8000$ and 10000 K. The models assume $M_* = 0.5 M_\odot$ and $R_* = 2 R_\odot$. For reference, the case B ratio is given as the dotted line.

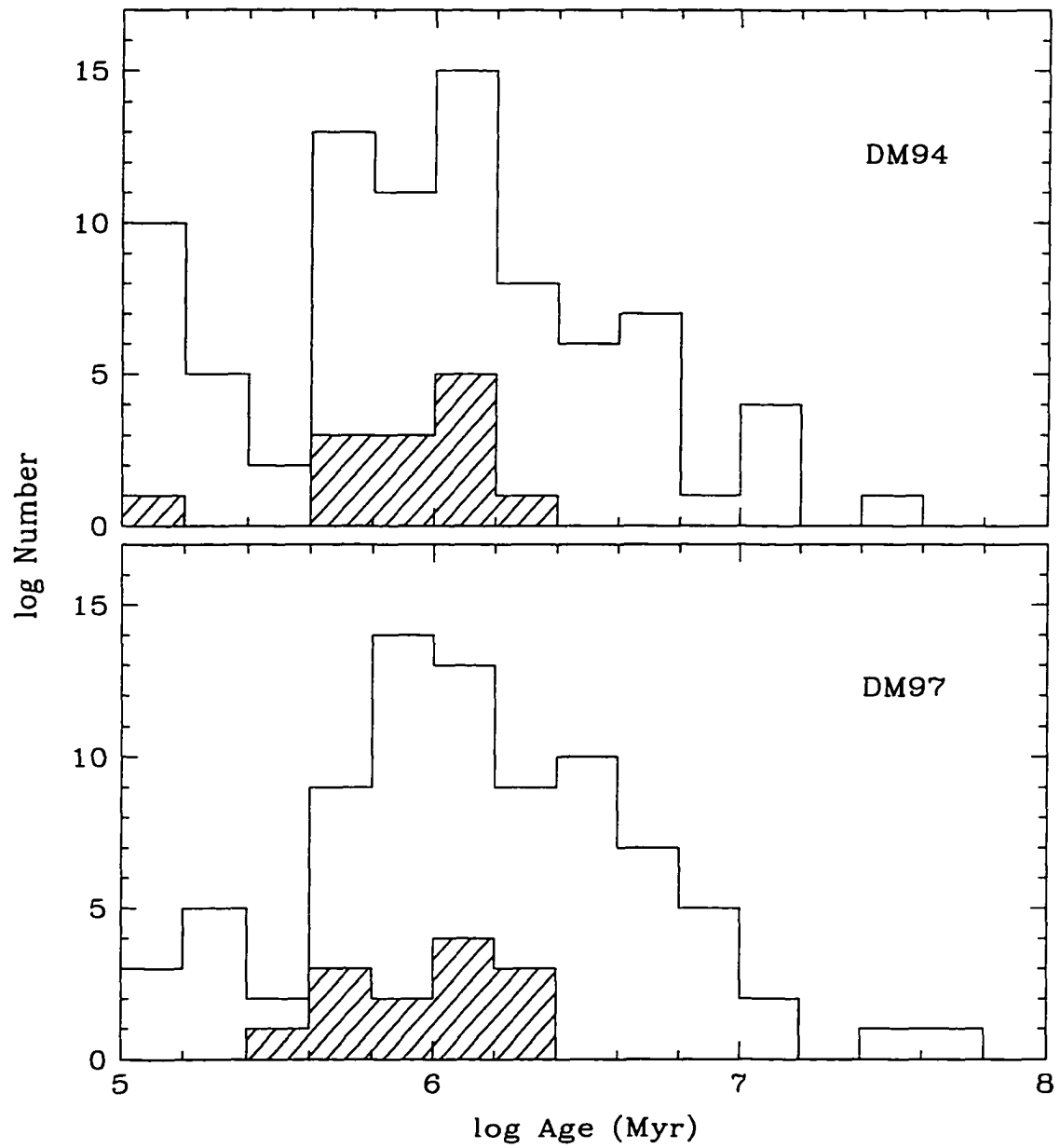


Figure 6.14 The distribution of ages for the core stars in IC 348 shown in the middle panels of Figures 6.7 and 6.8. The shaded histogram represents stars with disk activity.

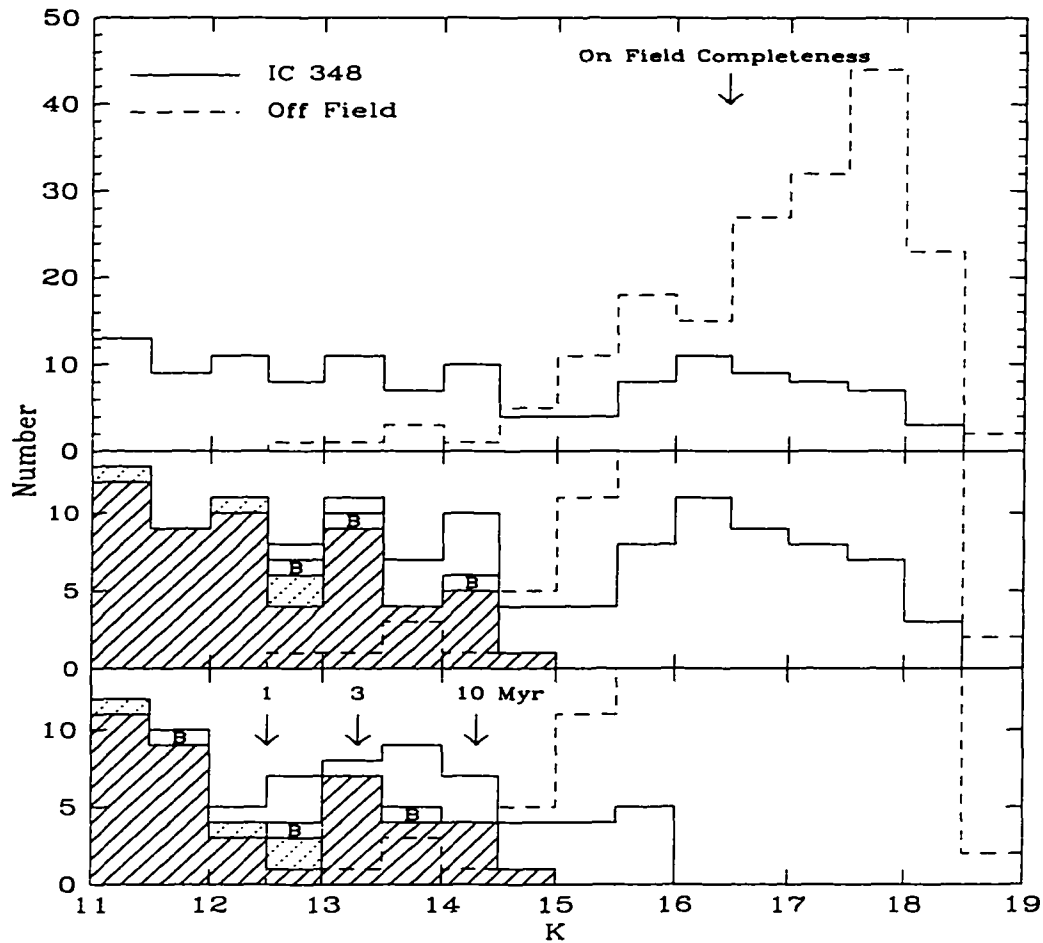


Figure 6.15 The K -band luminosity functions towards the $5' \times 5'$ core of IC 348 and a nearby off-field location of the same size are given in the top panel. The next panel shows magnified versions of these distributions, where solid stripes indicate stars which are plotted in the H-R diagrams in Figures 6.7 and 6.8. Sources with uncertain late-type spectral types ($>K5$) are represented by dotted stripes. In the lower panel, all sources brighter than $K = 16$ in IC 348 have been dereddened. The resulting KLF can be directly compared to the off-field KLF to estimate the number of background stars contaminating the IC 348 KLF at faint magnitudes. Sources identified as background stars in the spectroscopic sample are represented by "B". The arrows indicate the K -band magnitudes of DM94 corresponding to $0.08 M_{\odot}$ at 1, 3, and 10 Myr. If all stars are younger than 10 Myr, then the addition of sources without spectroscopy above $K = 14.5$ (open boxes) to the IMF in Figure 6.16 results in a mass completeness limit of $0.08 M_{\odot}$.

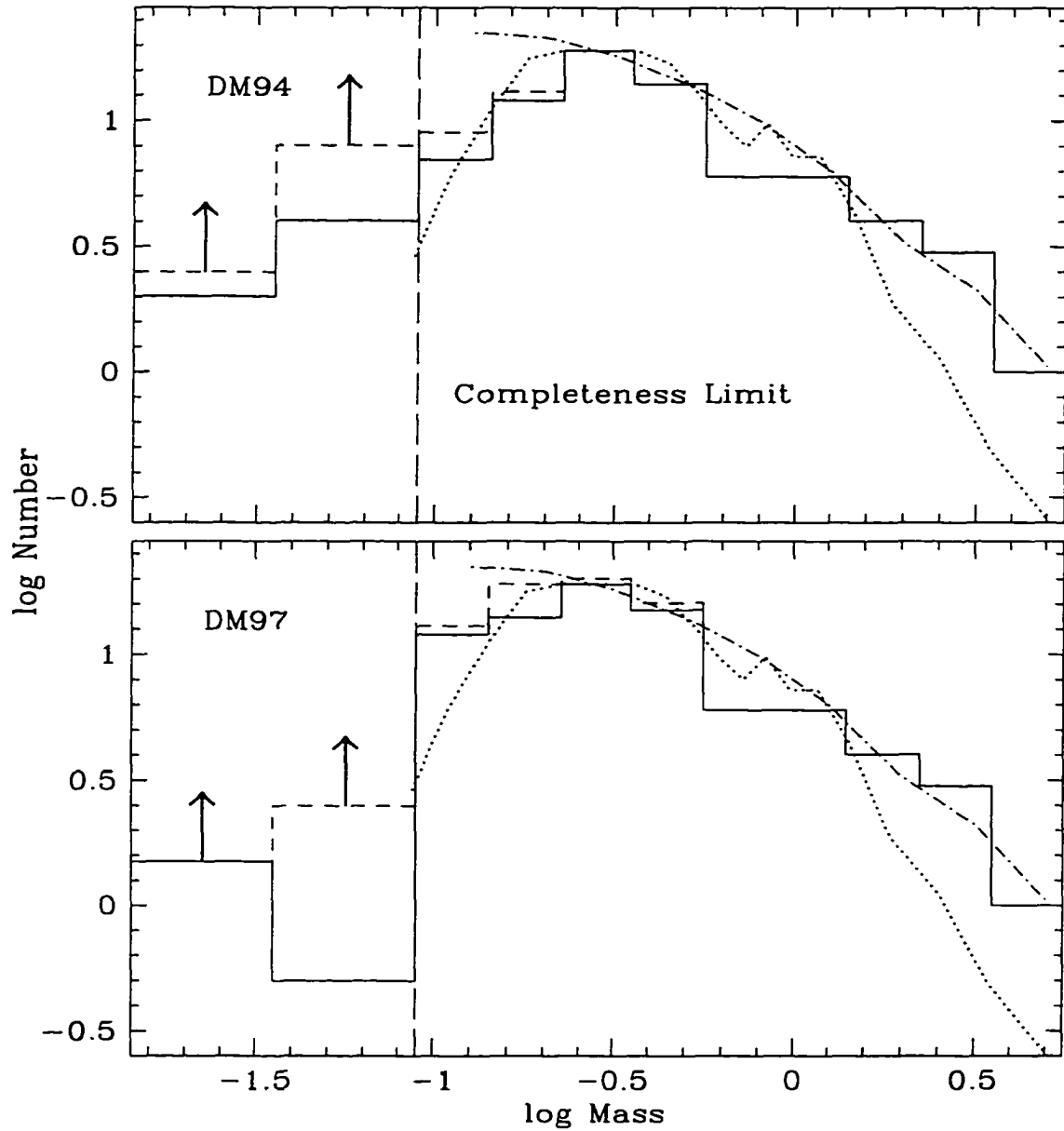


Figure 6.16 The solid histograms are the IMFs derived from the spectroscopic sample with the tracks of DM94 and DM97. The sources without spectroscopy in the lower panel of Figure 6.15 are added to the IMF as a completeness correction, represented by the dashed histogram. After such a correction, the completeness is indicated by the vertical dashed line and a lower limit to the substellar IMF is provided below this boundary. For reference, the field IMFs of Miller & Scalo (1979) (dot-dashed) and Scalo (1986) (dotted) are given.

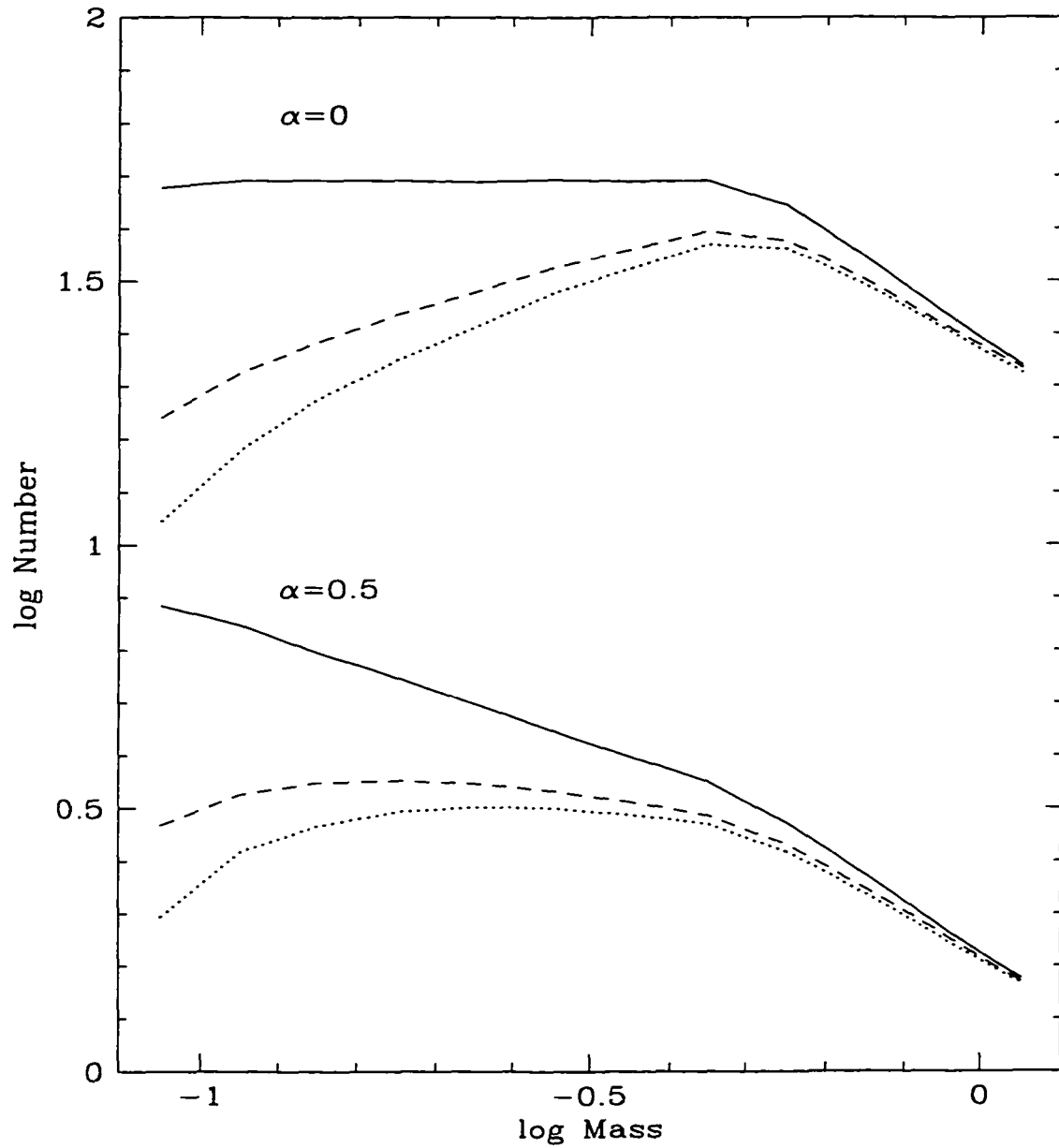


Figure 6.17 For two single star mass functions (solid lines) of $\alpha = 0$ and $\alpha = 0.5$ (Salpeter is 1.35), the simulated primary star mass functions (i.e., observed IMFs) are shown assuming binary fractions of 50% (dashed line) and 67% (dotted line).

CHAPTER 7

ρ OPHIUCHI

Young (< 10 Myr) stellar clusters within nearby ($d < 500$ pc) star forming regions offer insight into the birth of low-mass stars and brown dwarfs and the evolution of circumstellar disks. In particular, the distribution of masses in these populations directly reflects the initial mass function (IMF), as opposed to other regions (e.g., the field, globular clusters) where the present day mass function is the product of a complex evolution. By complementing optical techniques with modern infrared (IR) imaging and spectroscopy, we can estimate luminosities and spectral types for complete, well-defined samples of young objects within obscured star forming regions. Due to the luminous nature of newborn substellar objects, such data can be converted to mass functions which reach well below the hydrogen burning limit.

The ρ Ophiuchi dark cloud is an obvious region in which to perform such a study. The cloud core contains a very young (< 1 Myr), nearby ($d = 160$ pc), compact ($D \sim 20'$) population of ~ 100 low-mass stars. Due to the large extinction within the cloud, optical spectral types and photometry (e.g., Bouvier & Appenzeller 1992) and soft X-ray data (Montmerle et al. 1983; Casanova et al.

1995) are available for only a small fraction of the stars. Before the last few years, the ρ Oph members were studied primarily through their near- to mid-IR spectral energy distributions (SEDs), which were observed with single element detectors on the ground and aboard IRAS (Wilking, Lada, & Young 1989; Greene et al. 1994). Following the initial observations of ρ Oph with near-IR arrays (Barsony et al. 1989; Rieke, Ashok, & Boyle 1989), Greene & Young (1992) surveyed 650 arcmin² of the cloud at J , H , and K , providing a relatively sensitive ($K \sim 13$) photometric census of the stellar population. To reach young objects below the hydrogen burning limit, Rieke & Rieke (1990) obtained deep images ($K \sim 15.5$) of 200 arcmin² within the cloud core ($A_V \gtrsim 50$; Wilking & Lada 1983) and identified several brown dwarf candidates. The substellar nature of these sources has been supported by ISO mid-IR photometry (Comerón et al. 1998; hereafter CRCTL) and confirmed through spectroscopy in the optical (§ 4) and IR (Wilking, Greene, & Meyer 1998; hereafter WGM). After supplementing the data of Rieke & Rieke (1990) with $JHKL'$ aperture photometry, Comerón et al. (1993) (hereafter CRBR) found that the K -band luminosity function (KLF) of ρ Oph implied a logarithmically flat IMF (Salpeter is 1.35) down to and below the hydrogen burning limit. Williams et al. (1995) concluded that these results were consistent with the JHK modeling of Strom, Kepner, & Strom (1995). More recently, Barsony et al. (1997; hereafter BKLT) have obtained JHK photometry for thousands of sources across a square degree of around the cloud core complete to $K = 14$, from which Kenyon, Lada, & Barsony (1998) have measured a reddening law towards the cloud and examined the contamination by background stars.

Near-IR spectroscopy has recently been employed to study further the properties of the embedded stellar population in ρ Oph. After measuring K -band spectral types for 19 stars ($K < 10.5$, $R = 1000$), Greene & Meyer

(1995) constructed a Hertzsprung-Russell (H-R) diagram which implied an age of ~ 0.5 Myr for the cluster. Greene & Lada (1996) also observed ~ 100 young stars in Taurus and ρ Oph with lower resolution ($R = 500$) and broader wavelength coverage ($1.15\text{--}2.42\ \mu\text{m}$). The appearance of the spectra was closely correlated with SED class, indicating, as expected, that reddening increases and photospheric features weaken from Class III to Class I sources (Lada 1987). This trend is consistent with the large obscuration and strong continuum veiling expected from circumstellar material in the presumably younger, earlier SED classes. Finally, Green & Lada (1997) used very high resolution ($R = 21,000$) spectra to measure spectral types and continuum veilings for a small sample of flat-spectrum sources in ρ Oph. They demonstrated that the line profiles were consistent with absorption the originating in very young stellar photospheres rather than circumstellar disks, an important result which supports the validity of studying young stellar populations through IR spectral classification.

Expanding on the previous IR spectral classification in ρ Oph (Greene & Meyer 1995) and continuing my program started in L1495E (§ 5) and IC 348 (§ 6), I have performed K -band spectroscopy towards ~ 100 sources in the ρ Oph star forming region. This survey combines a magnitude-limited population in the cloud core ($K \lesssim 12$) with a representative sample from the outer regions of the cluster. The moderate spectral resolution ($R = 1200$) of the data allows both reasonably accurate spectral types ($\pm 1\text{--}2$ subclasses) and sensitivity to low-mass sources in ρ Oph ($\geq 0.1\ M_{\odot}$). I discuss the relation between the K -band spectroscopic properties ($\text{Br}\gamma$ emission and continuum veiling) and near and mid-IR SEDs in young low-mass stars, in addition to the detectability of photospheric absorption features in Class I and flat-spectrum sources. With the measured spectral types I construct an H-R diagram and use theoretical evolutionary tracks to derive

an IMF and star formation history for the cluster. Extending the IMF to lower masses, I include the likely substellar cloud members examined in § 4 and by WGM and CRCTL. Finally, I use a new KLF of the cloud core to develop a model of the reddened background population and identify likely cluster members lacking spectroscopy. After the addition of these sources, I arrive at an IMF complete to $\sim 0.08 M_{\odot}$, which is compared to results from studies of other young clusters.

7.1. Observations

I performed K -band spectroscopy on sources in ρ Ophiuchi using the near-IR long-slit spectrometer FSPEC (Williams et al. 1993) at the Steward 2.3 m Bok Reflector on Kitt Peak on 1994 July 15 and 1995 May 16, 17, 19 and at the Multiple Mirror Telescope (MMT) on Mount Hopkins on 1994 July 2-3, 1996 May 28-31, and 1996 June 3-6. Most of the spectra were obtained in 1996 with a grating providing a two-pixel resolution of $R = \lambda/\Delta\lambda = 1200$, while the data from 1994 and 1995 have a resolution of $R = 800$. The observations and data reduction procedures were identical to those described in § 6. I selected for spectroscopy ~ 30 sources with $K \lesssim 12$ appearing in IR images of the cloud core by CRBR. In addition, I observed ~ 70 sources surrounding the core, taken primarily from Greene & Young (1992). The spatial distribution of the spectroscopic sample is illustrated in Figure 7.1. The spectra are presented in Figs. 7.2-7.6, in order of IR spectral type and continuum veiling. Line identifications were made by comparison to the high-resolution ($R \geq 45,000$) spectra of cool stars obtained by Wallace & Hinkle (1996).

Imaging at K was performed at the Bok Reflector on the nights of 1998 April 12-15 using the Steward Observatory NICMOS3 256×256 near-IR camera at a plate

scale of $0''.64 \text{ pixel}^{-1}$, corresponding to a total field of $2'.7$ square. In 43 pointings, I observed the same region covered by CRBR (outlined by the dashed lines in Figure 7.1), in addition to a few extra positions, for a total of $\sim 250 \text{ arcmin}^2$. For followup observations at J and H during 1998 May 8-10, I selected three pointings which contained several faint, possibly low-luminosity K -band sources (outlined by dotted lines in Figure 7.1). At each position, I obtained images with dithers of $5''$ in a 4×4 grid, facilitating efficient flat-fielding and removal of bad pixels. Each exposure consisted of two coadded 30 s frames, producing a total exposure time of 16 minutes. A flat field was constructed by median combining frames which lacked bright sources. For calibration, I observed a photometric standard star, SR3, periodically during the night. After dark-subtracting and flat-fielding the images, the 16 frames at a given position were shifted and combined into one image. The tasks DAOFIND and PHOT under the package APPHOT were used in measuring the stellar coordinates and extracting photometry. The density of stars was low enough that I could measure the background emission in an annulus around each star and subtract it from the photometry. The data were calibrated with the CIT photometry of SR 3 from Elias et al. (1982) and are complete to $K \sim 17$. Using the coordinates measured by BKLT ($K < 14$) for nonsaturated ($K > 10$) stars in my images, I derived relatively precise ($\pm 1''$) coordinates for the fainter sources.

7.2. Individual Source Characteristics

7.2.1. IR Spectral Classification

In a study of the small stellar aggregate in L1495E in Taurus in § 5, I developed a technique of K -band spectral classification ($R \sim 1000$) to derive the spectral types and continuum veilings of young, late-type stars ($\sim 1 \text{ Myr}$, $> G0$). This method

was then used to classify ~ 100 stars in IC 348, where optical and IR spectral types were in reasonable agreement. The subtleties of K -band classification of young stars are discussed in § 5 and § 6. For instance, the surface gravity of pre-main-sequence stars is intermediate between that of dwarfs and giants, which results in weakened Na absorption at both $2.2 \mu\text{m}$ and 8200 \AA in young M stars relative to M dwarfs (§ 3; Martín, Rebolo, & Zapatero Osorio 1996). Comparing the data obtained in IC 348 ($R = 800$) and that presented here ($R = 1200$), I find that the higher resolution provides more accurate spectral types for G through M stars while maintaining sensitivity to faint sources. At the higher resolution I obtain more accurate measurements of Mg at $2.28 \mu\text{m}$, as illustrated in the observations of GY240A, GY240B, and GY250 at $R = 800$ and 1200 (Figure 7.3 and 7.4). The strength of Mg relative to Ca is important in the spectral classification of K through mid-M stars. As Mg disappears at later types, two other features (Ca and an unidentified line) replace it and at $R < 1000$ can be mistaken for Mg, while at $R \geq 1200$ the two lines are resolved and thus useful in the classification (see V410 Tau X-ray 6 in Figure 7.3). At types of M6 and later, lower resolution ($R \sim 500$) is sufficient for measuring spectral types from broad steam and CO absorption while maintaining greater sensitivity to faint, low-mass stars and brown dwarfs (see WGM).

I have extended my program of K -band classification to the obscured stellar cluster within the ρ Oph star forming region. The IR spectral types and measurements of $\text{Br}\gamma$ emission and continuum veiling at $2.2 \mu\text{m}$ ($r_K = I_{2.2}(\text{IR excess})/I_{2.2}(\text{star})$) are listed in Table 7.1. Typical uncertainties are 0.25-0.5 in r_K depending on the signal-to-noise, spectral type, and degree of veiling. I also list the spectral indices measured from the near- to mid-IR by Wilking, Lada, & Young (1989) and Greene et al. (1994). The spectra are shown in Figs. 7.2-7.6 in

order of spectral type and veiling. Following the Class I sources are stars I identify as background giants, which have very distinct spectra and are relatively easy to classify in moderate signal-to-noise data. A few spectra of lower quality are also given. The strong CO absorption in these sources could arise in either background giants or late-type cluster members, but the slopes, atomic lines, and mid-IR emission imply that most are probably the latter. Considering the various effects of veiling, surface gravity, and temperature on the appearance of these spectra, degeneracies in the classifications can occur. For instance, the sources classified as M4 are also matched by late-K stars with atomic lines weakened by veiling and CO enhanced by lower gravity. After comparison of IR and optical types in IC 348, I find that generally the simplest IR classification is the appropriate one, rather than a spectral type which requires simultaneous veiling and strengthening of CO. Previous optical and IR spectral types are listed in Table 7.1, which agree well with my measurements. Exceptions include SR20, GY410, and GY84. SR20 and GY410 were previously classified as G0: (Bouvier & Appenzeller 1992) and M6 (Greene & Meyer 1995), while I find very good fits with K5-M2 and K6-M0, respectively. The strength of Mg absorption in my data for GY84 indicates a spectral type of early M, in contrast to the M6 classification through steam features by WGM. In addition to the *K*-band sample presented here, I also give the sources recently classified in § 4 and by WGM.

On the northeast outskirts of the cloud, the bright IR source known as IRAS64A (Wilking, Lada, & Young 1989; Greene et al. 1994) does not appear to be a typical pre-main-sequence star. The *K*-band spectrum exhibits weak atomic lines and strong CO, indicative of a K giant. However, the near- and mid-IR excess emission towards this source implies youth and cluster membership. Furthermore, upon closer examination of the spectrum in Figure 7.7, I find that

the data matches that of FU Ori objects (Hartmann & Kenyon 1996), which all appear very similar in these spectra. One exception is the spectrum of RNO1C, which is more similar to the data for the K2III κ Oph (Kleinmann & Hall 1986). A well-known characteristic of FU Ori spectra is deep CO absorption, thought to arise in low-gravity disk atmospheres, which is seen in IRAS64A. I also find that the spectra from 2.15-2.3 μm are very similar among the FU Ori's shown in Figure 7.7 and distinct from that of a field giant. Some of this difference is likely due to broadening of lines from disk rotation. The FU Ori spectra also show two features on either side of where Mg appears in the giant (possibly the two lines seen in late M dwarfs) and unidentified absorption at 2.33 μm . These characteristics are also found in the spectrum of IRAS64A. While the FU Ori objects have strong CO absorption and late-type IR spectra, they tend to appear as F or G giants in the optical. However, I find that the optical spectrum (6000-9000 \AA) of IRAS64A is identical to the M8-M9III spectra presented by Kirkpatrick, Henry, & Irwin (1997). High-resolution spectroscopy on the CO band heads is necessary to determine whether a circumstellar disk is the origin of these peculiar optical and IR spectra.

Another unique source, GY182/WL16, is well-known for its strong CO band head emission, modeled successfully in terms of an inversion layer in a circumstellar disk (Carr et al. 1993; Najita et al. 1996). As seen in Figure 7.6, no photospheric features appear in the *K*-band spectrum of this Class I object. However, in observations of second overtone CO emission, Biscaya et al. (1998) detect absorption in the *H*-band Brackett series of hydrogen, presumably arising from the stellar photosphere of the central star. They conclude that the spectral type of WL16 is between B8 and A7, corresponding to $T_{\text{eff}} = 8000\text{-}12000$ K.

7.2.2. Derivation of A_J , T_{eff} , and L_{bol}

The recent survey by BKLT provides a homogeneous set of JHK photometry and coordinates for virtually the entire spectroscopic sample (see Table 7.1). The photometry is in the SQUID photometric system, which is similar to CIT (Kenyon et al. 1998). Photometry and coordinates for ROXs39 and SR22 are taken from Greene et al. (1994) and references therein. The photometry of these two stars was converted to CIT using transformations from Humphreys, Jones, & Sitko (1984) and Leggett (1992). Since the ρ Oph cloud core represents a relatively small fraction of the square degree observed by BKLT, most of the survey region has low reddening and background stars are likely to dominate the stellar counts. Under this assumption, Kenyon et al. (1998) used the IR color-color diagram to measure an extinction slope of $E(J - H)/(H - K) = 1.57 \pm 0.03$. I have spectroscopically identified several background stars, whose colors in Figure 7.8 are consistent with this reddening vector.

In an older cluster such as IC 348 (0.5-10 Myr), since much of the population consists of evolved Class III sources which show little evidence for disks, extinctions towards individual stars can be estimated by assuming the intrinsic colors of main sequence stars. On the other hand, in a very young cluster such as ρ Oph (< 1 Myr), most of the stars are Class I through Class II with IR colors affected substantially by emission from circumstellar disks and envelopes. By using $E(R - I)$ to deredden the $J - H$ and $H - K$ colors, Meyer (1995) derived a locus of intrinsic colors for classical T Tauri stars (CTTS) in Taurus, which are equivalent to Class II sources. The CTTS locus is shown as the dashed line in Figs. 7.8 and 7.9 and has been reproduced by models of star-disk systems (Lada & Adams 1992; Meyer, Calvet, & Hillenbrand 1997). To estimate extinctions for the stars in the spectroscopic

sample which have measured spectral types, I assume the CTTS locus measured in Taurus is applicable to ρ Oph. This is a reasonable assumption since the locus is consistent with CTTS studied in L1495E and IC 348 (§ 5; § 6). For stars within the reddening band of the CTTS locus ($H - K \leq J - H/1.57 + 0.3$), extinctions were calculated by dereddening the $J - H$ and $H - K$ colors to this locus. Since the CTTS locus is intermediate between dwarf and giant colors, this dereddening technique is also roughly consistent with the pre-main-sequence colors predicted in models of synthetic atmospheres (Bessell, Castelli, & Plez 1998). Extinctions were estimated for stars earlier than G0 by dereddening to the main sequence value of $J - H$ for a given spectral type. To convert spectral types and photometry to effective temperatures and bolometric luminosities, I have adopted the temperature scale and procedures discussed in detail in § 5 and § 6. I combined the dereddened J photometry with the bolometric corrections of Kenyon & Hartmann (1995) and distance modulus of 6.1 (Whittet 1974) to arrive at the bolometric luminosities. The source extinctions at J , effective temperatures, and bolometric luminosities are listed in Table 7.1, where the interstellar reddening law of Rieke & Lebofsky (1985) is used with A_J in the Johnson-Glass photometric system.

For the late-type sources observed by WGM, I have adopted their luminosity estimates while converting spectral types to effective temperatures with the scale used for the rest of my sample, which is 100-150 K warmer than found in WGM. No J photometry is available for two sources in the sample, GY244 and GY269. Since both show strong emission in the mid-IR, the $H - K$ color may be contaminated significantly by excess at K . Our measurements of r_K from the spectra could be used to correct for this effect, but since veiling can be variable (see § 7.3.2) and the spectra and colors were not measured simultaneously, I refrain from using $H - K$ to estimate reddening for these two objects. Although I cannot reliably place it

on the H-R diagram, I will use the spectral type of GY244 and a canonical age to arrive at an approximate mass which can be added to the IMF for the cloud core in § 7.3.4. Rather than use the above methods for the B star S1, I refer to the calorimetric luminosity derived by Wilking, Lada, & Young (1989).

7.3. The ρ Oph Stellar Population

7.3.1. Cluster Membership

Classic methods of determining cluster membership (e.g., proper motions, Li absorption) are unavailable for most of the stars in my spectroscopic sample. However, I can confidently distinguish cluster members from field contaminants, foreground stars and background giants, through other means. With K -band spectra of modest signal-to-noise, background giants are easily identified through their distinctive continuum structure and strong CO absorption. All of the background giants in the sample appear in the less reddened area surrounding the ρ Oph cloud core, as indicated in Figure 7.1. The sample of WGM includes one likely background giant and two background early-type stars. Most of the remaining sources are not background or foreground stars since they fall above the main sequence and have reddened colors. Three exceptions are WSB45, WSB46, and GY297, which show little or no reddening in the IR colors and have no other indications of youth and cluster membership, such as $H - K$ or mid-IR excess emission, weakening of Na expected for young M stars (§ 3; § 6), or Li absorption (WSB45; Bouvier & Appenzeller 1992). These are probable foreground stars and are omitted from further analysis. To examine cluster membership at fainter magnitudes beyond the limit of my spectroscopic sample, I will use a newly acquired KLF and diagrams of $H - K$ versus K to develop a model for the

background star population shining through the cloud core (§ 7.3.4).

7.3.2. Global Properties of the IR Spectra and Colors

Through low-resolution ($R = 500$) JHK spectroscopy, Greene & Lada (1996) examined the near-IR properties of a large number of young stars in ρ Oph and other star forming regions. A range of IR SED classes were represented in their sample, including Class I ($a > 0.3$), flat spectrum ($0.3 \geq a \geq -0.3$), II ($-0.3 > a \geq -1.6$), and III ($a < -1.6$), where a is the mid-IR spectral index (Lada 1987; Greene et al. 1994). Greene & Lada observed a trend of increasing line emission and reddening in addition to weakening absorption lines from Class III to Class I sources, consistent with the evolutionary interpretation of these observational classes. I can take this experiment further with the measurements of continuum veilings, r_K , from the K -band spectra. Figure 7.8 shows $H - K$ versus $J - H$ diagrams where the main sequence and CTTS locus are plotted with their respective reddening bands. In the first three panels I present the spectroscopic sample as a function of r_K . As one would expect, there is a clear sequence from sources with heavily veiled spectra and large $H - K$ excesses to objects with no detectable veiling and normal colors for reddened main sequence stars. The scatter in this correlation, where a few sources with large r_K have small excesses in $H - K$, can be explained by variability in the excess continuum emission. Such variability is evident in the data for GSS26 (flat spectrum) and GY51 (Class II). In May of 1996, these sources exhibited strong $\text{Br}\gamma$ emission and $r_K \sim 4$ and 2, while in July of 1994 the $\text{Br}\gamma$ emission was weaker and the veilings were only 0.75 and 0.5. Furthermore, when these spectra are flux calibrated, I find that GSS26 and GY51 were ~ 1.2 and 1.3 mag brighter at K in 1996 relative to 1994, consistent with an increase in excess continuum emission implied by r_K .

Previous studies (e.g., § 5; Greene & Meyer 1995) have shown that *K*-band spectroscopy can be used to measure spectral types for Class II and Class III sources. Can photospheric features also be detected in extremely young, Class I protostars? Greene & Lada (1997) observed absorption features in two flat-spectrum sources (GY21, GY279) and demonstrated that they likely originate in the photospheres of the central stars (rather than disks). With the large set of moderate-resolution spectra presented here, I can further examine the detectability of absorption features in flat-spectrum and Class I sources. Objects with featureless *K*-band spectra include GY6, GY20B, GY182, GY214, GY227, GY254, GY265, GY274, GY378 (Class I), GY224, GY205 (flat-spectrum), and GY129 (Class II). In addition to most of the Class II and Class III sources, absorption features are detected in GY111, GY192, GY240A, GY240B, GY244, GY269, GY304 (Class I), GSS26, GY21, GY128, GY239, GY252, GY273, GY279, and GY315 (flat-spectrum). Considering the heavy veiling expected from circumstellar disks and envelopes, it is surprising that absorption lines are seen in such a large fraction ($\sim 50\%$) of Class I and flat-spectrum objects. Since the signal-to-noise is rather low in some of the featureless spectra, higher quality data could reveal absorption features in still more of these Class I sources.

I now make a comparison of the IR characteristics of the stellar populations in the cloud core and in the surrounding region, which are separated by the dashed line in Figure 7.1. In the diagrams of $H - K$ versus $J - H$ in Figure 7.9, I find that a larger fraction of sources within the cloud core have near-IR excess emission. Another comparison can be made by designating sources with evidence for circumstellar disks as those exhibiting $W_\lambda(\text{Br}\gamma) > 1 \text{ \AA}$ or $r_K \geq 0.5$. In the H-R diagram at the bottom of Figure 7.10, I find that the sources with and without this disk signature have comparable ages on the tracks of DM97.

In a study of the older cluster IC 348 (0.5-10 Myr) in § 6, $\sim 24\%$ of sources within the core with ages less than 3 Myr met this criterion. In the core of ρ Oph, if I omit the B star and seven sources with uncertain K-M classifications and hence no veiling measurements, the frequency of disks is 17/27 (63%). The frequency is somewhat lower in the outer cluster, 23/45 (51%), after omitting the four earliest stars, two K-M stars, IRAS64A, and the foreground and background stars. The difference between the two populations is more pronounced when I compare the behaviors of the SEDs. For sources in the cloud core which have been observed in the mid-IR (Wilking, Lada, & Young 1989; Greene et al. 1994), the number distribution among Class I, flat spectrum, Class II, and Class III is 9, 5, 10, and 1, respectively. In the outer cluster, on the other hand, the SEDs are generally more evolved, where the distribution is 4, 5, 22, and 6. In IC348, the lower fraction of disk sources in the core relative to remainder of cluster was attributed to the accelerated truncation of disks at higher stellar densities (H98; § 6). In ρ Oph, since the densities are rather low throughout the region, the higher disk frequencies from the core outward are instead likely to be due to the birth of stars in the cloud core and their dispersal outward. Such an age gradient is supported by the ages implied by the H-R diagram of the inner and outer clusters, as discussed in § 7.3.3.

7.3.3. The H-R Diagram and Star Formation History

I use the estimates of T_{eff} and L_{bol} from § 7.2.2 to place the K -band spectroscopic sample on H-R diagrams in Figure 7.10. The sources of WGM and § 4 are also included. I have omitted the foreground and background stars and sources with uncertain spectral types ($< F8$, K-M, featureless). The diagram of $H - K$ versus K in Figure 7.12 indicates that the core spectroscopic sample is complete to $K_{\text{dereddened}} = 11$ for $H - K < 2$ ($A_K < 3$), which corresponds to the dashed line on

the H-R diagram for the core.

To interpret the H-R diagram of ρ Oph, several sets of low-mass evolutionary tracks are available, where those of D'Antona & Mazzitelli (1994) (hereafter DM94) have been used predominantly for young clusters. In § 2 and § 5, I describe the various model interiors at low masses and young ages and make comparisons of the model predictions with observations of YY Gem and CM Dra, Pleiades, the main sequence, and globular clusters. In § 6, I updated this discussion to include the latest evolutionary tracks of D'Antona & Mazzitelli (1997) (hereafter DM97). While calculations of both DM94 and DM97 were used in the analysis of data for IC 348 to provide continuity with previous studies, I will proceed with only DM97 in the following discussion. The isochrones and mass tracks of these two suites of models are very similar above $0.2 M_{\odot}$. In § 7.3.4 I describe in the general context of young clusters how the IMF derived with DM97 differs from that calculated with DM94.

As shown in Figure 7.10, the tracks of DM97 imply a median age of 0.3 Myr for the cloud core, with a few stars older than 1 Myr, particularly at the lowest masses where the scatter in ages is largest. A similar range of ages is found in the outer cluster sample, where the median age is slightly older. A trend towards older ages with increasing distance from the cloud core is more obvious in the H-R diagram plotted by Greene & Meyer (1995) for optically visible stars observed across three square degrees (Bouvier & Appenzeller 1992). Greene & Meyer also derived an H-R diagram for a sample observed with IR spectroscopy, composed of 5 stars from the core and 14 stars from the outer cluster. They found a distribution of ages very similar to that of the inner cluster in Figure 7.10, although the study was slightly deficient in stars older than 1 Myr relative to the work presented here.

Considering the uncertainties in evolutionary tracks and luminosity estimates at such early stages of evolution, absolute ages for these individual stars are not very meaningful. However, it is clear that ρ Oph is one of the youngest stellar populations relative to other clusters placed on the same evolutionary tracks.

7.3.4. The Initial Mass Function

The Spectroscopic Sample

In conjunction with the evolutionary tracks of DM97, I can use T_{eff} and L_{bol} to estimate masses for individual sources in ρ Oph and construct a cluster IMF. Since the cloud core provides an excellent screen against background stars, cluster membership and completeness are more readily addressed and I thus restrict the analysis of the mass function to sources within this region (see Figure 7.1). A total of 36 sources from the K -band spectroscopic sample fall within the cloud core. I have adopted the spectral types of WGM for three of these and refer to them as part of the WGM sample. Six sources exhibit heavily veiled, featureless spectra and are excluded from this calculation of the IMF. For the 16 stars from my sample and 12 stars from WGM and § 4 shown in the H-R diagram of the inner cluster, individual masses were determined from the evolutionary tracks. Because of uncertainties in the spectral types and subsequent mass estimates for two of the three early-type stars, the two highest mass bins are given widths of $\Delta \log M = 0.4$. In addition, for GY182/WL16 I use the H -band spectral type and a rough luminosity estimate to place it in the mass bin centered at $\log M = 0.35$ ($1.4\text{--}3.5 M_{\odot}$). The two lowest mass bins were also doubled in width since the evolutionary tracks and temperature scales are uncertain in this regime. Two other sources in my sample have uncertain reddenings and luminosities due to strong IR excess emission (GY51) and a lack of J photometry (GY244). By assuming these

objects have ages comparable to the rest of the inner cluster, I combined their spectral types with the evolutionary tracks to arrive at mass estimates.

Four sources in the cloud core had relatively uncertain late-type classifications (K-M) and hence were not plotted in the H-R diagrams. These are indicated by dotted circles in the figures. However, the spectral types are constrained well enough to estimate the mass bins these objects should fall within. Additional comments on the spectral types of these sources are given in the § 7.5. Combining the photometry and spectral type (\sim M5-M6) for GY29, I arrive at a luminosity of $0.12 L_{\odot}$ and a subsequent DM97 mass of $0.12 M_{\odot}$. Although GY192 is a Class I object and has a large $K - L'$ excess, the $J - H$ and $H - K$ colors show little excess and the K -band absorption features are strong. I find that the spectral type ($>$ M3) and luminosity estimate are consistent with the age of the cluster, implying a mass of $\sim 0.2 M_{\odot}$. Strong excess emission in $H - K$ and $K - L'$ and weak K -band features are found in 162712 – 243449. The spectrum of GY128 is very noisy and quantitative measurements of its features are not possible. It also exhibits a flat-spectrum SED and large $K - L'$ excess. Since these two objects cannot be classified and appear to be high-excess, heavily veiled objects similar to the six featureless sources mentioned previously, they are omitted from the IMF. The resulting IMF for the cloud core is composed of 36 sources, represented by the solid histogram in Figure 7.13.

Completeness Correction

A completeness correction can be applied to the above IMF by 1) developing a model for the background stars shining through the cloud core, 2) identifying likely cluster members which lack spectroscopy, and 3) estimating their masses

by combining canonical cluster ages from the H-R diagram with photometry and evolutionary tracks.

In a similar approach used in my studies of L1495E and IC 348 (§ 5; § 6), I have obtained deep K -band images of the cloud core ($A_V \gtrsim 50$), covering the same region surveyed by CRBR (see Figure 7.1). For the following discussion, I have merged my photometry with that of BKLT and CRBR. I use the data of BKLT when both H and K are provided ($H \lesssim 15.5$, $K \lesssim 15.0$), photometry of CRBR for the remaining sources detected in that work ($H \lesssim 17$, $K \lesssim 15.5$), and my new data for the faintest stars. The resulting set of photometry includes objects found in this survey and that of BKLT but not reported by CRBR: 162706 – 243811, 162713 – 243330, 162726 – 244045, 162648 – 242836, and 162622 – 242254 (GY12). The first four sources are faint companions to brighter objects while GY12 falls within bright nebulosity, explaining their absence from the photometry of CRBR. I reject five stars detected by BKLT which do not appear in my images or those of CRBR: 162718 – 243433, 162720 – 243820, 162703 – 243726, 162719 – 244156, and 162719 – 244122. The cloud core KLF for the combined BKLT and CRBR data is given in Figure 7.11, in addition to the deeper extension provided by my data. It is evident from the rapid rise in counts at $K > 16$ that the new KLF reaches the background star population behind the cloud core. To simulate this field population, I selected all BKLT sources within a $25' \times 10'$ area centered at $\alpha = 16^{\text{h}}24^{\text{m}}21^{\text{s}}30$, $\delta = -24^{\circ}42'00''$ (1950), which roughly equals size of the cloud core. This position is near the outskirts of the BKLT survey where the molecular column density associated with ρ Oph is quite low, likely containing only relatively unreddened field stars. This off-field KLF must be reddened by $A_K \sim 3.75$ to fit the background star KLF ($K > 16$) observed towards the core. Such an average extinction is also consistent with the lack of background stars at $K < 12$ in the

spectroscopic sample for the cloud core. Since only the brightest and least-reddened background stars will appear in the H -band luminosity function (HLF) towards the three fields imaged at J and H (see Figure 7.1), a comparison of the KLF and HLF implies a minimum extinction of $A_K \sim 3$ through the cloud. The off-field KLF is fit well with a function of the form $N(m)dm \propto 10^{\alpha m}dm$, where $\alpha = 0.31$, which is consistent with the Galactic field distribution observed by Wainscoat et al. (1992). When a KLF of this form is reddened, Comerón & Rieke (1998) found that the exponential form and value of α are preserved regardless of variable extinction or clumps. Thus, I show this fit to the background stars within the cloud core KLF in Figure 7.11. In a diagram of $H - K$ versus K in the third panel of Figure 7.12, I have reddened the off field by the best fit extinction, illustrating where background stars should appear in the photometry.

Eight stars showing either featureless spectra or weak features and high excess emission were rejected from the IMF in § 7.3.4 since I could not constrain their spectral types or place them on the H-R diagram. Estimates of reddening and luminosities for such heavily veiled objects are problematic, especially since half of them lack J photometry. Furthermore, the conversion of luminosities to ages for these objects would be highly uncertain since it is unclear what DM97 age is appropriate for such unevolved objects. Consequently, I do not attempt to add the high-excess, featureless objects to the IMF in the following completeness correction. The mass function derived from this analysis will therefore assume that these objects are not biased towards one mass regime. In addition to rejecting the sources which appear featureless in the spectroscopic sample, I must omit likely high-excess objects which are in the remainder of the KLF. Since many of the stars with no spectra at $K < 13$ have L' -band measurements, I will reject objects with $K - L' \gtrsim 2$, which is typical of Class I sources.

CRCTL detected mid-IR emission in ISO observations of several low-mass candidates in the cloud core, several of which have been classified by WGM and in § 4 and added to the IMF in § 7.3.4. Four remaining sources lacking spectroscopy show weak mid-IR excess emission and can be added to the IMF by photometric modeling described below. These objects (162623 – 242603, 162653 – 243236, 162710 – 242913, CRBR33) are indicated by the open stars in the figures.

Examination of the cloud core KLF reveals a number of sources in excess over the background model. In addition, many of the objects between $K = 12$ -13 have $H - K > 3$, much larger than expected for background stars, as shown in Figure 7.12. The simulated background KLF predicts that ~ 3 of the stars in this magnitude range are background. I therefore assume 3 moderately reddened stars are background and reject them from the completeness correction. Within 19 remaining objects, 9 show evidence for strong IR excess emission in $H - K$ or $K - L'$ and are rejected. The other 10 sources are added to the IMF as a completeness correction in the following manner. As in § 7.2.2, extinctions are calculated by dereddening the $J - H$ and $H - K$ colors to the CTTS locus. When J photometry is not available, an intrinsic color of $H - K \sim 1$ is assumed, which is the maximum expected on the CTTS locus. Given the star formation history implied by the DM97 tracks in Figure 7.10, I assume canonical ages of 0.5 and 1 Myr for these 10 objects and convert the dereddened J (or H) magnitudes to masses for each age. After adding these photometrically derived masses to the IMF for the spectroscopic sample, I arrive at the distributions indicated by dashed lines in Figure 7.13. With the exception of the sources with large IR excess and featureless spectra omitted from the IMF, the final mass function for the cloud core is complete to $\sim 0.08 M_{\odot}$.

General Behavior of the IMF

Although a large number of binary systems have been resolved ($> 0''.005$) in lunar occultation observations of ρ Oph (Simon et al. 1995), the IMF presented here includes only companions which are detected in the images of BKLT and CRBR ($\gtrsim 1''$). In this way, I consider only the primary star mass function, and thus can compare the IMF for ρ Oph to results in other clusters. As discussed in more detail § 6, under a broad range of assumptions the inclusion of binary companions in the IMF produces a single star mass function with a low-mass slope of ~ 0.2 - 0.7 greater than that of the primary star mass function.

As shown in Figure 7.13, the completeness corrections under the ages of 0.5 and 1 Myr are very similar. At masses higher than $\sim 0.4 M_{\odot}$, the DM97 IMF for ρ Oph matches that of Miller & Scalo (1979), while falling less steeply as that of Scalo (1986). After the peak at $\sim 0.4 M_{\odot}$, the IMF slowly declines to the hydrogen burning limit with a slope of ~ -0.5 in logarithmic units (where Salpeter is 1.35). These results are consistent with the logarithmically flat IMFs estimated by CRBR and Strom, Kepner, & Strom (1995) in IR luminosity function modeling of ρ Oph. The ρ Oph IMF also closely resembles that derived for IC 348 with DM97 (§ 6). Using the tracks of BCAH97, Bouvier et al. (1998) have recently measured a slope of -0.4 for the low-mass IMF in the Pleiades, which agrees with my results in ρ Oph and IC 348. The discussions in § 5 and § 6 and Scalo (1998) and compared the IMFs measured near $0.1 M_{\odot}$ in photometric and spectroscopic studies of young, open, and globular clusters. The new results for ρ Oph and the Pleiades further support their conclusion that these various regions do not show substantial variation in the low-mass IMF. However, there are significant differences in the mass functions derived between 0.5 and $2 M_{\odot}$ among these studies. Compared to

the IMFs of Miller & Scalo (1979) and Scalo (1986), the IMF in Orion (Hillenbrand 1997) is deficient in stars over this mass range. On the other hand, the Pleiades IMF of Bouvier et al. (1998) reaches above the field star mass functions, with my results in IC 348 and ρ Oph appearing consistent with Miller & Scalo (1979). Some of these variations may be due to differences in the techniques and tracks used in the young clusters. For instance, the Pleiades data were converted to masses with theoretical relations of $M_{\text{bol}}\text{-mass}$ ($> 0.7 M_{\odot}$, DM97) and $M_I\text{-mass}$ ($< 0.7 M_{\odot}$, BCAH97), whereas spectral types and H-R diagrams were used for Orion (DM94), IC 348 (DM94 and DM97), and ρ Oph (DM97).

New Substellar Candidates

Given the rapid increase of the background contribution to the cloud core KLF beyond $K = 13$, no completeness correction is feasible in this regime. Thus, below the hydrogen burning limit I can only provide a lower limit to the mass function. However, within the large population of background stars at $K > 13$, substellar cluster members should have less reddening than stars which are behind the entire thickness of the cloud core. Under the reddening model for the background population discussed previously, sources in the cloud core with $H - K \lesssim 2$ are possible cluster members. Using this criterion to search for brown dwarf candidates, in addition to the K -band images across the entire cloud core, I obtained deep J and H data towards three positions containing large numbers of faint K -band sources. In the resulting $H - K$ versus K diagram in Figure 7.12, I find several new objects with low reddening between $K = 15$ -18. If they are cluster members, the photometry implies extremely low masses for these sources ($< 10 M_J$). Furthermore, considering the number of these faint, low-reddening

objects relative to the brighter stars at these three positions, there may be rather large population of very low-mass brown dwarf candidates hidden within the background stars shining through the cloud core.

7.4. Conclusions

I have used IR spectroscopy and imaging to study the star formation history across the ρ Oph star forming region and examine the mass function within the cloud core. Our conclusions are as follows:

1. I have obtained moderate-resolution ($R = 1200$) K -band spectra for ~ 100 stars within and surrounding the cloud core of ρ Oph. I have measured spectral types and continuum veilings for $\sim 80\%$ of the sample.
 2. I detect absorption features in the spectra of $\sim 50\%$ of Class I and flat-spectrum sources, supporting the feasibility of studying the photospheres of extremely young protostars.
 3. Measurements of K -band continuum veiling and $\text{Br}\gamma$ emission from the spectra are strongly correlated with near- and mid-IR excess emission. These IR properties imply a slightly more evolved population distributed around the cloud core, suggesting the birth of stars within the core and their subsequent dispersal, which is also consistent with the ages implied by the H-R diagrams of the inner and outer clusters.
 4. Using the evolutionary tracks of DM97 to interpret the H-R diagram for ρ Oph, I measure stellar ages ranging between 0.1 and 1 Myr, with a few stars that may be slightly older.
-

5. With a deep KLF of the cluster core I developed a reddening model for the background star population and identified likely cluster members falling below the limit of the spectroscopic sample. After assuming the canonical ages of the cluster applied to these sources, I used the evolutionary tracks of DM97 to convert their luminosities to masses. With the addition of these sources as a completeness correction, the resulting IMF was complete to $\sim 0.08 M_{\odot}$.
6. With the tracks of DM97, the IMF for ρ Oph matches Miller Scalo (1979) at masses higher than $0.4 M_{\odot}$. The IMF peaks at this mass and slowly declines to the hydrogen burning limit with a slope (in logarithmic units) of ~ -0.5 , as compared to slopes of 1.35, 0, and -2.6 for Salpeter (1955), Miller & Scalo (1979), and Scalo (1986), respectively. The exact shape of the mass function remains dependent on the theoretical evolutionary tracks and temperature scales.
7. In deep images at J , H , and K of a limited region within the ρ Oph cloud core, I identified several faint sources ($K = 15-18$) which are possible cluster members by their low reddenings ($H - K < 2$), and thus are extremely low-mass ($< 10 M_J$) substellar candidates.

I thank M. Rieke for helping to obtain the IR spectra and M. Meyer for providing results prior to publication. I am grateful to F. Allard, I. Baraffe, A. Burrows, and F. D'Antona for providing their most recent calculations and useful advice. This work was supported by NASA grant NAGW-4083 under the Origins of Solar Systems program.

7.5. Notes on Individual Sources

GY20/DoAr24E is a binary system with a separation of $2''.06$ and component magnitudes of $K = 6.9$ and 7.9 (Simon et al. 1995). The curvature in the slope of the Class I secondary is due to its proximity to the primary and the resulting difficulties in extracting the spectrum. Since the companion is much redder than the primary, I assume the BKLT J photometry applies to only GY20A when deriving the luminosity.

GY29 exhibits strong CO absorption and weak atomic lines, indicative of a background K0III or M5-M6 cluster member. The lack of $\text{Br}\gamma$ absorption and the hint of Na absorption at $2.335\ \mu\text{m}$ support the latter classification.

In addition to absorption in $\text{Br}\gamma$, I clearly detect weak features of Na, Ca, and CO in the B star GY70/S1. The source of these metal lines is likely the fainter, unresolved secondary ($\Delta K = 1.8$, $0''.02$; Simon et al. 1995).

GY240/WL20 is a triple system (BKLT, references therein) appearing as one source in the data of BKLT and Wilking & Lada (1989) and two sources separated by $2\text{--}3''$ in the images of CRBR and Barsony et al. (1989). I refer to the west and east components as GY240A and B. Since GY240B has no J photometry and the $H - K$ colors of the two sources are similar, I derive the extinction from BKLT $J - H$ for the composite system and assume it applies to each component. To estimate a J magnitude for the individual sources, I assume a difference of ~ 1.2 mag, which is measured by CRBR at H and K .

GY250/SR12 is a binary system with a separation of $0''.3$ and component magnitudes of $K = 9.3$ and 9.4 (Simon et al. 1995). I assume the components have the same spectral types and divide the luminosity in half. Only one source is added

to the IMF, for reasons discussed in § 7.3.4.

GY372/VSSG14 is an unresolved binary system ($0''.1$; Simon et al. 1995) where the secondary is 0.8 mag fainter at K . As with GY70/S1, $\text{Br}\gamma$ is strong while I also detect absorption in metal lines and CO which may arise in the secondary. Due to possible line and continuum veiling (from either the secondary or IR excess emission), the classification of the primary is uncertain ($< \text{F8}$).

TABLE 7.1
DATA FOR SPECTROSCOPIC SAMPLE IN ρ OPHIUCHI

| BKLT | Other ID ^a | α (1950) min sec | δ (1950) " " | previous ^b | IR | adopt ^c | T_{eff} (K) | A_J | L_{bol} (L_{\odot}) | $J - H$ | $H - K$ | K | r_K ^d | B_{17} (Å) |
|----------------|--|----------------------------|------------------------|-----------------------|-------|--------------------|-------------------------|-------|-------------------------------------|---------|---------|-------|--------------------|-----------------|
| 162609-243411 | GSS25,VSS92,EL16 YLW28,SR3 | 23 07 84 | 27 26 6 | A0(SR) | <P3 | A0 | 9520 | 2.3 | 180 | 0.86 | 0.49 | 6.42 | 0 | 0 |
| 162711-242343 | GY228,IRS32 | 24 10 35 | 17 03 6 | | <P8 | | | | | 2.63 | 1.88 | 10.06 | 7 | 0 |
| 162737-243035 | GY304,YLW46A,IRS48 | 24 35 63 | 23 56 0 | | <P3 | | | | | 1.88 | 1.23 | 7.42 | 7 | 0 |
| 162634-242330 | GY70,S1,GSS35,VSS26 EL28,ROX*14,YLW36 | 23 32 78 | 16 47 1 | B2-B5(BA,GSS,CK) | <P8 | B3 | 18700 | | | 1.56 | 0.96 | 6.32 | 0 | 0 |
| 162749-242540 | GY372,VSSG14,EL36 | 24 48 37 | 19 02 5 | A7(GM) | <P8 | | | | | 1.20 | 0.82 | 7.32 | 0 | 0 |
| 162710-241914 | SR21,VSSG23,VSS31 EL30,YLW8 | 24 08 78 | 12 33 7 | | F0-F8 | F4 | 6590 | 2.7 | 51 | 1.23 | 1.03 | 6.30 | <1 | 0 |
| 162718-242853 | GY246,WL5,VSSG26 IRS38 | 24 16 65 | 22 12 6 | F7(GM) | <G0 | | | | | >2.68 | 4.04 | 10.28 | 7 | 0 |
| 162721-244142 | GY252,YLW13B,IRS42 | 24 19 63 | 35 02 5 | | <K0 | | | | | 3.90 | 2.90 | 8.41 | >1 | 0 |
| 162603-242337 | GSS23,DnA*21,EL14 ROX*8,VSS93 | 23 01 65 | 16 52 4 | K0(BA) | K0-K2 | K1 | 5080 | 1.6 | 18 | 1.26 | 0.59 | 6.16 | 0 | 0 |
| 162623-242101 | GY20A,DnA*24E,GSS31* EL22,ROX*10B,WSR50 | 23 22 01 | 14 17 8 | K0(BA) | K0-K2 | K1 | 5080 | 1.8 | 10 | 1.52 | 0.93 | 6.44 | 0 | 0.7±0.2 |
| 162536-241844 | IRS2 | 22 35 59 | 08 57 6 | K7(GM) | K3-K4 | K3.5 | 4690 | 1.9 | 2.1 | 1.39 | 0.70 | 8.36 | 0 | 0 |
| 162616-242228 | GSS29,EL18 | 23 16 46 | 15 40 7 | K7-M0(GM) | K5-K7 | K6 | 4205 | 3.0 | 3.1 | 1.88 | 1.04 | 8.19 | 0 | 0 |
| 162623-244511 | GY17,DnA*28 | 23 22 04 | 36 27 7 | K4(GM) | K5-K7 | K6 | 4205 | 0.0 | 1.0 | 0.93 | 0.79 | 7.57 | 0 | 0.9±0.2 |
| 162557-243032 | GSS20,IRS13,ROX*7 | 22 56 11 | 23 46 6 | K7(GM),K7(BA) | K5-K7 | K6 | 4205 | 0.9 | 1.1 | 1.12 | 0.63 | 8.37 | 0 | 0 |
| 162715-243843* | GY240B,WL20 | 24 14 08 | 32 02 9 | K-M(GM) | K5-K7 | K6 | 4205 | 4.9 | 6.3 | 2.67 | 1.57 | 9.21 | 0 | 0 |
| 162722-241759 | VSS122 | 24 21 51 | 11 19 1 | K7-M0(GM) | K5-K7 | K6 | 4205 | 4.6 | 1.8 | 2.48 | 1.38 | 9.41 | 0 | 0 |
| | ROX*39 | 27 33 8 | 27 51 0 | K5(BA) | K5-K7 | K6 | 4205 | 0.0 | 1.4 | 0.66 | 0.27 | 8.00 | 0 | 0 |
| 162649-242005 | GY135,VSSG13,LFAM18 | 23 47 86 | 13 23 0 | K7-M0(GM) | K5-K7 | K6 | 4205 | 4.4 | 4.4 | 2.33 | 1.20 | 8.62 | 0 | 0 |
| 162728-242721 | GY273,VSSG18,EL32 | 24 26 92 | 20 42 1 | | K5-M0 | K6.5 | 4132 | 5.0 | 0.86 | 2.99 | 2.09 | 9.39 | 0 | 0 |
| 162757-244004 | GY410 | 24 56 08 | 33 26 1 | M6(GM) | K5-M0 | K7 | 4060 | 2.7 | 0.64 | 1.72 | 0.92 | 9.78 | 0 | 0 |
| 162654-242231 | GY185,VSSG6,GSS40 | 23 53 58 | 15 49 4 | | K6-M1 | K6 | 3955 | 6.1 | 1.3 | 3.07 | 1.78 | 10.19 | 0 | 0 |
| 162622-242254 | GY12 | 23 20 99 | 16 10 8 | M2(GM) | K6-M1 | K6 | 3955 | 4.6 | 0.68 | 2.75 | 1.87 | 9.60 | 0 | 0 |
| 162643-241635 | VSSG11,IRS19 | 23 42 42 | 09 52 9 | M3(GM) | K6-M2 | M0 | 3850 | 4.0 | 1.1 | 2.27 | 1.27 | 9.58 | 0 | 0 |
| 162719-244139 | GY280,SR12,IRS40 ROX*21,YLW13A | 24 17 67 | 34 59 5 | K4/M2.5(BA) M1(CK) | K6-M2 | M0 | 3850 | 0.2 | 0.66 | 0.73 | 0.28 | 8.41 | 0 | 0 |
| 162715-245137 | WSR46,ROX*20B | 24 12 98 | 44 57 2 | M2(BA) | M0-M3 | f | | | | 0.90 | 0.46 | 9.51 | 0 | 0 |
| 162736-242833 | GY207 | 24 34 95 | 21 54 7 | | M0-M3 | f | | | | 0.68 | 0.25 | 11.04 | 0 | 0 |
| 162629-241908 | LFAM8 | 23 28 31 | 12 24 3 | | M0-M3 | M1.5 | 3595 | 6.6 | 0.46 | 3.37 | 2.05 | 11.19 | 0 | 0 |
| 162638-242324 | GY84 | 23 37 43 | 16 41 6 | M6(WGM) | M0-M3 | M1.5 | 3595 | 4.6 | 0.24 | 2.40 | 1.26 | 11.63 | 0 | 0 |
| 162615-241924 | 2615-1924,2314-1237 | 23 14 49 | 12 40 0 | | M0-M3 | M1.5 | 3595 | 4.6 | 0.80 | 2.81 | 1.46 | 9.98 | 0 | 0 |
| 162730-242457 | GY284 | 24 29 37 | 18 17 4 | | M0-M3 | M1.5 | 3595 | 2.4 | 0.35 | 1.89 | 0.97 | 10.04 | 0 | 0 |
| 162714-245132 | WSR45,ROX*20A | 24 12 34 | 44 51 7 | M5(BA) | M1-M4 | f | | | | 0.79 | 0.34 | 10.39 | 0 | 0 |
| 162721-244335 | GY253 | 24 19 95 | 36 55 5 | | M2-M4 | M3 | 3350 | 8.2 | 0.83 | 4.03 | 2.53 | 10.78 | 0 | 0 |
| 162738-243943 | GY306,IRS50 | 24 36 57 | 24 03 9 | | M4 | M4 | 3180 | 3.1 | 0.63 | 1.87 | 1.01 | 9.59 | 0 | 0 |
| 162659-243556 | GY172,WL14 | 23 57 42 | 29 14 7 | | M4 | M4 | 3180 | 5.1 | 0.14 | 2.74 | 1.64 | 11.74 | 0 | 0 |
| 162717-242856 | GY244,YLW12A,IRS37 VSS126 | 24 16 06 | 22 16 1 | | M4 | M4 | | | | >3.1 | 2.95 | 10.95 | 0 | 0 |
| 162735-243834 | GY295 | 24 33 50 | 31 55 0 | | M4 | M4 | 3180 | 1.3 | 0.36 | 1.13 | 0.51 | 9.64 | 0 | 0 |
| 162641-244015 | GY93,WSR37 | 23 39 72 | 33 33 0 | K-M(GM) | M4 | M4 | 3180 | 0.6 | 0.31 | 0.98 | 0.55 | 9.20 | 0 | 0 |
| 162559-242124 | | 22 58 32 | 14 38 3 | | M4 | M4 | 3180 | 0.0 | 0.21 | 0.65 | 0.45 | 9.52 | 0 | 0 |
| 162642-242031 | GY110,VSSG2,EL26 SR22 | 23 41 48 | 13 49 0 | M0(GM) | K6-M2 | M0 | 3650 | 2.9 | 3.5 | 1.78 | 0.93 | 8.00 | 0.25 | 0.6±0.2 |
| | | 22 22 7 | 22 55 0 | K7-M0(GM),M0(CK) | K6-M2 | M0 | 3650 | 0.6 | 0.76 | 0.93 | 0.45 | 8.70 | 0.25 | 1.9±0.4 |
| 162727-243116 | GY267,VSSG25,EL31 WL13 | 24 26 83 | 24 37 0 | K-M(GM) | K6-M2 | M0 | 3650 | 3.1 | 0.92 | 1.93 | 1.11 | 9.30 | 0.25 | 0 |
| 162654-242622 | GY153,VSSG15 | 23 53 04 | 19 40 2 | M2(GM) | K6-M2 | M0 | 3650 | 5.8 | 1.2 | 3.02 | 1.82 | 9.88 | 0.25 | 1.7±0.4 |

TABLE 7.1 - Continued

| BKLT | Other ID ^a | α (1950) min sec | δ (1950) ° | previous ^b | IR | adopt ^c | T_{eff} (K) | A_J | L_{bol} (L_{\odot}) | $J - H$ | $H - K$ | K | r_K ^d | B_{r} (Å) |
|----------------------------|---|----------------------------|----------------------|----------------------------|--------------------|--------------------|-------------------------|-------|-------------------------------------|---------|---------|---------|----------------------------|----------------------------|
| 162715 245843 ^e | GY240A,WL20 | 24 14 08 | 32 02 9 | K7-M0(GM) | K6-M2 | M0 | 3850 | 4.9 | 2.5 | 2.67 | 1.57 | 9.21 | 0.25 | 0 |
| 162718 242900 | GY247,WL4,IRS39 VSSG26 | 24 16 05 | 22 25 6 | M(GM) | M0-M3 | M1.5 | 3595 | 5.4 | 1.6 | 3.00 | 1.93 | 9.13 | 0.25 | 0 |
| 162739 245914 | GY314 | 24 37 55 | 32 35 6 | M(GM) | K6-M2 | M0 | 3850 | 2.0 | 1.4 | 1.55 | 0.92 | 8.35 | 0.5 | $1.6 \pm 0.3, < 0.5$ |
| 162755 242619 | GY400,SR10 | 24 53 07 | 19 41 0 | M1.5(CK) | K6-M2 | M0 | 3850 | 0.0 | 0.55 | 0.50 | 0.60 | 8.74 | 0.5 | 2.6 ± 0.3 |
| 162617 242023 | GSS28,DoAr24,EL19 ROXs10A,WSH27 | 23 15 71 | 13 39 3 | K7-M0(GM),K5(BA) | K6-M2 | M0 | 3850 | 0.8 | 1.2 | 1.05 | 0.58 | 8.09 | 0.5 | 1.9 ± 0.15 |
| 162645 242309 | GY110,GSS39,EL27 VSSG28 | 23 43 42 | 16 26 9 | M(GM) | K5-M2 | K8 | 3955 | 4.7 | 2.1 | 2.64 | 1.62 | 8.88 | 0.75 | 2.1 ± 0.15 |
| 162709 245408 | GY211,WL10 | 24 07 48 | 27 27 0 | | K5-M2 | K8 | 3955 | 3.6 | 1.4 | 2.22 | 1.39 | 8.85 | 0.75 | $1.4 \pm 0.2, < 0.5$ |
| 162816 245657 | WSH60,YLW58 | 25 14 58 | 30 20 9 | K-M(GM) | K5-M2 | K8 | 3955 | 0.7 | 0.28 | 1.16 | 0.78 | 9.43 | 0.75 | 0 |
| 162624 242449 | GY25,S2,GSS32 EL23 | 23 22 44 | 18 05 6 | K(GM) | K5-M2 | K8 | 3955 | 3.1 | 3.9 | 2.15 | 1.48 | 7.20 | 0.75 | 0 |
| 162730 242744 | GY279,VSSG17,EL33 IRS47 | 24 28 65 | 21 04 6 | M(GM), \geq M2(OL) | K5-M2 | K8 | 3955 | 6.9 | 1.8 | 3.50 | 2.69 | 8.95 | 0.75 | 0 |
| 162738 245658 | GY305,IRS49 | 24 36 57 | 30 19 1 | | K5-M2 | K8 | 3955 | 2.9 | 1.7 | 1.95 | 1.24 | 8.31 | 0.75 | $0.8 \pm 0.2, < 2$ |
| 162740 242205 | GY319,SR0,EL34,ROXs29 IRS52,DoAr34,WSH54 | 24 38 53 | 15 24 4 | K4(GM),K7(CK) K4/K6(BA) | K5-M2 | K8 | 3955 | 0.0 | 2.0 | 0.77 | 0.51 | 7.20 | 0.75 | 0 |
| 162646 241203 | WSH38,VSS27,ROXs16 | 23 45 16 | 05 20 9 | K(GM),G9 (BA) | K5-M2 | K8 | 3955 | 1.9 | 3.4 | 1.47 | 0.82 | 7.51 | 0.75 | 0.6 ± 0.15 |
| 162623 242241 | SR20,ROXs33,DoAr38 WSH61 | 25 21 82 | 16 05 7 | G0 (BA) | K5-M2 | K8 | 3955 | 2.1 | 0.95 | 1.69 | 1.13 | 8.55 | 1 | 0 |
| 162733 244115 | GY292 | 24 31 29 | 34 36 2 | | K5-M2 | K8 | 3955 | 2.9 | 2.1 | 2.04 | 1.37 | 7.92 | 1 | $1.0 \pm 0.4, 0.5 \pm 1$ |
| 162728 245934 | GY269,YLW16A,IRS44 | 24 26 22 | 32 54 5 | | K5-M2 | K8 | | | > 3.91 | 3.44 | 9.55 | 1 | 0 | |
| 162610 242056 | GSS26 | 23 08 07 | 14 11 6 | | K5-M2 | K8 | 3955 | 6.0 | 1.3 | 3.34 | 2.25 | 9.38 | 4.0 75 | $2.9 \pm 0.2, 1.7 \pm 0.3$ |
| 162637 242302 | GY81,VSSG4 | 23 36 42 | 16 19 4 | | K5-M2 | K8 | 3955 | 4.6 | 0.20 | 2.79 | 1.91 | 10.92 | 1.2 | 3.0 ± 0.5 |
| 162556 242050 | SR4,EL13,YLW25,IRS12 ROXs6,WSH25,DoAr20 | 22 54 82 | 14 04 5 | K6(BA),K7(CK) | K5-M2 | K8 | 3955 | 0.5 | 1.9 | 1.05 | 0.72 | 7.25 | $1.5, 2.1, 5$ | $6.7 \pm 0.3, 4.5 \pm 0.5$ |
| 162658 244529 | GY168,SR24N,IRS24 EL28 | 23 55 55 | 38 48 1 | K2(GM),M0.5(CK) | K5-M2 | K8 | 3955 | 2.0 | 2.3 | 1.70 | 1.18 | 7.42 | 2 | 1.3 ± 0.2 |
| 162726 245933 | GY292 | 24 24 07 | 32 44 0 | | K7-M3 | M1 | 3680 | 6.4 | 1.0 | 3.46 | 2.30 | 9.77 | 1 | 2.2 ± 0.3 |
| 162630 242258 | GY51,VSSG27 | 23 29 12 | 16 15 3 | | K3-M1 | | | | 3.23 | 2.74 | 10.72 | 2.0 5 | $5.0 \pm 0.5, 1.5 \pm 0.5$ | |
| 162658 244534 | GY167,SR24S,IRS25 EL28 | 23 55 04 | 38 52 9 | K2(GM),K2 (CK) | G5-K7 | K2 | 4900 | 1.2 | 2.4 | 1.50 | 1.17 | 7.08 | 1.3 | 4.7 ± 0.15 |
| 162624 241616 | EL24,YLW32 | 23 22 55 | 09 32 0 | | G5-K7 | | 2.3 | | 1.95 | 1.46 | 6.77 | 1.3 | 2.7 ± 0.2 | |
| 162649 245823 | GY129,WL16 | 23 47 47 | 31 41 3 | | ? | | | | 1.99 | 1.39 | 9.82 | > 1 | 13.7 ± 0.5 | |
| 162739 244316 | GY315,YLW45,IRS51 | 24 37 97 | 36 37 0 | | G5-K7 | | 9.5 | | 4.70 | 3.49 | 6.93 | 1.3 | 2.0 ± 0.6 | |
| 162644 243447 | GY111,WL12,YLW2 VSSG30 | 23 42 06 | 28 04 7 | | G5-K7 | | 7.1 | | 3.79 | 2.89 | 10.18 | 1.3 | 1.8 ± 0.4 | |
| 162623 242101 | GY208,DoAr24EN ^e | 23 22 01 | 14 17 6 | | ? | | | | 1.52 | 0.93 | 6.44 | > 2 | 1.5 ± 0.4 | |
| 162729 245917 | GY274,YLW16B,IRS46 | 24 27 53 | 32 37 2 | | ? | | | | > 2.35 | 3.19 | 11.45 | > 1 | 2.0 ± 0.6 | |
| 162621 242306 | GY6,GSS30 | 23 19 99 | 16 22 1 | | ? | | | | 3.05 | 2.51 | 8.32 | > 2 | $2.0 \pm 0.2, < 0.5$ | |
| 162711 244046 | GY224 | 24 09 38 | 34 05 7 | | ? | | | | > 3.31 | 2.90 | 10.79 | > 0.5 | 8.5 ± 1.0 | |
| 162751 245145 | GY375,YLW52,IRS54 | 24 50 28 | 25 07 6 | | ? | | | | 5.13 | 2.63 | 10.87 | > 2 | 4.3 ± 0.4 | |
| 162706 245814 | GY205,WL17 | 24 05 06 | 31 33 3 | | ? | | | | 3.33 | 3.29 | 10.26 | > 0.5 | 5.9 ± 0.4 | |
| 162721 242953 | GY254,YLW14,WL5 | 24 20 28 | 23 12 9 | | ? | | | | > 2.61 | 4.35 | 10.04 | > 1 | 6.2 ± 0.4 | |
| 162726 244051 | GY265,YLW15A,IRS43 | 24 25 09 | 34 11 5 | | ? | | | | > 3.53 | 5.71 | 9.45 | > 1 | $1.5 \pm 0.7, < 0.5$ | |
| 162711 245552 | GY227,WL19 | 24 10 00 | 31 51 2 | | ? | | | | > 4.27 | | 11.23 | > 0.5 | 0 | |
| 162709 243716 | GY214,EL29,WL15 YLW7 | 24 07 71 | 30 37 4 | | ? | | | | 5.20 | 4.47 | 7.54 | > 2 | 3.0 ± 0.1 | |
| 162702 243726 | GY182,WL16 | 24 00 54 | 30 45 0 | | D6-A7 ^f | | | | 3.55 | 2.65 | 7.92 | ? | 7.2 ± 0.2 | |
| 162630 245841 | GY45 | 23 28 45 | 31 57 4 | | G8-III | b | | | 2.40 | 1.36 | 6.31 | | 0 | |
| 162757 243761 | GY411 | 24 56 19 | 31 13 3 | | G8-III | b | | | 2.20 | 1.21 | 9.52 | | 0 | |
| 162653 242229 | GY160,GSS40,VSSG6 IRS21 | 23 52 47 | 15 47 6 | | K0-III | b | | | 2.65 | 1.07 | 9.55 | | 0 | |
| 162603 242632 | GY453,VSSG16,EL37 IRS58 | 25 02 13 | 19 55 5 | | K2-III | b | | | 1.10 | 0.77 | 6.69 | | 0 | |
| 162809 242322 | EL38,VSSG15 | 25 07 71 | 16 45 0 | | K2-III | b | | | 1.52 | 0.82 | 7.12 | | 0 | |
| 162746 242323 | GY351,VSSG13,EL35 | 24 45 25 | 16 45 2 | | M0-III | b | | | 2.20 | 1.12 | 7.29 | | 0 | |
| 162713 244133 | GY232 | 24 11 44 | 34 52 5 | | M0-III | b | | | > 4.45 | 2.95 | 9.58 | | 0 | |
| 162633 243625 | GY65 | 23 31 34 | 29 42 4 | | M2-III | b | | | 2.55 | 1.49 | 8.91 | | 0 | |
| 162558 242203 | | 22 57 23 | 15 17 7 | | K0-K2-III | b? | | | 2.57 | 1.45 | 11.41 | ? | 0 | |

TABLE 7.1 — Continued

| BKLT | Other ID ^a | α (1950) min sec | δ (1950) ° ' " | previous ^b | IR | adopt ^c | T_{eff} (K) | A_J | L_{bol} (L_{\odot}) | $J - H$ | $H - K$ | K | r_K ^d | B_{17} (Å) |
|---------------|--------------------------------|----------------------------|--------------------------|-----------------------|-------|--------------------|-------------------------|------------------|-------------------------------------|---------|---------|-------|--------------------|-----------------|
| 162626-242446 | GY29 | 23 23 67 | 18 02 7 | | M5-M6 | na | | | | 2 95 | 2 11 | 10 86 | ? | 0 |
| 162704-242830 | GY192,WL1,YLW6 IRS29,VSSG31 | 24 02 61 | 21 49 3 | | >M3 | | | | | 5 15 | 2 26 | 10 81 | ? | 0 |
| 162621-242692 | GY8 | 23 20 27 | 19 17 74 | M7(WGM) | >M5 | M7 | 2720 | 1 3 ^E | 0 063 ^E | 1 13 | 0 66 | 10 91 | | |
| 162631-242631 | GY59 | 23 20 25 | 18 47 99 | M6(WGM) | M4-M6 | M6 | 2840 | 3 1 ^E | 0 061 ^E | 1 86 | 1 21 | 11 68 | | |
| 162923-241359 | IRAS564A | 26 22 00 | 07 27 1 | | h | | | | | 1 79 | 0 61 | 8 46 | ? | 0 |
| 162601-242521 | | 23 00 01 | 18 36 2 | | K-M | | | | | 1 90 | 1 23 | 11 10 | ? | 0 |
| 162712-243449 | | 24 10 49 | 28 08 4 | | K-M | | | | | 2 37 | 1 76 | 11 53 | ? | 0 |
| 162618-242416 | | 23 17 56 | 17 32 16 | M5(WGM) | K-M | M5 | 3010 | 4 8 ^E | 0 048 ^E | 2 46 | 1 95 | 11 94 | | |
| 162623-242441 | GY21,LFAM3 | 23 22 14 | 17 57 4 | K-M(GM),M0(GL) | K-M | M0 | 3850 | 3 8 | 0 36 | 2 46 | 1 69 | 9 94 | ? | 2 0 ± 0.7, <1 |
| 162715-242640 | GY239,IRS34,YLW10B | 24 13 99 | 19 59 9 | K(GM) | K-M | | | | | >3 53 | 2 81 | 10 66 | ? | 0 |
| 162648-242640 | GY128,WL2 | 23 47 05 | 21 57 9 | K-M(GM) | K-M | | | | | >2 98 | 3 06 | 10 99 | ? | 0 |
| 162618-242611 | | 23 17 54 | 19 27 36 | M7 5(WGM) | | M7 5 | 2660 | 2 8 ^E | 0 026 ^E | 1 75 | 1 20 | 12 18 | | |
| 162622-242354 | GY10 | 23 20 16 | 17 10 17 | M8 5(WGM) | | M8 5 | 2500 | 3 9 ^E | 0 036 ^E | 2 16 | 1 34 | 12 26 | | |
| 162622-242409 | GY11 | 23 20 69 | 17 28 08 | M6 5(WGM) | | M6 5 | 2780 | 1 4 ^E | 0 002 ^E | 1 15 | 1 22 | 14 15 | | |
| 162625-242326 | GY31 | 23 23 86 | 16 41 68 | M5 5(WGM) | | M5 5 | 2925 | 1 6 ^E | 0 71 ^E | | 3 96 | 13 09 | | |
| 162627-242643 | GY37,VSSG29 | 23 26 38 | 19 59 46 | M6(WGM) | | M6 | 2840 | 1 8 ^E | 0 024 ^E | 1 31 | 0 95 | 11 99 | | |
| 162632-242656 | GY64 | 23 31 11 | 19 53 37 | M8(WGM) | | M8 | 2600 | 3 1 ^E | 0 0085 ^E | 1 87 | 1 43 | 13 33 | | |
| 162642-242224 | GY107 | 23 41 32 | 18 42 04 | M3?(WGM) | | b | | | | 2 02 | 0 97 | 11 40 | | |
| 162651-243242 | GY141 | 23 49 82 | 26 00 42 | M8 5(LLR) | | M8 5 | 2500 | 0 ¹ | 0 0026 ¹ | 0 76 | 0 50 | 13 57 | | |
| 162656-242838 | GY163 | 23 55 47 | 21 56 79 | M2 5(WGM) | | M2 5 | 3430 | 9 0 ^E | 0 18 ^E | >2 06 | 2 28 | 12 66 | | |
| 162706-242837 | GY202 | 24 04 47 | 21 56 00 | M7(WGM) | | M7 | 2720 | 3 7 ^E | 0 013 ^E | 2 09 | 1 70 | 12 97 | | |
| 162606-242451 | | 23 03 64 | 18 05 93 | early(WGM) | | b | | | | >1 1 | 1 91 | 15 99 | | |
| 162618-242818 | | 23 18 61 | 21 33 60 | early(WGM) | | b | | | | 2 57 | 1 43 | 12 93 | | |
| 162738-243838 | GY310 | 24 36 90 | 31 59 07 | M8 5(WGM) | | M8 5 | 2600 | 1 6 ^E | 0 085 ^E | 1 29 | 0 83 | 11 08 | | |
| 162742-243849 | GY326 | 24 40 96 | 32 10 94 | M4(WGM) | | M4 | 3180 | 3 1 ^E | 0 20 ^E | 1 78 | 0 88 | 10 59 | | |

^a SR=Struve & Rudkjøbing (1949), DoAr=Donati & Arakelyan (1959), S and GSS=Grasdalen, Strom, & Strom (1973), VSSG=Vrba et al. (1975), VSS=Vrba, Strom, & Strom (1976), EL=Elias (1978), ROX=Montmerle et al. (1983), WL=Wilking & Lada (1983), YLW=Young, Lada, & Wilking (1986), WSB=Wilking, Schwartz, & Blackwell (1987), IRAS=Table 1 of Wilking, Lada, & Young (1989), LFAM=Lecus et al. (1991), GY=Greene & Young (1992).

^b IR spectral types of Greene & Meyer (1995), Greene & Lada (1997), and Wilking, Greene, & Meyer (1998). Optical spectral types of Struve & Rudkjøbing (1949), Grasdalen, Strom, & Strom (1973), Cohen & Kuhl (1979), Bouvier & Appenauer (1992), and Luhman, Liebert, & Rieke (1997).

^c Background and foreground stars are indicated by "h" and "f".

^d Derived from the IR spectra in this work.

^e GY20 and GY240 are each binary systems which appear as one source in the coordinates and photometry of BKLT and the measurements of $\alpha(\lambda)$.

^f H-band classification by Hecaya et al. (1998).

^g Wilking, Greene, & Meyer (1998).

^h The optical spectral type is M8 M0III while the IR spectrum exhibits CO absorption equivalent to K4III and is very similar to spectra of FU Ori objects.

ⁱ Luhman, Liebert, & Rieke (1997).

NOTE — JHK photometry and coordinates are taken from BKLT. The data for ROX39 and SR22 are from GWAYL and references therein. Photometry for GY31 from Cameron et al. (1993). Coordinates are prefixed by 16^h and -24°.

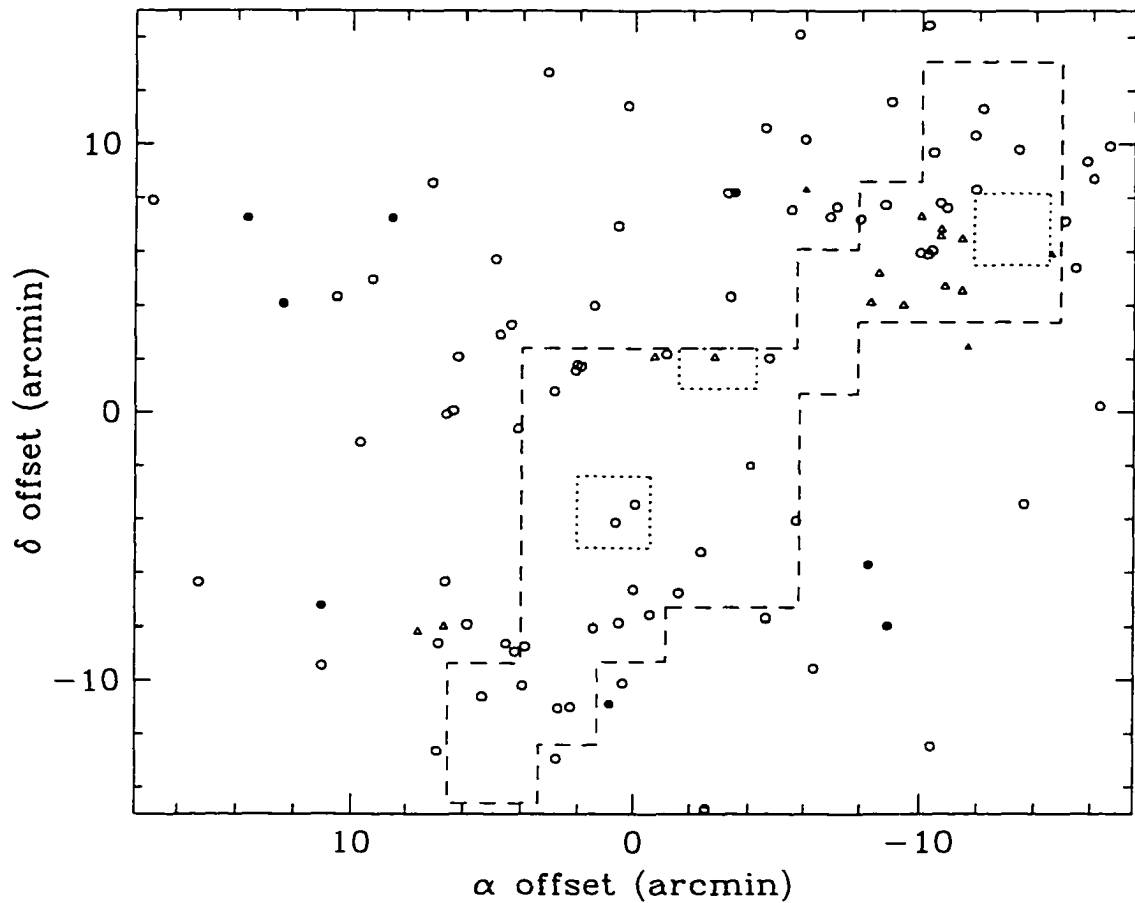


Figure 7.1 All sources in ρ Oph observed with K -band spectroscopy, with the exception of seven objects falling outside of this region (IRS2, IRAS64A, SR22, WSB38, WSB45, WSB46, ROXs39). Filled circles represent stars classified as background giants in this work and open circles are all other sources in my sample. Open triangles and the open square are the low-mass sources observed spectroscopically by WGM and in § 4. Filled triangles are identified as likely background stars by WGM. The area within the dashed line was surveyed through IR images by CRBR and corresponds to the cloud core ($A_V \gtrsim 50$; Wilking & Lada 1983). Deeper K -band photometry of the same region was obtained for this work, in addition to J and H images towards the three positions outlined by dotted lines. The origin corresponds to $\alpha = 16^{\text{h}}24^{\text{m}}07.7$, $\delta = -24^{\circ}24'00''$ (1950).

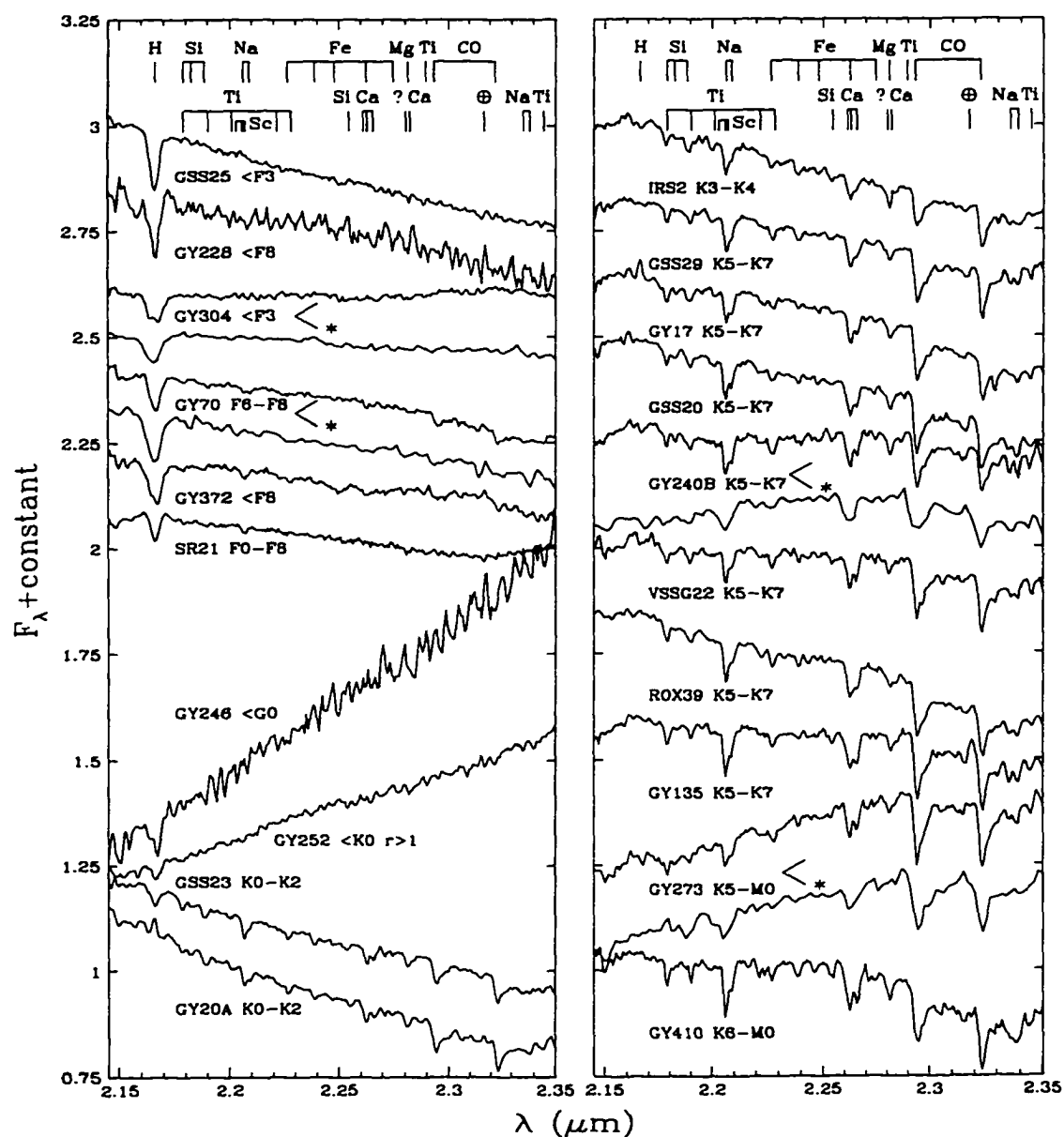


Figure 7.2 K -band spectra at $R = 1200$ of early-type stars and sources exhibiting no detectable continuum veiling ($\tau_K < 0.25$), with additional data at $R = 800$ (*). Spectra are normalized at $2.2 \mu\text{m}$ with constant offsets.

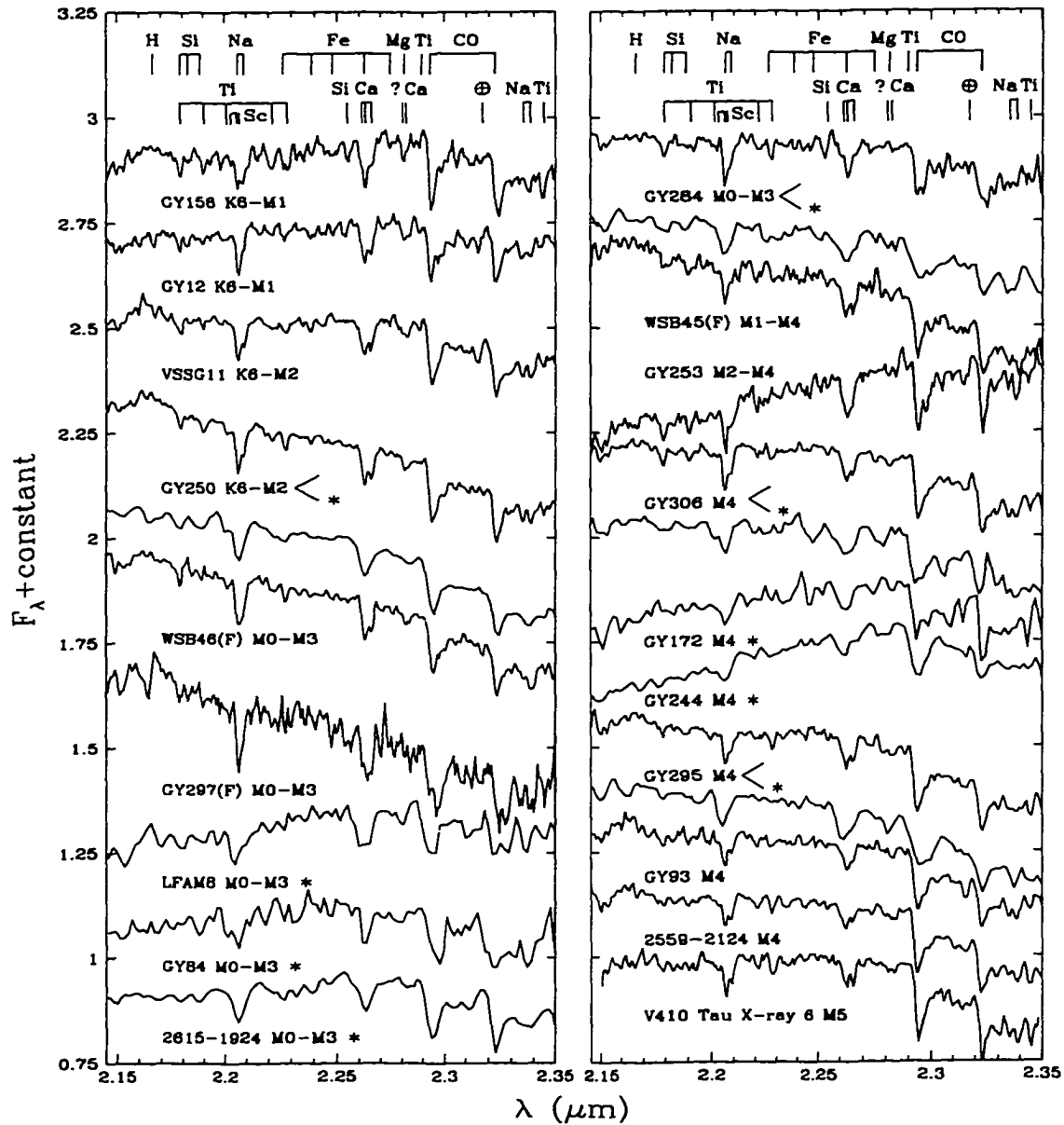


Figure 7.3 K -band spectra at $R = 1200$ of late-type sources exhibiting no detectable continuum veiling ($r_K < 0.25$), with additional data at $R = 800$ (*). Spectra are normalized at $2.2 \mu\text{m}$ with constant offsets. Probable foreground stars (F) are also indicated. The IR spectrum of V410 Tau X-ray 6 (§ 5), which is classified in the optical as M5 (SS94), is shown for comparison. The spectra classified as M4 are also fit marginally by veiled late-K stars with enhanced CO absorption. Spectra are normalized at $2.2 \mu\text{m}$ with constant offsets.

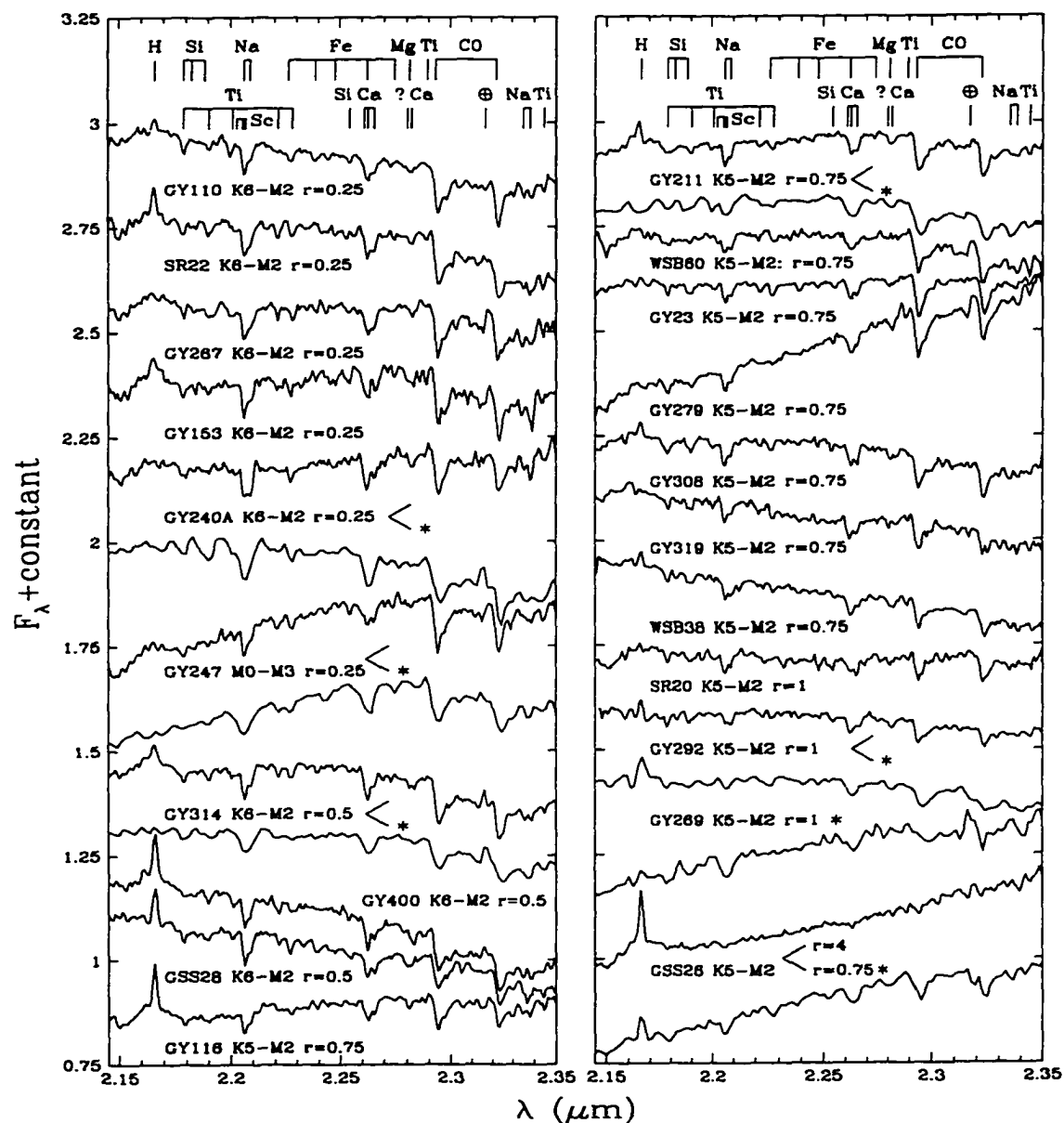


Figure 7.4 K -band spectra at $R = 1200$ of moderately veiled sources ($0.25 \leq r_K \leq 1$), with additional data at $R = 800$ (*). Spectra are normalized at 2.2 μm with constant offsets. K -band ($R = 1200$) spectra of moderately veiled sources

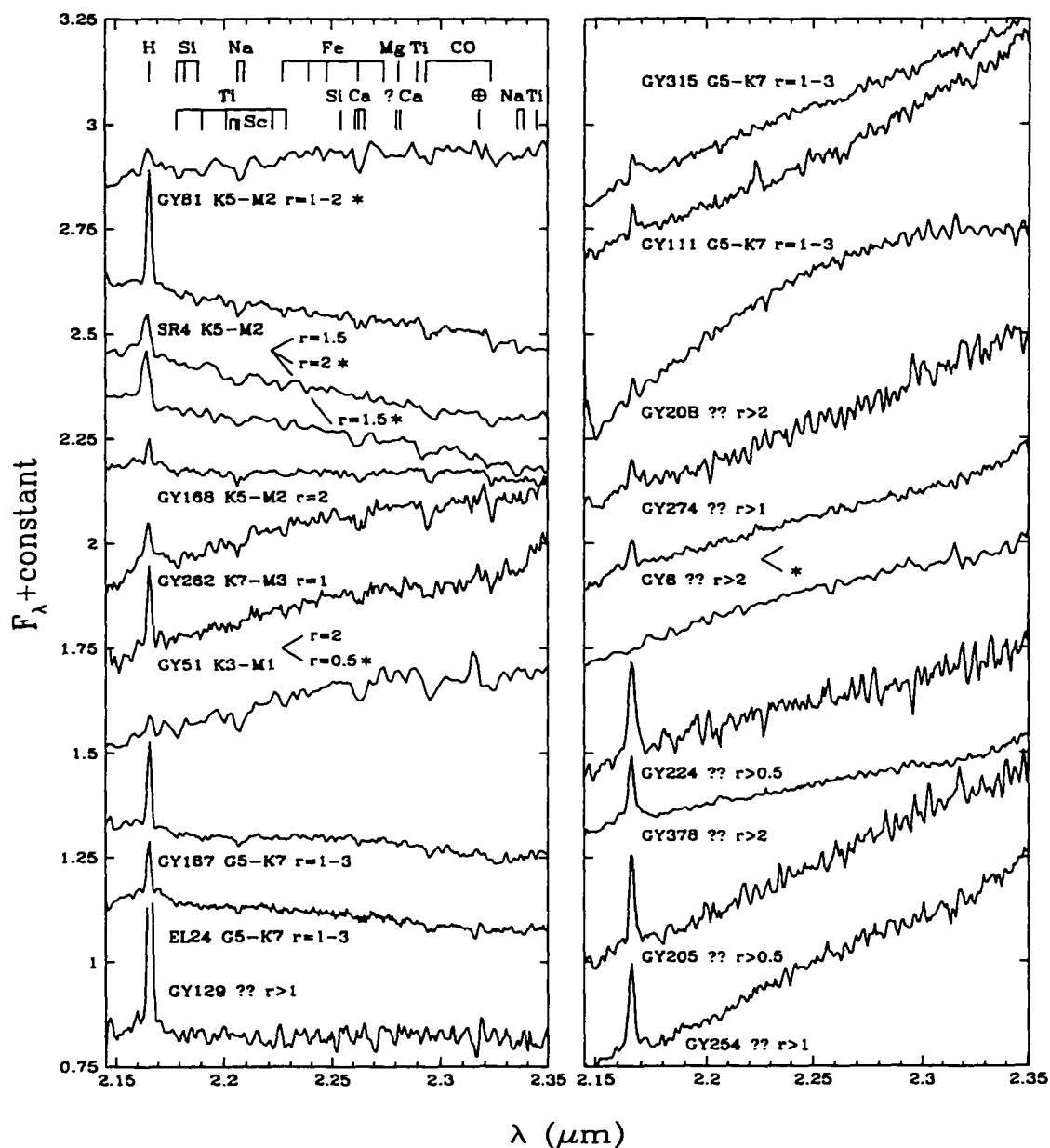


Figure 7.5 K -band spectra at $R = 1200$ of heavily veiled ($\tau_K \geq 1$), likely Class I sources, with additional data at $R = 800$ (*). Spectra are normalized at 2.2 μm with constant offsets.

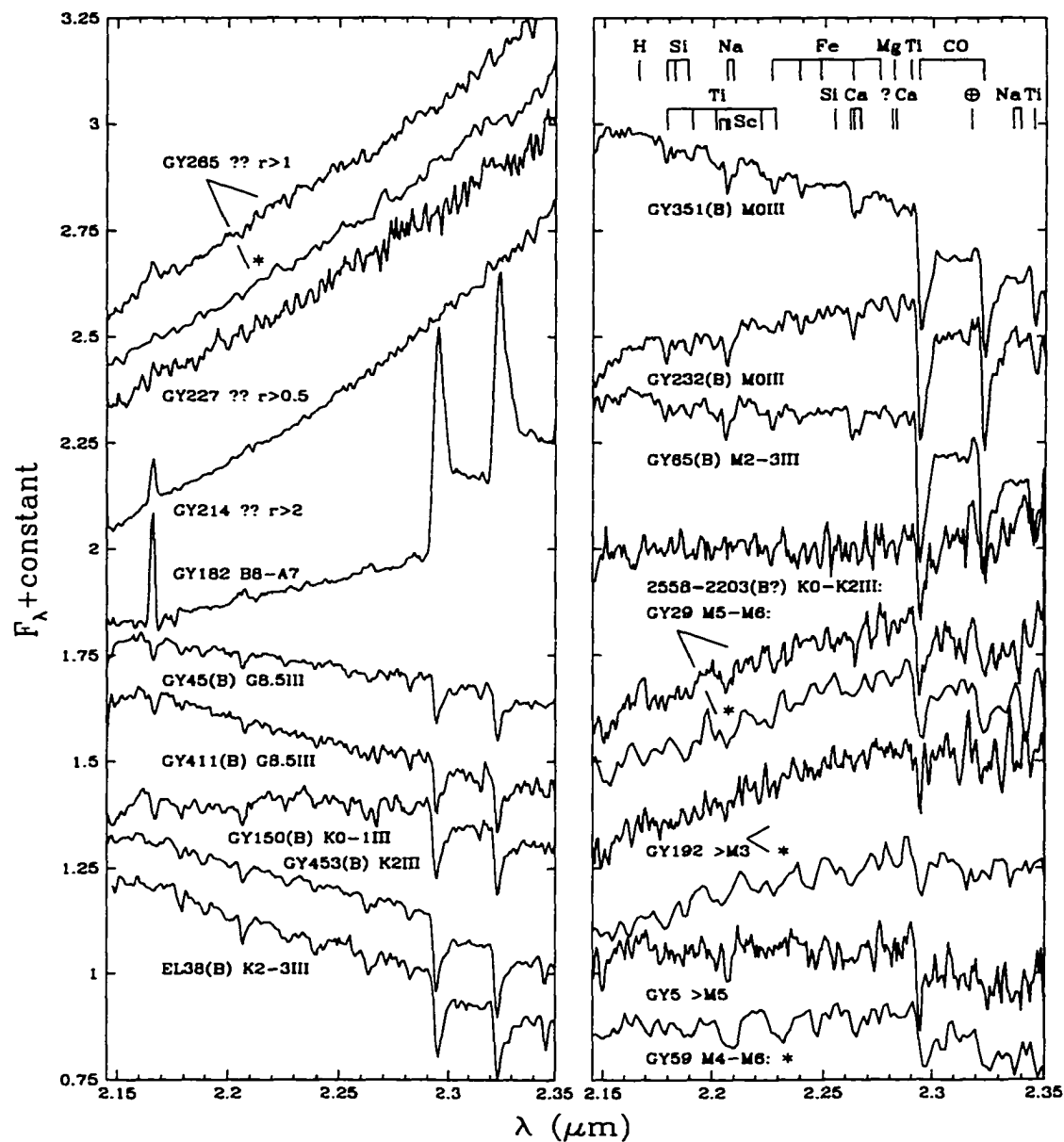


Figure 7.6 K -band spectra at $R = 1200$ of spectra of heavily veiled ($r_K \geq 1$) sources, background giants (B), and sources showing uncertain late-type classifications, with additional data at $R = 800$ (*). The curvature in the spectrum of GY20B is not real and is due to difficulties in extracting the spectrum separately from the nearby companion GY20A. Spectra are normalized at $2.2 \mu\text{m}$ with constant offsets.

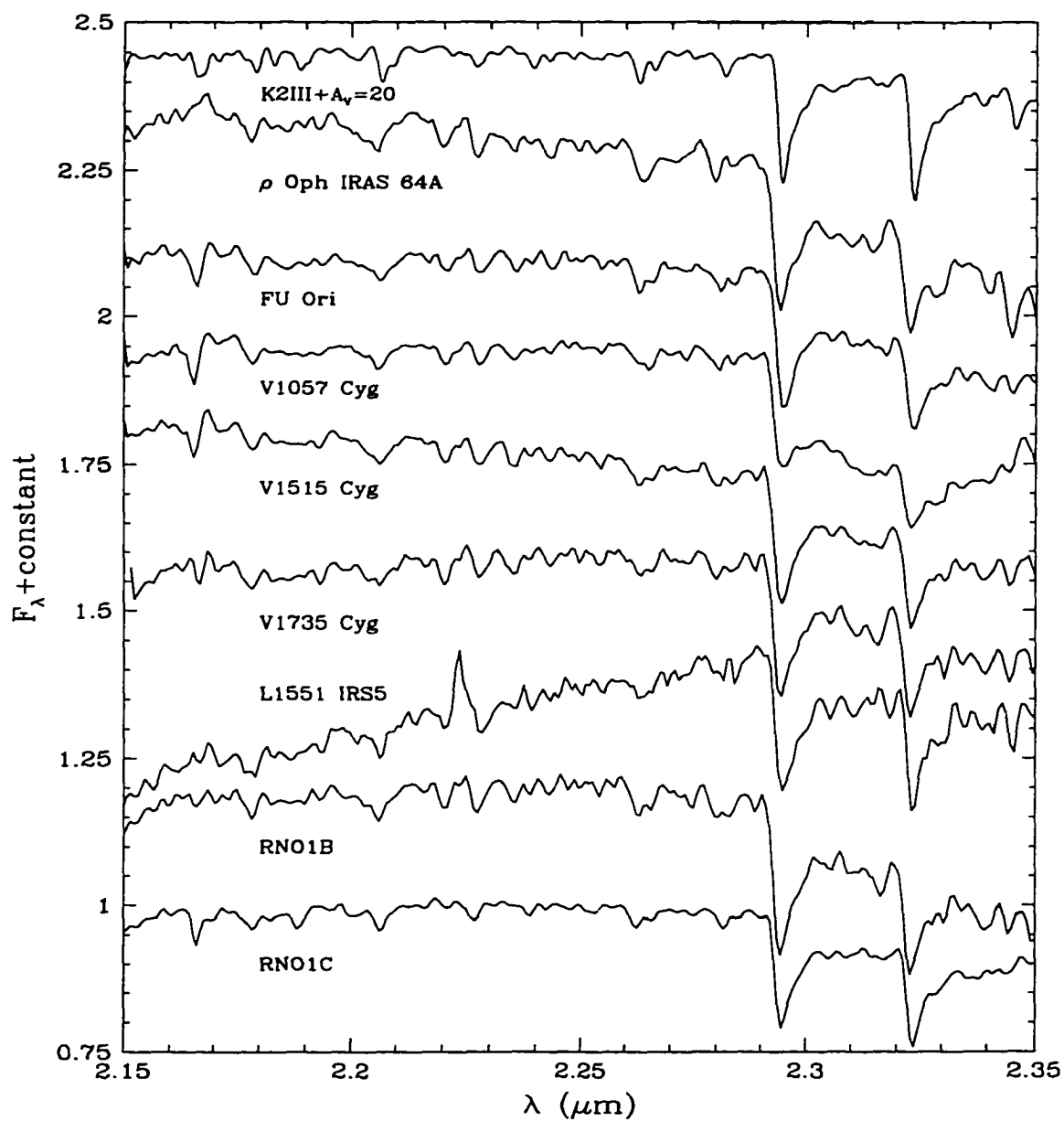


Figure 7.7 The K -band spectrum of IRAS64A is compared to data for several FU Ori objects and a typical field K giant (reddened by $A_V = 20$.) Spectra are normalized at 2.2 μm with constant offsets.

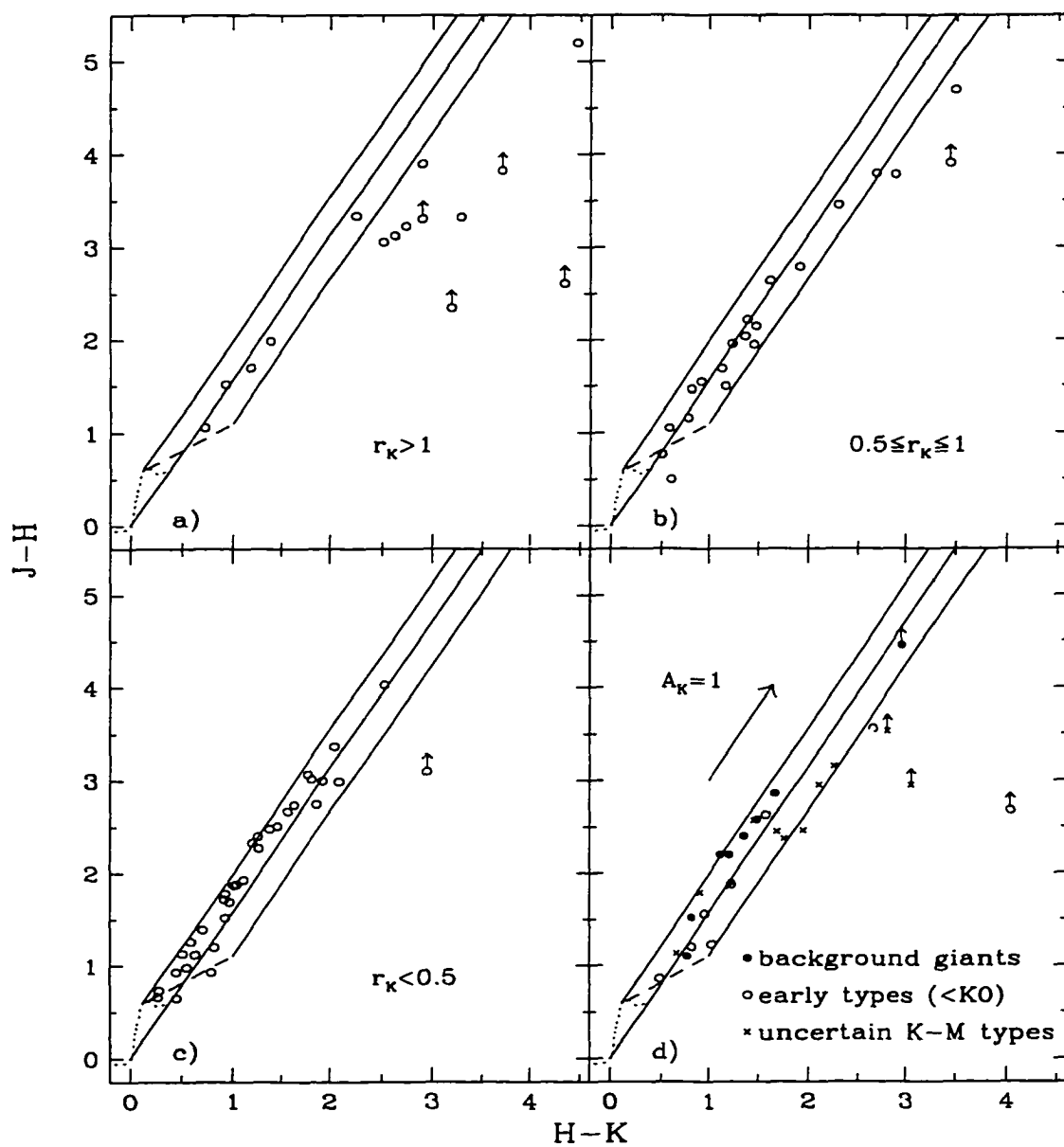


Figure 7.8 $H-K$ vs. $J-H$ for the K -band spectroscopic sample is given in a), b), and c) as a function of the continuum veiling, r_K , measured in the spectra. Background giants, early-type stars, and sources with uncertain late-type classifications are given in the d).

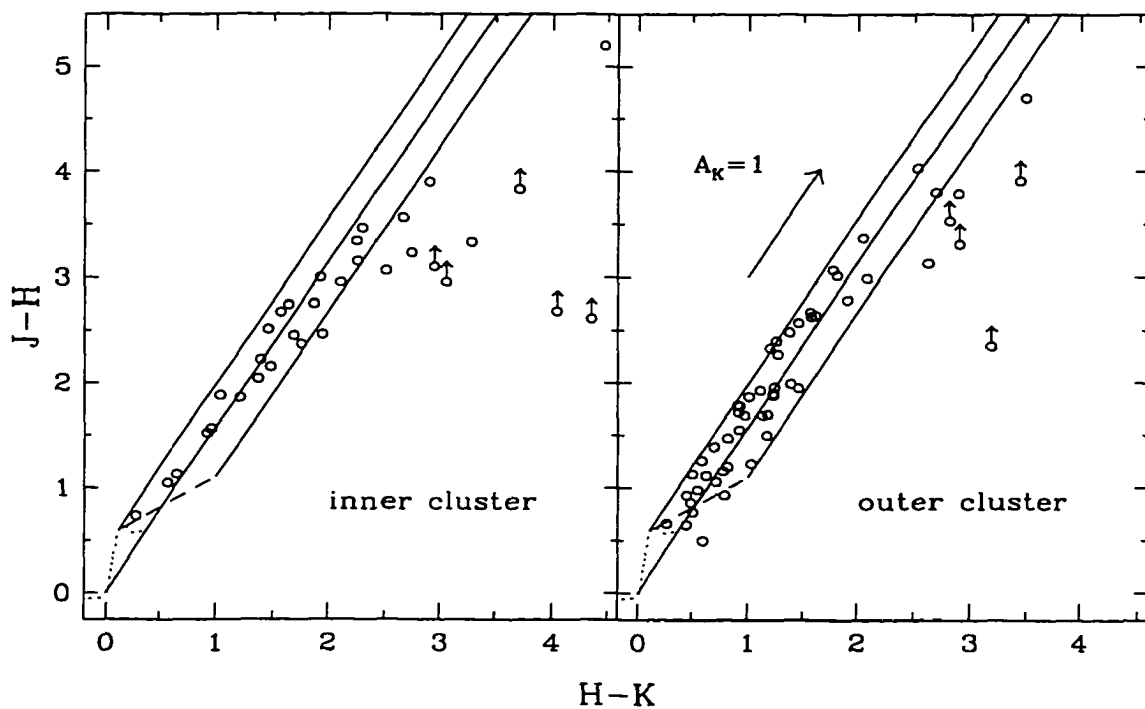


Figure 7.9 $H - K$ vs. $J - H$ for the K -band spectroscopic sample within and outside the cloud core, as defined by dashed boundary in Figure 7.1. Background and foreground stars have been omitted. The main sequence (dotted line) and CTTS locus (dashed line) are shown along with the reddening bands of each, where the reddening vectors were derived from BKLT data by Kenyon et al. (1998).

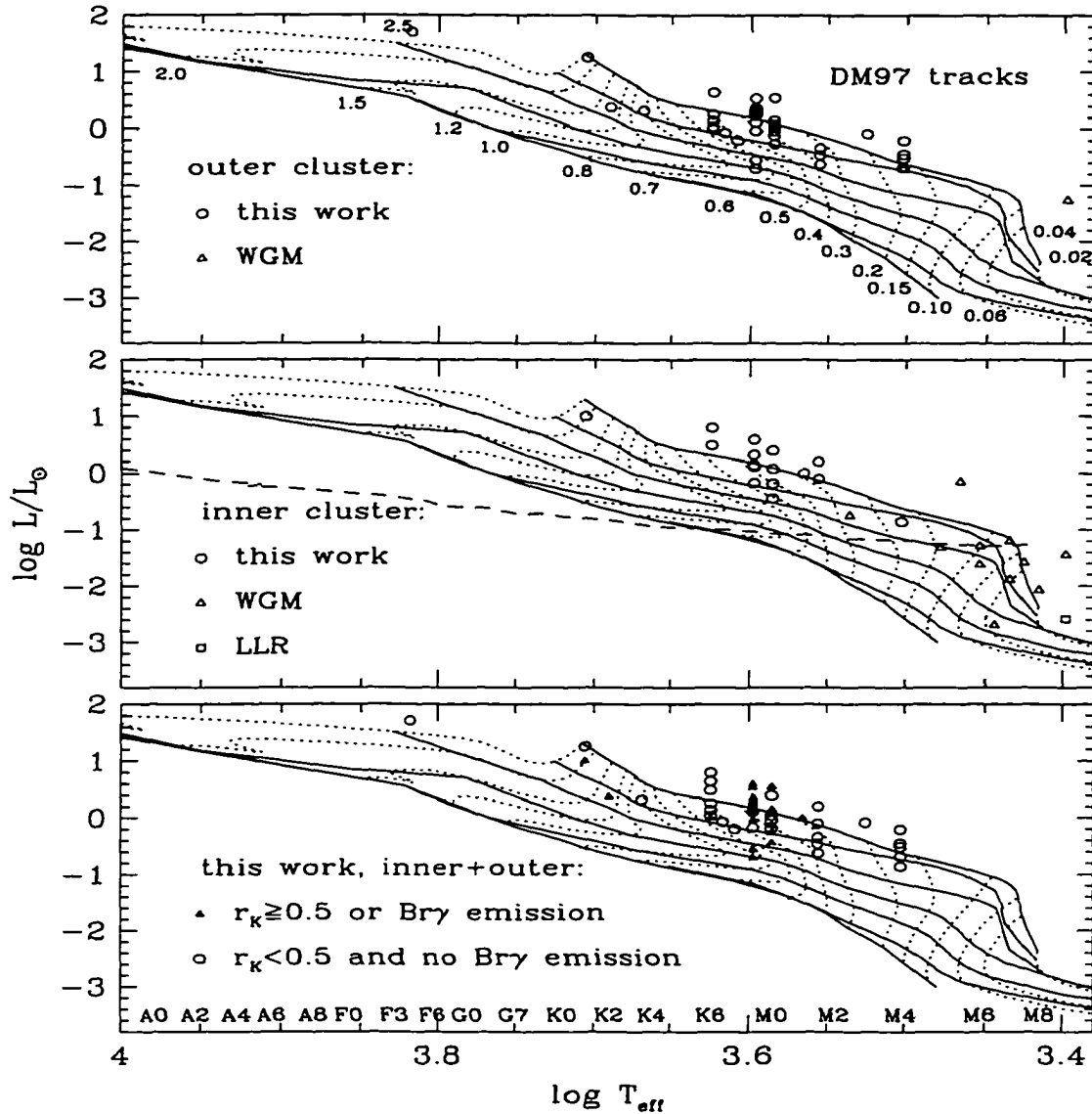


Figure 7.10 The H-R diagram of the ρ Oph star forming region within (upper panel) and outside (middle panel) the cloud core, as defined by the dashed boundary in Figure 7.1. Low-mass sources observed by WGM and in § 4 are also shown. The lower panel compares sources in the sample with and without signs of disk activity. The theoretical evolutionary tracks of DM97 are given, where the horizontal solid lines are isochrones representing ages of 0.3, 1, 3, 10, 30, and 100 Myr, from top to bottom. The dashed line in the H-R diagram for the cloud core represents $K_{\text{dereddened}} = 11$, which is the approximate completeness limit of the that spectroscopic sample for $A_K < 30$.

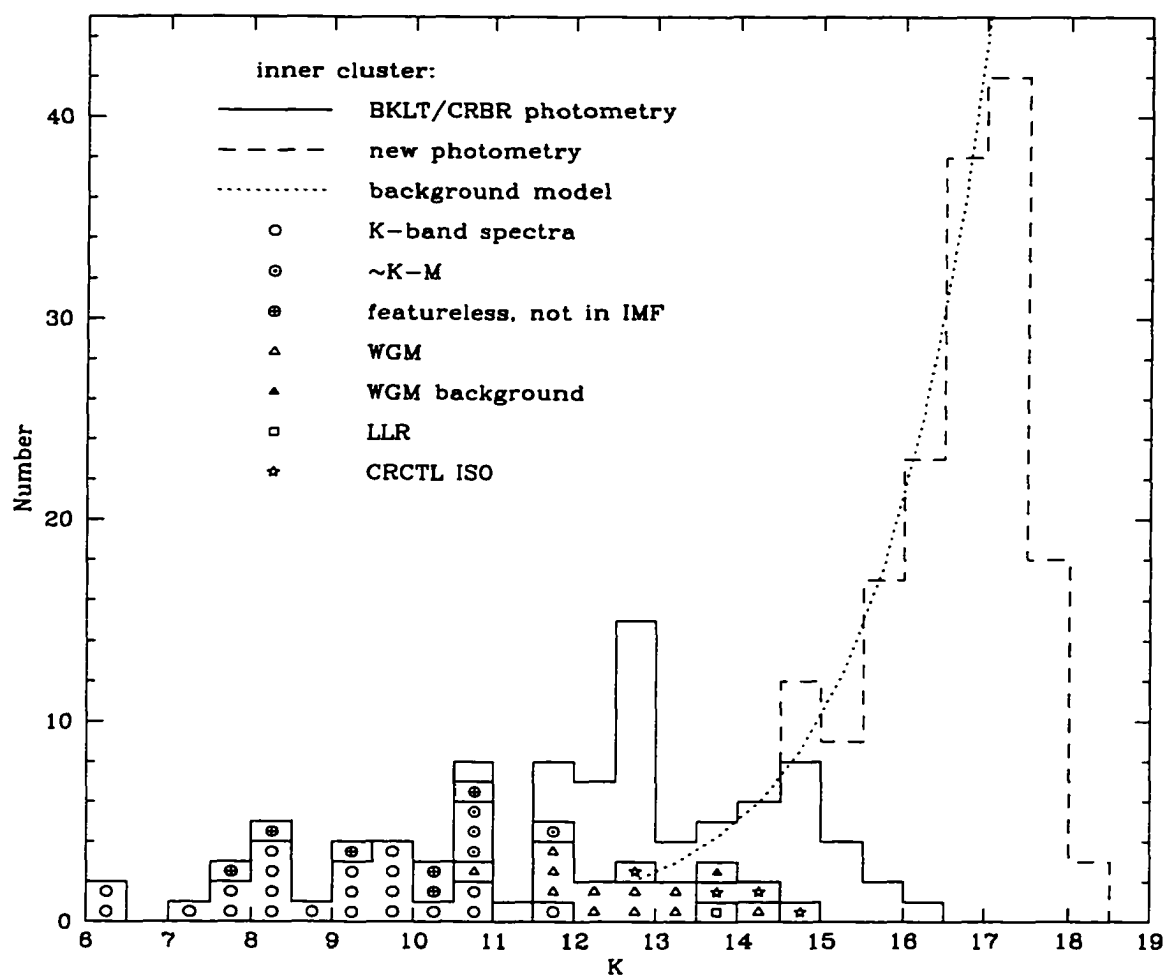


Figure 7.11 The K -band luminosity function of the cloud core of ρ Oph. The dotted line is a model for the distribution of background stars.

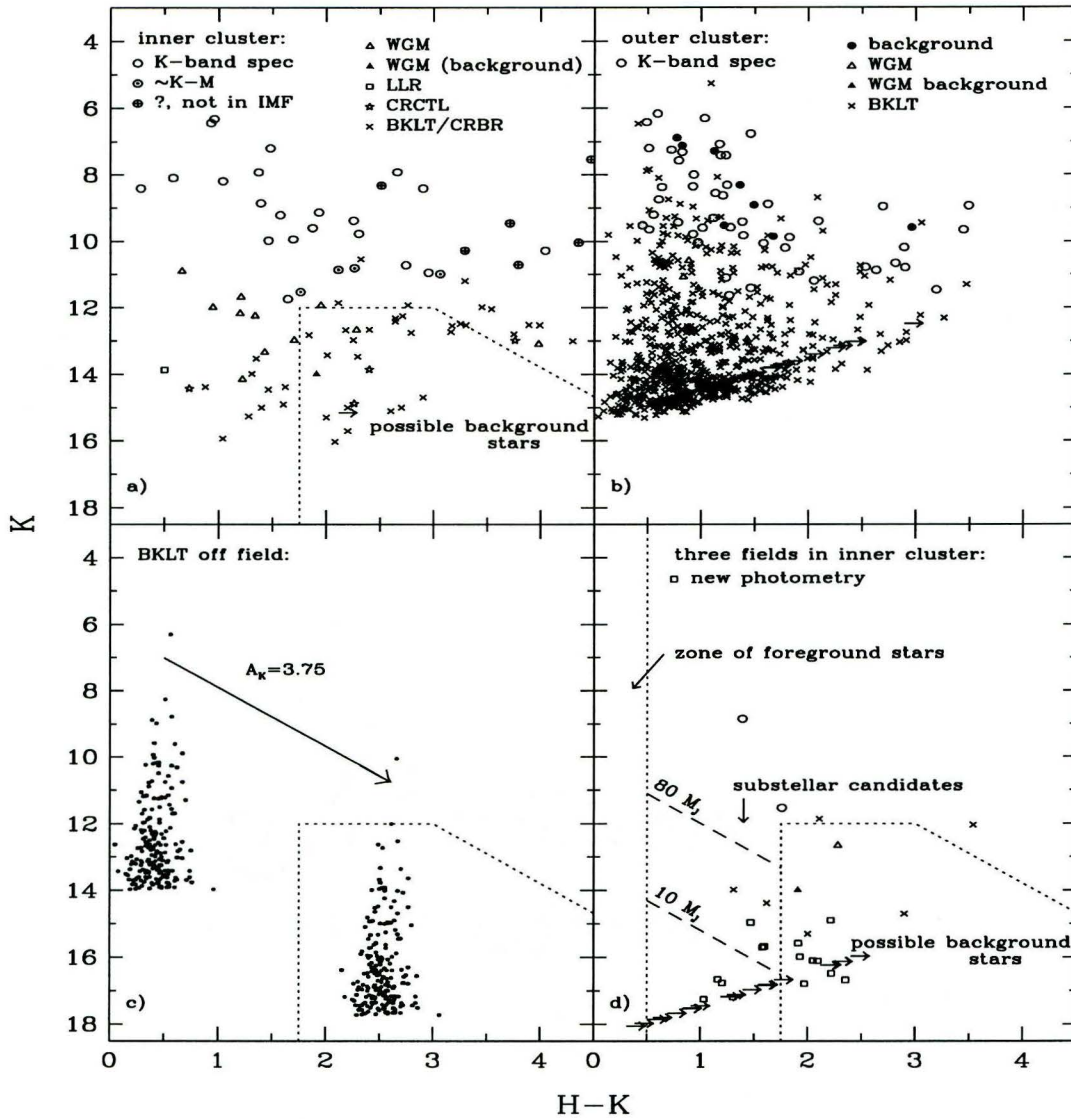


Figure 7.12 $H-K$ vs. K for the area a) within and b) outside the cloud core of ρ Oph, c) an off-field observed by BKLT equal in area to the inner cloud core, and d) three fields in the inner cluster (outlined by dotted lines in Figure 7.1) which I observed at J , H , and K . In a) and b), in addition to the sources in the K -band spectroscopic sample, I indicate those observed by WGM (K -band spectra), in § 4 (optical spectrum), CRCTL (ISO photometry), and BKLT and CRBR (JHK photometry). Analysis of the inner cluster KLF implies an average extinction of $A_K \sim 3.75$ towards the background stars behind the cloud core, which is simulated in d) by reddening the off-field population. The region enclosed by the dotted lines is therefore where background stars are expected to appear in a) and d). The dashed lines in d) are the theoretical K magnitudes of substellar objects at 1 Myr (A. Burrows, private communication).

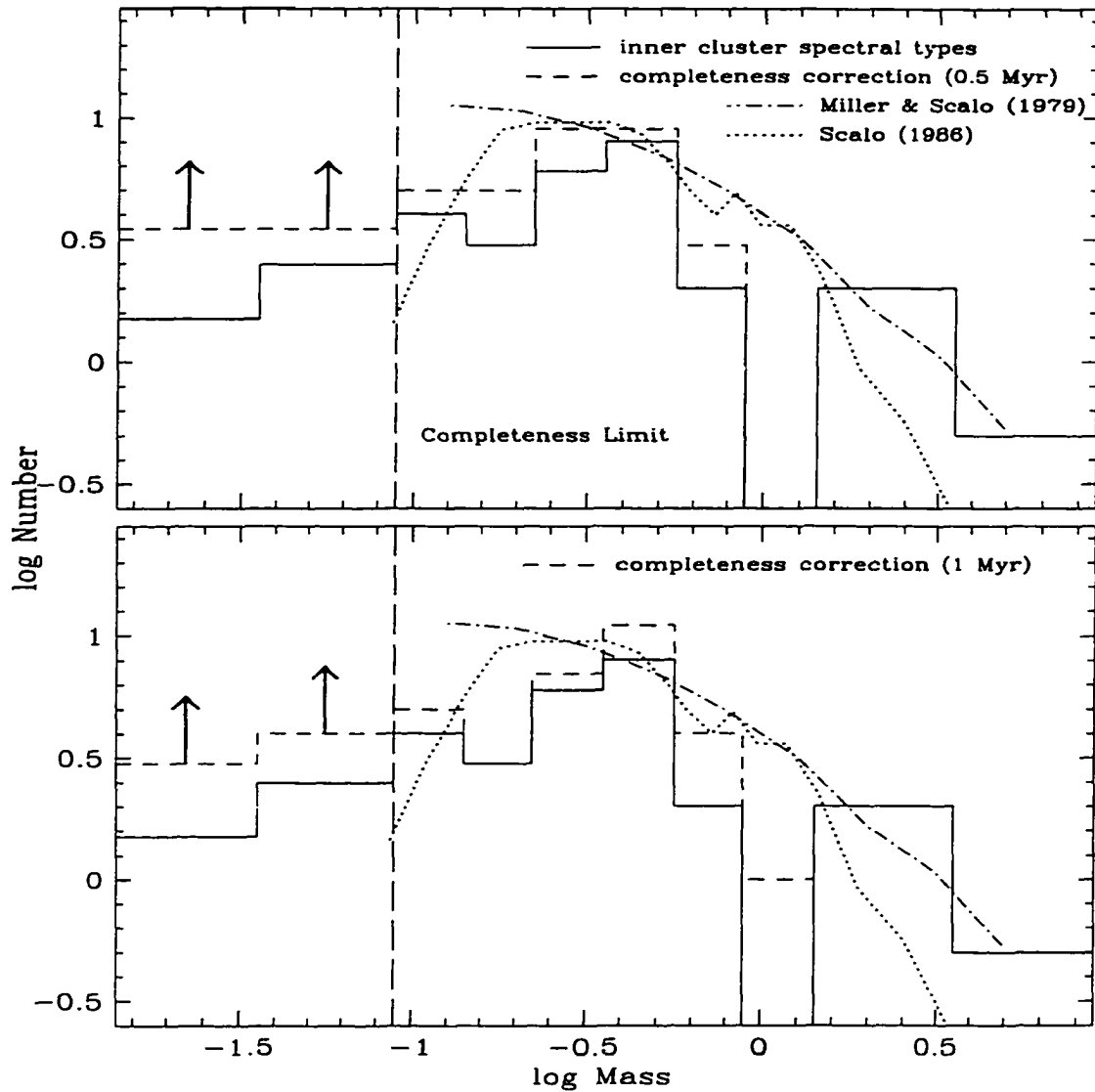


Figure 7.13 The solid histogram is the IMF derived by combining the evolutionary tracks of DM97 with the spectroscopic sample. The dashed histogram includes sources which 1) have uncertain late-type spectral types, 2) are identified as likely cluster members in ISO observations by CRCTL, or 3) lack spectra and fall above the background population in the KLF in Figure 7.11. Sources with featureless spectra (labeled as “?”), all of which are flat spectrum or Class I, are not included in the IMF. After such a correction, the completeness is indicated by the vertical dashed line and a lower limit to the substellar IMF is provided below this boundary. For reference, the field IMFs of Miller & Scalo (1979) and Scalo (1986) are given. The two lowest and two highest mass bins were given widths of $\log M = 0.4$ due to uncertainties in mass estimates.

CHAPTER 8

FUTURE WORK

A few years ago:

1. Spectral classification of young stars was restricted to optical spectroscopy of unobscured sources ($A_V < 5$) meeting specific criteria (e.g., emission in X-rays or $H\alpha$).
2. Studies of the accretion process in T Tauri stars relied on UV and optical photometry and optical emission lines.
3. Near-IR imaging surveys were beginning to constrain the IMF in young clusters.
4. No confirmed brown dwarfs had been identified, with only a few young stars as late as M6 known ($\sim 0.1 M_\odot$).

At the conclusion of this thesis:

1. Unbiased, magnitude-limited ($K \lesssim 12.5$) IR spectroscopic surveys of young, nearby (< 500 pc) stellar populations have been performed.

2. The global properties of near-IR continuum and line emission in T Tauri stars have been studied.
3. Spectral classification and KLF modeling have been combined to derive the IMF down to the hydrogen burning limit ($0.08 M_{\odot}$) and lower limits to the mass function in the substellar regime.
4. In addition to brown dwarfs recently found in the field (e.g., GL 229B), several candidates identified in early photometric surveys of open (e.g., Pleiades) and young clusters (ρ Oph) have been confirmed as substellar.

Several important questions will be addressed over the next five years:

1. What is the nature of Class I sources?

The photospheres of these very young protostars will be probed through sensitive, moderate- to high-resolution IR spectroscopy.

2. How is the accretion and formation process of brown dwarfs characterized?

Observations of optical and IR emission lines (≥ 6 meter class telescopes) and mid- to far-IR continuum emission (SIRTF, WIRE) in young brown dwarfs will provide insight into the birth of these transitional objects between stars and planets.

3. What is the IMF for brown dwarfs? Where is the bottom of the mass function for free-floating objects? $10 M_J$? $5 M_J$?

Accurate substellar mass functions will be measured in several clusters with NICMOS grism spectroscopy (NGC 2024, Trapezium; E. Young), NICMOS narrow-band imaging (IC 348; J. Najita), and Keck multi-object optical

spectroscopy (IC 348; K. Luhman). Although these projects may reach the bottom of the mass function, the most promising technique for obtaining a complete census of all brown dwarfs in a given cluster is broad and narrow-band imaging in the near- to mid-IR with SIRTf.

4. What is the frequency of binary brown dwarfs and planetary systems?

High-resolution imaging ($\sim 0.05\text{--}0.1''$) from the ground (adaptive optics) and space (HST) will be used to search for binary brown dwarfs and planets in young clusters.

5. Are theoretical models of pre-main-sequence evolution valid?

Low-mass stellar and substellar spectroscopic binaries will be identified through high-resolution optical and near-IR spectroscopy on large ground-based telescopes (≥ 6 meter), providing direct tests of these models through measurements of stellar temperatures, radii, and luminosities.

REFERENCES

- Adams, F. C., & Fatuzzo, M. 1996, *ApJ*, 464, 256
- Ali, B., Sellgren, K., DePoy, D. L., Carr, J. S., Gatley, I., Merrill, K. M., & Lada, E. 1997, in prep
- Allard, F. 1990, Ph.D. thesis, Univ. Heidelberg
- Allard, F., Hauschildt, P. H., Baraffe, I., & Chabrier, G. 1996, *ApJ*, 465, L123
- Allard, F., & Hauschildt, P. H. 1995, *ApJ*, 445, 433
- Allard, F., & Hauschildt, P. H., Alexander, D. R., & Starrfield, S. 1997, *ARA&A*, 35
- Allen, L. E., & Strom, K. M. 1995, *AJ*, 109, 1379
- Alonso, A., Arribas, S., & Martinez-Roger, C. 1996, *A&A*, 313, 873
- Andersson, B-G., & Wannier, P. G. 1997, *ApJ*, 491, L103
- Baraffe, I. 1997, private communication
- Baraffe, I., Chabrier, G., Allard, F., & Hauschildt, P. H. 1995, *ApJ*, 446, L35
- Baraffe, I., Chabrier, G., Allard, F., & Hauschildt, P. H. 1997, *A&A*, 327, 1054 (BCAH97)
- Barsony, M., Burton, M. G., Russel, A. P. G., Carlstrom, J. E., & Garden, R. 1989, *ApJ*, 346, L93
- Barsony, M., Kenyon, S. J., Lada, E. A., & Teuben, P. J. 1997, *ApJS*, 112, 109 (BKLT)
- Basri, G., Marcy, G. W., & Graham, J. R. 1996, *ApJ*, 458, 600
- Basri, G., & Martín, E. L. 1997, ASP Conf. Series, "Brown Dwarfs and Extrasolar Planets" Proceedings, R. Rebolo, E. L. Martín, M. R. Zapatero-Osorio (eds), in press
- Basu, S. & Rana, N. C. 1992, *ApJ*, 393, 373
- Bell, R. A., & Gustafsson, B. 1989, *MNRAS*, 236, 635
- Berriman, G., Reid, N., & Leggett, S. K. 1992, *ApJ*, 392, L31
- Berriman, G., & Reid, I. N. 1987, *MNRAS*, 227, 315
- Bertiau, F. C. 1958, *ApJ*, 128, 533
- Bessell, M. S. 1979, *PASP*, 91, 589
- Bessell, M. S. 1990a, *A&AS*, 83, 357
- Bessell, M. S. 1990b, *PASP*, 102, 1181
- Bessell, M. S. 1991, *AJ*, 101, 662
-

- Bessell, M. S., & Brett, J. M. 1988, *PASP*, 100, 1134
- Bessell, M. S., Castelli, F., & Plez, B. 1998, *A&A*, 333, 231
- Biscaya, A. M., Calvet, N., Rieke, G. H., & Luhman, K. L. in prep
- Blaauw, A. 1952, *B. A. N.*, 11, 412
- Bonnell, I. A., Bate, M. R., Clarke, C. J., & Pringle, J. E. 1997, *MNRAS*, 285, 201
- Boulard, M.-H., Caux, E., Monin, J.-L., Nadeau, D., & Rowlands, N. 1995, *A&A*, 300, 276
- Bouvier, J., & Appenzeller, I. 1992, *A&AS*, 92, 481
- Bouvier, J., Stauffer, J. R., Martín, E. L., Barrado y Navascués, Wallace, B., & Bejar, V. J. S. 1998, *A&A*, in press
- Brett, J. M. 1995, *A&A*, 295, 736
- Bryja, C. 1994, *BAAS*, 185, 103.03
- Budding, E., Butler, C. J., Doyle, J. G., Etzel, P. B., Oláh, K., Zeilik, M., & Brown, D. 1996, *Ap&SS*, 236, 215
- Burrows, A. 1997, private communication
- Burrows, A., Hubbard, W. B., & Lunine, J. I. 1989, *ApJ*, 345, 939
- Burrows, A., Hubbard, W. B., Saumon, D., & Lunine, J. I. 1993, *ApJ*, 406, 158 (BHSL93)
- Burrows, A., & Liebert, J. 1993, *Rev Mod Phy*, 65, 301
- Carr, J. S., Tokunaga, A. T., Najita, J., Shu, F. H., & Glassgold, A. E. 1993, *ApJ*, 411, 37
- Casali, M. M., & Eiroa, C. 1996, *A&A*, 306, 427
- Casali, M. M., & Matthews, H. E. 1992, *MNRAS*, 258, 399
- Casanova, S., Montmerle, T., Feigelson, E. D., & André, P. 1995, *ApJ*, 439, 752
- Cayrel de Strobel, G., Hauck, B., Francois, P., Thevenin, F., Friel, E., Mermilliod, M., & Borde, S. 1992, *A&AS*, 95, 273
- Chabrier, G., & Baraffe, I. 1995, *ApJ*, 451, L29
- Cohen, M., & Kuhl, L. V. 1979, *ApJS*, 41, 743
- Comerón, F., Rieke, G. H., Burrows, A., & Rieke, M. J. 1993, *ApJ*, 416, 185 (CRBR)
- Comerón, F., Rieke, G. H., Claes, P., Torra, J., & Laureijs, R. J., 1998, *A&A*, 335, 552 (CRCTL)
- Comerón, F., & Rieke, G. H. 1998, submitted
-

- Comerón, F., Rieke, G. H., Burrows, A., & Rieke, M. J. 1993, *ApJ*, 416, 185
- Comerón, F., Rieke, G. H., & Rieke, M. J. 1996, *ApJ*, 473, 294
- D'Antona, F., & Mazzitelli, I. 1994, *ApJS*, 90, 467 (DM94)
- D'Antona, F., & Mazzitelli, I. 1997, in "Cool stars in Clusters and Associations", eds. R. Pallavicini & G. Micela, *Mem.S.A.It.*, 68, n.4
- De Marchi, G. & Paresce, F. 1995, *A&A*, 304, 211
- Dolidze, M. V., & Arakeylan, M. A. 1959, *Soviet Astron*, 3, 434
- Duquennoy, A., & Mayor, M. 1991, *A&A*, 248, 485
- Dyck, H. M., Benson, J. A., van Belle, G. T., & Ridgway, S. T. 1996, *AJ*, 111, 1705
- Eggen, O. J. 1996, *AJ*, 111, 466
- Elias, J. H. 1978, *ApJ*, 224, 453
- Elias, J. H., Frogel, J. A., Matthews, K., & Neugebauer, G. X. 1982, *AJ*, 87, 1029
- Favata, F., Micela, G., & Sciortino, S. 1997, *A&A*, 326, 647
- Feigelson, E. D., Casanova, S., Montmerle, T., & Guilbert, J. 1993, *ApJ*, 416, 623
- Fredrick, L. W. 1956, *AJ*, 61, 437
- Frogel, J. A., Persson, S. E., Matthews, K., & Aaronson, M. 1978, *ApJ*, 220, 75
- Gauvin, L. S., & Strom, K. M. 1992, *ApJ*, 385, 217
- Gingrich, C. H. 1922, *ApJ*, 56, 139
- Gliese, W., 1969, *Veroeff. Astron. Rechen-Inst.*, 22, 1
- Gonzalez, G. 1997, *ASP Conf. Series*, "Brown Dwarfs and Extrasolar Planets" Proceedings, R. Rebolo, E. L. Martín, M. R. Zapatero Osorio (eds), in press
- Gorgas, J., Faber, S. M., Burstein, D., Gonzalez, J. J., Courteau, S., & Prosser, C. 1993, *ApJS*, 86, 153
- Grasdalen, G. L., Strom, K. M., & Strom, K. E. 1973, *ApJ*, 184, L53
- Greene, T. P., Wilking, B. A., André, P., Young, E. T., & Lada, C. J. *ApJ*, 434, 614
- Greene, T. P., & Lada, C. J., 1996, *AJ*, 112, 2184
- Greene, T. P., & Lada, C. J., 1997, *AJ*, 114, 2157
- Greene, T. P., & Meyer, M. R. 1995, *ApJ*, 450, 233
- Greene, T. P., & Young, E. T. 1992, *ApJ*, 395, 516
- Gullbring, E., Hartmann, L., Briceño, C., & Calvet, N. 1998, *ApJ*, 492, 323
- Harris, D. L., Morgan, W. W., & Roman, N. G. 1954, *ApJ*, 119, 622
-

- Hartigan, P. 1993, *AJ*, 105, 1511
- Hartigan, P., Edwards, S., & Ghandour, L. 1995, *ApJ*, 452, 736
- Hartmann, L., & Kenyon, S. J. 1996, *ARA&A*, 34, 207
- Hawley, S. L., Gizis, J. E., & Reid, I. N. 1996, *AJ*, 112, 2799
- Hearnshaw, J. B. 1974, *A&A*, 30, 203
- Henry, T. J., Kirkpatrick, J. D., & Simons, D. A. 1994, *AJ*, 108, 1437
- Herbig, G. H. 1998, *ApJ*, 497, 736
- Hillenbrand, L. A. 1997, *AJ*, 113, 1733
- Hodapp, K.-W., & Deane, J. 1993, *ApJS*, 88, 119
- Hughes, J., Hartigan, P., Krautter, J., & Kelemen, J. 1994, *AJ*, 108, 1071
- Humphreys, R. M., Jones, T. J., & Sitko, M. L. 1984, *AJ*, 89, 1155
- Jones, H. R. A., Longmore, A. J., Allard, F., & Hauschildt, P. H. 1996, *MNRAS*, 280, 77
- Jones, H. R. A., Longmore, A. J., Jameson, R. F., & Mountain, C. M. 1994, *MNRAS*, 267, 413
- Kalas, P., & Jewitt, D. 1997, *Nature*, 386, 52
- Keenan, P. C., & McNeil, R. C. 1976, *An Atlas of the Spectra of the Cooler Stars* (Columbus: Ohio State University Press)
- Keenan, P. C., & McNeil, R. C. 1989, *ApJS*, 71, 245
- Kenyon, S. J., Lada, E. A., & Barsony, M. 1998, *AJ*, 115, 252
- Kenyon, S. J., & Hartmann, L. 1990, *ApJ*, 349, 197
- Kenyon, S. J., & Hartmann, L. 1995, *ApJS*, 101, 117
- King, I. R., Anderson, J., Cool, A. M., & Piotto, G. 1998, *ApJ*, 492, L37
- Kirkpatrick, J. D., Henry, T. J., & Irwin, M. J. 1997, *AJ*, 113, 1421
- Kirkpatrick, J. D., Henry, T. J., & McCarthy, D. W. 1991, *ApJS*, 77, 417
- Kirkpatrick, J. D., Kelly, D. M., Rieke, G. H., & Liebert, J. 1993, *ApJ*, 402, 643
- Kleinmann, S. G., & Hall, D. N. B. 1986, *ApJS*, 62, 501
- Kroupa, P., Tout, C. A., Gilmore, G. 1991, *MNRAS*, 251, 293
- Lacy, C. H. 1977, *ApJ*, 218 444
- Lada, C. J. 1987, in *Star Forming Regions*, ed. M. Peimbert and J. Jugaku (Dordrecht: Reidel), p. 1
- Lada, C. J., Alves, J., & Lada, E. A. 1996, *AJ*, 111, 1964
-

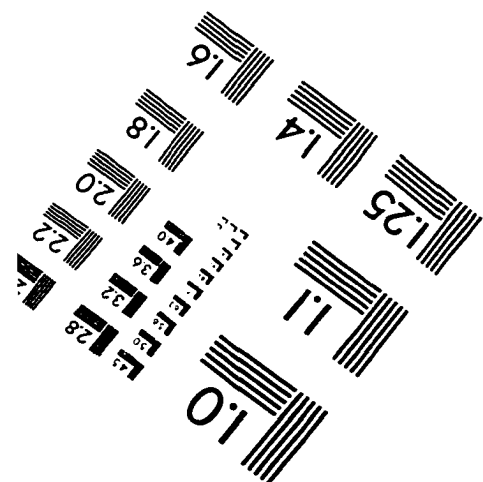
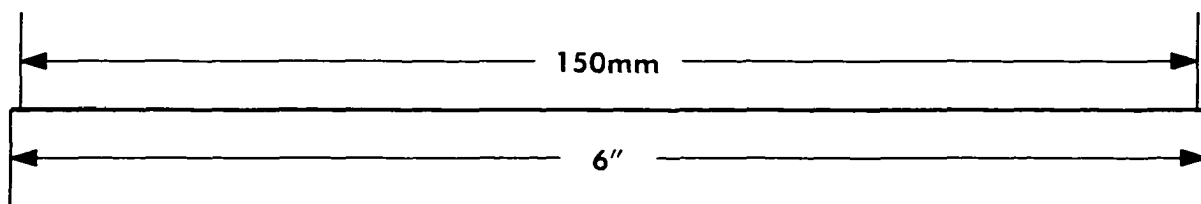
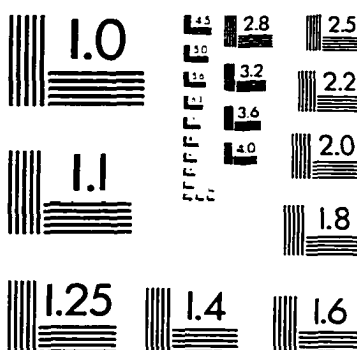
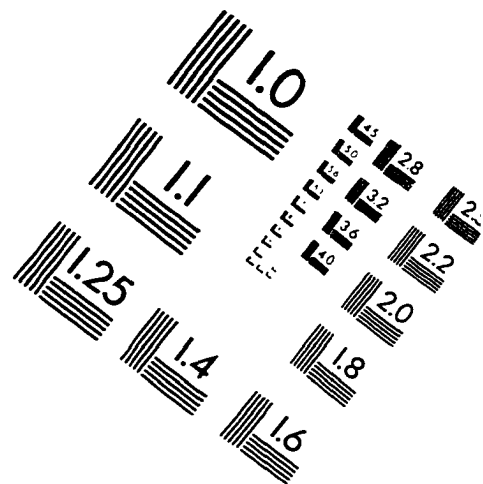
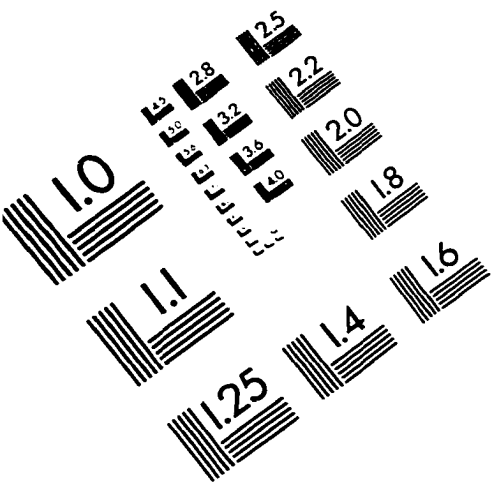
- Lada, C. J., Young, E. T., & Greene, T. P. 1993, *ApJ*, 408, 471
- Lada, C. J., & F. C. Adams, 1992, *ApJ*, 393, 278
- Lada, E. A., DePoy, D. L., Evans, N. J., & Gatley, I. *ApJ*, 1991, 371, 171
- Lada, E. A., & Lada, C. J. 1995, *AJ*, 109, 1682
- Laird, J. B. 1985, *ApJS*, 57, 389
- Landolt, A. U. 1992, *AJ*, 104, 340
- Larson, R. B. *MNRAS*, 1992, 256, 641
- Lawson, W. A., Feigelson, E. D., & Huenemoerder, D. P. 1996, *MNRAS*, 280, 1071
- Leggett, S. K. 1989, *A&A*, 208, 141
- Leggett, S. K. 1992, *ApJS*, 82, 351
- Leggett, S. K., Allard, F., Berriman, G., Dahn, C. C., & Hauschildt, P. H. 1996, *ApJS*, 104, 117
- Leous, J. A., Feigelson, E. D., André, P., & Montmerle, T. 1991, *ApJ*, 379, 683
- Leung, K.-C., & Schneider, D. P. 1978, *AJ*, 83, 618
- Liebert, J., Saffer, R. A., Norsworthy, J., Giampapa, M. S., & Stauffer, J. R. 1992, *Seventh Cambridge Workshop on Cool Stars, Stellar Systems, and the Sun*, Ed. Giampapa, A.S.P. Conference Series V.26, 282
- Magazzù, A., Martín, E. L., & Rebolo, R. 1991, *A&A*, 249, 149
- Maiolino, R., Rieke, G. H., & Rieke, M. J. 1996, *AJ*, 111, 537
- Marley, M. S., Saumon, D., Guillot, T., Freedman, R. S., Hubbard, W. B., Burrows, A., & Lunine, J. I. 1996, *Science*, 272, 1919
- Martín, E. L., Rebolo, R., & Zapatero Osorio, M. R. 1996, *ApJ*, 469, 706
- Martín, E. L., Rebolo, R., & Zapatero Osorio, M. R. 1997, *ASP Conf. Series*, "Brown Dwarfs and Extrasolar Planets" Proceedings, R. Rebolo, E. L. Martín, M. R. Zapatero Osorio (eds), in press
- McCaughrean, M. J., Rayner, J. T., & Zinnecker, H. 1994, *ApJ*, 436, L189
- McCaughrean, M. J., & Stauffer, J. R. 1994, *AJ*, 108, 1382
- Metcalf, T. S., Mathieu, R. D., Latham, D. W., & Torres, G. 1996, *ApJ*, 456, 356
- Meyer, M. R. 1995, Ph.D. thesis, Univ. Massachusetts
- Meyer, M. R., Calvet, N., & Hillenbrand, L. A. 1997, *AJ*, 114, 288
- Miller, G. E., & Scalo, J. M. 1979, *ApJS*, 41, 513
- Montmerle, T., Koch-Miramonde, L., Falgarone, E., & Grindlay, J. E., 1983, *ApJ*, 269, 182
-

- Morgan, W. W., Abt, H. A., & Tapscott, J. W. 1978, Revised MK Spectral Classification for Stars Earlier than the Sun (Yerkes Observatory, University of Chicago and Kitt Peak Nationaly Observatory)
- Muench, A., Lada, E. A., & Lada, C. J. in preparation
- Muzerolle, J., Calvet, N., & Hartmann, L. 1998, *ApJ*, 492, 743
- Najita, J., Carr, J. S., Glassgold, A. E., Shu, F. H., & Tokunaga, A. T. 1996, *ApJ*, 462, 919
- Najita, J., Carr, J. S., & Tokunaga, A. T. 1996, *ApJ*, 456, 292
- Nakajima, T., Oppenheimer, B. R., Kulkarni, S. R., Golimowski, D. A., Matthews, K., & Durrance, S. T. 1995, *Nature*, 378, 463
- Natta, A., Giovanardi, C., & Palla, F. 1988, *ApJ*, 332, 921
- Nelson, L. A., Rappaport, S., & Joss, P. C. 1993, *ApJ*, 404, 723
- Oppenheimer, B. R., Kulkarni, S. R., Nakajima, T., & Matthews, K. 1995, *Science*, 270, 1478
- Perrin, G., Coudé du Foresto, V., Ridgway, S. T., Mariotti, J.-M., Traub, W. A., Carleton, N. P., & Lacasse, M. G. 1997, *A&A*, in press
- Preibisch, T., Zinnecker, H., & Herbig, G. H. 1996, *A&A*, 310, 456
- Price, N. M., & Podsiadlowski, Ph. 1995, *MNRAS*, 273, 1041
- Pulone, L., De Marchi, G., Paresce, F., & Allard, F. 1998, *ApJ*, 492, L41
- Rebolo, R., Martín, E. L., Basri, G., Marcy, G. W., & Zapatero Osorio, M. R. 1996, *ApJ*, 469, L53
- Rebolo, R., Zapatero Osorio, M. R. & Martín, E. L. 1995, *Nature*, 377, 129
- Reid, I., Hawley, S. L., & Gizis, J. E. 1996, *AJ*, 111, 2469
- Ridgway, S. T., Joyce, R. R., White, N. M., & Wing, R. F. 1980, *ApJ*, 235, 126
- Rieke, G. H., Ashok, N. M., & Boyle, R. P. 1989, *ApJ*, 339, L71
- Rieke, G. H., & Lebofsky, M. J. 1985, *ApJ*, 288, 618
- Rieke, G. H., & Rieke, M. J. 1990, *ApJ*, 362, L21
- Salpeter, E. E. 1955, *ApJ*, 121, 161
- Scalo, J. 1986, *Fund. Cosmic Phys.*, 11, 1
- Scalo, J. 1998, The Stellar Initial Mass Function Proceedings of the 38th Herstmonceux Conference, ed. G. Gilmore, I. Parry & S. Ryan, in press
- Schmidt-Kaler, T. 1982, in *Landolt-Bornstein, Group VI, Vol. 2*, ed. K.-H. Hellwege (Berlin: Springer), 454
- Silk, J. 1995, *ApJ*, 438, 41

- Simon, M., et al. 1995, *ApJ*, 443, 625
- Stauffer, J. R., Hamilton, D., & Probst, R. G. 1994, *AJ*, 108, 155
- Stauffer, J. R., Hartmann, L. W., & Barrado, D. 1995, *ApJ*, 454, 910
- Stevenson, D. J. 1991, *ARA&A*, 29, 163
- Strom, K. M., Kepner, J., & Strom, S. E. 1995, *ApJ*, 438, 813
- Strom, K. M., Strom, S. E., Edwards, S., Cabrit, S., & Skrutskie, M. F. 1989, *AJ*, 97, 1451
- Strom, K. M., & Strom, S. E. 1994, *ApJ*, 424, 237 (SS94)
- Strom, S. E., Edwards, S., & Skrutskie, M. F. 1993, in *Protostars and Planets III*, ed. E. H. Levy, J. I. Lunine, & M. S. Mathews (University of Arizona Press, Tucson), 837
- Strom, S. E., Strom, K. M., & Carrasco, L. 1974, *PASP*, 86, 798
- Struve, O., & Rudkjøbing, M. 1949, *ApJ*, 109, 92
- Swenson, F. J. 1996, private communication (FJS)
- Terlevich, E. 1987, *MNRAS*, 224, 193
- Thé, P. S., Thomas, D., Christensen, C. G., & Westerlund, B. E. 1990, *PASP*, 102, 565
- Tinney, C. G., Mould, J. R., & Reid, I. N. 1993, *AJ*, 105, 1045
- Torres-Dodgen, A. V., & Weaver, W. B. 1993, *PASP*, 105, 693
- Trullols, E. & Jordi, C. 1997, *A&A*, 324, 549
- Valenti, J. A., Basri, G., Johns, C. M. 1993, *A&A*, 106, 2024
- Veeder, G. J. 1974, *AJ*, 79, 1056
- Vesperini, E., & HEGGIE, D. C. 1997, *MNRAS*, 289, 898
- Vrba, F. J., Strom, K. M., Strom, S. E., & Grasdalen, G. L. 1975, *ApJ*, 197, 77
- Vrba, F. J., Strom, S. E., & Strom, K. M. 1976, *AJ*, 81, 958
- Wainscoat, R. J., Cohen, M., Volk, K., Walker, H. J., Schwartz, D. E. 1992, *ApJS*, 83, 111
- Wallace, L., & Hinkle, K. 1996, *ApJS*, 107, 312
- Wallace, L., & Hinkle, K. 1997, *ApJS*, 111, 445
- Whittet, D. C. B. 1974, *MNRAS*, 168, 371
- Wiling, B. A., Greene, T. P., & Meyer, M. R. 1998, submitted
- Wiling, B. A., Lada, C. J., & Young, E. T. 1989, *ApJ*, 340, 823
- Wiling, B. A., Schwartz, R. D., & Blackwell, J. H. 1987, *AJ*, 94, 106
-

- Willing, B. A., & Lada, C. J. 1983, *ApJ*, 274, 698
- Williams, D. M., Boyle, R. P., Morgan, W. T., Rieke, G. H., Stauffer, J. R., & Rieke, M. J. 1996, *ApJ*, 464, 238
- Williams, D. M., Comerón, F., Rieke, G. H., & Rieke, M. J. 1995, *ApJ*, 454, 144
- Williams, D. M., Rieke, G. H., & Stauffer, J. R. 1995, *ApJ*, 445, 359
- Williams, D., Thompson, C. L., Rieke, G. H., & Montgomery, E. F. 1993, *ProcSPIE*, 1308, 482
- Wyse, R. F. G., & Gilmore, G., 1995, *AJ*, 110, 2771
- Young, E. T., Lada, C. J., & Wilking, B. A. 1986, *ApJ*, 304, L45
- Zapatero Osorio, M. R. 1997, ASP Conf. Series, "Brown Dwarfs and Extrasolar Planets" Proceedings, R. Rebolo, E. L. Martín, M. R. Zapatero Osorio (eds), in press
- Zapatero Osorio, M. R., Rebolo, R., Martín, E. L., Basri, G., Magazzù, A., Hodgkin, S. T., Jameson, R. F., & Cossburn, M. R. 1997, *ApJ*, 491, L81
- Zapatero Osorio, M. R., Rebolo, R., Martín, E. L., & López García, R. J. 1996, *A&A*, 305, 519
- Zapatero Osorio, M. R., Rebolo, R., & Martín, E. L. 1997, *A&A*, 317, 164
- van Altena, W. F., Lee, J. T.-L., & Hoffleit, D. 1991, The General Catalogue of Trigonometric Stellar Parallaxes (1991): A Preliminary version (New Haven Univ. Obs: Yale) ADS catalog a1174

IMAGE EVALUATION TEST TARGET (QA-3)



APPLIED IMAGE, Inc
1653 East Main Street
Rochester, NY 14609 USA
Phone: 716/482-0300
Fax: 716/288-5989

© 1993, Applied Image, Inc., All Rights Reserved

